ABSTRACT

TITLE OF DOCUMENT: ACYCLIC CUCURBIT[N]URIL CONGENERS: SYNTHESIS, BINDING PROPERTIES AND MEDICINAL APPLICATIONS

Ben Zhang, Doctor of Philosophy, 2014

Directed By: Professor Lyle Isaacs
Department of Chemistry and Biochemistry

An urgent problem for pharmaceutical industry is that the water solubility of an estimated 40-70% of the newly developed active pharmaceutical ingredients (API) are so poor that they cannot be formulated on their own. One interesting topic is to use molecular containers as the solubilizing agents. Supramolecular chemistry has always been an interesting research area and during the past decades, various new supramolecular host•guest systems have been developed. Cucurbit[n]urils (CB[n]) are very promising molecular containers as drug delivery vehicles due to their outstanding recognition properties. In order to discover the most suitable CB[n]-type containers as solubilizing agents, acyclic CB[n]-type containers have been synthesized and their recognition and formulation properties have been studied. In this thesis, three chapters have been included to investigate the possibility of using CB[n]-type containers as solubilizing agents for pharmaceutical agents.

Chapter 1 gives an introduction to supramolecular chemistry and formulation techniques using molecular containers. A literature review on the synthesis, functionalization and applications of cucurbit[n]uril is given and the application of cyclodextrins and CB[n] containers in formulation techniques is discussed.

Chapter 2 describes a series of acyclic CB[n]-type molecular containers (**II-2a** – **II-2h**) with different solubilizing groups bearing different charges for evaluation as potential drug solubilizing agents. The X-ray crystal structures of the negative, positive and neutral hosts (host **II-2b**, **II-2f**, and **II-2h**) are reported. For neutral (**II-2h**) and positively charged (**II-2f**) hosts, intramolecular H-bonds and ion-dipole interactions between the solubilizing arms and the ureidyl C=O portals are observed as well as intrahost π–π stacking interactions which results in a self-filling of the cavity. ^{1}H NMR and UV/Vis spectroscopy are used to measure the K_a values of hosts **II-2a**, **II-2h**, and **II-2f** toward guests with different charge and significant decrease is noted in binding affinities of the neutral (**II-2h**) and positive (**II-2f**). The pK_a of **7**H^+ alone and in the presence of differently charged hosts **II-2a, II-2h**, and **II-2f** are measured and the **II-2a** induces the largest pK_a shift. The poor recognition properties of hosts **II-2h** and **II-2f** are reflected in their phase-solubility diagrams with insoluble drugs (tamoxifen, 17-α–ethynylestradiol, and indomethacin). In all cases, the anionic host **II-2a** functions more efficiently as a solubilizing agent than either neutral **II-2h**, or cationic host **II-2f**.

In chapter 3, we compare the ability of **III-1a** – **III-1e** to solubilize insoluble drugs relative to HP-β-CD. Phase solubility diagrams are created for mixtures of containers **III-1a** – **III-1e** and HP- β-CD with 19 drugs. We find that the solubilizing

ability of the best container (**III-1a** – **III-1e**) is superior to HP-β-CD in all cases. A notable achievement is the solubilization of the developmental anticancer agent PBS-1086. The acyclic CB[n]-type containers display an affinity for the steroid ring system, aromatic moieties of insoluble drugs, and cationic ammonium groups. Compound **III-1b** is generally the most potent (K_a up to and exceeding 10^6 M^{-1}) container whereas both **III-1a** and **III-1b** display excellent solubility enhancement toward a broad range of insoluble drugs. The broad scope of insoluble drugs that can be formulated with **III-1a** and **III-1b** – in many cases where HP-β-CD fails completely – makes acyclic CB[n]-type containers particularly attractive alternatives to cyclodextrins as solubilizing excipients for practical applications.

ACYCLIC CUCURBIT[N]URIL CONGENERS: SYNTHESIS, BINDING PROPERTIES AND MEDICINAL APPLICATIONS

By

Ben Zhang

Dissertation submitted to the Faculty of the Graduate School of the
University of Maryland, College Park, in partial fulfillment
of the requirements for the degree of
Doctor of Philosophy
2014

Advisory Committee:
Professor Lyle Isaacs, Chair
Professor Jeffery Davis
Associate Professor Herman Sintim
Professor Philip DeShong
Associate Professor Volker Briken, Dean's Representative

Dedication

To my parents, Jianfeng Zhang and Chunxia Kong

and my grandparents, Zhengying Zhang, and Xizhi Xiang

Acknowledgements

I would like to thank my advisor Professor Lyle Isaacs for his guidance throughout my Ph.D. life. From his precious knowledge and experience, I learned a lot about chemistry and how to become a successful researcher.

I would like to thank the former group members of Isaacs group for passing down their knowledge and laboratory skills. I would like to thank Dr. Da Ma for his advice in my initial stages. I also would like to thank Dr. James Wittenberg and Dr. Liping Cao for their generous help and continual friendship.

I would like to thank all of the current Isaacs group members for being supportive in both science and daily life. It was my great pleasure to work in such a pleasing and productive environment. Thank you to Dr. Yu-Fai Lam and Dr. Yinde Wang for your help in NMR experiments and Dr. Peter Zavalij for your assistance with X-ray crystallography.

I would like to thank our collaborators, Dr. Pavel Anzenbacher, Dr. Volker Briken, Dr. Matthias Eikermann, and Dr. Gaya Hettiarachchi for the achievements we have made together.

Finally, I would like to specially thank my parents Jianfeng Zhang and Chunxia Kong. I could not have made these achievements without their wholehearted support, understanding and encouragement.

Table of Contents

Dedication…… ii

Acknowledgements…….. iii

Table of Contents……. iv-v

List of Tables…… vi

List of Schemes…… vii

List of Figures…… viii-x

List of Abbreviations…… xi-xii

Chapter 1: Introduction to Acyclic CB[n]-type Molecular Containers …… 1

1.1 Introduction …… 1

1.2 Molecular Containers …… 2

1.2.1 Examples of Molecular Containers …… 2

1.2.2 Introduction to CB[n]-type Molecular Containers ……..…… 3

1.2.3 Applications of CB[n] Containers ……..…… 5

1.2.4 Functionalization of CB[n] Containers ……..…… 8

1.3 Drug Delivery Using CB[n]-type Molecular Containers ……....…… 17

1.3.1 Technology in Drug Delivery ……...… 18

1.3.2 Cyclodextrin in Formulation Techniques ……...… 19

1.3.3 CB[n]-type Containers in Formulation Techniques ……....… 24

Chapter 2: Acyclic CB[n]-Type Molecular Containers: Effect of Solubilizing Group on their Function as Solubilizing Excipients …….……..... 28

2.1 Introduction ……...… 28

2.2 Results and Discussion …….……..... 31

2.2.1 Design and Synthesis of Acyclic CB[n] Acyclic CB[n]-Type Receptors **II-2a – II-2h** ..…… 28

2.2.2 X-ray Crystal Structures of Hosts **II-2b**, **II-2f**, and **II-2h** that differ in the charge on their solubilizing groups …… 33

2.2.3 Hosts **II-2a**, **II-2f**, and **II-2h** Do Not Undergo Self-Association …… 36
2.2.4 Binding Studies Between Acyclic CB[n]-Type Receptors and
Guests **II-4** – **II-8**……..... 37
2.3 Conclusions……..... 52
2.4 Experimental Section……..... 53
2.5 Supporting Information……..... 54

Chapter 3. Acyclic Cucurbit[n]uril-Type Molecular Containers: Influence of
Aromatic Walls on their Function as Solubilizing Excipients for Insoluble Drugs …… 127
3.1 Introduction……..... 127
3.2 Results and Discussion……... 127
3.2.1 Design and Synthesis of Acyclic CB[n]-Type Containers
III-1a – **III-1e** ……..……..……... 128
3.2.2 Solubility Properties of the Acyclic CB[n] Type Containers
III-1a – **III-1e** ……..……..……..……. 129
3.2.3 Self-Association Properties of Acyclic CB[n] Type Containers
III-1a – **III-1e** ……....……..……..……..…… 130
3.2.4 Theoretical Treatment of Phase Solubility Diagrams …….. 131
3.2.5 Use of **III-1a** – **III-1e** as Solubilizing Agents for Insoluble Drugs …….. 134
3.2.6 Comparison of the Binding Affinity of **III-1a** – **III-1e** with
HP-β-CD Toward Insoluble Drugs …… 143
3.3 Conclusions…… 144
3.4 Experimental Section…….. 144
3.5 Supporting Information……... 149
Bibliography…….. 243

List of Tables

Chapter 2

Table II-1. Binding Constants (K_a, M^{-1}) obtained for the interaction between host **II-2a** – **II-2f** with various guests..…… 45

Table II-2. pK_a values and binding constants (K_a) obtained for compound **II-7** with host **II-2a**, **II-2h** and **II-2f** ……...……..……..…… 48

Chapter 3

Table III-1. Inherent solubility (S_0) of selected drugs and values of slope calculated from the linear region of the PSDs for containers **III-1a** – **III-1e** and HP- β-CD with drugs **III-8** – **III-26** …….…….…….…….…….……. 134

List of Schemes

Chapter 2

Scheme II-1. Synthesis of Acyclic CB[n] solubilizing excipients **II-2a** – **II-2h**. …… 32

Chapter 3

Scheme III-1. Structures of known acyclic CB[n] solubilizing excipients **III-1b** and **III-1c** and synthesis of **III-1d** and **III-1e.** …… 129

List of Figures

Chapter 1

Figure I-1. Synthesis and structure of CB[*n*]……. 3
Figure I-2. Structure of *ns*-CB[6]. …… 4
Figure I-3. Structure of bis-*ns*-CB[10]. ……..…….. 4
Figure I-4. Chemically controlled molecular machine. …… 5
Figure I-5. Supramolecular cross-linked networks based on CB[8] ternary complex … 6
Figure I-6. CB[7] can be used to regulate enzyme activity …… 7
Figure I-7. Oxidation of CB[5] – CB[8] ……..…….. 9
Figure I-8. Supramolecular velcro based on CB[7]- and Fc- modified surfaces ……. 10
Figure I-9. Synthesis of glycoluril hexamer …… 11
Figure I-10. Synthesis of monofunctionalized CB[6]…… 12
Figure I-11. Synthesis of monofunctionalized CB[7] ……. 12
Figure I-12. Self-assembly of monofunctionalized CB[7] ……... 13
Figure I-13. Synthesis of an elongated CB[6] analogue ……. 14
Figure I-14. Synthesis of acyclic CB[n] congeners ……. 15
Figure I-15. Synthesis of highly soluble acyclic CB[n]-type container …… 16
Figure I-16. Biopharmaceutics Classification System (BSC) for active pharmaceutical ingredients (APIs) …… 18
Figure I-17. Supramolecular containers as drug delivery vehicles. …….. 19
Figure I-18. Cyclodextrin family …….. 20
Figure I-19. Phase diagram showing different solubility behaviors …….. 21
Figure I-20. Compounds for drug solubility enhancement with cyclodextrin derivatives …….. 22
Figure I-21. Cyclodextrin increases stability of drugs …….. 23
Figure I-22. Structure of monofunctionalized biotin-CB[7] encapsulating oxaliplatin for targeted delivery …….. 25
Figure I-23. Solubility enhancement for water-insoluble host with acyclic CB[n]-type containers …….. 26

Chapter 2

Figure II-1. Structures of molecular containers used previously as solubilizing agents for insoluble drugs: HP- β-CD**,** Captisol^{TM}, CB[n], and acyclic CB[n]-type container ……. 30

Figure II-2. Cross-eyed stereoviews of the X-ray crystal structures of: a) **II-2b**, b) **II-2f**, and c&d) two different conformations of **II-2h** in the crystal …… 36

Figure II-3. Chemical structures of guests used in this study …… 37

Figure II-4. ^{1}H NMR recorded (400 MHz, RT, 20 mM sodium phosphate buffered D_2O, pH 7.4) for: a) **II-6**, b) an equimolar mixture of **II-2f** (positive host) and **II-6**, (c) and equimolar mixture of **II-2h** (neutral host) and **II-6**, and (d) and equimolar mixture of **II-2a** (negative host) and **II-6**.) …… 39

Figure II-5. (a) UV/vis spectra obtained during the titration of a fixed concentration of **II-4** (10.0 μM) with **II-2a** (0 – 0.45 mM) and (b) plot of absorbance versus [**II-2a**] used to determine the K_a value of the **II-2a•II-4** complex by nonlinear least-square fitting ……..…… 41

Figure II-6. Plot of absorbance change (%) versus pH to determine the pK_a values of 6-aminocoumarin ..……..…… 47

Figure II-7. Chemical structures of water-insoluble drugs used in this study..…… 50

Figure II-8. Phase solubility diagrams constructed using solutions of hosts **II-2a**, **II-2h** and **II-2f** of known concentrations and an excess of solid drug: a) tamoxifen, b) 17α-ethynylestradiol, and c) indomethacin. ..…… 51

Chapter 3

Figure III-1 Chemical structures of drugs used in this study ……..... 131

Figure III-2. Simulations of the phase solubility behavior of hypothetical container•drug 1:1 systems that obey equation III-1. a) Plot of [Drug] versus [Container] for a system with S_0 = 1 μM and five different K_a values. B) Plot of slope of the PSD versus K_a (M^{-1}) for five different values of S_0 (1 mM, 100 μM, 10 μM, 1 μM, 100 nM)..…… 133

Figure III-3. Phase solubility diagrams constructed for mixtures of containers with selected insoluble drugs: a) Estradiol, b) PBS-1086, c) Camptothecin. Conditions: 20 mM sodium phosphate buffered D_2O (pH = 7.4, RT).……. 138

Figure III-4. MMFF minimized models of the trans-1,4-cyclohexanediammonium ion complexes of truncated versions of: a) **III-1a**, b) **III-1b**, c) **III-1c**, d) **III-1d**, e) **III-1e**. …… 139

Figure III-5. ^{1}H NMR recorded (400 MHz, RT, 20 mM sodium phosphate buffered D_2O, pH 7.4) for: a) estradiol (in DMSO-d_6), b) **III-1a** (10 mM) with estradiol, c) **III-1b** (10 mM) with estradiol, d) camptothecin (in DMSO-d_6), e) **III-1d** (15 mM) with camptothecin, and f) **III-1b** (10 mM) with camptothecin ……..... 140

List of Abbreviations

Å	angstrom
br	broad
CB[n]	cucurbit[n]uril
CH_3Cl	chloroform
CH_3CN	acetonitrile
D	diffusion coefficient
d	doublet
D_2O	deuterium oxide
CH_2Cl_2	dicholromethane
DMF	dimethylformamide
DMSO	dimethylsulfoxide
DOSY	diffusion-ordered spectroscopy
ESI-MS	electrospray ionization-mass spectrometry
EtOH	ethanol
g	gram
h	hour
HCl	hydrochloric acid
H_2SO_4	sulfuric acid
Hz	herts
K	kelvin
IR	infrared
J	coupling constant
m	multiplet
M	molar
M^+	molecular ion
MeOH	methanol
MHz	megahertz
min	minute
mM	millimolar

MMFF	Merck molecular force field
M.p.	melting point
MW	molecular weight
m/z	mass to charge ratio
NaOH	sodium hydroxide
NMR	nuclear magnetic resonance
o	*ortho*
p	*para*
ppm	parts per million
RT	room temperature
s	singlet
t	triplet
TFA	trifluoroacetic acid

Chapter 1: Introduction to Acyclic CB[n]-type Molecular Containers

1.1 Introduction

Supramolecular macrocycles has been arousing increasing interest over the past decades. Supramolecular chemistry has been defined by Jean-Marie Lehn as the "chemistry of molecular assemblies and of the intermolecular bond". Usually, these interactions involve non-covalent bonds established between the interacting species, and the majority of these interactions can be categorized as host-guest type interactions. In a host-guest type interaction, a host is usually a larger molecule with a certain kind of binding sites or cavity, and a guest is usually a smaller molecule, which can be encapsulated into the binding site or cavity of the host molecule and non-covalent bonds are formed when a host molecule and a guest molecule are combined together. The chemical nature of different host-guest systems can vary greatly from each other and there are a wide variety of host molecules, including enzymes and synthetic molecular containers. During the past decades, chemists have found large success in design, synthesis, characterizing and applications of different synthetic molecular containers, including crown ethers, cyclodextrin (CD), calixarene, and cucurbit(n)urils (CB[n]). These molecular containers may differ greatly in their physical and chemical properties like solubility and reactivity. But their recognition properties are the most interesting feature for this category of compounds. For example, CDs prefer to bind with hydrophobic compounds and CB[n]-type containers have high affinity towards cations. As a result, lots of applications have been developed based on the molecular

encapsulation principle. CDs are the most widely used class of molecular containers. Applications of molecular containers include odor elimination, drug delivery, separation techniques, and catalysis. CB[n]-type containers, as the new generation of molecular containers, are well known for their high affinity towards cationic guests, especially ammonium alkanes and are showing great potentials in applications in various fields. Nevertheless, CB[n]-type containers have some weakness to overcome before they can be used in wider applications. For example, most of CB[n] family members have limited aqueous solubility and they are difficult to functionalize.

1.2 Molecular Containers

Host-guest chemistry is often referred to as the confinement of the guest molecule inside the cavity of a supramolecular host molecule. In such situations the host molecules are also often referred to as molecular containers.

1.2.1 Examples of Molecular Containers

Crown ethers were first discovered by Charles Pedersen in 1967.[1] These cyclic polyethers were synthesized from aromatic viyinal diols. This category of compounds assumes a ring conformation and can vary greatly in terms of the ring size, ranging from 9 to 60 atoms. The presence of the oxygen atoms in the macrocycle ring provided the crown ethers with the ability to interact with different cations by ion-dipole interactions. Crown ethers with 5 to 10 oxygen atom are known to be able to form salt-polyether complex with a wide range of cations, including Li+, Na^+, NH_4^+, RNH_3^+, K^+, Rb^+, Cs^+, Ag^+, Au^+, Ca^{2+}, Sr^{2+}, Ba^{2+}, Cd^{2+},

Hg^{+}, Hg^{2+}, La^{3+}, Tl^{+}, Ce^{3+}, and Pb^{2+}. After the discovery of crown ethers, a lot of work has been done to discover new type of molecular containers with different host-guest chemistry. For example, chemists have discovered various new molecular containers including calixarenes, which are macrocycle oligomers based on hydroxyl alkylation products of phenol derivatives and aldehydes, cyclodextrins, which are macrocyclic oligomers of saccharides, and cucurbiturils (CB[n]s), which are macrocycle oligomers of glycolurils linked by methylene bridges. Among them, CB[n]-type molecular containers are of special interest to us.

1.2.2 Introduction to CB[n]-type Containers.

The synthesis of CB[n]s was first reported in 1905 by Behrend.[2] In his report, he described an insoluble polymer from the condensation reaction between glycoluril and formaldehyde in concentrated HCl. Mock, in 1981, has discovered that the compound synthesized by Behrend 75 years earlier was a macrocycle comprising six glycoluril units and linked with twelve methylene bridges.[3] This compound was named as cucurbituril since the shape of the molecule looks like a pumpkin.

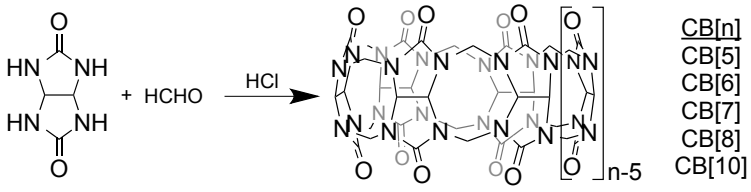

Figure I-1. Synthesis and structure of CB[*n*].

Ever since the report of CB[6], new CB[n] family members including CB[5], CB[7], CB[8] CB[10] and CB[5]•CB[10] complex have been discovered successively.[4-7] Other CB[n]

derivatives have also been identified. Inverted CB[6] has been reported in 2005[8], which is a CB[6] container with one glycoluril pointing inside the cavity. Another CB[6] analogue, *ns*-CB[6] (Figure I-2) was also reported recently.[9] It is a host with one methylene bridge missing from the CB[6] structure. It was obtained from the condensation reaction between glycoluril (1 eq.) and inadequate amount of paraformaldehyde (2 eq.). Further functionalization can be achieved by reacting this host with *o*-phthaladehyde to close up the opening between the two neighbouring un-bridged urea nitrogens.

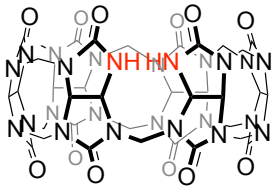

Figure I-2. Structure of *ns*-CB[6].

Besides the analogues with only a single cavity, a dual-cavity, bis-*ns*-CB[10] (Figure I-3), was also reported[10] to be able to encapsulate two guest molecules with one guest in each of its cavities. By reacting bis-*ns*-CB[10] with paraformaldehyde and imidazolidone under acid conditions, the two open cavities can be clipped by the imidazolidone units. With this clipping mechanism, a [3]rotaxane was synthesized based on the encapsulation of 1,6-hexanediamine derivatives in bis-*ns*-CB[10] followed by clipping with imidazolidone.[11]

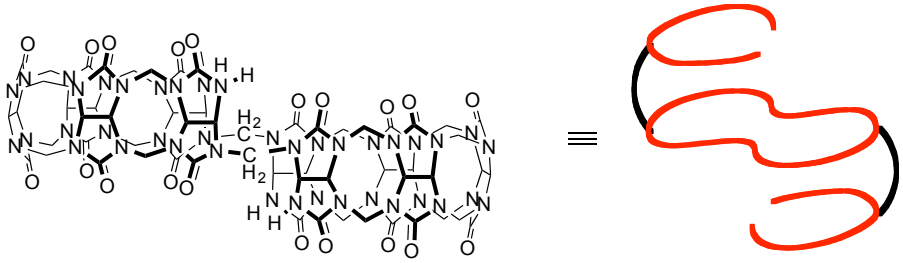

Figure I-3. Structure of bis-*ns*-CB[10].

The different CB[n] homologues contain different numbers of glycoluril unites and have different cavity sizes. Due to the difference in the size of the cavities, different CB[n] containers also have different binding properties towards different guest molecules.

1.2.3 Applications of CB[n]-type Containers.

CB[n] type containers are well known to bind selectively with cationic gusts with high binding affinities, especially alkane diammoniums. Based on their outstanding recognition properties, a lot of applications have been developed for CB[n]-type containers.

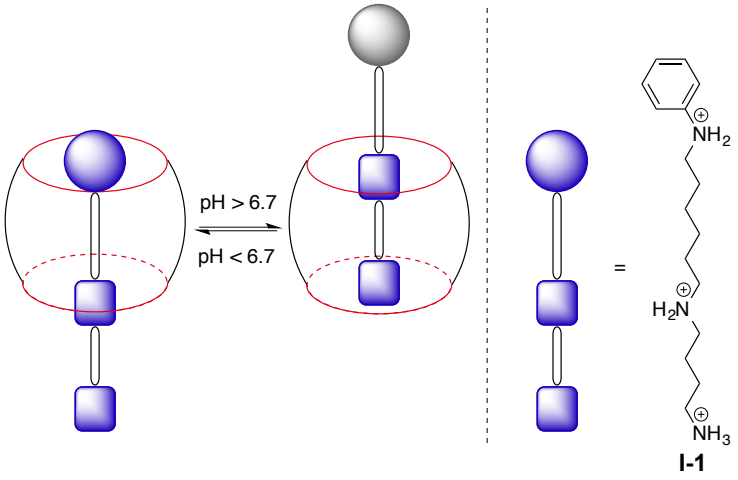

Figure I-4. Chemcially controlled molecular machine.

Molecular machines formed by self-assembly processes have aroused great interest and CB[n]s have shown great potential in this area. By providing chemical, electrochemical, or photochemical stimuli, the binding affinity of CB[n]s towards different guests can be manipulated easily and the host•guest system can be switched between different binding states.[12-15]

For example, Mock developed a pH-dependent molecular switch in 1990.[13] In his study, a pseudo-rotaxane system was formed with CB[6] and triamine **I-1** (Figure I-4), and the switch was controlled by the protonation of the aniline moiety. CB[6] tended to bind with hexanediammonium moiety when the pH is lower than the pK_a of the anilinium group. When the pH is higher than 6.7, the aniline nitrogen atom was deprotonated which decreased the affinity of CB[6] towards hexanediammonium moiety and CB[6] shifted to the butanediammonium moiety. In this way, CB[6] is able to shuttle along the guest, triamine, by changing the pH value.

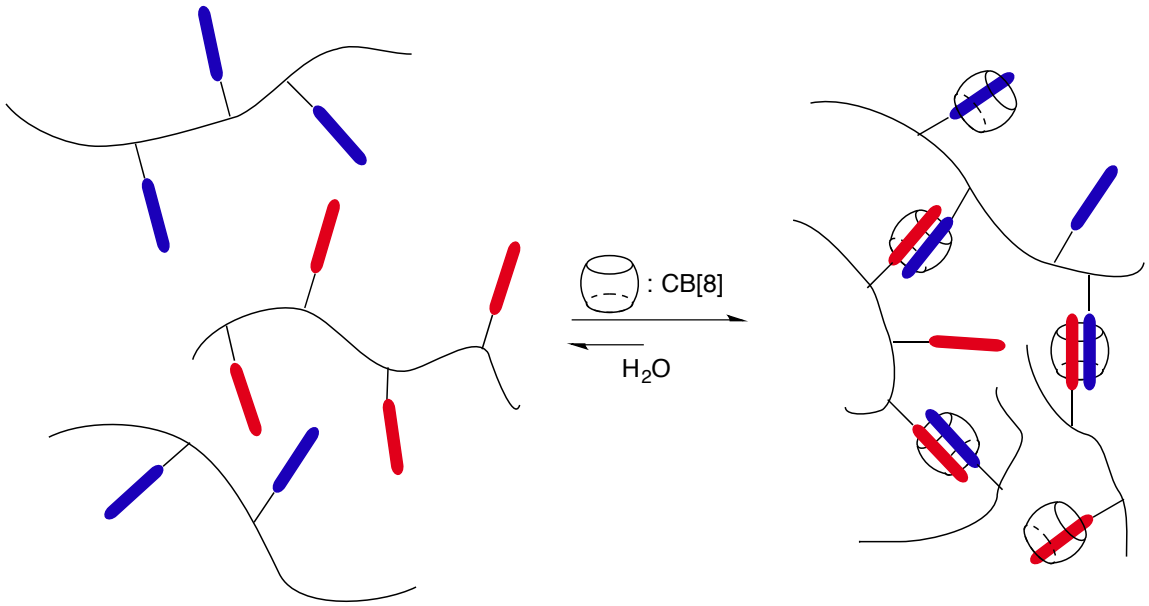

Figure I-5. Supramolecular cross-linked networks based on CB[8] ternary complex.

Besides using the stimuli-responsive CB[n] complex to make molecular machines, chemist can also use the recognition properties of CB[n] complexes to build up other complicated supramolecular architectures. Due to relatively large cavity size, CB[8] is known to be able to encapsulate two guest molecules and form a ternary complex.[16,17,18] Various applications

have utilized this recognition property of CB[8] to build self-assembled supramolecular polymers, networks, and vesicles. For example, Scherman in 2010 has reported the supramolecular cross-linked network via CB[8] complexes (Figure I-5).[19] In his report, two different polymers were prepared bearing different side-chains: viologen groups or naphthoxy groups. These two polymers do not cross-link with each other in aqueous solutions. However, since methylviologen and hydroxynaphthalene will form a strong three-component complex with CB[8] through a two-steps process (methylviologen is the first guest, and hydroxynaphthalene is the second guest), the polymer scaffold will be cross-linked by the two different pendants upon the addition of CB[8] and a porous hydrogel was obtained. This hydrogel showed thermal reversibility and subsequent facile modulation of microstructure upon futher addition of CB[8] and thermal treatment.

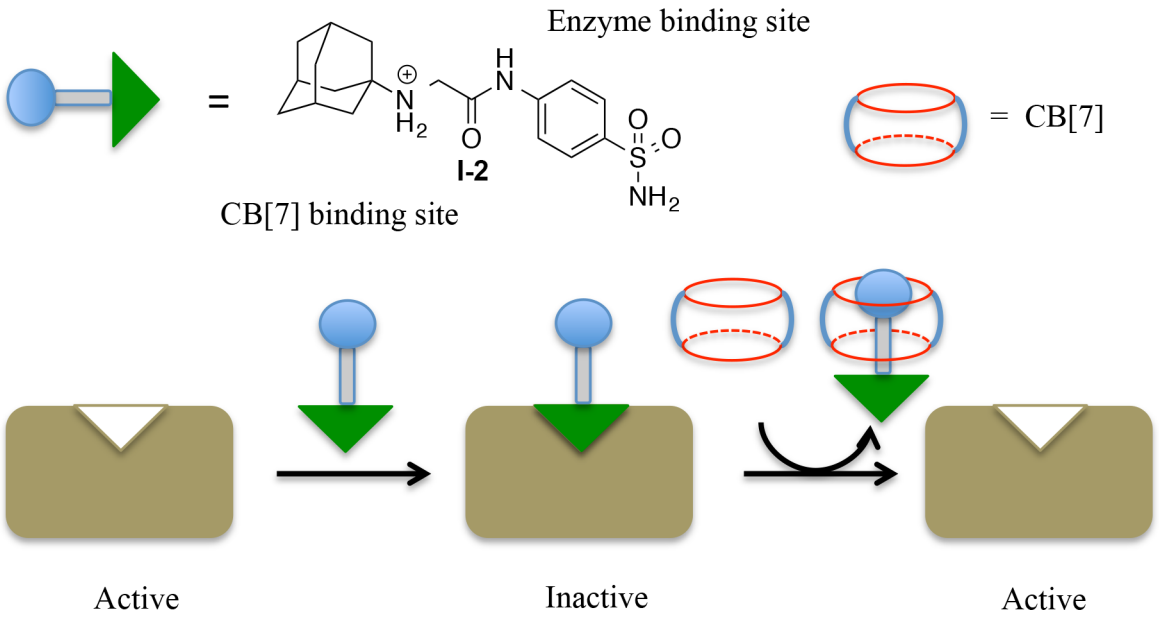

Figure I-6. CB[7] can be used to regulate enzyme activity.

Applying host-guest systems in biochemistry and medicinal chemistry have

always been an interesting topic, and CB[n] compounds are of great potential in this area. With a careful designed system, the features of CB[n] host-guest systems like high selectivity and low toxicity can be fully taken advantage of. One good example is from the Isaacs' group, where CB[7] was successfully used to regulate the catalytic activity of bovine carbonic anhydrase (BCA) (Figure I-6).[20] In this study, a special inhibitor of BCA, compound **I-2**, was synthesized. Compound **I-2** contains a benzenesulfonamide unit which binds to the Zn co-factor of BCA, and an adamantylammonium unit which is the preferred guest for CB[7] ($K_a \approx 10^{12}$ M^{-1}). The addition of the compound **I-2** turns off the catalytic activity of BCA due to the formation of a stable complex BAC• **I-2** ($K_a = 2.7 \times 10^{7}$ M^{-1}). It was observed that the catalytically activity of BCA was then recovered after the addition of CB[7] as the result of the formation of a more stable complex CB[7]• **I-2** sequestering the inhibitor **I-2** from BCA.

1.2.4 Functionalization of CB[n] Containers

Despite all the advantages and outstanding properties regular CB[n]-type containers still have their weaknesses, including limited solubility in water, rigid skeleton and challenge to modify internal or external molecular surface of the CB[*n*] molecules. Over the past years, numerous analogues and derivatives of CB[n]-type containers prepared in order to overcome these weaknesses. The goal of these research projects was to manipulate the shape and size of the binding cavities of CB[n] molecules to alter their binding properties or directly introducing different functional groups to the host molecule so that eventually the applications of CB[n]-type containers can be expanded.

One of the pathway is to utilize the formation reaction of CB[n] molecules and use substituted glycoluril derivatives to derivatize CB[n] compounds. The first example was reported in 1992 by Stoddart and co-workers. They reported the first characterized CB[*n*] derivative with the synthesis of Me_{10}CB[5] from dimethylglycoluril and formaldehyde under acidic conditions.[21]

Another important way to functionalized CB[n] molecules was discovered by Kim in 2003 (Figure I-7). They reported the direct oxidation reactions using $K_2S_2O_8$ to obtain derivatives of CB[5] – CB[8].[22,23] From the reaction between CB[n] molecules and $K_2S_2O_8$ in water, perhydroxylated compound $(HO)_{2n}$CB[n] were obtained and could be subsequently derivatized. For example, $(HO)_{2n}$CB[*n*] can be alkylated by treatment with allyl bromide to yield CB[6] with 12 allylic groups on the surface ($(CH_2{=}CHCH_2O)_{12}$CB[6]).

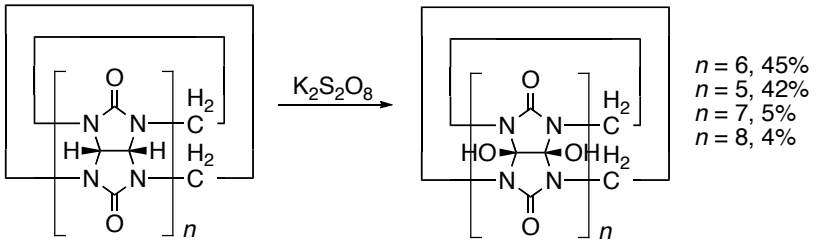

Figure I-7. Oxidation of CB[5] – CB[8].

The oxidation reaction has become an important pathway for functionalization of CB[n]s and various applications of functionalized CB[n] containers has been developed based on this method. By reacting the $(CH_2{=}CHCH_2O)_{12}$CB[6] with pentanethiol through photochemical reactions, CB[6] containers were anchored onto a glass surface granting the glass surface the ability to bind to fluorescent guests.[22] Similarly, allylated CB[7] can be obtained

through the same pathway and Kim and co-workers have anchored modified CB[7] onto gold surface.[24] Then glucose oxidase (GOx) was used as a model protein and decorated with ferrocenemethylammonium ions. Through the non-covalent interactions between CB[7] and ferrocenemethylammonium ions, the protein was attached on the gold solid surface, and hence they obtained a biosensor for glucose concentrations via supramolecular host•guest systems.

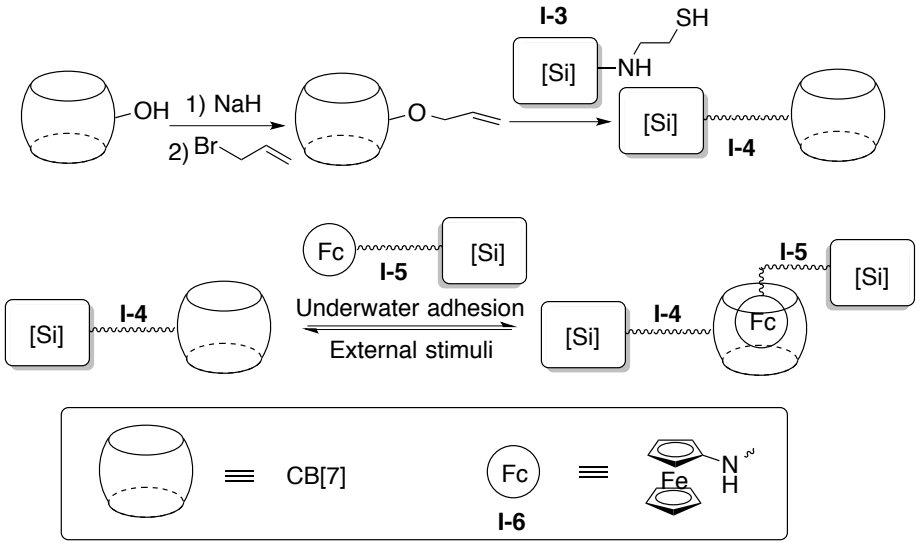

Figure I-8. Supramolecular velcro based on CB[7]- and Fc- modified surfaces.

Recently, Kim and co-workers have attached mono allylated CB[7] to a thiol poly ethylene imine (PEI) functionalized silica surface (Figure I-8).[25] The surface (PEISH-[Si], **I-3**) was obtained by reacting ethylene sulfide with PEI decorated silica surface (PEI-[Si]). It was then reacted with alkene-functionalized monoallyloxy-CB[7] to yield CB[7]-[Si] (**I-4**). Similarly, aminomethylferrocene (Fc , **I-6**) decorated silica surface (FC-[Si], **I-5**) was also obtained. Fc moieties are known to bind very tightly with CB[7] in water ($K_a \approx 10^{12}$ M^{-1}), which made the

FC-[Si] (**I-5**) and CB[7]-[Si] (**I-4**) ideal for under water adhesion applications. Like commercial velcro, these two functionalized surfaces hook up with each other with great strength in aqueous environment (maximum lap shear strength of the supramolecular velcro was 1.12 MPa). Moreover, the adhesion can be reversed when Fc was oxidized to Fc^+, since the affinity of CB[7] towards Fc^+ is much weaker.

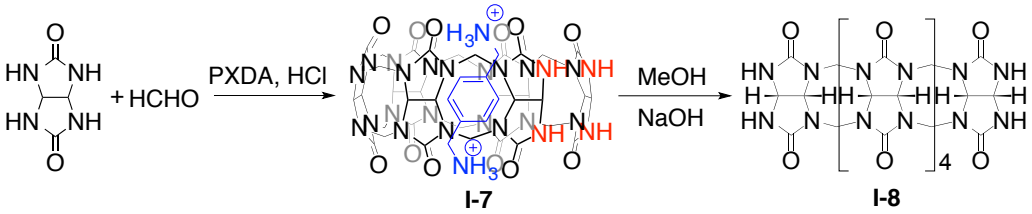

Figure I-9. Synthesis of glycoluril hexamer**.**

In order to obtain mono-functionalized CB[n] containers, the Isaacs' group has discovered the synthetic route to make glycoruil hexamer (**I-8**).[26,27,28] As has been reported, in CB[n] forming reactions, glycoluril oligomers linked by methylene bridges will form first. Once the oligomer chain has grown to a certain length, for example, hexamers, the cyclization will happen to the give the corresponding cyclic CB[n]. Once the oligomer is cyclized, the reaction becomes irreversible. In 2011, the isaacs group reported the template synthesis of glycoluril oligomers[28], where *p*-xylenediammoiun salt was used as the template molecule. Due to the flexible nature of the oligomers before cyclization, the guest molecule can expand the cavity of the host, separating the two unbridged glycoluril units, and prevent the NH tips (Figure I-9, atoms shown in red) from cyclizing into CB[6]. This compound is a very important building block for mono-functionalized CB[n]s.

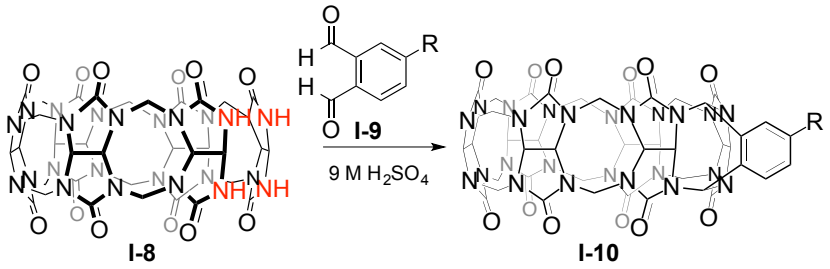

Figure I-10. Synthesis of monofunctionalized CB[6].

With The new glycoluril hexamer building block available, Isaacs and co-workers have synthesized a series of monofunctionalized CB[6] derivatives using the condensation reaction between the free ureidyl nitrogens and *o*-phthaladehyde derivative **I-9** (Figure I-10).[27,29] This derivative have a very similar cavity with CB[6] but can be easily functionalized on the aromatic ring. CB[6] derivatives **I-10** made through this synthetic route has been applied in various fields including fluorescent sensor[27,30], where the aromatic ring is a naphthalene ring, and self-assemble daisy chain[29], where R group in Figure I-9 is a hydroxy group and was then further transferred into a isopropylamine group.

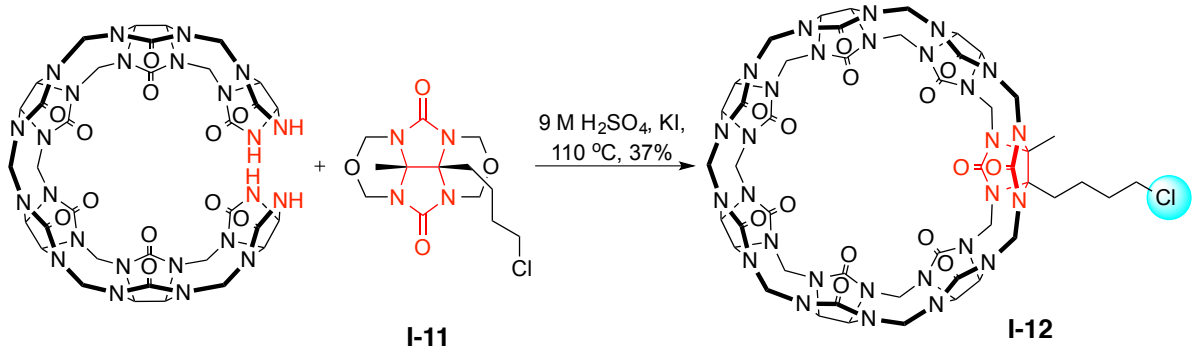

Figure I-11. Synthesis of monofunctionalized CB[7].

Besides monofunctionalized CB[6] derivatives, glycoluril hexamer is also a very ideal

building block for CB[7] derivatives, which is even more interesting due to the relatively larger cavity size and higher solubility compared with CB[6] derivatives. Instead of condensing glycoluril hexamers with *o*-phthaladehyde derivatives, a functionalized glycoluril was used in the condensation reaction with glycoluril hexamers.[31] Figure I-11 shows the example of monofunctionalized CB[7] with a chloride on the posterior. The chloride was then turned into an azide group and other functional groups can be attached to the host with click reactions.

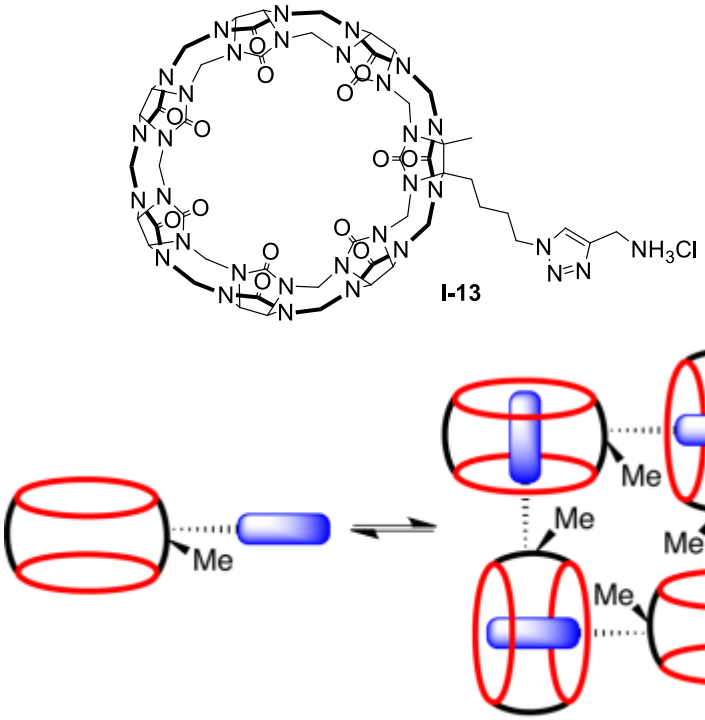

Figure I-12. Self-assembly of monofunctionalized CB[7].

In 2012, Isaacs and co-workers have reported the CB[7] derivative by attaching a primary amine moiety to the CB[7] host with click chemistry (Figure I-12).[31] The attached alkyl amine moiety is a good binding site for CB[7] and the CB[7] derivative undergoes a self-assembly process to give the supramolecular cyclic tetramer.

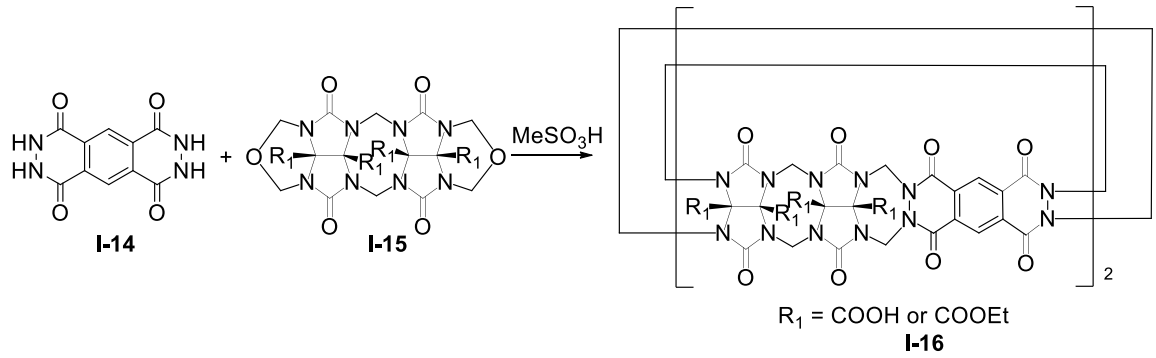

Figure I-13. Synthesis of an elongated CB[6].analogue.

Thanks to all the methods mentioned above, the CB[n] family has been greatly expanded and more functional CB[n] type container derivatives have been discovered and applied in various fields. In order to expand the CB[n] family to even a larger range with more desirable properties, like higher aqueous solubility, different cavity size, or more flexible backbones, researchers have synthesized more CB[n] analogues based on the understanding of the step-wise mechanism of CB[n] formation reactions. Isaacs and co-workers have synthesized compound **I-16** in high yield (Figure I-13) from the condensation reaction between compound **I-14** and a building block glycoluril dimer **I-15**.[32] It was discovered that in the formation reaction of CB[n]s, phthalhydrazides serve as nucleophilic glycoluril surrogates. And based on this mechanism, compound **I-14** and glycoluril dimer **I-15** should be able to cyclize and give cyclic CB[n] analogues **I-16**. As expected, a CB[6] analogues was obtained with electrochemically, UV/Vis and fluorescent active aromatic "walls". Moreover, the introduction of the aromatic walls has elongated the shapes of the containers (5.9 × 11.2 × 6.9 Å when R is COOEt) compared with the original circular CB[n] container and the solubility of the containers in organic or aqueous solvents can also be

modified depending on the substituent R groups.

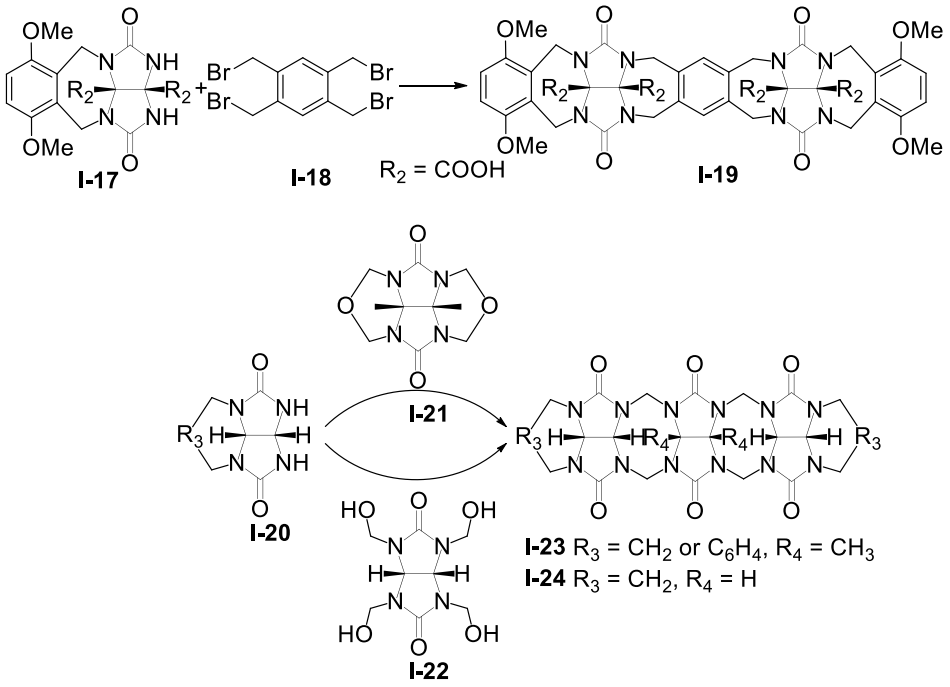

Figure I-14. Synthesis of acyclic CB[n] congeners.

Recently, a lot of attention has also been focused on the synthesis of acyclic CB[n]-type containers which turns out to be an ideal pathway for functionalization CB[n] molecules. Many years ago, the Isaacs group reported the synthesis of an acyclic CB[n] congener **I-19**[33] with alternating glycoluril and aromatic units from the S_N2 reaction between functionalized glycoruil **I-17** and aromatic wall **I-18** (Figure I-14). The congener would preorganize into an a,a,a,a-conformation amd binds to positive charged guests tightly although relatively weaker than cyclic CB[n] (K_a is 10^4 M^{-1} towards hexanediamine, compared to 10^6 M^{-1} for CB[6]). Sindelar also reported the discovery of glycoluril trimer **I-23** and **I-24** from the condensation reaction of glycoluril derivative **I-20** with glycoluril bisether **I-21** or tetrakis hydroxyl methyl glycoluril **I-22** (Figure I-14).[34] The products has retained some of the recognition properties of CB[n] containers towards positive guests (for bispyridinium ethylene, $K_a = 8.4 \times 10^4$ M^{-}

[1], and for methylviologen $K_a = 7.5 \times 10^4\ M^{-1}$).

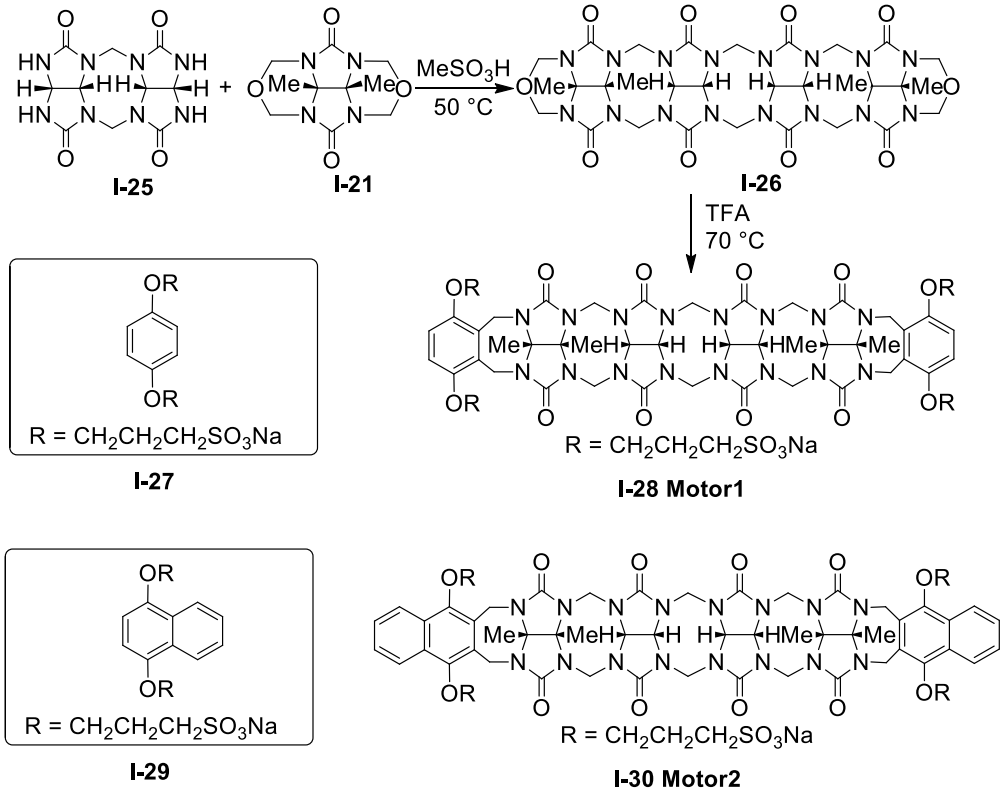

Figure I-15. Synthesis of highly soluble acyclic CB[n]-type container

Another very important category of acyclic CB[n] analogues was discovered in 2010 by Isaacs' group.[35] In this study, a glycoluril tetramer building block **I-26** was synthesized first through a step-wise synthetic route and was then reacted with two equivalents of sulfonated hydroquinone derivative **I-27** to yield acyclic CB[n] congener **I-28** (Figure I-15) in high yield. Similarly, by using a naphthalene derivative **I-29** instead of **I-27** as the aromatic wall, another acyclic container **I-30** was obtained. The two acyclic congeners possess excellent binding properties toward typical positive guests for cyclic CB[n]'s. There are several reasons for this: 1) the acyclic host molecule contains four glycoluril units which can provide sufficient ion-dipole and H-bond interactions at the uriedyl carbonyl portal on both ends of

the host; 2) the container assumes a C-shape conformation due to the glycoluril tetramer backbone which creates a hydrophobic cavity for the binding of hydrophobic compounds; 3) introduction of aromatic side walls will boost the π–π interaction with species with aromatic systems. More importantly, due the four sulfonate groups attached to the aromatic wall, the aqueous solubility of the hosts have been dramatically enhance (346 mM in water for **I-16**) compare with cyclic CB[n]s. These two leading compounds (XX and XX) have been proven of profound importance in various applications, and one of their most successful applications is to be used as drug delivery vehicles.

1.3. Drug delivery Using CB[n]-type Molecular Containers.

One core issue in pharmaceutical industry is the formulation of active pharmaceutical ingredients (APIs).[36,37] There have been increasing numbers of newly discovered drug candidates with promising therapeutic effects in recent years. However, according to the Biopharmaceutics Classification System (BSC), about 40 – 70% of them belong to the Class II with low solubility but high intestinal permeability (Figure I-16).[38] To revive those drug candidates with poor aqueous solubility, there is an urgent need for the development of new formulation tools

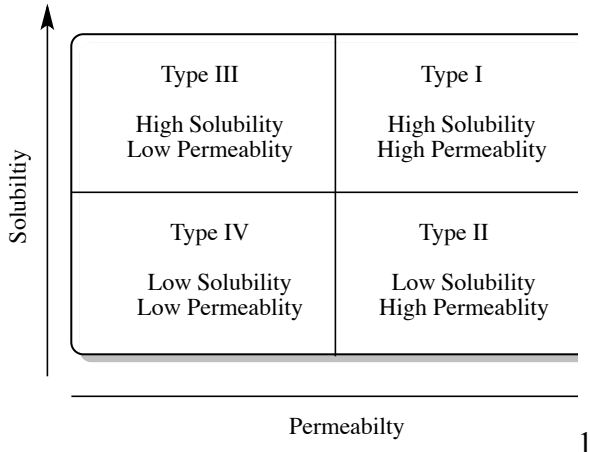

Figure I-16. Biopharmaceutics Classification System (BSC) for active pharmaceutical ingredients (APIs)

Various formulation methods are known and they can mainly be divided into two categories: 1) increasing the rate of dissolution (kinetic solubility) and 2) increasing the solubility at equilibrium. The first category includes methods based on kinetically stabilizing the API at a higher free energy form which dissolve faster and initially reaches a higher concentration compared with the lower free energy form of the API, but eventually, the API will be transformed in the most stable low free energy form, which is why APIs formulated with these methods have problems in storage. Methods including preparation of nanocrystal or solid dipersions of the API fall into this category.[39,40] The other way is to increase solubility at equilibrium which includes methods like preparation of highly soluble pro-drugs, formation of salts, encapsulation into soluble drug delivery vehicles.[41-45] Among those different methods, using supramolecular containers as drug delivery vehicles is of special interest to us.

1.3.1 Molecular Container Technology in Drug Delivery.

A variety of water-soluble containers including calix[n]arenes, cyclodextrins, and cucurbit[n]urils (Figure I-17) are known to have the ability to encapsulate smaller molecules. Theoretically, they will be able to form water-soluble host•guest complexes with appropriate APIs, and hence increase the solubility of those drug candidates.

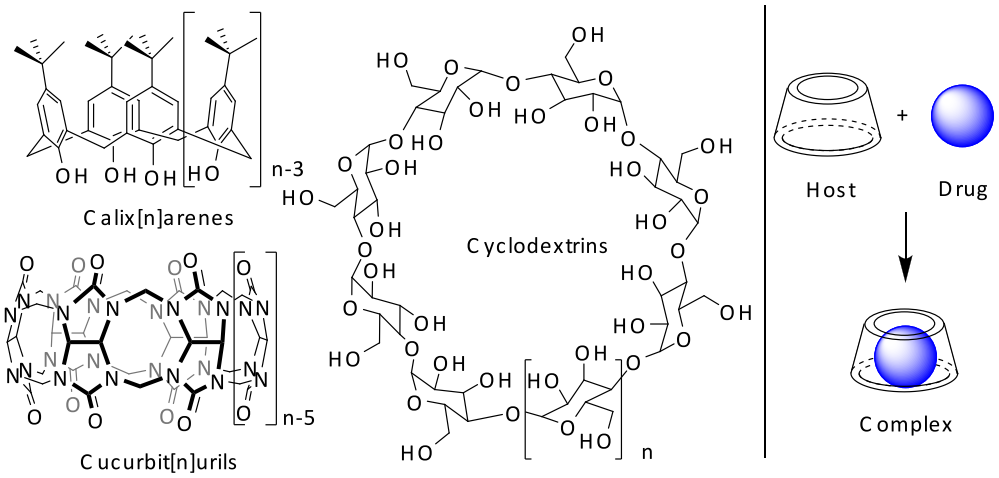

Figure I-17. Supramolecular containers as drug delivery vehicles.

1.3.2 Cyclodextrins in Formulation Techniques

Cyclodextrin was first discovered in 1891 by Villiers[46], and it mainly comprises a family of three members and other derivatives. These three major cyclodextrins are crystalline, homogeneous, non-hygroscopic substances, which are torus-like macro-rings built up from glucopyranose units. The α-cyclodextrin comprises six glucopyranose units, β-CD comprises seven such units, and γ-CD comprises eight such units (Figure I-18). The shape of cyclodextrin is also displayed in Figure I-17. It has a hydrophobic cavity and hydrophilic portals and outer walls.[47,48,49]

Cyclodextrins (CD) have been one of the most widely used supramolecular containers in drug delivery systems. They have achieved generally regarded as safe status by FDA and have been applied as solubilizing agents for different drugs. The recognition properties of cyclodextrins make them suitable for drug delivery systmes: cyclodextrins have relatively low selectivity and affinity towards most of their guests (lower than 10^4 M^{-1}), and they also

have fast kinetics for the association and dissociation process.[45,50,51] These properties make cyclodextrins able to encapsulate a wide range of different guests, increase their solubility to the desired level and release them rapidly upon dilution.

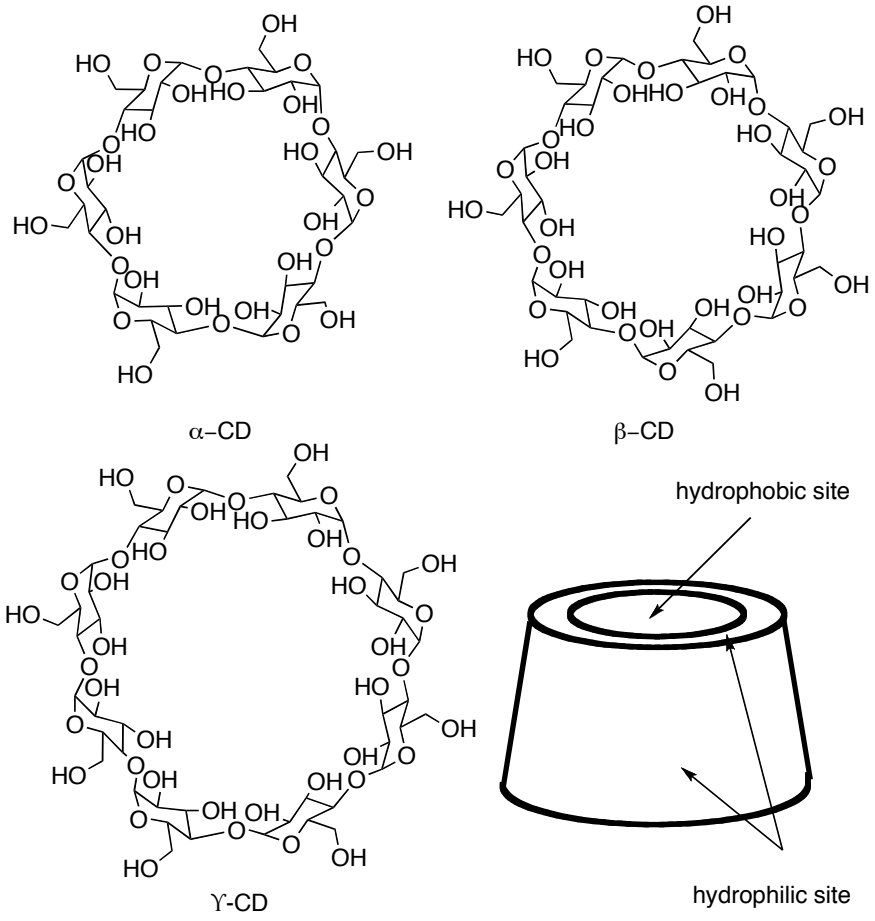

Figure I-18. Cyclodextrin family.

Numerous experiments have been done to improve aqueous solubility of drug candidates using cyclodextrins as the solubilzing agent. To evalutate the efficiency of solubility enhancement that can be achieved with a given container requires the creation of a phase-solublity diagram. It was first proposed by Higuchi and Connors[52,53], and is a plot of the total concentration of the solubilized drug candidate versus the concentration of the solubilizing agent. There a two basic types of phase solubility diagrams: type A and type B

(Figure I-19).

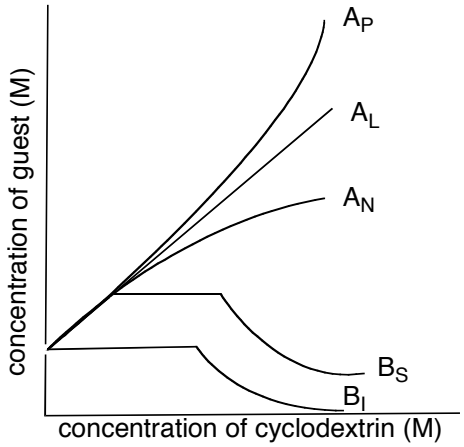

Figure I-19. Phase diagram showing different solubility behaviors.

Type A indicates a highly soluble complex is formed with cyclodextrin, and can be further divided in to A_p, A_L, and A_N type. A_L type plots correspond to 1:1 binding while A_p and A_n plots usually indicates different binding modes. A_n plots are sometimes due to the limited solubility of the host•drug complex or the self-association of the host. The slope of the A_L type plots or the slope of the linear region of A_p and A_n plots can be used to calculate the value of K_a using the equation I-1 shown below where S_0 is the intrinsic solubility of the drug.

$$K_a = \frac{\text{slope}}{S_0\,(1\text{-slope})} \qquad \text{(I-1)}$$

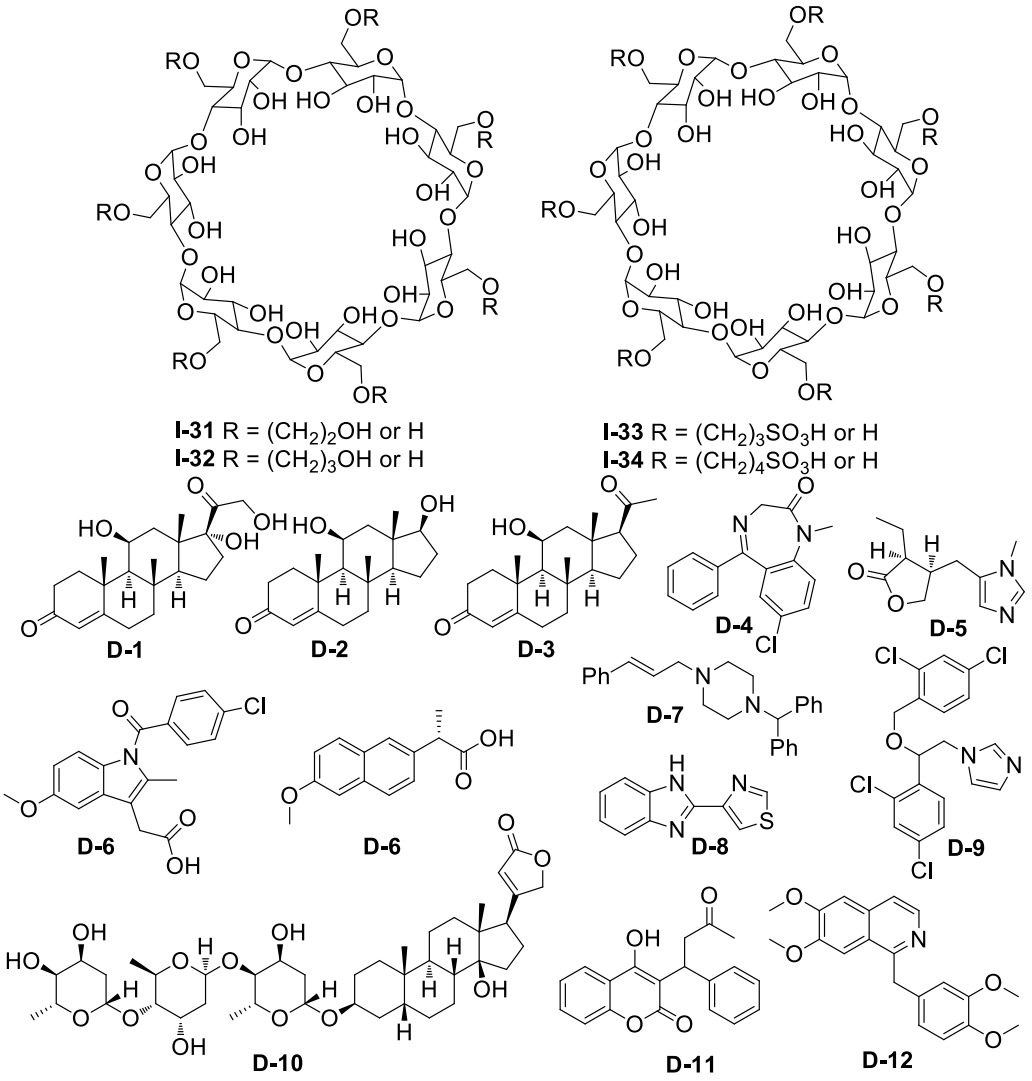

Figure I-20. Compounds for drug solubility enhancement with cyclodextrin derivatives.

In order to better perform in the solubility enhancement, functionalized cyclodextrin derivatives have been made. Among them, hydroxyalkylated *β*-CDs (**I-31** and **I-32**), and sulfonated *β*-CDs (**I-33** and **I-34**) have been proven to be of great importance.[54] Compared to their parent *β*-CD, whose low intrinsic solubility has limited their effectiveness in solubility enhancement, these functionalized *β*-CDs poccess the A_L-type diagram pattern with the guest solubility increasing linearly up to 10% (w/v) concentration of the hosts. Müller and Brauns have reported that the hydroxyalkylated *β*- CDs (**I-31** and **I-32**) with different numbers

of substitutions were efficient in solubilizing several water-insoluble drug (Figure I-20) like hydrocortisone (**D-1**), diazepam (**D-4**), indomethacin (**D-6**), and digitoxin (**D-10**).[55] The sulfonated *β*-CDs (**I-33** and **I-34**) is another important solubilizing agent, where the sulfonate group is introduced to improve the intrinsic solubility. However, it was discovered that an alkyl linker was needed to separate the charges on the sulfonate groups form the CD cavity, which explained why the sulfobutyl-*β*-CD (**I-34**) has better affinity that sulfopropyl-*β*-CD (**I-33**). Also, a variety of water-insoluble drugs including testosterone (**D-2**), progesterone (**D-3**), pilocarpine (**D-5**), naproxen (**D-7**), cinnarizine (**D-8**), indomethcin, thiabendazole (**D-9**), miconazole (**D-11**), warfarin (**D-12**), and papaverin (**D-13**), have been successfully solubilized by sulfobutyl-*β*-CD (**I-34**) (Figure I-20).[56,57,58]

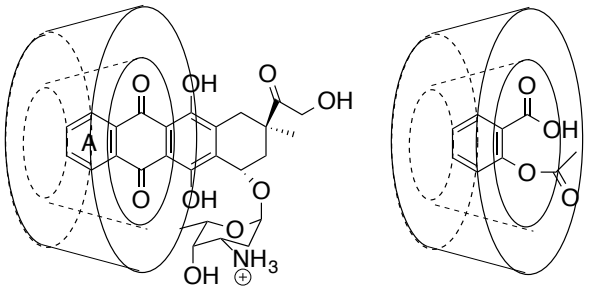

Figure I-21. Cyclodextrin increases stability of drugs.

Besides the increase of solubility, the encapsulation of the drug molecules into the cyclodextrin cavity can also increase the stability.[59] Once the drug molecule is encapsulated, the cyclodextrins can act as a shield, at least partially, to protect the drug molecule form other reactive compounds or restrain the conformation the molecule. Lots of hydrolysis, oxidation, isomerization and rearrangement can be prevented in this way. For example, doxorubicin (Figure I-21) is known to be unstable in water and undergoes acid-catalyzed

hydrolysis, cleavage of the 9-hydroxymethyl ketone moiety followed by A-ring aromatization, and photodecomposition.[60,61] When forming a supramolecular complex with γ-cyclodextrin, the A-ring of the doxorubicin was shielded by the cyclodextrin cavity and greatly slow down the decomposition the drug molecule. Also, the hydrolysis of Aspirin (acetylsalicyclic acid) under acid conditions can be slowed down by 4 – 6 time at the presence of β-cyclodextrin. This can be explained by the fact that when forming a stable complex, benzene ring of the drug molecule stays inside the cyclodextrin cavity and the steric hindrance results in a decrease in the rate of hydrolysis.[62]

1.3.2 CB[n]-type Containers in Formulation Techniques

Considering the outstanding properties of cucurbit[n]urils, potential successes may be achieved in drug delivery systems. CB[n]-type containers have been well known for their outstanding affinities, selectivity and stimuli responsiveness for positive charged guests, especially alkylammoniums (up to 10^{15} M^{-1}), which makes CB[n]-type containers a suitable vehicles for those drug candidates with solubility problems.[63-68] Lots of work has been done to explore the application of CB[n]-type containers as drug delivery vehicles. Kim and co-workers has reported the self-assembled hollow nanocapsules (diameter 190 nm) of CB[6] derivatives[69] as delivery vehicles for drugs like doxorubicin. The nanocapsule can also be decorated noncovalently with targeting ligands like folate groups to achieve targeting effects.

CB[7] and its derivatives are more interesting in this area due to its relatively higher solublity (~ 20 mM) and larger cavity size. The low toxicity has been proved by Anthony Day's group

and Isaacs-Briken team.[70] Day's group have done *in vitro* cytotoxicity study of CB[7] and CB[8] as well as *in vivo* oral and IV administration in mice.[71] The biocompatibility of CB[7] and CB[5] was tested on HepG2 and HEK293 cells by Isaacs-Briken team. There are several reports on the encapsulation of drug molecules with CB[7] to ether increase the solubility or protect the drug molecule.[72-78] For example, Kim have reported the formation of CB[7] with an anticancer agent: oxaliplatin, and it was discovered that encapsulation can increase the stability of the drug.[72]

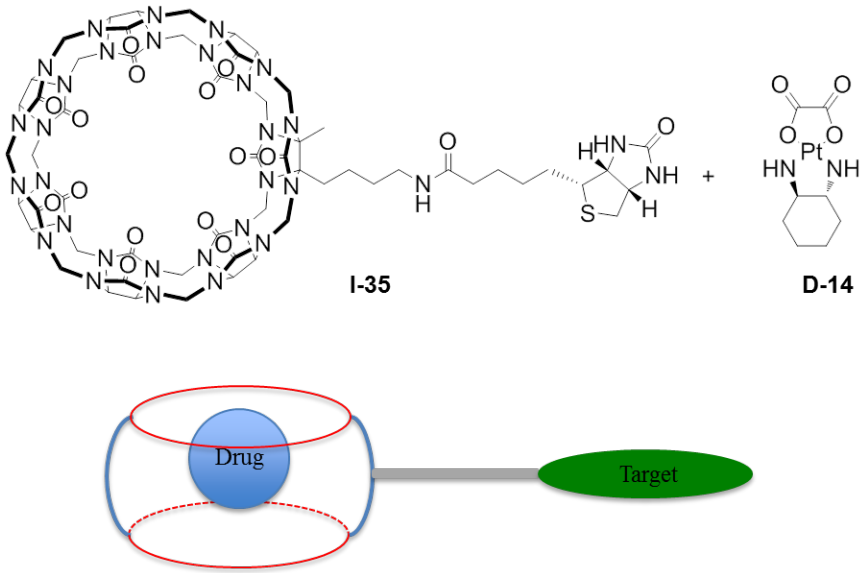

Figure I-22. Structure of monofunctionalized biotin-CB[7] encapsulatiing oxaliplatin for targeted delivery.

Besides simply encapsulating drug molecules and enhancing solubility or stability, more complicated goals can be achieved with functionalized CB[7] derivatives, liking targeting effects, which has been widely explored recently and may greatly enhance the therapeutic effects and reduce side effects. The Isaacs-Briken group have proposed a monofunctionalized biotin-CB[7] host **I-35** (Figure I-22) for the targeted delivery of different

drug molecules.[79] This CB[7] derivative **I-35** has retained the binding properties of CB[7] and is able to encapsulate a variety of different drug while the biotin moiety act as the targeting ligand. It was proven with L1210 cells which have overexpressed the biotin receptors that this biotin-CB[7] does selectively delivery oxaliplatin into the targeted cells, which implies a potential reduction in cumulative oxaliplatin doses which could result in reduction incidence of peripheral neuropathy.

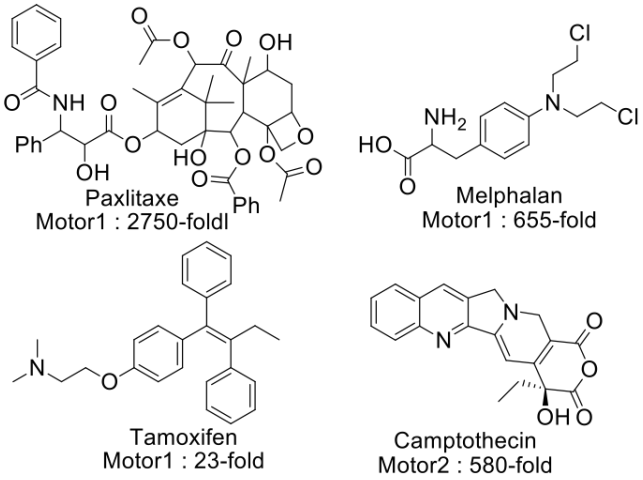

Figure I-23. Solubility enhancement for water-insoluble host with acyclic CB[n]-type containers.

Acyclic CB[n]-type containers are very interesting compounds and have great potentials in drug delivery applications.[35,80] Due to the acyclic structure, these containers are less rigid compared with the cyclic CB[n] containers, and they are much easier to functionalize. The previously mentioned acyclic CB[n]-type container motor1 (**I-16**) and motor2 (**I-18**) synthesized by Isaacs' group have been used as general solubilizing agents for a variety of water-insoluble drugs[35] (Figure I-23). With excellent aqueous solubility (up to 346 mM in water) and binding properties, these acyclic containers are very efficient in solubilizing their

guest molecules. For example, Motor1 container (**I-16**) is able to enhance the solubility of paclitaxel by approximately 2750-fold, melphalan by 655-fold and tamoxifen by 23-fold. Motor2 container (**I-18**) bind to camptothcin very well and solubilizes it up to 580-fold at a 1:1 concentration ratio. The huge success of these two acyclic compounds has implied a bright future of using acyclic CB[n] containers as drug solubilizing agents. It is possible and necessary to develop a broader family of acyclic CB[n] containers that can enhance the solubility of a even broader range of poorly soluble pharmaceuticals.

Chapter 2. Acyclic CB[n]-Type Molecular Containers: Effect of Solubilizing Group on their Function as Solubilizing Excipients

2.1 Introduction.

A major thrust in the area of supramolecular chemistry is the development of macrocyclic compounds that act as molecular containers.[81,82] Accordingly, the synthesis and basic molecular recognition properties of numerous classes of macrocycles including cyclodextrins, calixarenes, cyclophanes, crown ethers, self-assembled systems, and most recently pillararenes have been extensively studied.[45,81,84-89] Importantly, the properties of guest compounds bound within molecular containers are distinct from those of the same compounds free in solution. For example, the lifetime of high energy molecules like cyclobutadiene can be greatly extended,[90] the photophysical properties of encapsulated dyes can be improved,[91] the conformation of natural and non-natural molecules can be controlled,[87,92] the pK_a of included guests can be shifted,[93] and the reactions of certain substrates can be catalyzed.[88,89] Over the past decade, the supramolecular chemistry of the cucurbit[n]uril family (Figure 1) of molecular containers[12] has developed rapidly due in large part to the remarkable affinity and selectivity displayed by CB[n] toward their guests in water[23,63,94] and the stimuli responsiveness of the resultant CB[n]•guest complexes.[67] Accordingly, CB[n] have been used as components of a large number of functional systems including molecular machines,[67] sensing ensembles,[95] supramolecular catalysts,[96] supramolecular polymers and materials,[97] supramolecular velcro,[25] membrane protein fishing,[98] and non-covalent inducers of dimerization.[99,100]

A major problem facing the pharmaceutical industry over the past 20 years has been the increase in the percentage of new chemical entities with excellent biological activity but such poor solubility characteristics that they cannot be formulated on their own.[36,37] Accordingly, the pharmaceutical industry has developed numerous techniques to increase the solubility of these poorly soluble drugs including solid dispersions,[39] the generation of nanocrystal solid forms,[101] the preparation of amorphous solid forms of the API,[102] the application of co-solvents systems (e.g. EtOH / Cremophore), the formation of salts,[43] higher solubility pro-drugs,[44] co-crystals,[41] the encapsulation within or attachment to the outside of a dendrimer construct,[42] and complexation within cyclodextrin molecular containers (e.g. HP-β-CD and Captisol^{TM}).[50,103] Accordingly, researchers in the CB[n] area have begun to investigate the *in vitro* and *in vivo* toxicology of *macrocyclic* CB[n] containers,[71,70,74] their ability to increase the solubility of insoluble drugs (e.g. camptothecin, albendazole, chlorambucil),[73,75,76,77,104,105] protect them against degradation,[72,78] promote transformation into their biologically active form,[106] and target them to specific cells.[69,79]

Over the years, the Isaacs group has investigated the mechanism of CB[n] formation,[26,27,107] and used that mechanistic knowledge to prepare a variety of CB[n]-type receptors including CB[n] analogues,[108] inverted CB[n],[8] nor-seco-CB[n],[9,10,109,110] and CB[n] derivatives.[9,27,29,31,79] Most recently, we have synthesized acyclic CB[n]-type receptors comprising a central C-shaped glycoluril tetramer backbone, two terminal substituted aromatic rings derived from **II-1**, and four arms bearing anionic sulfonate solubilizing

groups.[30,35,111,112] Previously we reported that **II-2b** is highly water soluble (346 mM), increases the solubility of insoluble drugs in water by factors of up to 2750-fold, is not toxic in *in vitro* and *in vivo* tests, and that the **II-2b•**paclitaxel complex efficiently kills HeLa cells.[35] In complementary work we showed that related acyclic CB[n]-type receptors are capable of reversing the biological activity of the neuromuscular blocking agent rocuronium in rats.[112] In this chapter we examine the influence of the nature of the solubilizing group (e.g. anionic, neutral, cationic) and the linker connecting the solubilizing group to the aromatic walls on the ability to act as a solubilizing agent.

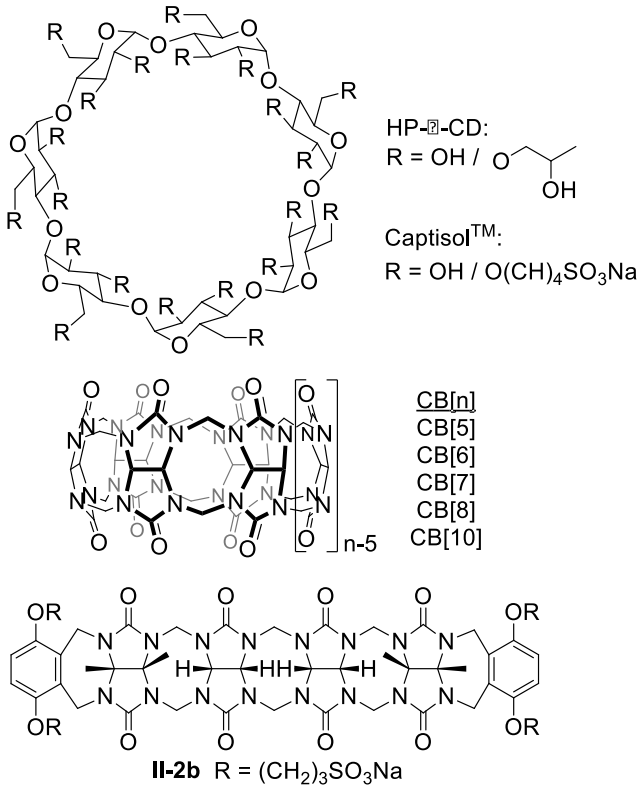

Figure II-1. Structures of molecular containers used previously as solubilizing agents for insoluble drugs: HP-β-CD**,** Captisol™, CB[n], and acyclic CB[n]-type container.

2.2 Results and Discussion.

This results and discussion section is organized as follows. First, we discuss the design and synthesis of a series of acyclic CB[n]-type receptors **II-2a** – **II-2h** and x-ray crystallographic determination of their solid state structures. Subsequently, we show that these containers do not self-associate and study their container•guest recognition properties by ^{1}H NMR and UV/Vis spectroscopy. Finally, we describe the use of these compounds as containers for insoluble drugs as a function of charge of the solubilizing group employed.

2.2.1 Design and Synthesis of Acyclic CB[n]-Type Receptors II-2a – II-2h.

Previously, we have published the design and synthesis of compound **II-2b** and its use as a solubilizing excipient for insoluble pharmaceutical agents.[35] Acyclic CB[n]-type receptor **II-2b** is composed of a central glycoluril tetramer to which two aromatic walls have been attached. The central glycoluril tetramer imparts an overall C-shape to compound **II-2b** which allows it to preferentially bind to and solubilize hydrophobic and cationic drugs whereas the aromatic walls were incorporated to allow **II-2b** to interact by π–π interactions with the wide variety of insoluble drugs which contain aromatic rings in their structures. Finally, container **II-2b** features four anionic sulfonate (SO_3^-) solubilizing groups which greatly enhance its solubility in water.[35] In this paper, we prepare derivatives of **II-2b** – compounds **II-2a** – **II-2h** – that contain different solubilizing groups and study the influence on their ability to act as a host and a solubilizing agent for drugs in water.

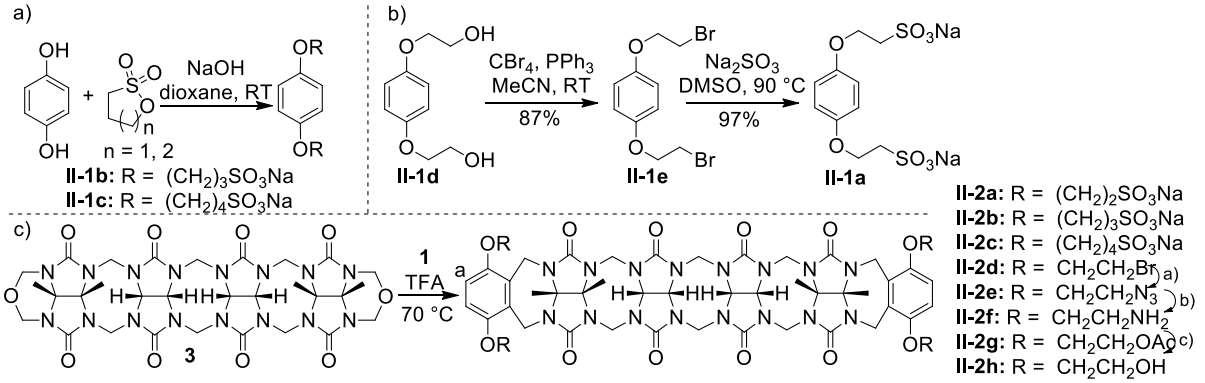

Scheme II-1. Synthesis of Acyclic CB[n] solubilizing excipients **II-2a** – **II-2h**. Conditions: a) NaN_3, DMSO, 90 °C, 95% yield, b) PPh_3, H_2O, DMF, 50 °C, 39% yield, c) LiOH, then HCl, 67% yield.

Synthetically, the preparation of compound **II-2b** involves the reaction of glycoluril tetramer **II-3** with aromatic sidewall **II-1b** by a double electrophilic aromatic substitution reaction as described previously.[35] Accordingly, to prepare derivatives of **II-2b** which differ in the nature of the solubilizing groups we needed to prepare a series of aromatic sidewalls. In analogy to the preparation of **II-1b**, we allowed hydroquinone to react with butanesultone under basic conditions (aq. NaOH) to deliver **II-1c** in 80% yield. To prepare aromatic sidewall **II-1a** with a shorter linker between the aromatic ring and the SO_3^- groups we first reacted commercially available diol **II-1d** with CBr_4 and PPh_3 to give **II-1e** in 91% yield according to the literature report.[113] Next, **II-1e** was reacted with Na_2SO_3 in DMF to give aromatic sidewall **II-1a** in high yield (88%). Reaction of glycoluril tetramer **II-3** with the new anionic sidewalls **II-1a** and **II-1c** in trifluoroacetic acid (TFA) yielded acyclic CB[n]-type receptors **II-2a** and **II-2c** in good yield (61 and 40%), respectively. The series of hosts **II-2a** – **II-2c** differ only in the number of CH_2-groups between the aromatic sidewall and the anionic SO_3^- solubilizing groups.

To prepare acyclic CB[n]-type receptor **II-2f** we first reacted glycoluril tetramer **II-3** with **II-2e** in hot TFA for 3 hours to obtain host tetra-bromo host **II-2d** in good yield (79%). Transformation of **II-2d** into the corresponding tetra-azido compound **II-2e** proceeded smoothly with NaN_3 in DMSO. Reduction of the tetra-azide host **II-2e** with PPh_3 in DMF/H_2O gave the corresponding tetra-amine host which was isolated in pure form as its tetrahydrochloride salt **II-2f** in 39% yield. Lastly, we targeted the preparation of acyclic CB[n] type container **II-2h** which contains uncharged solubilizing arms. For this purpose we reacted commercially available diol **II-1d** with glycoluril tetramer **II-3** with in a mixed solvent of TFA and Ac_2O (v/v = 1:1)[114] which delivered tetraacetoxy compound **II-2g** in 90% yield. Hydrolysis of **II-2g** with an aqueous solution of LiOH followed by acidification with HCl gives host **II-2h** in 67% yield.

2.2.2 X-ray Crystal Structures of Hosts II-2b, II-2f, and II-2h that differ in the charge on their solubilizing groups.

We were fortunate to obtain the crystal structures for host **II-2b**,[35] **II-2f** and **II-2h**, which are the representatives of the negative, neutral and positive hosts (Figure II-2). As we expected, all of the three structures assume a C-shaped conformation, which can be attributed to the polycyclic nature of the glycoluril tetramer backbone. In the crystal structure of **II-2b** (Figure II-2a), the substituted *o*-xylylene tips interact with by CH•••π interactions whereas the $O(CH_2)_3SO_3^-$ arms are extended away from the cavity; the cavity is filled by a solvating CF_3CO_2H molecule. To quantify the size of the cavity we measure the distance between the

opposing quaternary (MeC) carbon atoms (10.92 and 11.44 Å) on the glycoluril tetramer backbone of **II-2b**. In the crystal the individual molecules of **II-2b** form tapes along the c-axis. The formation of tapes is driven by π–π interactions between the *o*-xylylene rings of **II-2b**; the mean separation between the planes of the aromatic rings amounts to 3.49 Å. The tapes stack parallel to one another along the a-axis. For the cationic host **II-2f** (Figure II-2b) the distance between the opposing quaternary (MeC) carbon atoms amounts to 10.50 Å and 10.62 Å which is slightly smaller than that observed for **II-2b**. We attribute this decreased dimension of **II-2f** relative to **II-2b** to the folding of one aromatic wall into the cavity of **II-2f**. This self-complexation is driven by the formation of N-H•••O=C H-bonds / ion-dipole interactions between the $OCH_2CH_2NH_3^+$ solubilizing arms and the carbonyl portal (N•••O distance = 2.790 Å; N-H•••O angle = 160˚). In order for **II-2f** to act as a container for guests the self-complexation process would need to be reversed. The self-complexation also results in an out-of-plane twist which extends one $OCH_2CH_2NH_3$ arm toward a neighboring molecule of **II-2f** in the crystal which reciprocates and forms a dimeric motif driven by N-H•••O=C H-bonds / ion-dipole interactions (N•••O distance = 2.790 Å; N-H•••O angle = 165˚). The dimers pack in the ac-plane which stack along the b-axis separated by chloride counterions. A similar self-complexation phenomenon was observed in the crystal structure of **II-2h** (Figure II-2c). Once again, the folding of the *o*-xylylene ring of **II-2h** into the cavity results in a decreased distance between the opposing quaternary (MeC) carbon atoms which amounts to 10.88 Å and 11.00 Å. In this case the self-complexation is driven by O-H•••O=C H-bonding interactions between on of the OCH_2CH_2OH arms and the carbonyl portal (HO•••O=C distance = 2.799 Å; O-H•••O angle = 164˚). In the crystal the self-folded forms

of **II-2h** appear as dimeric pairs driven by π–π interactions (mean interplanar separation = 3.5 Å). Quite interestingly, a second conformation of **II-2h** is also observed in the crystal (Figure II-2d). In this second conformation, the size of the cavity is increased as evidenced by the larger distance between the opposing quaternary (MeC) carbon atoms (12.23 and 13.70 Å) and the centroid – centroid distance between the two terminal aromatic rings (10.29 Å). This result is significant because it provides direct evidence for the highly flexible nature of methylene bridged glycoluril oligomers in general and acyclic CB[n]-type receptors in general which had previously been surmised based on their ability to solubilize drugs with a range of sizes and single walled carbon nanotubes.[35,115] These expanded conformers of **II-2h** occur in dimeric pairs within the crystal; the $ArOCH_2CH_2OH$ wall and arm of one molecule fills the cavity of its partner and vice versa.[116] Overall, the x-ray crystal structures point to a high level of conformational flexibility of the acyclic CB[n]-type receptors and highlight the possibility of both self-complexation and dimerization.

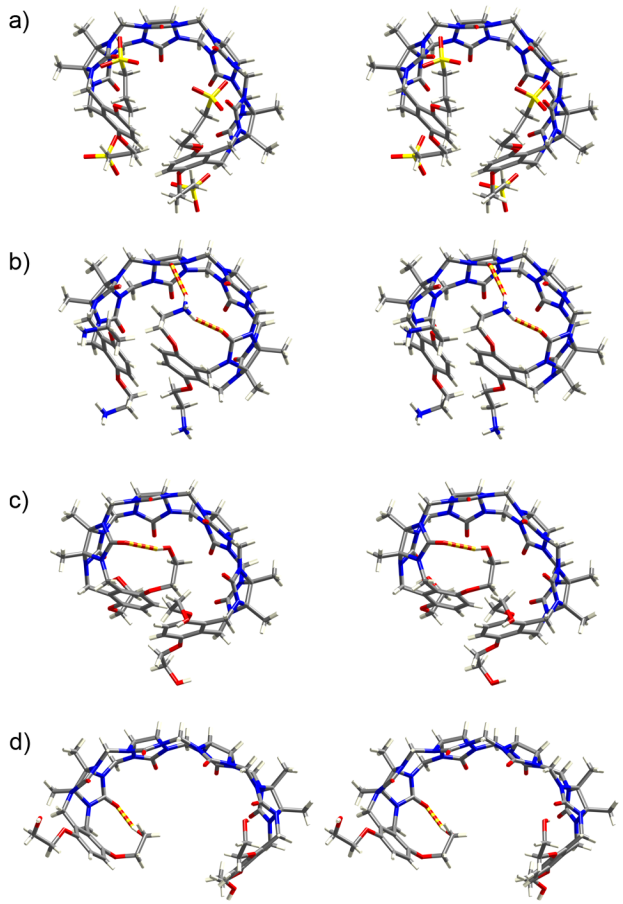

Figure II-2. Cross-eyed stereoviews of the X-ray crystal structures of: a) **II-2b**, b) **II-2f**, and c&d) two different conformations of **II-2h** in the crystal. Color code: C, gray; H, white; N, blue; O, red; H-bonds, red-yellow striped.

2.2.3 Hosts II-2a, II-2f, and II-2h Do Not Undergo Self-Association.

A prerequisite for the use of negative, neutral and positive hosts as solubilizing agents for insoluble drugs is that they do not undergo strong self-association in water which would compete with the formation of the host•drug complexes. Previously, we have performed ^{1}H NMR dilution experiments with negatively charged host **II-2b** and determined a self-association constant K_s = 47 M^{-1} by fitting the change in observed chemical shift as a function of host concentration.[35] The low value of K_s (47 M^{-1}) ensures that the majority of the host molecules are uncomplexed and ready to bind to drug molecules.

Accordingly, we performed related ^{1}H NMR dilution experiments[117] with the newly prepared neutral (**II-2h**) and positively charged (**II-2f**) hosts. We did not observe any significant change in chemical shift of H_a over the accessible concentration ranges (**II-2h**: 1.3 mM – 0.05 mM; **2f**: 10.5 mM – 0.05 mM). These result establish that hosts **II-2f** and **II-2h** do not undergo significant self-association in the 20 mM sodium phosphate buffered D_2O (pH 7.4) used in the drug solubilization experiments described below.

2.2.4 Binding Studies Between Acyclic CB[n]-Type Receptors and Guests II-4 – II-8.

This section describes our investigation of the binding between hosts **II-2a** – **II-2c**, **II-2f**, and **II-2h** toward guests **II-4** – **II-8** (Figure II-3) by a combination of ^{1}H NMR spectroscopy and direct and competition UV/Vis spectroscopic titrations.

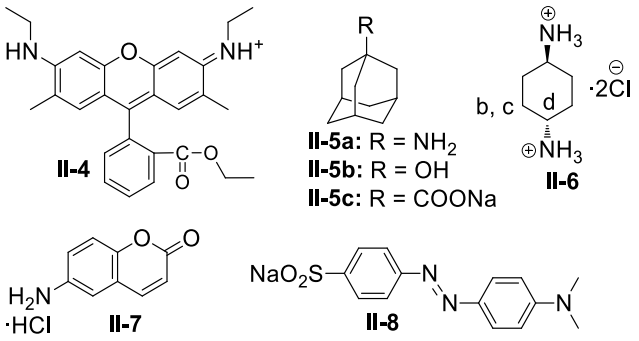

Figure II-3. Chemical structures of guests used in this study.

^{1}H NMR INVESTIGATIONS OF THE BINDING INTERACTIONS. In this section we use ^{1}H NMR experiments to qualitatively and quantitatively study the geometrical features and association constants of the host•guest complexes. Initially, we performed a

qualitative ^{1}H NMR study of the difference in binding of guest **II-6** toward hosts **II-2a**, **II-2f**, and **II-2h**. Figure II-4a – c shows the ^{1}H NMR spectra recorded for **II-6** (1.0 mM), and equimolar mixtures of **II-6** (1.0 mM) with hosts **II-2a** (1.0 mM), **II-2h** (1.0 mM) and **II-2f** (1.0 mM). Interestingly, for an equimolar mixture of host **II-2f** and guest **II-6** we do not observe any changes in chemical shift for protons H_b, H_c and H_d on guest **II-6** or protons H_a on host **II-2f**. We surmise that the interaction between host **II-2a** and guest **II-6** is simply too weak to be detected at the 1 mM concentrations used. In contrast, however, we do observe significant upfield shifts of the protons H_b**,** H_c and H_d on guest **II-6** in the presence of neutral host **II-2h** (Figure II-4c) and negative host **II-2a** (Figure II-4d). The upfield nature of the changes in chemical shift is indicative of guest **6** binding within the cavity of **II-2h** and **II-2a** as observed previously for (acyclic) CB[n]-type receptors.[35,112,118,119] The larger upfield shift observed for protons H_b, H_c and H_d within the mixture of negative host **II-2a** (Figure II-2d) and guest **II-6** relative to neutral host **II-2h** and guest **II-6** (Figure II-4c) indicates that the negatively charged host **II-2a** binds the dicationic guest significantly stronger than the neutral host **II-2h**. It was also observed that the resonances for protons H_a on the aromatic sidewalls of hosts **II-2h** and **II-2a** undergo a downfield shift upon complexation with guest **II-6**. This observation can be explained by the fact that the neutral and positive hosts undergo π–π interactions between their aromatic walls within the uncomplexed host (Figure II-2) which shifts the resonances for protons H_a upfield (≈ 6.45 ppm). Binding to guest **II-6** breaks the π–π interactions and shifts the resonances for H_a downfield (≈ 7.4 ppm).

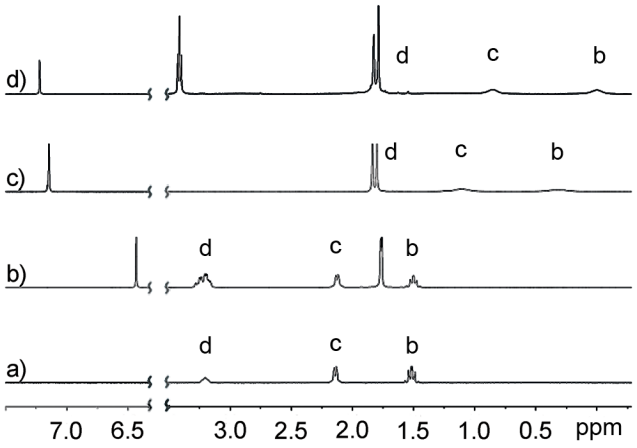

Figure II-4. ^{1}H NMR recorded (400 MHz, RT, 20 mM sodium phosphate buffered D_2O, pH 7.4) for: a) **II-6**, b) an equimolar mixture of **II-2f** (positive host) and **II-6**, (c) and equimolar mixture of **II-2h** (neutral host) and **II-6**, and (d) and equimolar mixture of **II-2a** (negative host) and **II-6**.

After performing these initial ^{1}H NMR experiments which showed substantial differences in the complexation behavior of negative, neutral, and positively charged hosts **II-2a**, **II-2f**, and **II-2h** toward diammonium ion **II-6** we decided to determine the binding constants for these complexes by suitable titration experiments. To measure the binding constant for complex **II-2a• II-5c**, we performed a direct ^{1}H NMR titration experiment. A solution containing a fixed concentration of host **II-2a** (0.5 mM) in 20 mM sodium phosphate buffer (pH 7.4) was titrated with increasing concentrations of compound **II-5c** (Supporting Information). We monitored the change in the ^{1}H NMR chemical shift of proton H_a of host **II-2a** as a function of [**II-5c**] and fitted the data to a 1:1 host:guest binding model which allowed us to determine the K_a value for **II-2a• II-5c** ($K_a = 3.33 \times 10^3\ M^{-1}$). In an analogous manner, we performed direct ^{1}H NMR titration experiments to obtain the K_a values (Table **II-**1) for the complexes

between host **II-2b** and guests **II-5b**, **II-5c**, host **II-2h** and guests **II-5b** and **II-5c**, and host **II-2f** and guests **II-5c** and **II-6** (Supporting Information).

DIRECT UV/VIS TITRATIONS. The ^{1}H NMR titration experiments described above were not applicable for the determination of the K_a values for the tighter host guest complexes and complexes with poor solubility characteristics. Accordingly, we decided to measure the K_a values for the remaining host-guest complexes by UV/Vis competition assays referenced to K_a values determined by direct UV/Vis titration. Dye **II-4** was used in displacement assays to determine the K_a values of negative host **II-2a** towards different guests. However, the application of **II-4** in the detection of the K_a values of neutral host **II-2h** was limited by the fact that the dye induces precipitation of the host in the displacement experiments. To avoid that problem, we chose dye **II-8** as the indicator for competition experiments involving neutral host **II-2h**. Figure II-3a shows the UV/Vis spectra recorded when a fixed concentration of dye **II-4** (10.0 μM) was titrated with negative host **II-2a** (0 – 0.45 mM). We observed an isosbestic point at 533 nm which is indicative of the formation of a well defined **II-2a• II-4** complex. Figure II-3b shows the best nonlinear least-squares fit of the absorbance at 550 nm versus concentration data to a 1:1 binding model which allowed us to determine the binding constant for complex **II-2a• II-4** ($K_a = (1.83 \pm 0.08) \times 10^5$ M^{-1}). Similar experiments were carried out to determine the binding constant constants for complex **II-2h• II-8** ($K_a = (1.32 \pm 0.01) \times 10^3$ M^{-1}, Supporting Information). With those binding constants in hand we were able to perform the indicator displacement assays[120] to determine the K_a values for a larger variety of

guests.

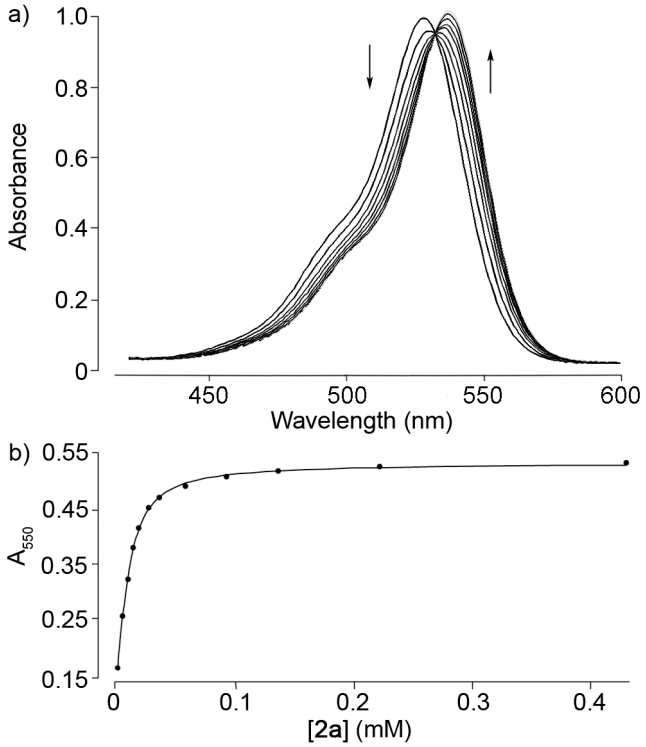

Figure II-5. (a) UV/vis spectra obtained during the titration of a fixed concentration of **II-4** (10.0 μM) with **II-2a** (0 – 0.45 mM) and (b) plot of absorbance versus [**II-2a**] used to determine the K_a value of the **II-2a• II-4** complex by nonlinear least-square fitting.

UV/VIS COMPETITION ASSAYS. To measure the values of K_a for guests whose binding affinity exceeds that measurable by direct ^{1}H NMR titrations (approx. 10^4 M^{-1}) we turned to UV/Vis competition assays[120] involving a colorimetric indicator as guest. In these UV/Vis competition assays a complex between host and indicator (of known K_a) is initially formed – which shows a UV/Vis change upon host•indicator formation – and then titrated with an increasing concentration of UV/Vis silent guest. Upon competitive formation of the host•guest complex the indicator is released and the UV/Vis change is reversed. Fitting of a plot of UV/Vis absorbance values versus

[guest] to the competitive binding model (Supporting Information) as described previously[112,118] then yields the unknown K_a value for host•guest. For example, we performed a UV/Vis competition assay employing fixed concentrations of dye **II-4** (10.0 μM) and host **II-2a** (9.15 μM) and increasing concentrations of **II-5a** (0 – 65.0 μM). The absorbance of dye **II-4** was monitored and was then plotted against the concentration of guest **II-5a**. Fitting the data to a competitive binding model, we determined the K_a value of **II-2a• II-5a** to be $(1.68 \pm 0.09) \times 10^6$ M^{-1}. Similar experiments were also performed for hosts **II-2a**, **II-2b**, **II-2c** and **II-2h** with guest **II-5a** – **II-5c**, and **II-6** (Table II-1, Supporting Information).

Table II-1. Binding Constants (K_a, M^{-1}) obtained for the interaction between host **II-2a** – **II-2f** with various guests.

	II-2a	**II-2b**	**II-2c**	**II-2h**	**II-2f**
II-4	$1.83 \times 10^{5\,a}$	$4.23 \times 10^{5\,a}$	$1.29 \times 10^{5\,a}$	ppt.	n.d.
II-5a	$1.68 \times 10^{6\,b}$	$1.78 \times 10^{6\,b}$	$1.94 \times 10^{5\,b}$	$3.64 \times 10^{3\,d}$	–
II-5b	$4.47 \times 10^{4\,b}$	$1.67 \times 10^{5\,d}$	$5.54 \times 10^{4\,b}$	$2.36 \times 10^{3\,d}$	–
II-5c	$3.33 \times 10^{3\,d}$	$1.87 \times 10^{3\,d}$	345^{d}	$108^{\,d}$	645^{d}

II-6	4.59×10^{6} [b]	4.37×10^{6} [b]	1.12×10^{6} [b]	1.13×10^{4} [c]	327[d]
II-8	n.d.	n.d.	n.d.	1.32×10^{3} [a]	n.d.

[a]Measured by direct titration monitored by UV/Vis absorption spectroscopy. [b]Measured by competition with guest **II-4** monitored by UV/Vis spectroscopy. [c]Measured by competition with guest **II-8** monitored by UV/Vis spectroscopy. [d]Measured by direct titration monitored by ^{1}H NMR. n.d.: not determined. –, below detection limit of ^{1}H NMR titration. ppt. = precipitate formed.

TRENDS IN THE K_A VALUES BETWEEN HOSTS II-2A, II-2H, AND II-2F AND GUESTS II-5A – II-5C, AND II-6. Hosts **II-2a**, **II-2h**, and **II-2f** differ in the nature of the charge on the solubilizing arms with a constant OCH_2CH_2 linker connecting them to the aromatic sidewall. In previous work, we reported the x-ray crystal structure of host **II-2b** which showed that the sulfonate solubilizing groups extend away from the cavity and portals of the acyclic CB[n]-type receptor.[35] However, the x-ray crystal structures of hosts **II-2h** and **II-2f** reveal the presence of intramolecular H-bonds between the solubilizing arms and the ureidyl C=O portal of the host. In addition, the presence of intramolecular H-bonds prompts the attached substituted o-xylylene sidewall to fold into the cavity to undergo offset π–π stacking. Accordingly, for hosts **II-2h** and **II-2f** to undergo guest binding these intramolecular H-bonds, ion-dipole interactions, and π–π interactions need to be disrupted which should result in lower binding strength

relative to anionic host **II-2a**. In accord with these expectations we note that adamantaneammonium ion **II-5a** binds 461-fold more tightly to anionic host **II-2a** than to neutral host **II-2h**; binding of **II-5a** to positively charged host **II-2f** was too weak to be detected. Similarly, cyclohexanediammonium ion **II-6** binds 406-fold more tightly to **II-2a** than it does to neutral host **II-2h** which in turn binds 35-fold more tightly to **II-6** than cationic host **II-2f** does. The effect of solubilizing group charge on the binding process toward neutral guests is somewhat different. For a neutral guest like adamantanol **II-5b** the main driving force for complexation is the hydrophobic effect; the presence of a RO-H•••O=C H-bond is of no consequence to the binding because **II-5b** is H-bonded in both water and the complex. We find that host **II-2a** binds **II-5b** only 19-fold more tightly than **II-2h** which can be attributed to the loss of intrahost π–π interactions upon formation of the **II-2h• II-5b** complex. Host **II-2f** does not complex **II-5b** at all because it is energetically unfavorable to sacrifice intrahost ammonium•O=C ion-dipole interactions. Interestingly, the influence of solubilizing group charge on the binding of negatively charged guests is different still. For example, negatively charged host **II-2a** binds 30-fold more tightly to adamantane carboxylate **II-5c** than neutral host **II-2h** does again because of the loss of intrahost π–π interactions upon formation of the **II-2h• II-5c** complex. However, host **II-2f** forms a relatively stable complex with **II-5c** (K_a = 645 M^{-1}) which is 6-fold stronger than **II-2h• II-5c**. We suggest that this increase in K_a is due to the presence of direct ammonium-carboxylate (H_3N^+•••^-O_2C) electrostatic interactions between the solubilizing arms of cationic host **II-2f** and guest **II-5c**. Apparently, these electrostatic

interactions are sufficiently strong to compensate for the loss or reduction of ion-dipole interactions and π–π stacking interactions in uncomplexed host **II-2f**. A related trend is noted in the recognition properties of anionic host **II-2a** toward cationic (**II-5a**), neutral (**II-5b**), and negatively (**II-5c**) charged adamantane derivatives where **II-5a** binds 38-fold more tightly than **II-5b** and 505-fold more tightly than **II-5c**. Overall, these results suggest that the charge on the solubilizing arms (e.g. anionic, neutral, cationic) has a major impact on the molecular recognition capabilities of the hosts.

We also studied the length of the linker ($O(CH_2)_nSO_3^-$; n = 2, 3, 4) between the aromatic wall and the anionic solubilizing group. For example, the binding affinities of **II-2a**, **II-2b**, and **II-2c** toward a common guest (e.g. **II-5b**) differ by only 4-fold from one another. Because the magnitude of the differences in K_a for hosts **II-2a**, **II-2b**, and **II-2c** toward a given guest are small we will not speculate further on the reasons for any observed differences.

ACYCLIC CB[N]-TYPE RECEPTORS THAT DIFFER IN CHARGE INDUCE pK_A SHIFTS OF BOUND GUESTS OF DIFFERENT MAGNITUDE. It is well known in the literature that the pK_a values for the guest within CB[n]-guest complexes can differ substantially from the pK_a for guest alone; the magnitude of these complexation induced pK_a shifts can exceed 4 pK_a units.[73,121] The origin of these pK_a shifts can be traced to the strong ion-dipole interactions that occur between CB[n] host and cationic guests that are not possible with the corresponding neutral guests. In this paper, we studied the influence of the charges on the solubilizing groups on the pK_a shift of 6-aminocoumarin (**II-7**)

when binding with acyclic CB[n] type receptors. UV/Vis spectroscopy was used to monitor the protonation and deprotonation process of **II-7**. Figure **II-**6 shows the plot of the percentage of the absorbance change of **II-7** at 345 nm versus pH; the pK_a value (Table **II-**2) was obtained by non-linear fitting of the data to the Equation **II-**1 (Supporting Information).[122,123] From Table **II-**2, we can observe an increase in pK_a values in the presence of neutral host **II-2h** (pK_a = 4.1) and negative host **II-2a** (pK_a = 4.9) compared with dye **II-7** alone (pK_a = 3.6), while a small decrease was observed in the presence of positive host **II-2f** (pK_a = 3.4). These changes in pK_a are consistent with our expectations based on the net charge of the host. For example, protonation of guest **II-7** to give **7**H^+ is more favorable in the presence of neutral host **II-2h** because **II-2h** establishes ion-dipole interactions in the **II-2h• II-7**H^+ that are not formed in the **II-2h• II-7** complex. Protonation of guest **II-7** to give **II-7**H^+ is even more favorable (larger pK_a shift to 4.9) in the presence of anionic host **II-2a** not only because of ion-dipole interactions in **II-2a• II-7**H^+ complex but also because of the favorable ion-ion electrostatic interactions between the SO_3^- groups and **II-7**H^+. Finally, the pK_a of the **II-7**H^+ in the presence of cationic host **II-2f** is comparable to that of **II-7**H^+ which probably reflects the weak binding between **II-2f** and **II-7**H^+ due to binding of the $OCH_2CH_2NH_3^+$ arms of **II-2f** to its C=O portals and unfavorable ion-ion electrostatic interactions in the putative **II-2f• II-7**H^+ complex.

$$A_{obs} = \frac{A_{7H+}}{(1 + 10^{pH-pKa})} + \frac{A_7}{(1 + 10^{pKa-pH})} \qquad \text{(II-1)}$$

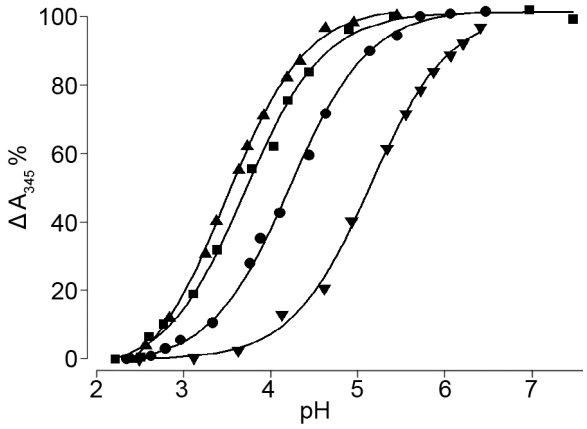

Figure II-6. Plot of absorbance change (%) versus pH to determine the pK_a values of 6-aminocoumarin (35.6 μM) by itself (■), and with **II-2f** (cationic host, 1.5 mm, ▲), **II-2h** (neutral host, 1.2 mM, ●), and **II-2a** (anionic host, 1.5 mM, ▼).

Table II-2. pK_a values and binding constants (K_a) obtained for compound **II-7** with host **II-2a**, **II-2h** and **II-2f**.

	II-7	**II-2a• II-7**	**II-2h• II-7**	**II-2f• II-7**
pK_a	3.6	4.9	4.1	3.4
K_a $(M^{-1})^a$	n.a.	2.74×10^5	9.59×10^3	678

n.a. = not applicable. – = no changes in ^{1}H NMR chemical shift observed. a) Conditions: 20 mM sodium phosphate buffer, pH 7.4, RT.

Phase Solubility Diagrams for Acyclic CB[n] Type Receptors with Insoluble Drugs of Different Charges. Our purpose in preparing and studying hosts **II-2a**, **II-2h**, and **II-2f** was to determine whether the charge on the solubilizing arms of the acyclic CB[n]-type receptor effects their ability to act as a solubilizing excipient for insoluble

drugs. Given that we observed significantly weaker binding of neutral (**II-2h**) and positively charged (**II-2f**) hosts toward most soluble guests as described above we anticipated that the anionic host **II-2a** would be the superior solubilizing agent for insoluble drugs. Accordingly, we decided to test the ability of hosts **II-2a**, **II-2h** and **II-2f** to enhance the solubility of three insoluble drugs: tamoxifen, 17α–ethynylestradiol, and indomethacin (Figure II-7). We selected these three drugs because they differ in their net charge in neutral aqueous solution (tamoxifen, positive; 17α–ethynylestradiol, neutral; indomethacin, negative). For this purpose, we constructed phase solubility diagrams (plots of [drug] versus [host])[117] for the each of the three hosts with each of the three water insoluble drugs (Figure II-8). Experimentally, a series of solutions containing known concentrations of host **II-2a** (or **II-2h** or **II-2f**) in sodium phosphate buffer (20 mM, pH 7.4) were stirred with excess of solid insoluble drug (e.g. tamoxifen, 17α–ethynylestradiol, or indomethacin) at RT until equilibrium was established. The mixture was then filtered and the supernatant was collected. A known concentration of benzene-1,3,5-tricarboxylic acid was added into the supernatant as an internal standard. The concentration of the solubilized drug was then determined by ^{1}H NMR spectroscopy using the integrals of the resonances of the known concentration of internal standard versus those of solubilized drug. Figure II-8a-c shows the phase solubility diagrams constructed for tamoxifen, 17α–ethynylestradiol, and indomethacin with hosts **II-2a**, **II-2h**, and **II-2f**. As is readily apparent, negatively charged host **II-2a** is able to solubilize substantially more drug than neutral or positively charged hosts **II-2h** and **II-2f**. This behavior can

be further rationalized based on an analysis of the phase solubility diagrams.[117] For linear (A_L) phase solubility diagrams, the initial slope of the PSD obeys equation 2 where S_0 is the intrinsic solubility of the drug, slope is the slope of the PSD, and K_a is the binding constant for the host•drug complex.[117] In this manner, we calculated the binding constant for host **II-2a** towards all three drugs (1.83×10^3 M^{-1} for tamoxifen, 1.73×10^4 M^{-1} for 17α - ethynylestradiol, and 6.07×10^3 M^{-1} for indomethacin). It is also possible to use the phase solubility diagram to compare the behavior for a given drug (with common S_0) with different hosts. In this situation, the relative slopes of the phase solubility diagrams reflect the relative binding affinities of the different host-drug complexes. Accordingly, the inability of hosts **II-2h** and **II-2f** to solubilize any of the three drugs can be traced to their poor abilities as hosts (e.g. low K_a values). In turn, this may be attributed to the blockade of the host cavity in **II-2h** and **II-2f** which was induced by intramolecular H-bonds, ion-dipole interactions, and π–π stacking.

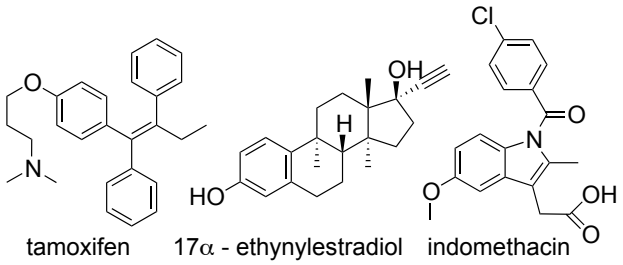

Figure II-7. Chemical structures of water-insoluble drugs used in this study.

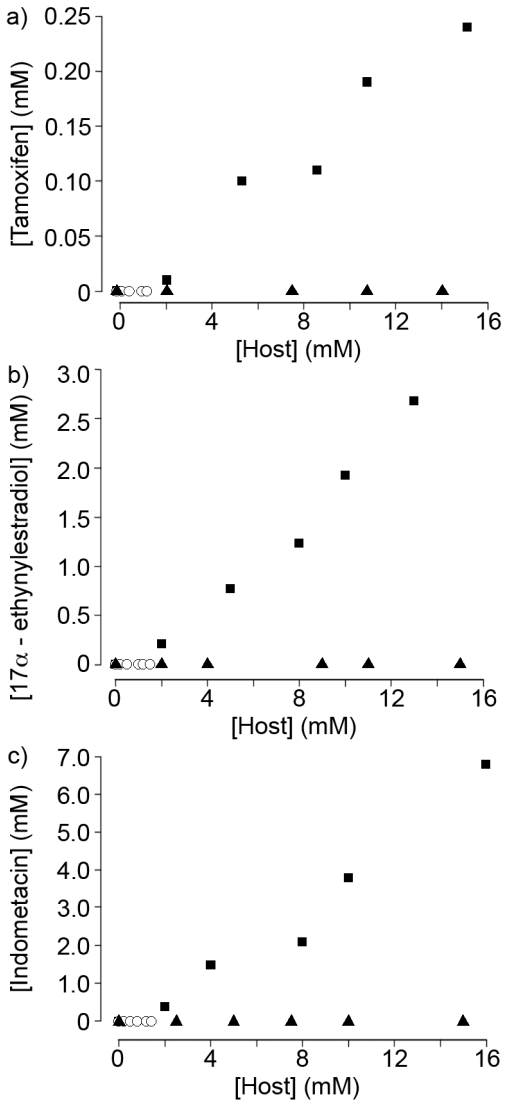

Figure II-8. Phase solubility diagrams constructed using solutions of hosts **II-2a** (■),**II-2h** (○) and **II-2f** (▲) of known concentrations and an excess of solid drug: a) tamoxifen, b) 17α-ethynylestradiol, and c) indomethacin. Conditions: 20 mM sodium phosphate buffered D_2O (pH = 7.4, RT). Solubility data were collected from single experiments.

$$K_a = \text{slope} / [S_0(1\text{-slope})] \qquad \text{(II-2)}$$

2.3 Conclusion

In summary, we have synthesized a series of acyclic CB[n]-type molecular containers (**II-2a** – **II-2h**) with different solubilizing groups bearing different charges for evaluation as potential drug solubilizing agents. The X-ray crystal structures of the negative, positive and neutral hosts (host **II-2b**, **II-2f**, and **II-2h**) show us that all of these acyclic hosts assume a C-shaped configuration. However, for neutral (**II-2h**) and positively charged (**II-2f**) hosts, we observed intramolecular H-bonds and ion-dipole interactions between the solubilizing arms and the ureidyl C=O portals as well as intrahost π–π stacking interactions which result in a self-filling of the cavity. We used ^{1}H NMR and UV/Vis spectroscopy to measure the K_a values of hosts **II-2a**, **II-2h**, and **II-2f** toward guests with different charge and noted significant decrease in binding affinities of the neutral (**II-2h**) and positive (**II-2f**) hosts towards most guests. There are exceptions, however, with adamantane carboxylate **II-5c** binding more tightly to positively changed host **II-2f** than to neutral host **II-2h** probably due to ion-ion electrostatic interactions. We measured the pK_a of **7**H^+ alone and in the presence of **II-2a, II-2h**, and **II-2f** and noted that the **II-2a** induces the largest pK_a shift which we attribute to the presence of ion-ion electrostatic interactions in the **II-2a• II-7**H^+ complex. Both the K_a and pK_a measurements indicate that the solubilizing groups are not innocent bystanders. The poor recognition properties of hosts **II-2h** and **II-2f** are reflected in their phase-solubility diagrams with insoluble drugs (tamoxifen, 17-α–ethynylestradiol, and indomethacin). In all cases, the anionic host **II-2a** functions more efficiently as a solubilizing agent that either neutral **II-2h**, or cationic host **II-2f**.

In conclusion, we have established that host **II-2a** which bears anionic sulfonate solubilizing

groups is far more efficient as a solubilizing agent than either **II-2h** or **II-2f**. The work reinforces the need to employ solubilizing groups that do not impinge upon the innate recognition abilities of the host cavity by either self-association or self-folding due to H-bonds, ion-dipole interaction, or π–π interactions. Accordingly, further development of acyclic CB[n]-type receptors as solubilizing excipients for insoluble drugs will focus on derivatives with sulfonate solubilizing groups. Because the synthesis of acyclic CB[n]-type receptors is modular, we are able to attach different aromatic sidewalls (e.g. naphthalene) to create tailor made analogues of **II-2**. Ongoing work targets an understanding of the role of aromatic walls on the performance of analogues of **II-2** as solubilizing excipients

2.4 Experimental Section

General Experimental. Starting materials were purchased from commercial suppliers and were used without further purification or were prepared by literature procedures. Compound **II-1b**, **II-1e**, **II-2b** and **II-3** were prepared according to literature procedures.[35,113,118] Melting points were measured on a Meltemp apparatus in open capillary tubes and are uncorrected. IR spectra were measured on a JASCO FT/IR 4100 spectrometer and are reported in cm^{-1}. NMR spectra were measured at 400 MHz or 600 MHz for ^{1}H and 125 MHz for ^{13}C. Mass spectrometry was performed using a JEOL AccuTOF electrospray instrument using the electrospray ionization (ESI) technique. UV/Vis spectra were measured on a Varian Cary 100 UV/Visible spectrophotometer.

Compound **II-2a**. Compound **II-1a** (0.28 g, 0.23 mmol) was added into a solution of **II-3**

(0.18 g, 0.77 mmol) in TFA (2.0 mL). The mixture was stirred and heated at 70 ˚C for 4 h. The solvent was removed with under reduced pressure and the solid was further dried under high vacuum. The solid was washed with the mixture of water and acetone (1:2, v/v, 30 mL) twice and then dissolved in water and adjusted to pH = 7 by adding 1 M aqueous NaOH. The solvent was removed under reduced pressure and then the solid was further dried under high vacuum to yield **II-2a** as a white solid (0.21 g, 61%). M.p. > 300 ˚C. IR (ATR, cm^{-1}): 2990w, 1726s, 1480s, 1381m, 1318m, 1182, 1087s, 968m, 938m, 822m, 799s, 759m, 526m. ^{1}H NMR (400 MHz, D_2O): 6.93 (s, 4H), 5.67 (d, *J* = 15.5, 2H), 5.56 (d, *J* = 16.0, 4H), 5.44 (d, *J* = 7.6, 2H), 5.38 (d, *J* = 7.6, 2H), 5.35 (d, *J* = 16.3, 4H) 4.45 - 4.25 (m, 8H), 4.24 (d, *J* =16.0, 4H), 4.21 (d, *J* = 16.3, 4H) 4.10 (d, *J* = 15.5, 2H), 3.55 -3.40 (m, 4H), 3.35-3.20 (m, 4H), 1.79 (s, 6H), 1.75 (s, 6H). ^{13}C NMR (125 MHz, D_2O, 1,4-dioxane as internal reference): δ 168.3, 167.8, 161.5, 139.5, 126.3, 90.3, 89.0, 82.8, 82.7, 77.4, 64.2, 62.0, 59.9, 46.7, 27.5, 26.5. High-Res MS (ESI): *m/z* 708.1271 ($[M - 3Na + H]^{2-}$), calculated 708.1256.

2.4 Support Information

General Experimental. Starting materials were purchased from commercial suppliers and were used without further purification or were prepared by literature procedures. Compound **II-1b**, **II-1e,** and **II-2b** were prepared according to literature procedures.[35,118] Melting points were measured on a Meltemp apparatus in open capillary tubes and are uncorrected. IR spectra were measured on a JASCO FT/IR 4100 spectrometer and are reported in cm^{-1}. NMR spectra were measured on Bruker DRX-400 instrument operating at 400 MHz for ^{1}H and 125 MHz for ^{13}C. Mass spectrometry was performed using a JEOL AccuTOF

electrospray instrument (ESI). UV-Vis absorbance was measured on Varian Cary 100UV spectrophotometer.

Synthetic Procedures and Characterization. The synthesis of **II-1e** and **II-2b** have been reported previously in literature.[35,118]

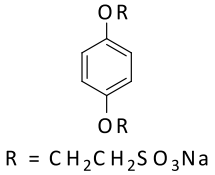

Compound II-1a. Compound **II-1e** (2.00 g, 6.13 mmol) and Na_2SO_3 (3.10 g, 24.5 mmol) was mixed and dissolved in H_2O (20 mL). The mixture was stirred at 100 ^oC under N_2 for 12 h. The mixture was allowed to cool to RT and then acetone (40 mL) was added The product precipitated as white crystals. The solid was collected by filtration and then purified by recrystalization from water. Drying under high vacuum gave **II-1a** as a white solid (2.01 g, 88%). M.p. > 270 ^oC. IR (ATR, cm^{-1}): 3053w, 2994w, 2972w, 2882w, 1618w, 1512s, 1478m, 1265m, 1169s, 1038s, 817w, 747m, 597m, 477m. ^1H NMR (400 MHz, D_2O): 6.98 (s, 4H), 4.35 (t, J = 6.2, 4H), 3.32 (t, J = 6.2, 4H). ^{13}C NMR (125 MHz, D_2O, 1,4-dioxane as internal reference): δ 151.5, 115.5, 63.3, 49.3. High-Res MS (ESI): *m/z* 162.0120 ($[M - 2Na]^{2-}$), calculated for $C_{10}H_{12}O_8S_2^{2-}$ 161.9987.

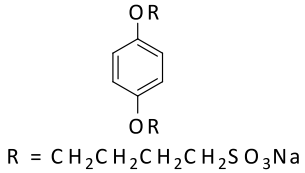

Compound II-1c. A solution of butanesultone (24.50 g, 200 mmol) in 1,4-dioxane (160 mL) was added into a solution of hydroquinone (8.80 g, 80.0 mmol) in aqueous NaOH solution (10 wt%, 120 mL). The mixture was stirred at RT. for 12 h then filtered to collect the crude solid.

The solid was stirred with acetone (200 mL) then dried under high vacuum to yield **II-1c** as a white solid (25.112 g, 80%). M.p. > 270 ˚C. IR (ATR, cm^{-1}): 2961w, 2857w, 1622w, 1510s, 1475w, 1237s, 1184s, 1049s, 822m, 604m, 534m, 479w. ^{1}H NMR (400 MHz, D_2O): 6.98 (s, 4H), 4.05 (t, *J* = 5.7, 4H), 2.95 (t, *J* = 7.0, 4H), 1.80 - 2.00 (m, 8H). ^{13}C NMR (125 MHz, D_2O, 1, 4-dioxane as internal reference): δ 152.1, 115.8, 68.3, 50.1, 26.8, 20.3 (6 out of 6 resonances were observed). High-Res MS (ESI): *m/z* 381.0677 ($[M - 2Na + H]^-$), calculated for $C_{14}H_{20}O_8S_2H^-$ 381.0678.

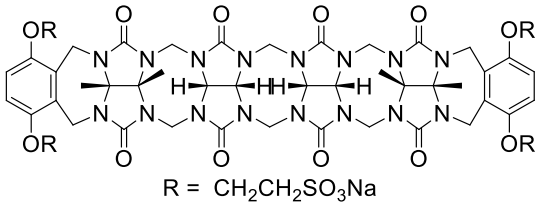

Compound **II-2a.** Compound **II-1a** (0.28 g, 0.77 mmol) was added into a solution of **II-3** (0.181 g, 0.23 mmol) in TFA (2.0 mL). The mixture was stirred and heated at 70 ˚C for 4 h. The solvent was removed with under reduced pressure and the solid was further dried under high vacuum. The solid was washed with the mixture of water and acetone (1:2, v/v, 30 mL) twice and then dissolved in water and adjusted to pH = 7 by adding 1 M aqueous NaOH. The solvent was removed under reduced pressure and then the solid was further dried under high vacuum to yield **II-2a** as a white solid (0.208 g, 61%). M.p. > 300 ^{o}C. IR (ATR, cm^{-1}): 2990w, 1726s, 1480s, 1381m, 1318m, 1182, 1087s, 968m, 938m, 822m, 799s, 759m, 526m. ^{1}H NMR (400 MHz, D_2O): 6.93 (s, 4H), 5.67 (d, *J* = 15.5, 2H), 5.56 (d, *J* = 16.0, 4H), 5.44 (d, *J* = 7.6, 2H), 5.38 (d, *J* = 7.6, 2H), 5.35 (d, *J* = 16.3, 4H) 4.45 - 4.25 (m, 8H), 4.24 (d, *J* =16.0, 4H), 4.21 (d, *J* = 16.3, 4H) 4.10 (d, *J* = 15.5, 2H), 3.55 - 3.40 (m, 4H), 3.35-3.20 (m, 4H), 1.79 (s, 6H), 1.75 (s, 6H). ^{13}C NMR (125 MHz, D_2O, 1,4-dioxane as internal reference): δ 168.3, 167.8, 161.5, 139.5, 126.3, 90.3, 89.0, 82.8, 82.7,

77.4, 64.2, 62.0, 59.9, 46.7, 27.5, 26.5 (16 out of 16 resonances were observed). High-Res MS (ESI): *m/z* 708.1271 ($[M - 3Na + H]^{2-}$), calculated for $C_{50}H_{57}N_{16}O_{24}S_4Na^{2-}$ 708.1256.

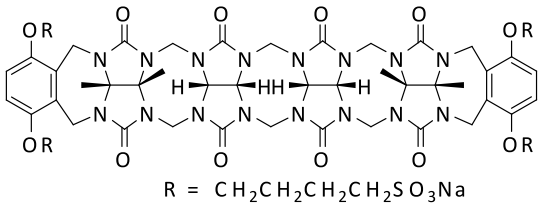

Compound **II-2c.** Compound **II-1c** (6.50 g, 15.4 mmol) was added into a solution of **II-3** (3.000 g, 3.84 mmol) in TFA (30 mL). The mixture was stirred and heated at 70 ^oC for 4 h. The solvent was removed with under reduced pressure and the solid was further dried under high vacuum. The solid was washed twice with the mixture of water and acetone (1:2, v/v, 300 mL) twice and then dissolved in water and adjusted to pH = 7 by adding 1 M aqueous NaOH. The solvent was removed under reduced pressure and then the solid was further dried under high vacuum to yield **II-2c** as a white solid (2.331 g, 40%). m.p. > 300 ^oC. IR (ATR, cm^{-1}): 3936w, 1729s, 1474s, 1380m, 1185s, 1088s, 1043s, 963m, 974m, 823m, 799s, 760m, 603m. ^1H NMR (400 MHz, D_2O): 7.00 (s, 4H), 5.62 (d, *J* = 15.2, 2H), 5.51 (d, *J* = 16.0, 4H), 5.45(d, *J* = 8.9, 2H), 5.35 (d, *J* = 8.9, 2H), 5.24 (d, *J* = 16.0, 4H), 4.30(d, *J* = 16.0, 4H), 4.25 (d, *J* = 16.0, 4H), 4.04 (d, *J* = 15.2, 2H), 3.90 - 3.75(m, 8H), 2.90 - 2.75 (m, 4H), 2.70 - 2.55 (m, 4H), 1.72 (s, 12H), 1.80 - 1.40 (m, 16H). ^{13}C NMR (125 MHz, D_2O, 1,4-dioxane as internal reference): δ 162.5, 162.3, 156.8, 134.1, 122.4, 85.2, 83.8, 77.5, 76.8, 57.1, 54.6, 41.3, 34.2, 27.4, 22.1, 21.4 (16 out of 18 resonances were observed). High-Res MS (ESI): *m/z* 753.1977 ($[M - 4Na + 2H]^{2+}$), calculated for $C_{58}H_{74}N_{16}O_{24}S_4^{2-}$ 753.1972.

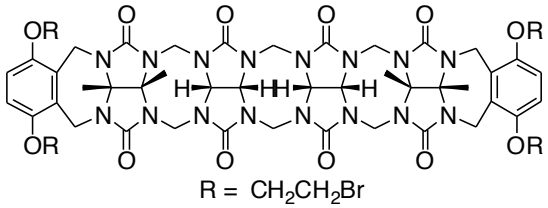

Compound **II-2d.** Compound **II-1e** (1.70 g, 5.21 mmol) and compound **II-3** (1.20 g, 1.53 mmol) were mixed in a round bottom flask. TFA (12 mL) was added, and the mixture was stirred at 70 °C for 3 h. The reaction mixture was poured into MeOH (100 mL), and the solid was collected with filtration. The crude product was stirred with water (150 mL) and then acetone (150 mL) at RT and the solid was isolated by filtration. Drying at high vacuum gave the product **II-2d** as a white powder (1.71 g, 79 %). M.p. 283 - 285 ^{o}C. IR (ATR, cm^{-1}): 3000br, 1704m, 1456m, 1311m, 1225s, 1177s, 1080s, 966m, 922m, 818m, 794s, 754m, 666m. ^{1}H NMR (400 MHz, DMSO): 6.91 (s, 4H), 5.59 (d, *J* = 14.4, 2H), 5.51 (d, *J* = 15.2, 4H), 5.38 (d, *J* = 9.0, 2H), 5.30-5.25 (m, 6H), 4.50-4.40 (m, 4H), 4.25-4.20 (m, 10H), 4.06 (d, *J* = 15.2, 4H), 3.90-3.80 (m, 8H), 1.69 (s, 6H), 1.66 (s, 6H). ^{13}C NMR (125 MHz, DMSO): δ 155.3, 154.0 150.3, 128.8, 116.0, 77.3, 76.2, 70.1, 70.8, 70.7, 70.3, 52.9, 48.2, 34.5, 32.8, 16.6, 15.6, (16 out of 16 resonances were observed). MS (ESI): *m/z* 765 ([M + *p* - xylenediamine + 2H]$^{2+}$)

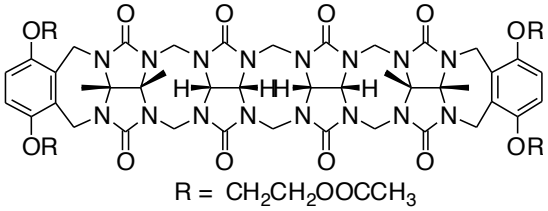

Compound **II-2g.** Compound **II-1d** (1.021 g, 5.12 mmol) and **II-3** (1.000 g, 1.28 mmol) was mixed as solid and then dissolved in a mixture of TFA and Ac_2O (1:1, 10 mL). The mixture was stirred at 70 ^{o}C for 3.5 h and then was poured into MeOH (150 mL). The solid was collected by filtration and was washed with acetone (100 mL) and water (100 mL). After drying under high vacuum, compound **II-2g** was obtained as a white powder (1.512 g, 90 %). M.p. > 300 ^{o}C. IR (ATR, cm^{-1}): 2925w, 1732s,

1464s, 1377m, 1314m, 1228s, 1184s, 1083m, 974m, 822m, 797m. ^{1}H NMR (400 MHz, DMSO): 6.84 (s, 4H), 5.58 (d, *J* = 16.3, 2H), 5.48 (d, *J* = 15.6, 4H), 5.37 (d, *J* = 9.0, 2H), 5.27 (d, *J* = 9.0, 2H), 5.23 (d, *J* = 16.0, 4H), 4.45-4.30 (m, 4H), 4.30-4.05 (m, 16H), 3.50-3.45 (m, 4H), 2.06 (s, 12H), 1.67 (s, 6H), 1.63 (s, 6H). ^{13}C NMR (125 MHz, DMSO): δ 170.4, 155.3, 153.9, 150.3, 128.4, 115.0, 77.3, 76.2, 71.8, 70.4, 68.6, 63.1, 53.1, 48.3, 34.4, 20.7, 16.6, 15.6 (18 out of 18 resonances were observed). MS (ESI): *m/z* 745 ([M + *p* - xylenediamine + 2H]$^{2+}$).

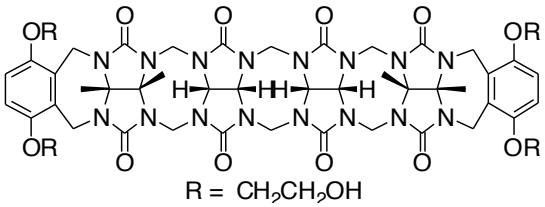

Compound **II-2h.** Compound **II-2g** (0.400 g, 0.305 mmol) was added into an aqueous solution of LiOH (2.5 M, 7.5 mL). The mixture was stirred at 50 ºC for 0.5 h and then the solid was collected by filtration. The solid was wash with 0.1 M HCl to nertral and then stirred with EtOH (30 mL), and water (30 mL). After drying under high vacuum, a white solid was obtained (0.234 g, 67%). M.p. > 300 ^{o}C. IR (ATR, cm^{-1}): 3428br, 2932w, 1728s, 1476s, 1379s, 1256s, 1184m, 1085m, 967m, 798m. ^{1}H NMR (400 MHz, D_2O): 6.95 (s, 4H), 5.62 (d, *J* = 15.3, 2H), 5.52 (d, *J* = 15.7, 4H), 5.43 (d, *J* = 8.0, 2H), 5.20 (d, *J* = 8.0, 2H), 4.72 (d, *J* = 16.2, 4H), 4.28 (d, *J* = 15.7, 4H), 4.23 (d, *J* = 16.2, 4H), 4.19 (d, *J* = 15.3, 2H), 3.85-3.50 (m, 8H), 3.45-2.85 (m, 8H), 1.76 (s, 12H). ^{13}C NMR (125 MHz, D_2O, 1,4-dioxane as internal reference): δ 155.8, 149.8, 127.2, 114.7, 78.8, 77.4, 71.0, 70.2, 60.0, 52.0, 47.8, 34.6, 15.7, 14.8 (16 out of 18 resonances were observed). High-Res MS (ESI): *m/z* 639.2886 ([M + *p* - xylenediamine + 2H]$^{2+}$), calculated for $C_{58}H_{74}N_{18}O_{16}^{2+}$ 639.2765.

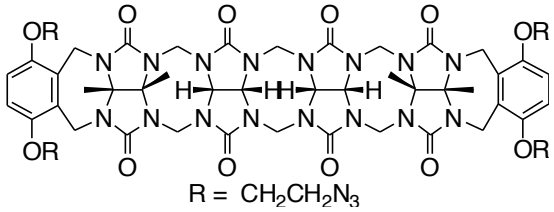

Compound **II-2e.** Compound **II-2d** (0.500 g, 0.359 mmol) and NaN_3 (0.281 g, 4.32 mmol) were mixed together and was then dissolved in DMSO (5.0 mL). The mixed was stirred at 80 °C for 12 h and was then poured into H_2O (50 mL). The solid was collected by filtration and was then washed with MeOH (50 mL). After drying under vacuum, a white solid was obtained (0.423 g, 95%). M.p. > 300 ^oC. IR (ATR, cm^{-1}):2932w, 2106m, 1730s, 1466s, 1378m, 1314m, 1230m, 1086m, 973w, 798m, ^1H NMR (400 MHz, DMSO): 6.88 (s, 4H), 5.57 (d, *J* = 14.6*,* 2H), 5.47 (d, *J* = 15.1*,* 4H), 5.37 (d, *J* = 8.7*,* 2H), 5.25 (d, *J* = 8.7*,* 2H), 5.24 (d, *J* = 16.1, 4H), 4.25 – 4.20 (m, 4H), 4.14 (d, *J* = 16.1, 4H), 4.15 – 4.05 (m, 4H), 4.05 (d, *J* = 14.6, 4H), 4.03 (d, *J* = 15.1, 2H), 3.85-3.75 (m, 4H), 3.55-3.45 (m, 4H), 1.69 (s, 6H), 1.66 (s, 6H). ^{13}C NMR (125 MHz, DMSO,): δ 155.1, 153.8, 150.2, 128.3, 115.0, 77.1, 76.0, 70.6, 70.2, 69.6, 52.8, 50.4, 34.2, 16.5, 15.4 (16 out of 16 resonances were observed). High-Res MS (ESI): *m/z* 689.3025 ([M + *p* - xylenediamine + 2H]$^{2+}$), calculated for $C_{58}H_{70}N_{30}O_{12}^{2+}$ 689.2894.

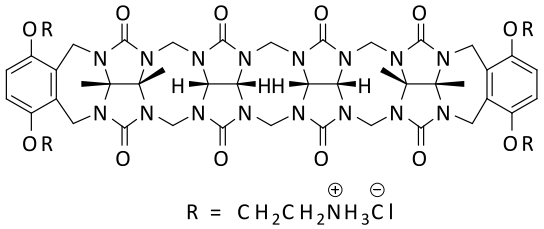

Compound **II-2f.** Compound **II-2e** (0.031 g, 0.0242 mmol) was mixed with triphenylphosphine (0.051 g, 0.193 mmol) and was then dissolved in the mixed solvent of DMSO (4 mL) and H_2O (1 mL). The mixture was stirred at 80 °C for 6 h and pH was adjusted to 1 with 6M HCl. The resulting solution was poured into acetone (80 mL) and the solid was collected by filtration. The crude product was

then crystallized with a mix solvent of H_2O (0.5 mL) and acetone (1.5 mL). The solid was then collected by centrifuge and after drying under vacuum, a white solid was obtained (0.012 g, 39%). M.p. > 300 ^oC. IR (ATR, cm^{-1}): 3435br, 3045m, 1726s, 1479s, 1379w, 1318s, 1257s, 1231s, 1180s, 1093s. ^1H NMR (400 MHz, D_2O): 6.44 (s, 4H), 5.58 (d, *J* = 15.3*,* 2H), 5.52 (d, *J* = 15.8*,* 4H), 5.46 (d, *J* = 9.2*,* 2H), 5.28 (d, *J* = 9.2*,* 2H), 5.27 (d, *J* = 16.5, 4H), 4.31 (d, *J* = 15.8, 4H), 4.29 (d, *J* = 16.5, 4H), 4.13 (d, *J* = 15.3, 2H), 3.85 - 3.75 (m, 4H), 3.65-3.55 (m, 4H), 3.350-3.10 (m, 8H), 1.78 (s, 6H), 1.77 (s, 6H). ^{13}C NMR (125 MHz, D_2O, 1,4-dioxane as internal reference): δ 155.9, 155.7, 148.2, 126.8, 112.1, 78.6, 77.5, 70.1, 70.0, 64.0, 51.5, 47.8, 38.4, 34.5, 17.0, 15.5, (16 out of 16 resonances were observed). High-Res MS (ESI): *m/z* 1137.5092 ($[M - 4HCl + H]^+$), calculated for $C_{50}H_{65}N_{20}O_{12}^+$ 1137.5091.

References

1) Ma, D.; Hettiarachchi, G.; Nguyen, D.; Zhang, B.; Wittenberg, J. B.; Zavalij, P. Y.; Briken, V.; Isaacs, L., *Nat. Chem.* **2012,** *4*, 503-510.

2) George, W. N.; Giles, M.; McCulloch, I.; De Mello, J. C.; Steinke, J. H. G., *Soft Matter.,* **2007***, 3,* 1381-1387.

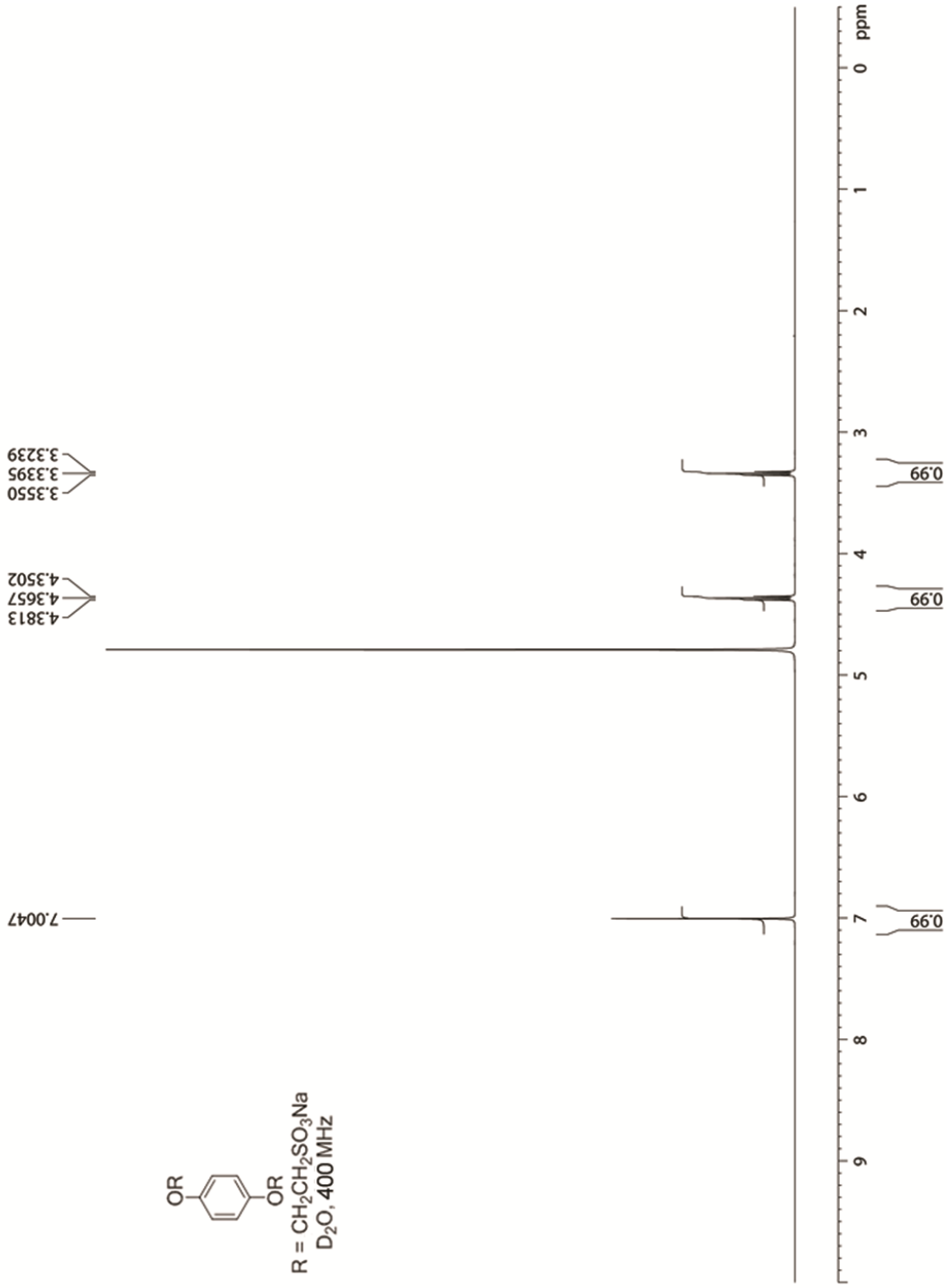

Figure S II-1. ^{1}H NMR spectra (400 MHz, D_2O, RT) recorded for **II-1a**.

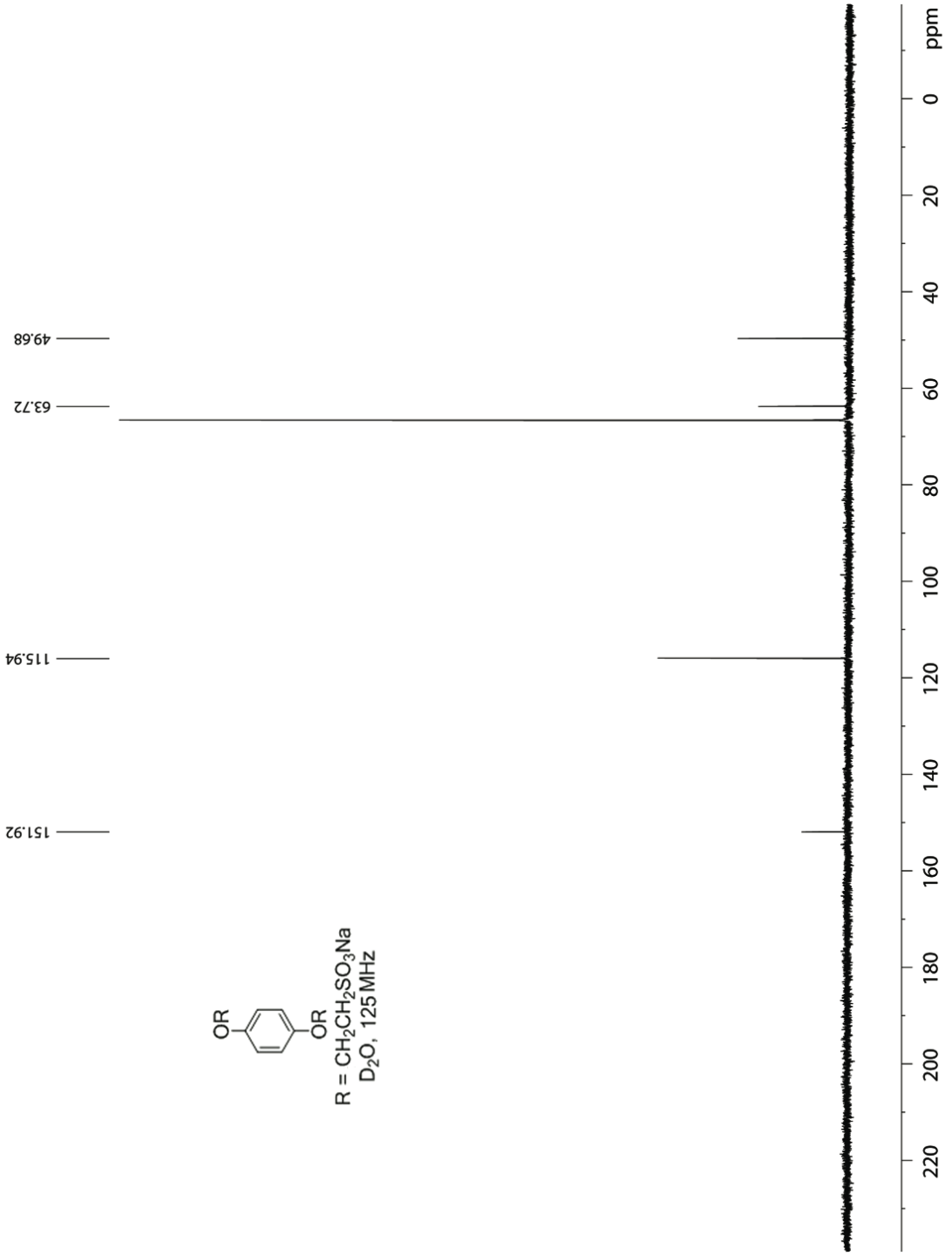

Figure S II-2. ^{13}C NMR spectra (125 MHz, D_2O, RT, 1,4-dioxane as internal reference) recorded for **II-1a**.

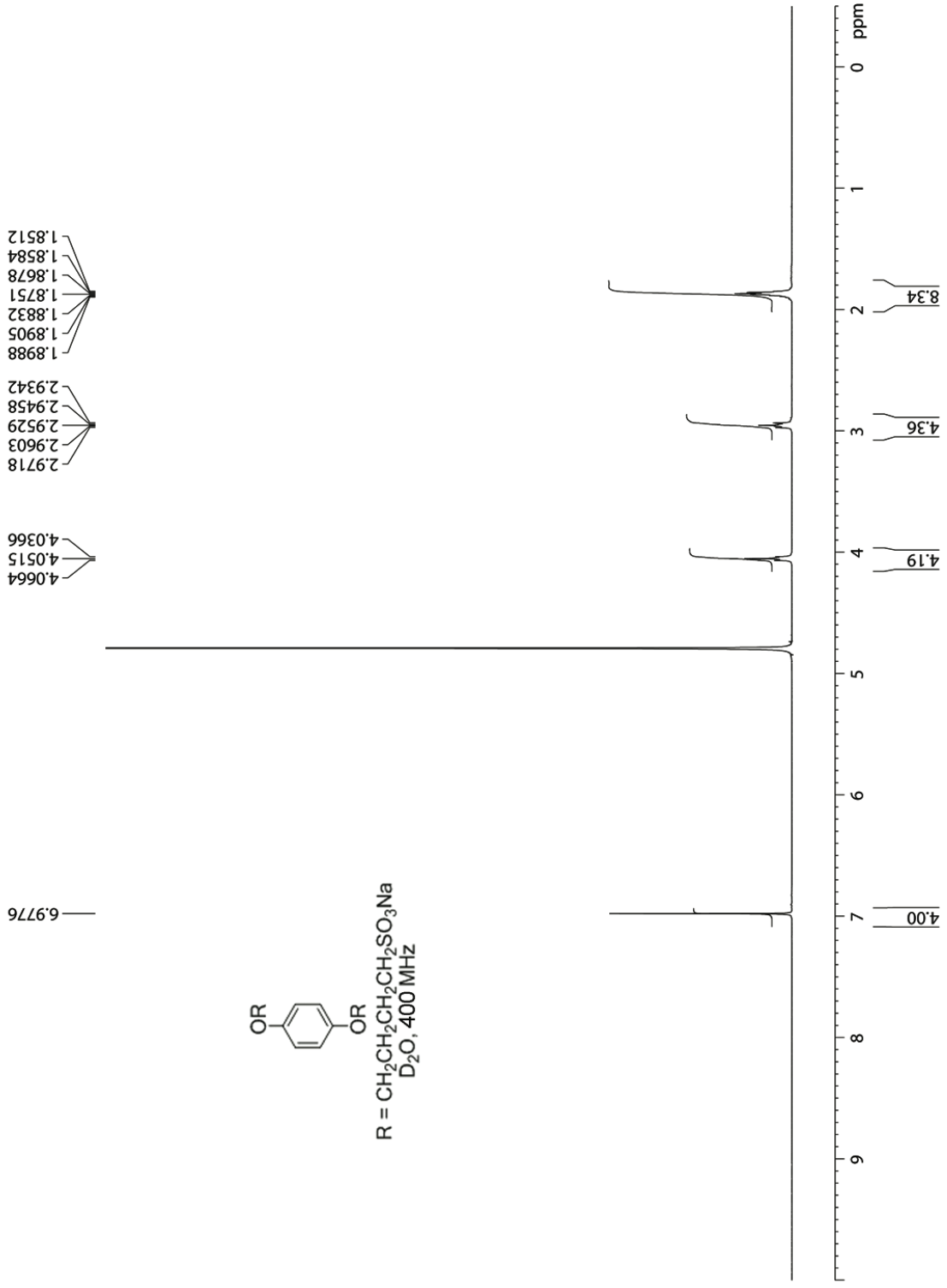

Figure S II-3. ^{1}H NMR spectra (400 MHz, D_2O, RT) recorded for **II-1c**.

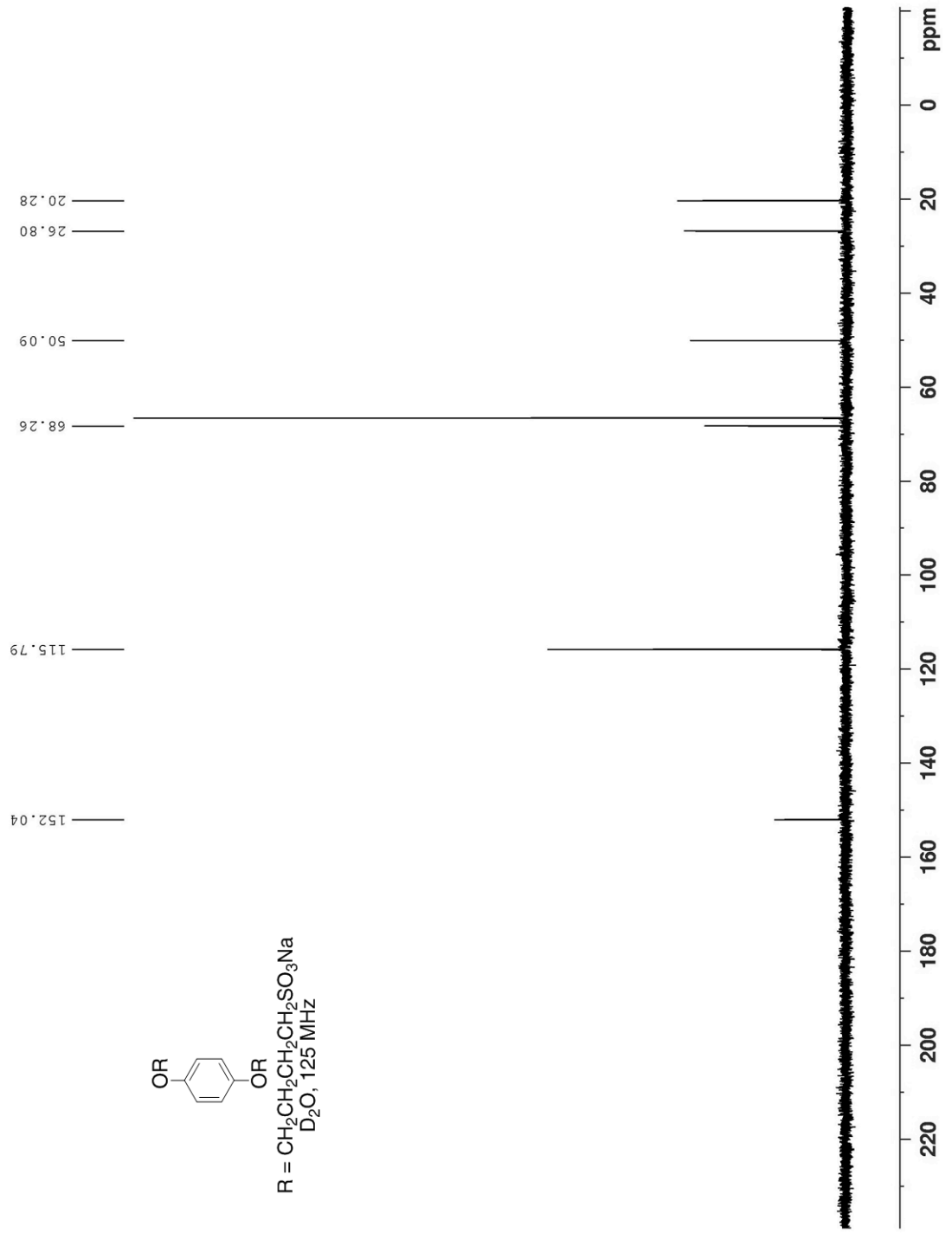

Figure S II-4. ^{13}C NMR spectra (125 MHz, D_2O, RT, 1,4-dioxane as internal reference) recorded for **II-1c**.

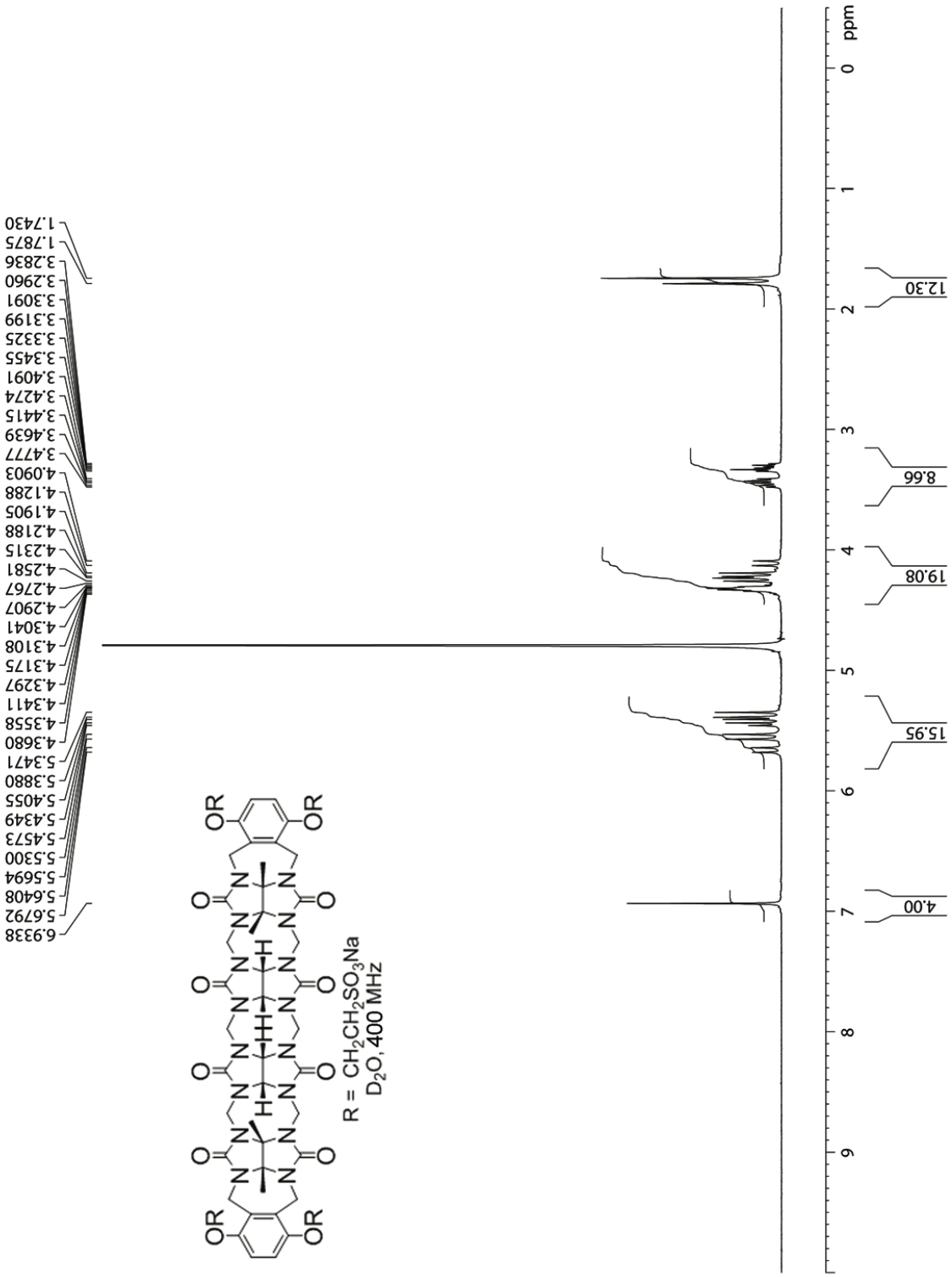

Figure S II-5. ^{1}H NMR spectra (400 MHz, D_2O, RT) recorded for **II-2a**.

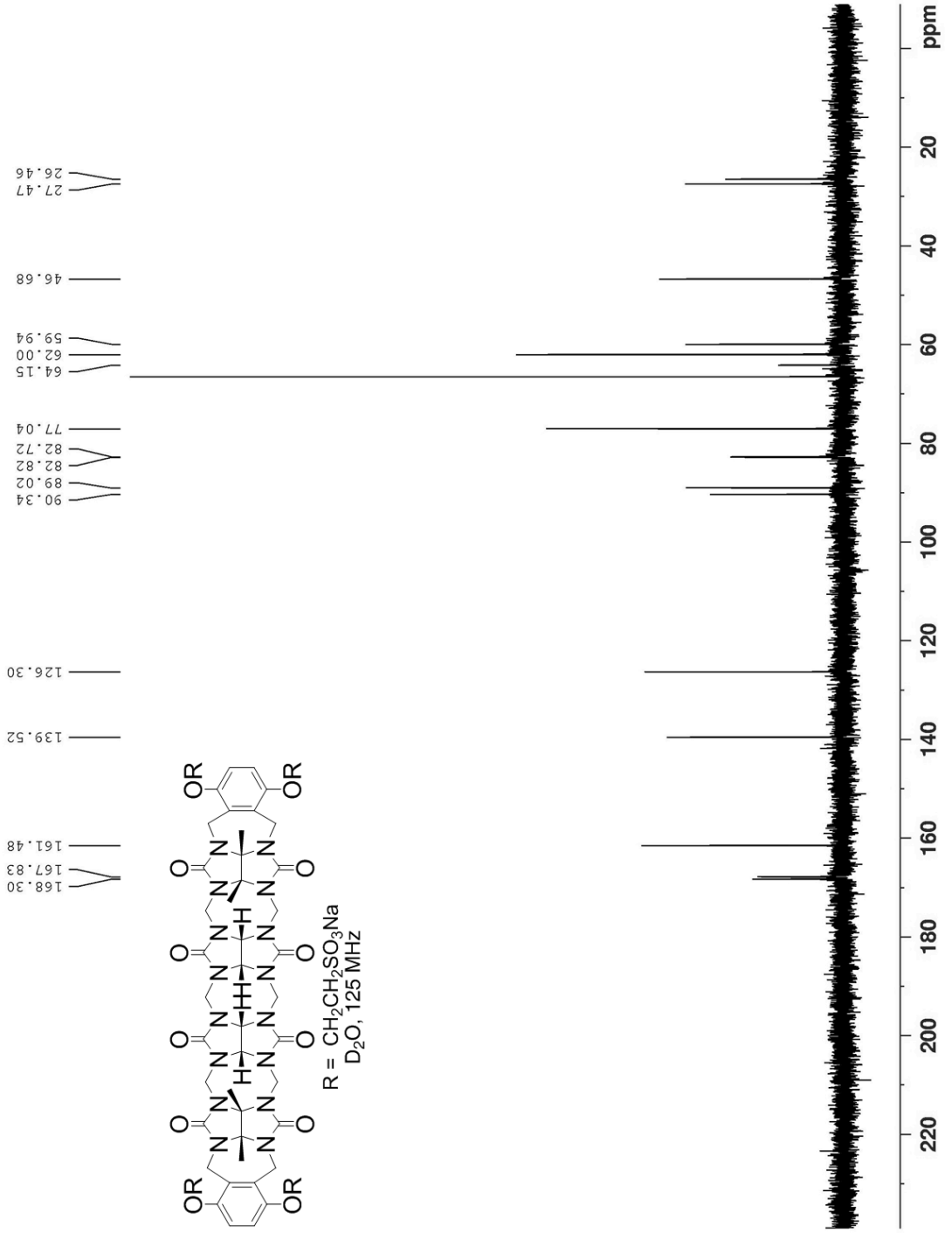

Figure S II-6. ^{13}C NMR spectra (125 MHz, D_2O, RT, 1,4-dioxane as internal reference) recorded for **II-2a**.

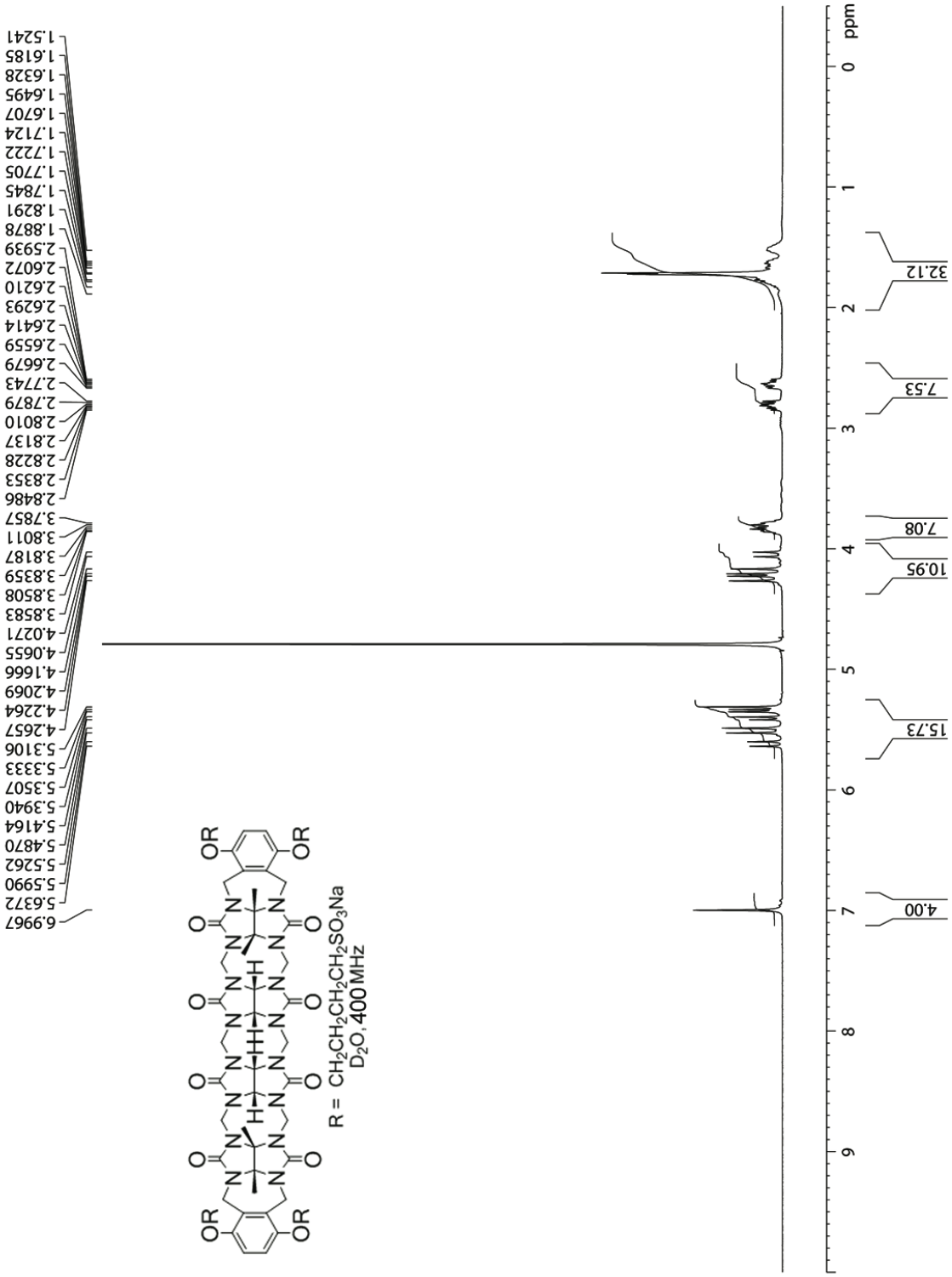

Figure S II-7. ^{1}H NMR spectra (400 MHz, D_2O, RT) recorded for **II-2c**.

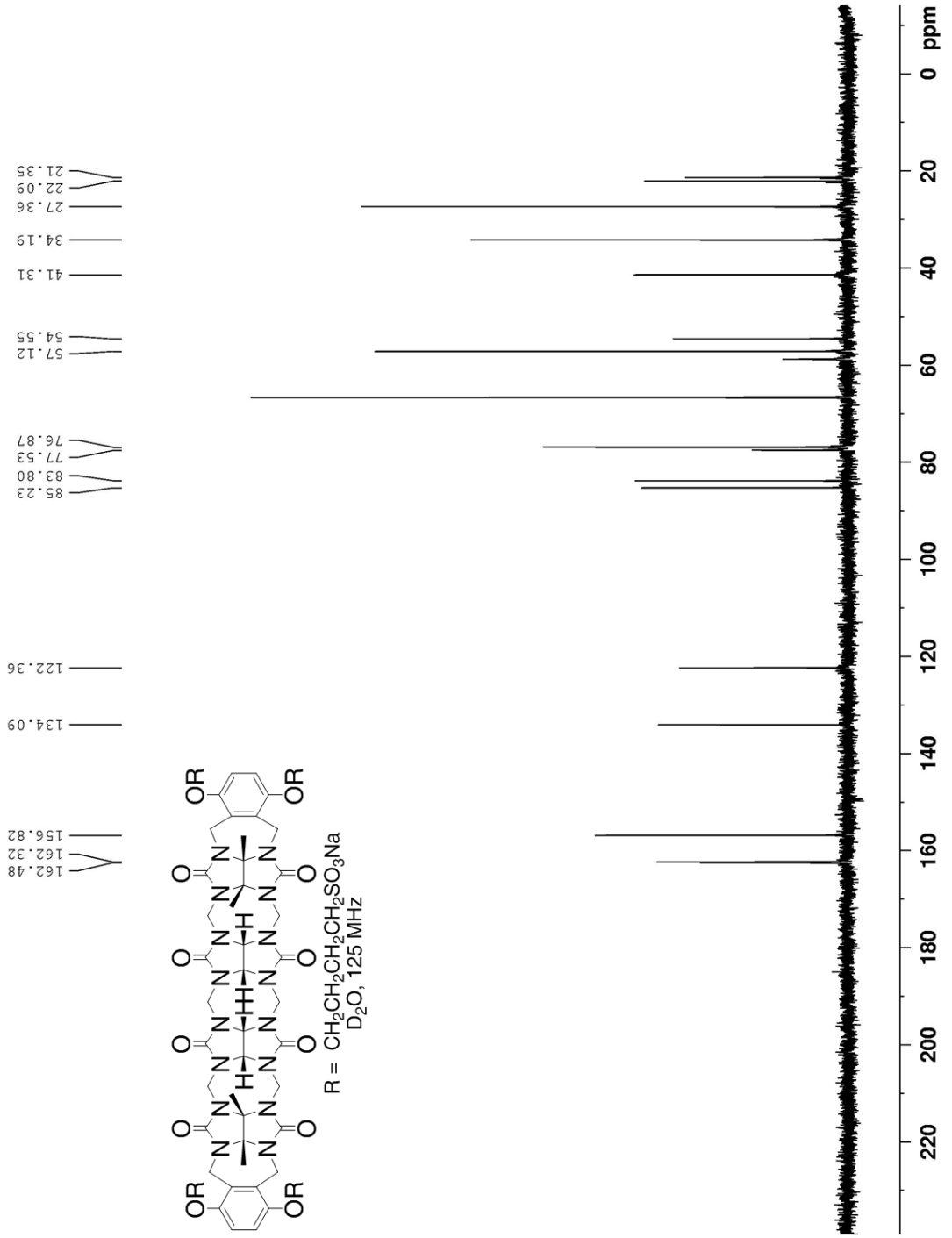

Figure S II-8. ^{13}C NMR spectra (125 MHz, D_2O, RT, 1,4-dioxane as internal reference) recorded for **II-2c**.

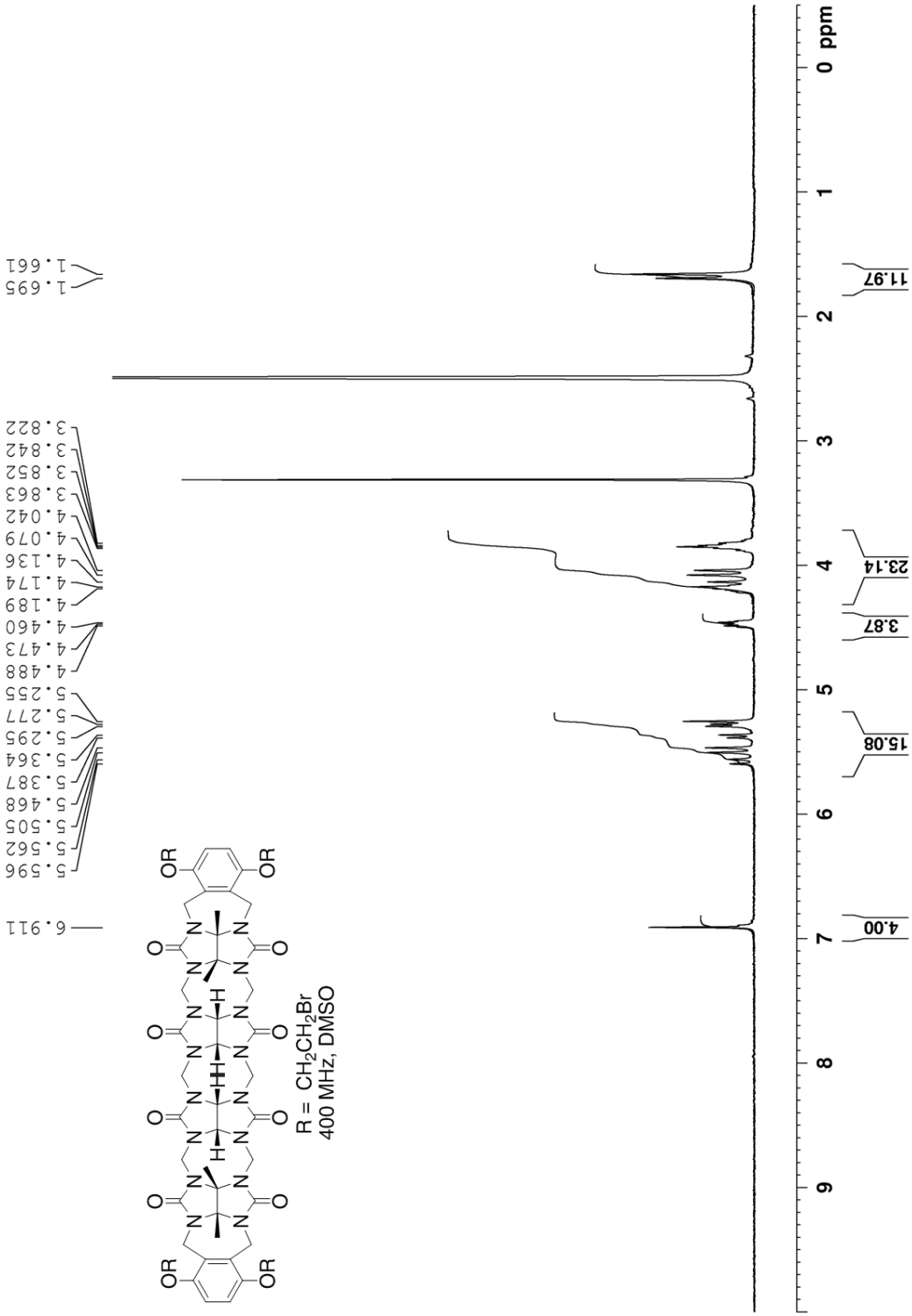

Figure S II-9. ^{1}H NMR spectra (400 MHz, DMSO, RT) recorded for **II-2d**.

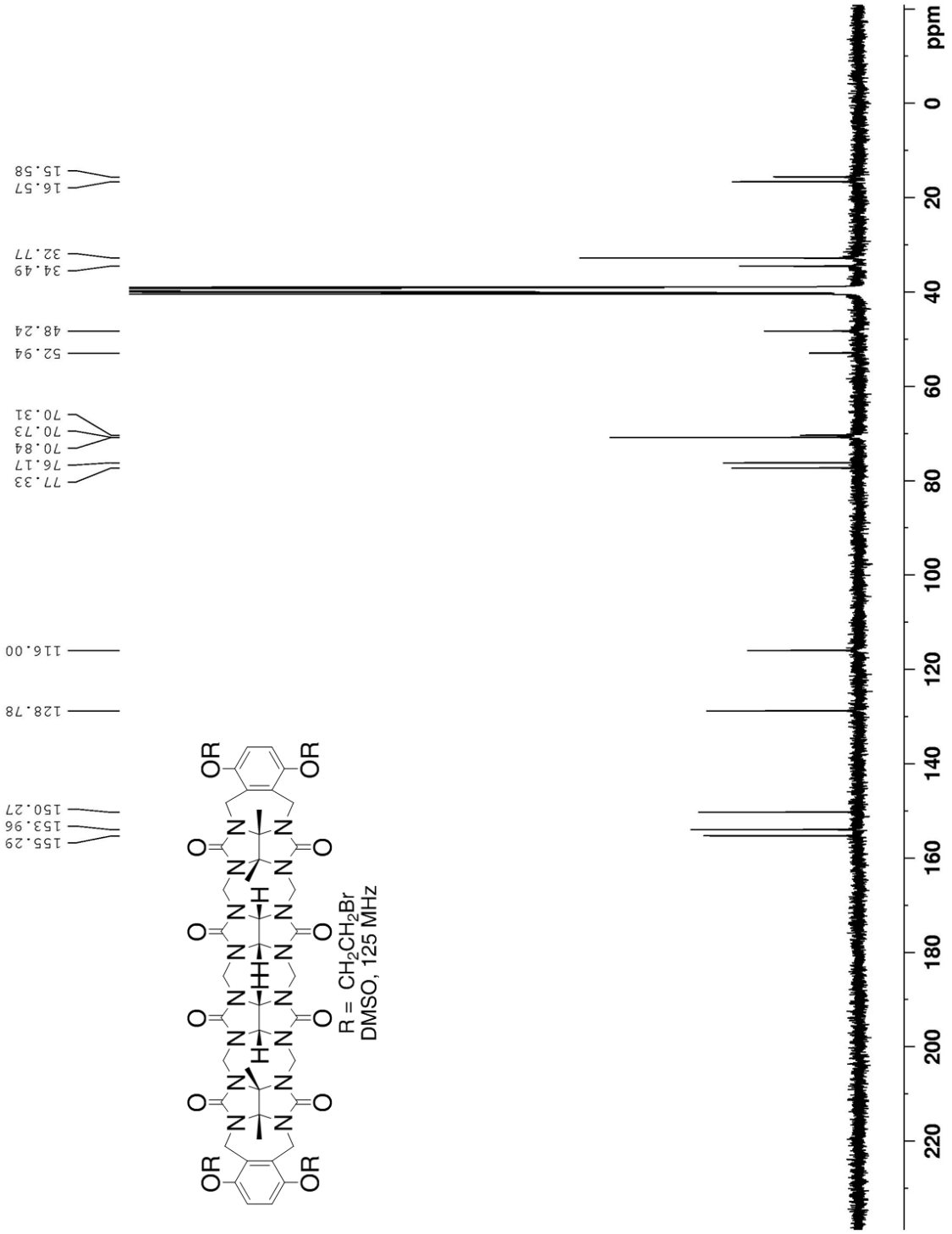

Figure S II-10. ^{13}C NMR spectra (125 MHz, DMSO, RT) recorded for **II-2d**.

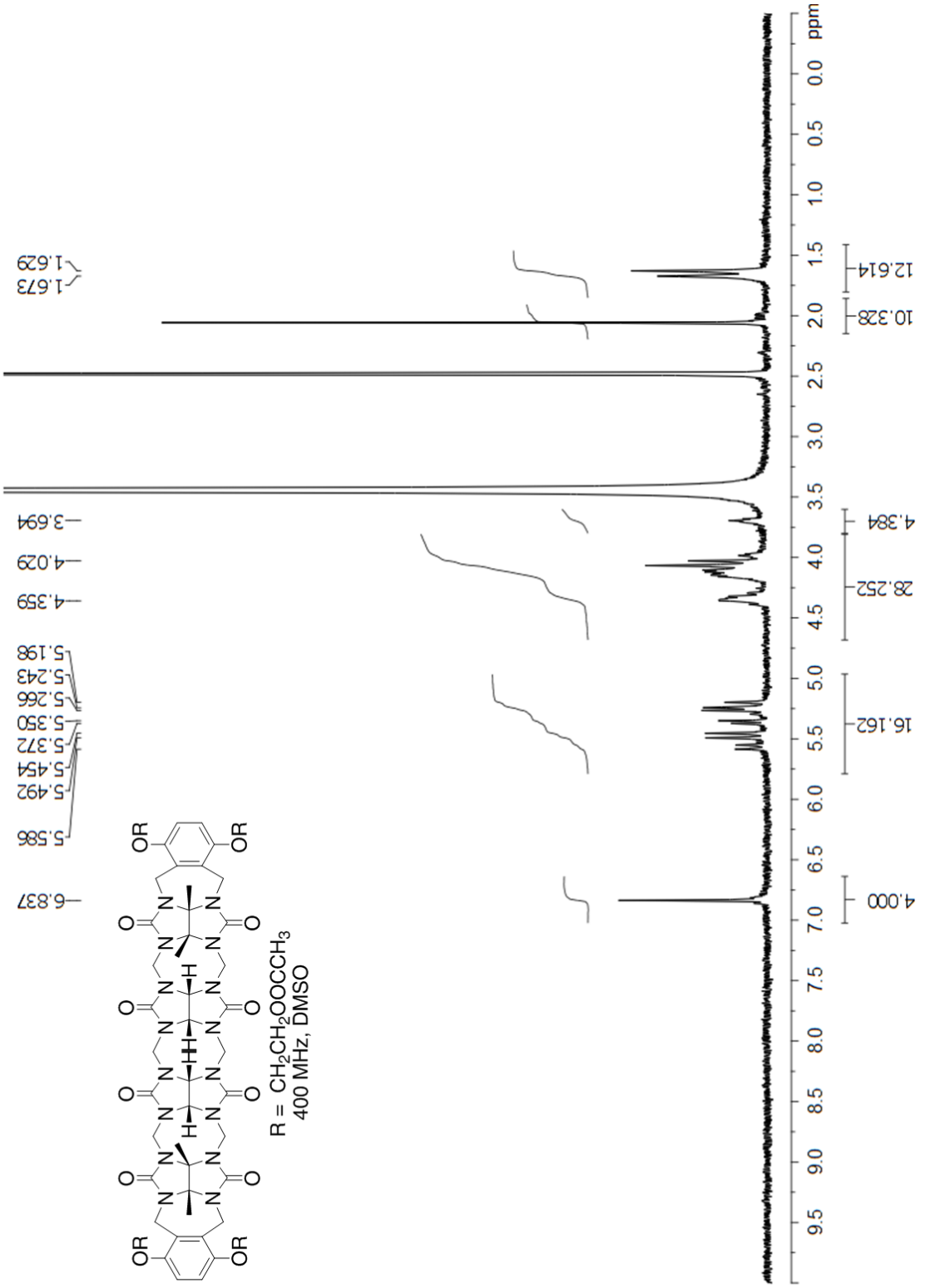

Figure S II-11. ^{1}H NMR spectra (400 MHz, DMSO, RT) recorded for **II-2g**.

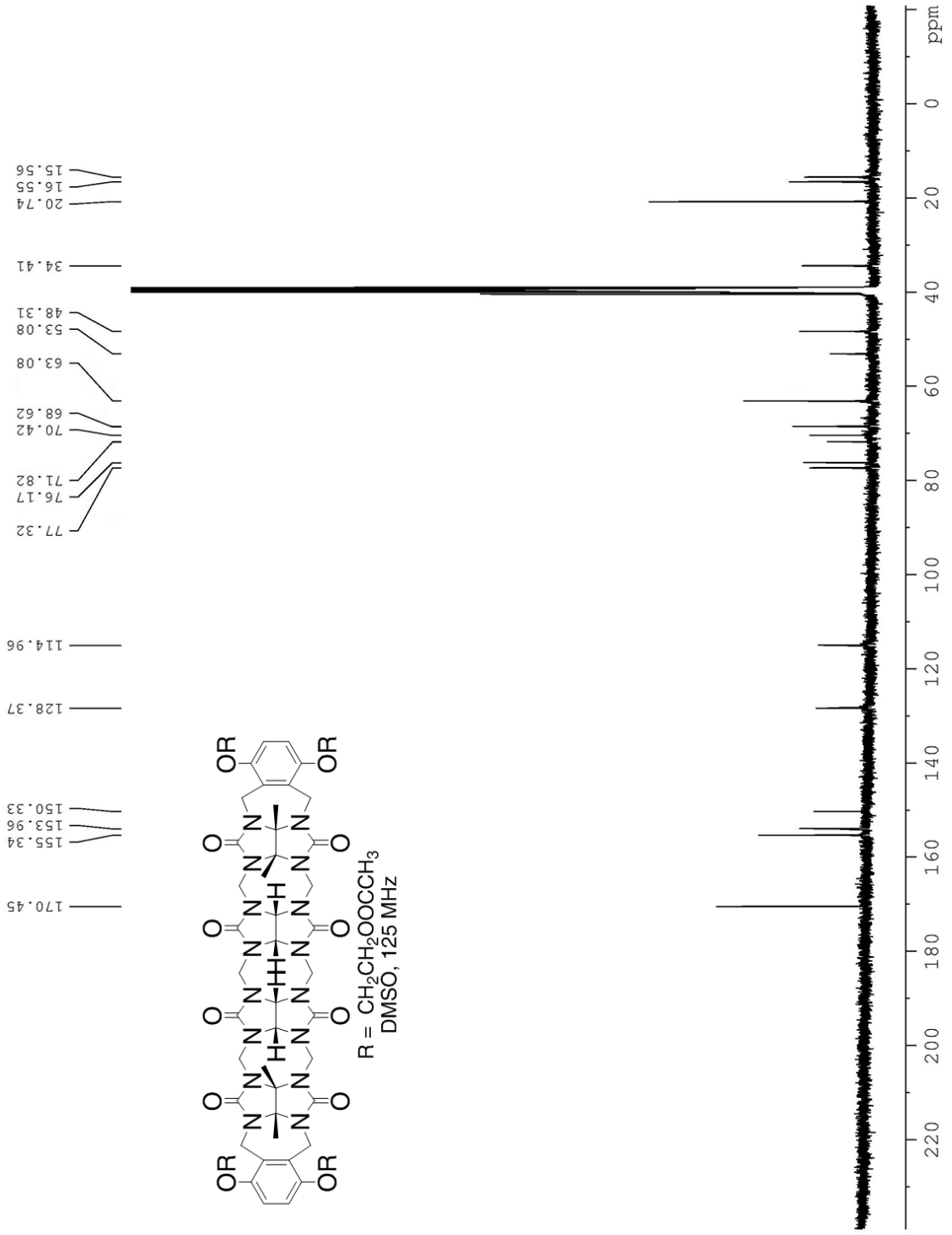

Figure S II-12. ^{13}C NMR spectra (125 MHz, DMSO, RT) recorded for **II-2g**.

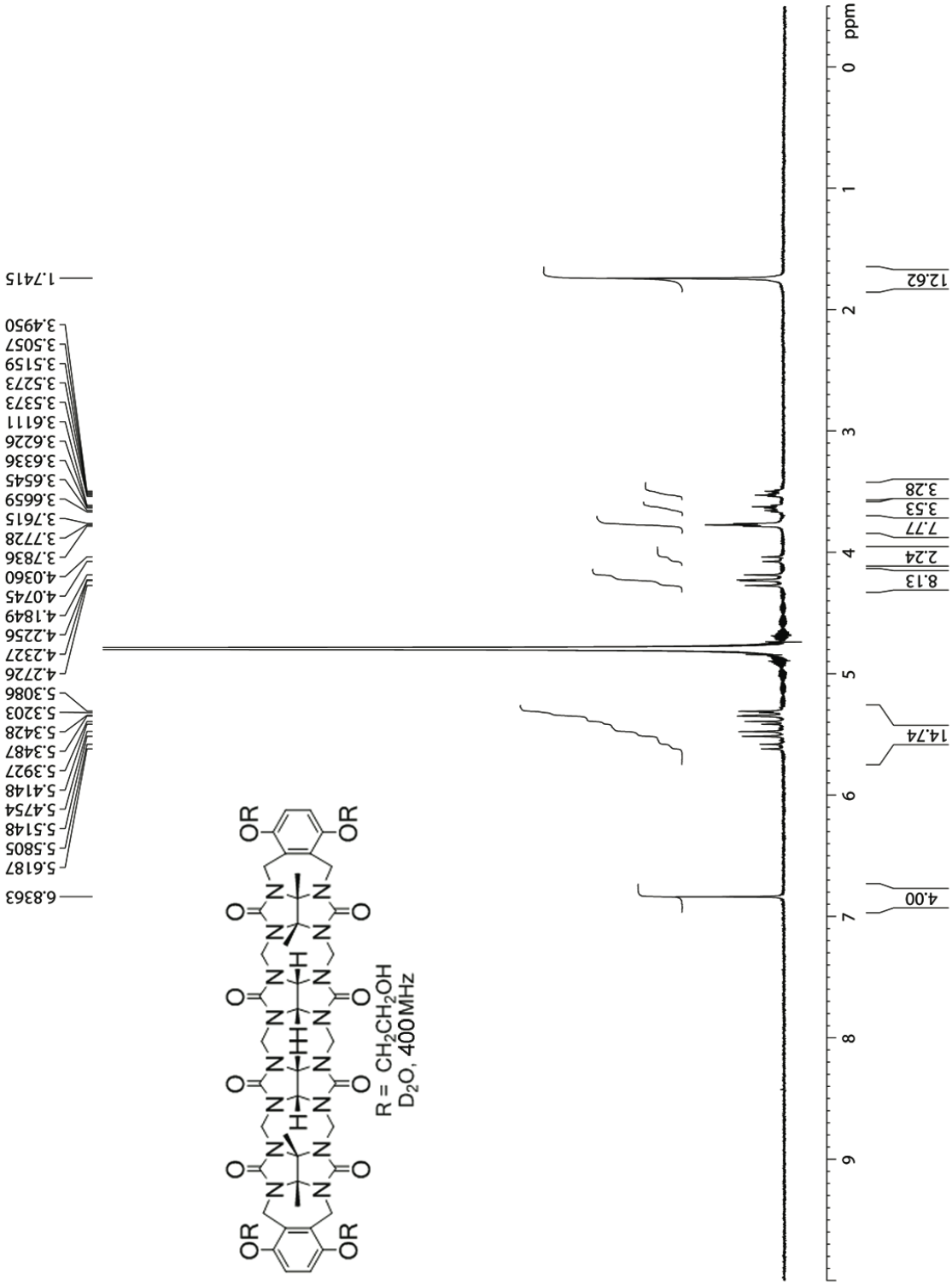

Figure S II-13. ^{1}H NMR spectra (400 MHz, D_2O, RT) recorded for **II-2h**.

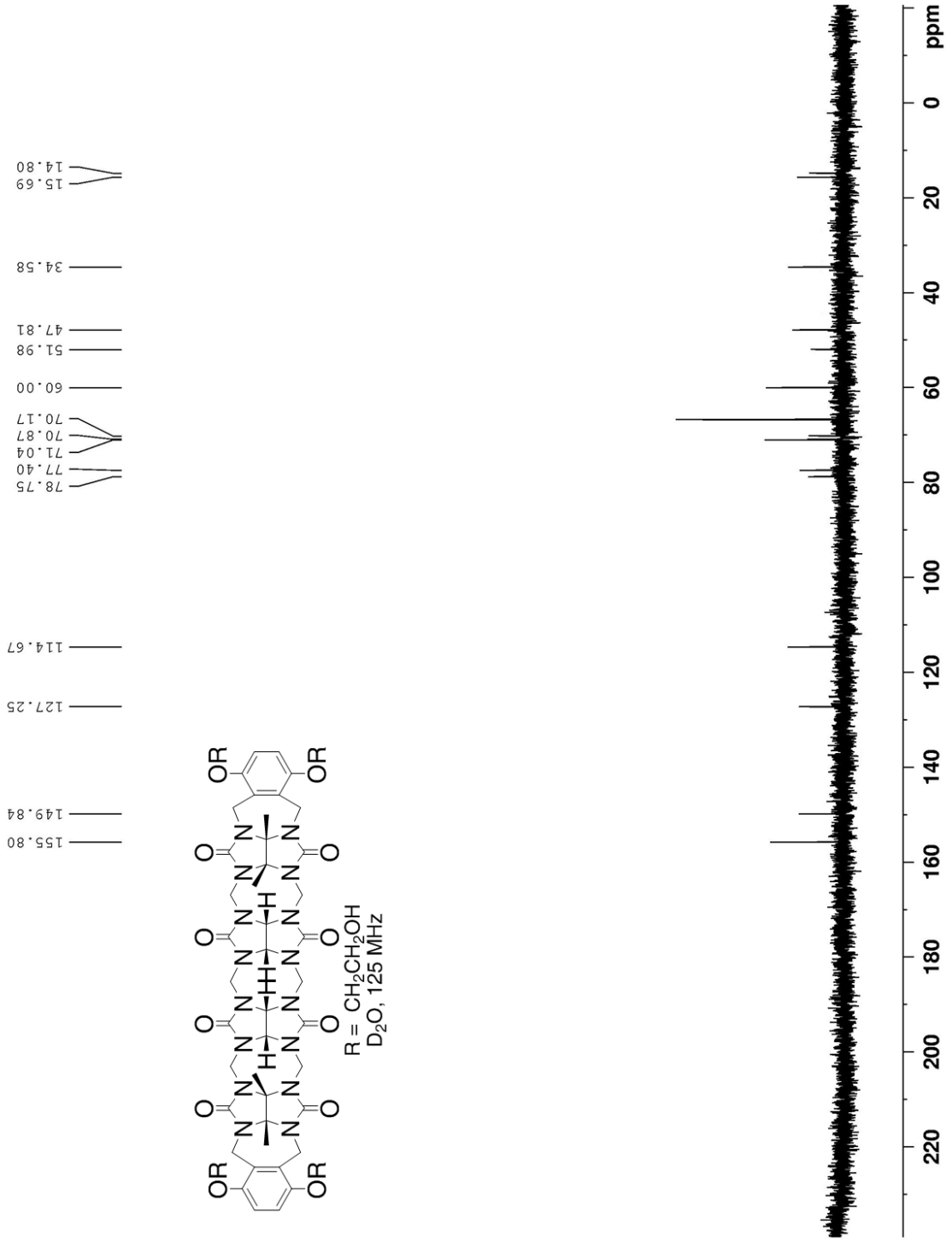

Figure S II-13. ^{13}C NMR spectra (125 MHz, D_2O, RT, 1,4-dioxane as internal reference) recorded for **II-2h**.

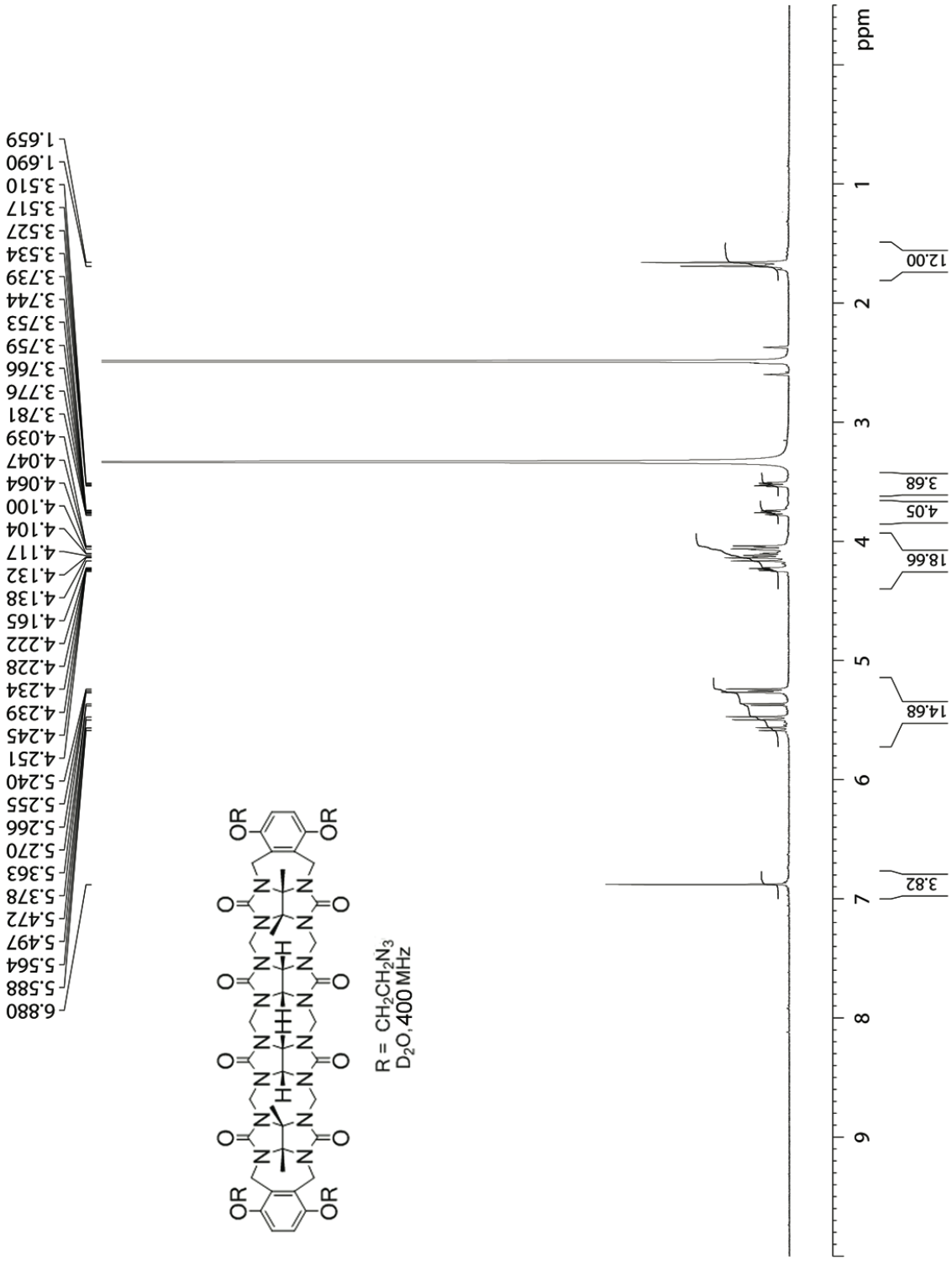

Figure S II-14. ^{1}H NMR spectra (400 MHz, DMSO, RT) recorded for **II-2e**.

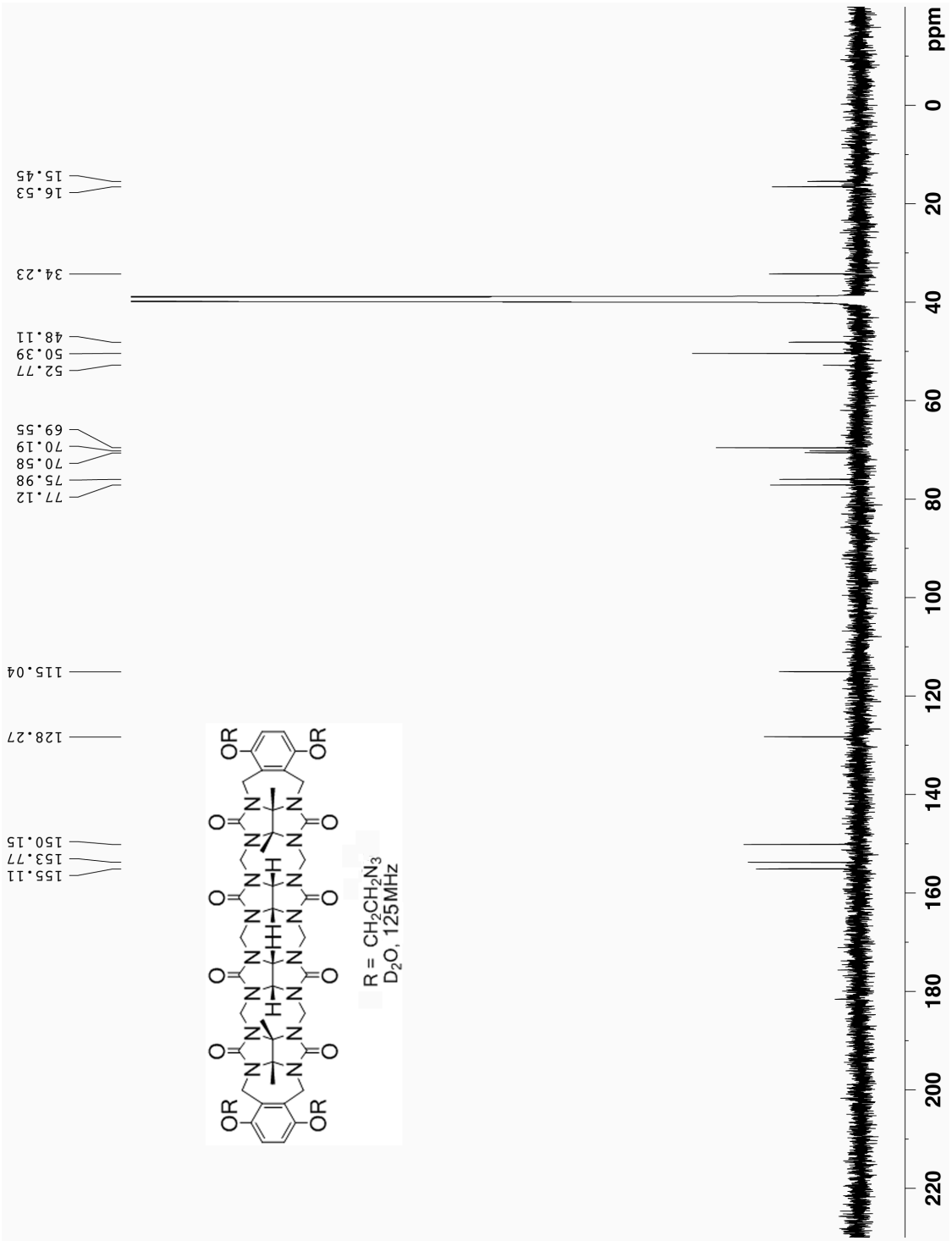

Figure S II-15. ^{13}C NMR spectra (125 MHz, D_2O, RT, 1,4-dioxane as internal reference) recorded for **II-2e**.

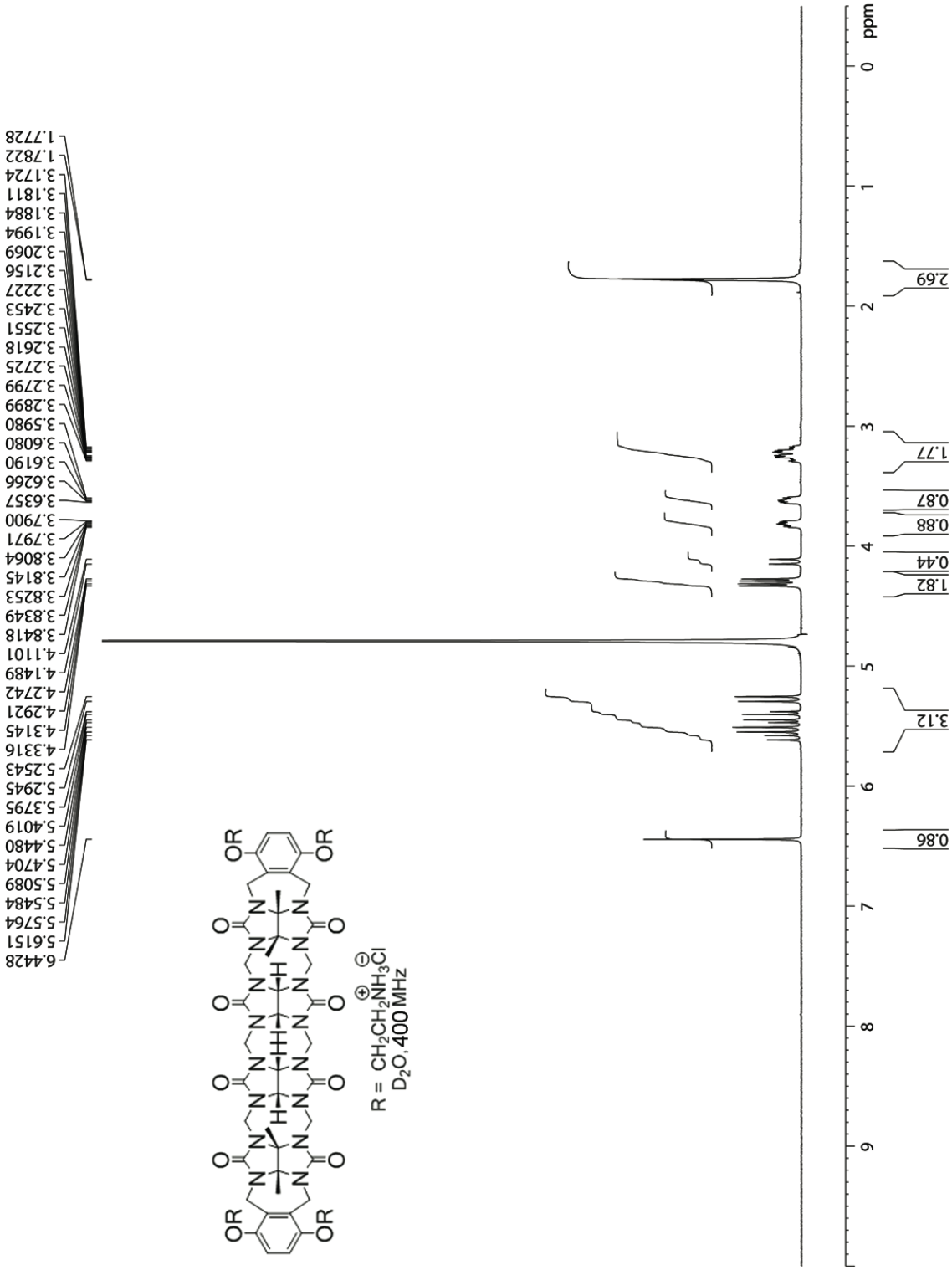

Figure S II-16. ^{1}H NMR spectra (400 MHz, D_2O, RT) recorded for **II-2f**.

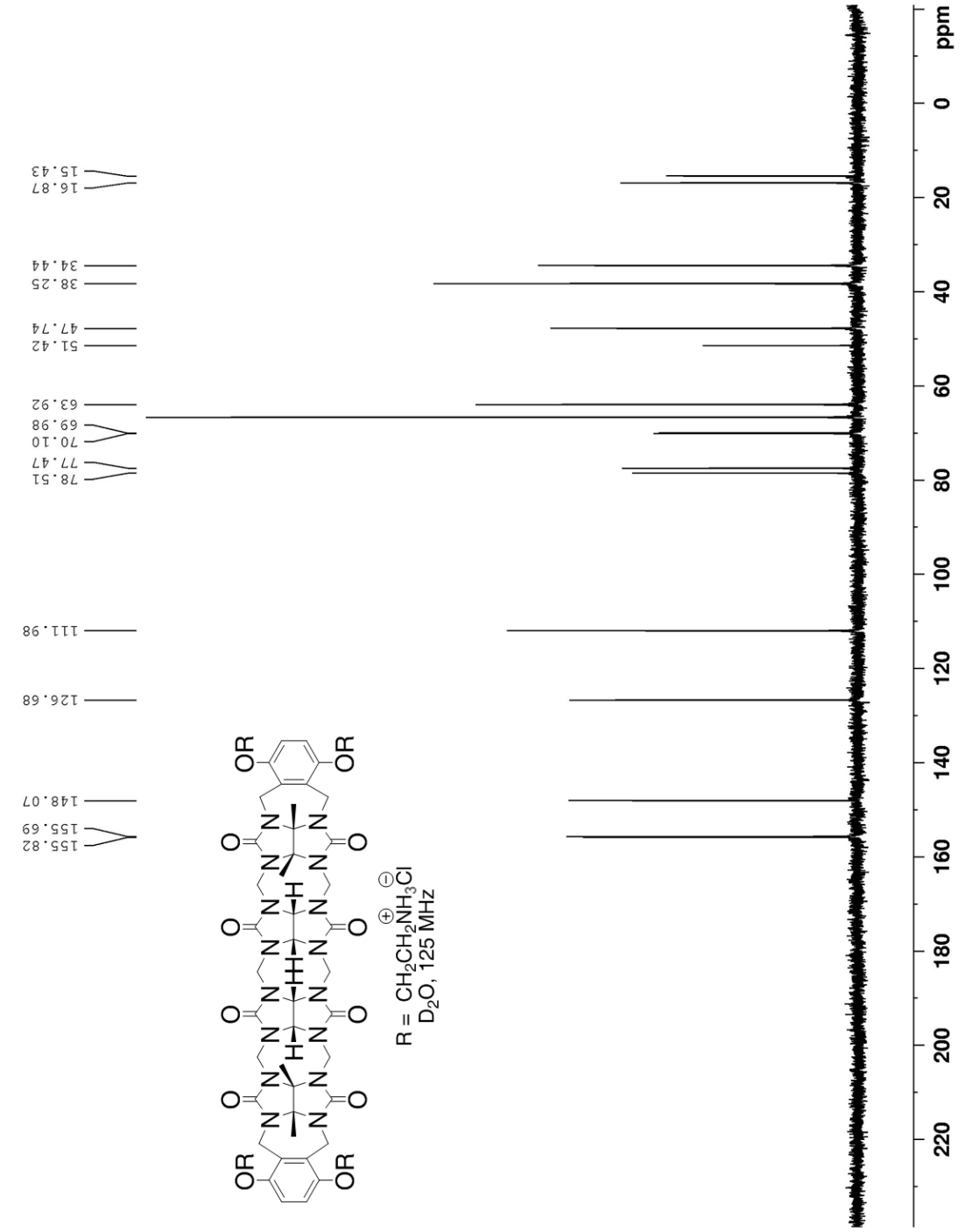

Figure S II-17. ^{13}C NMR spectra (125 MHz, D_2O, RT, 1,4-dioxane as internal reference) recorded for **II-2f**.

Procedure to measure the solubility of drugs with Host II-2a, II-2h and II-2f. Excess amount of drug was added into a solution of host **II-2a**/ **II-2f**/ **II-2h** of known concentration in deuterated sodium phosphate buffer (20 mM, pD = 7.4). The suspended mixture was magnetically stirred at room temperature for 6 h. During this period, the pD value of the solution was monitored and adjusted back to 7.4 if it changed. The mixture was then centrifuged twice (4200 rpm, 10 min). The 1H NMR spectrum of the supernatant was measured (400 MHz) with 1,3,5-benzenetricarboxylic acid (1.03 mM) as internal standard. The signal for the reference shows up at 8.35 ppm (s, 3H). Diagnostic signals for the dissolved drug were also integrated. From the ratio of integrations of reference peak relative to the drug peak, and the concentration of reference, the concentration of the drug can be calculated.

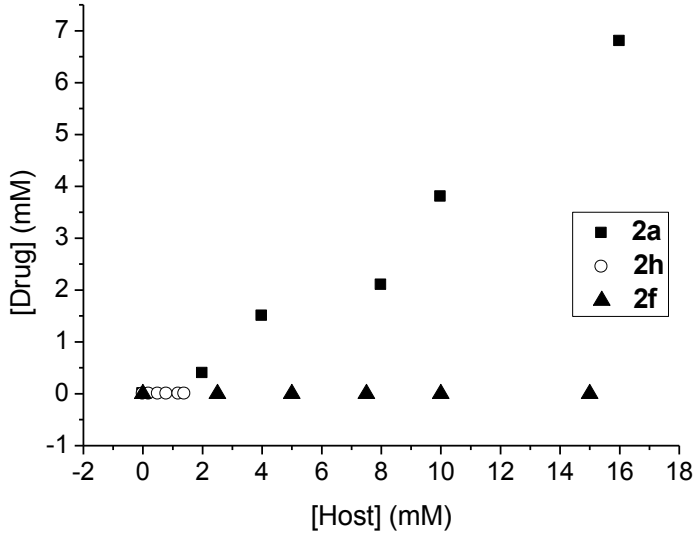

Figure S II-18. Phase diagram of mixtures of indomethacin and host **II-2a**, **II-2f** and **II-2h**, in 20 mM sodium phosphate buffer (pH = 7.4).

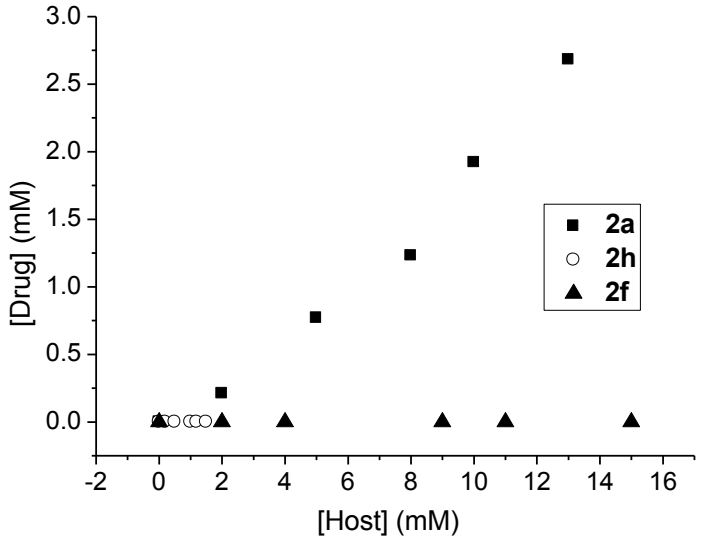

Figure S II-19. Phase diagram of mixtures of 17α-ethynylestradiol and host **II-2a**, **II-2f** and **II-2h**, in 20 mM sodium phosphate buffer (pH = 7.4).

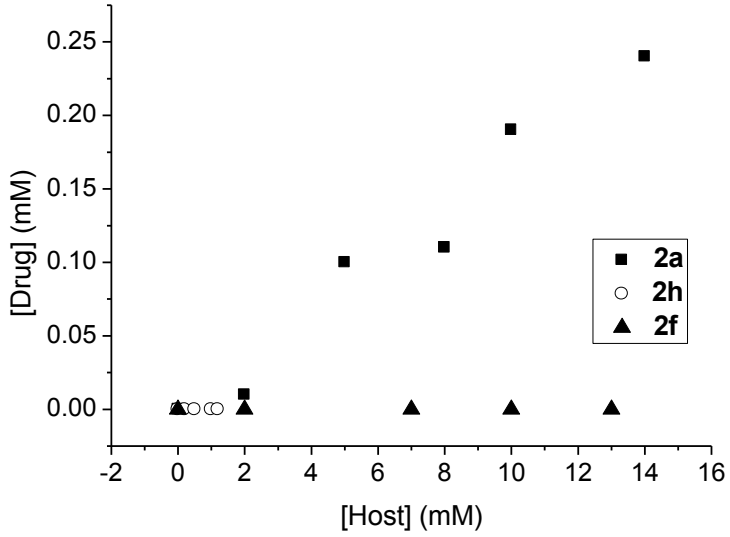

Figure S II-20. Phase diagram of mixtures of tamoxifen and host **II-2a**, **II-2f** and **II-2h**, in 20 mM sodium phosphate buffer (pH = 7.4).

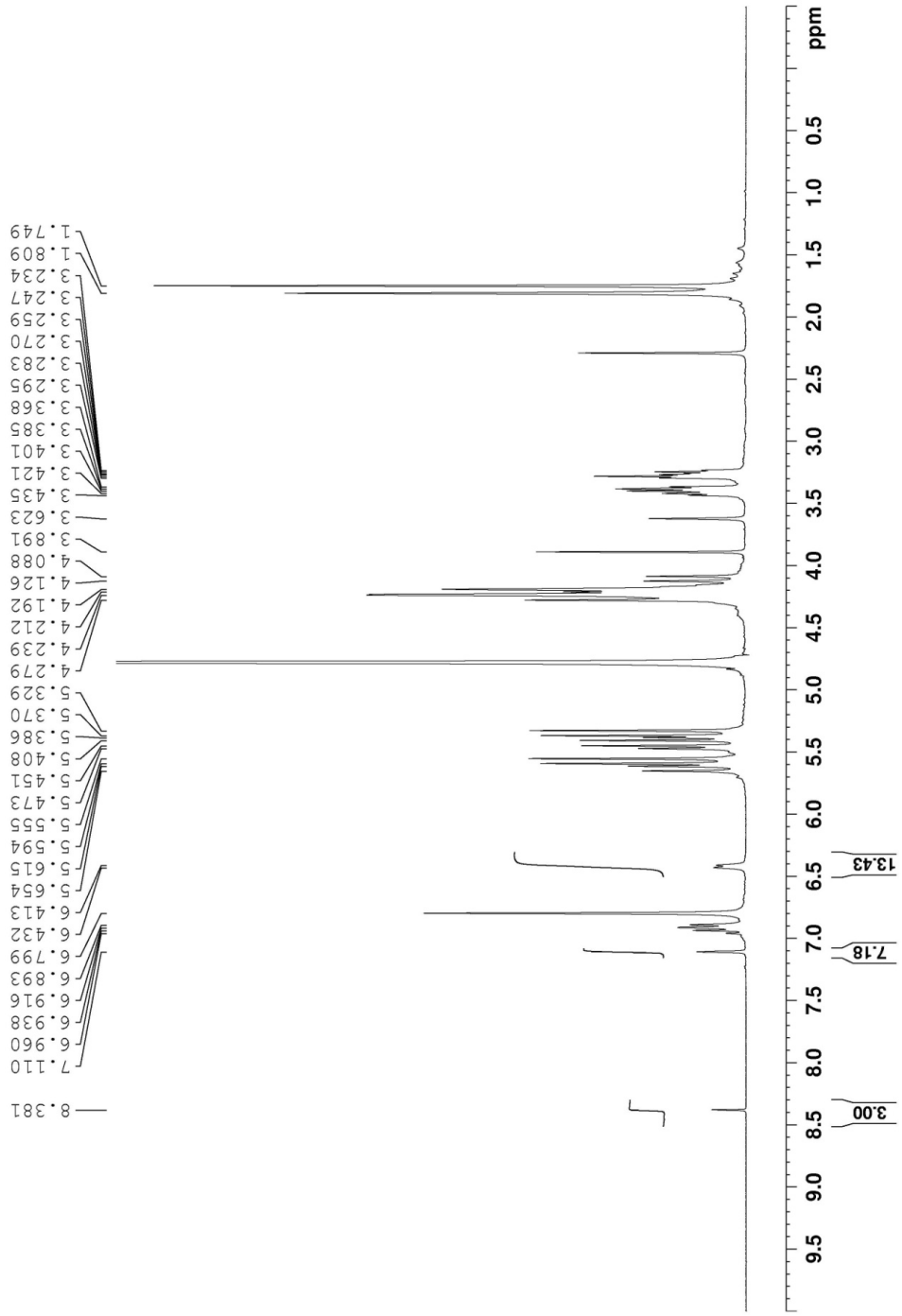

Figure S II-21. ^{1}H NMR recorded for pharmaceutical agent indomethacin with **II-2a** (16 mM) (400 MHz, 20 mM NaD_2PO_4, pD = 7.4, RT, 1,3,5-benzenetricarboxylic acid as reference).

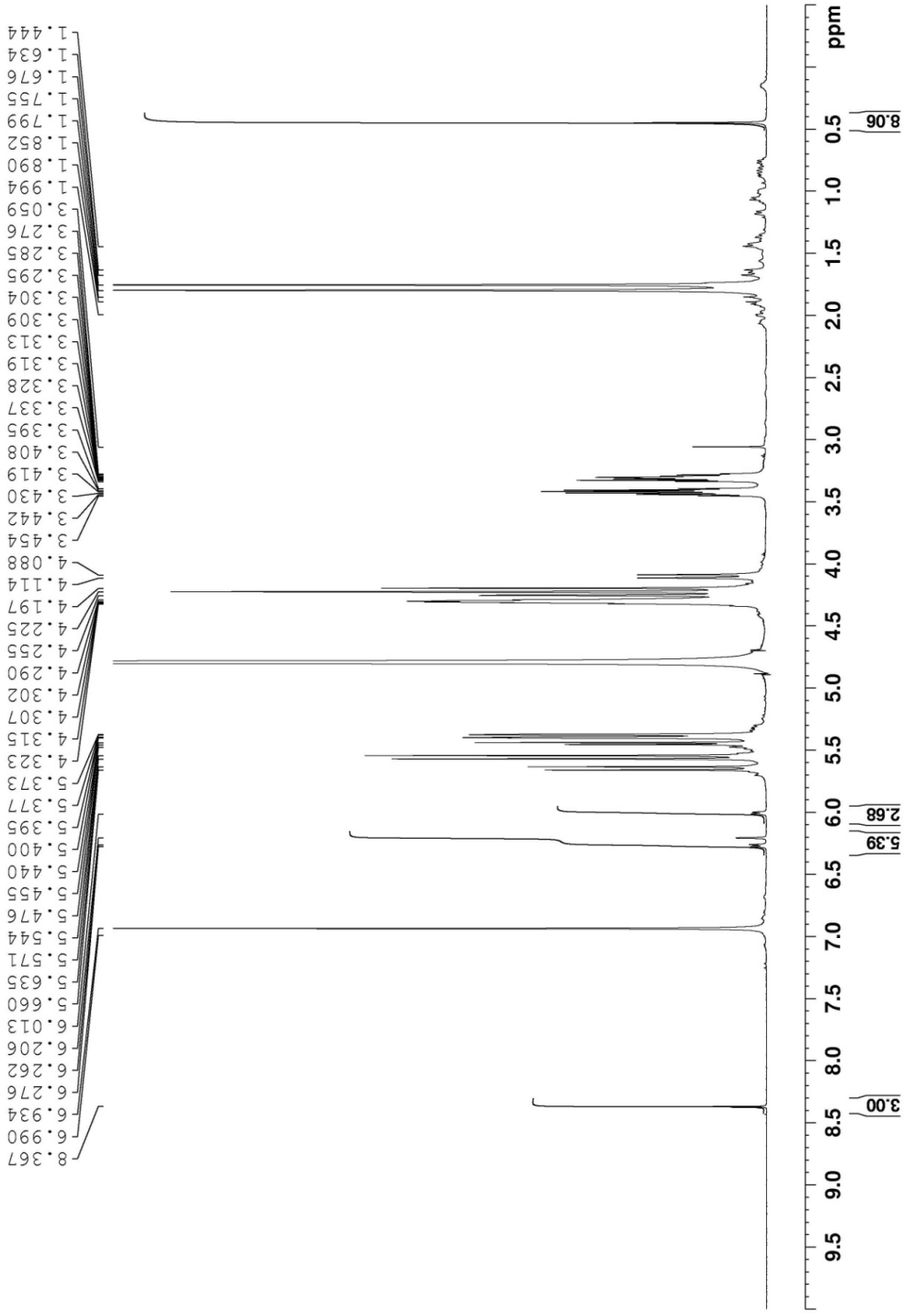

Figure S II-22. ^{1}H NMR recorded for pharmaceutical agent 17α-ethynylestradiol with **II-2a** (13 mM) (400 MHz, 20 mM NaD_2PO_4, pD = 7.4, RT, 1,3,5-benzenetricarboxylic acid as reference).

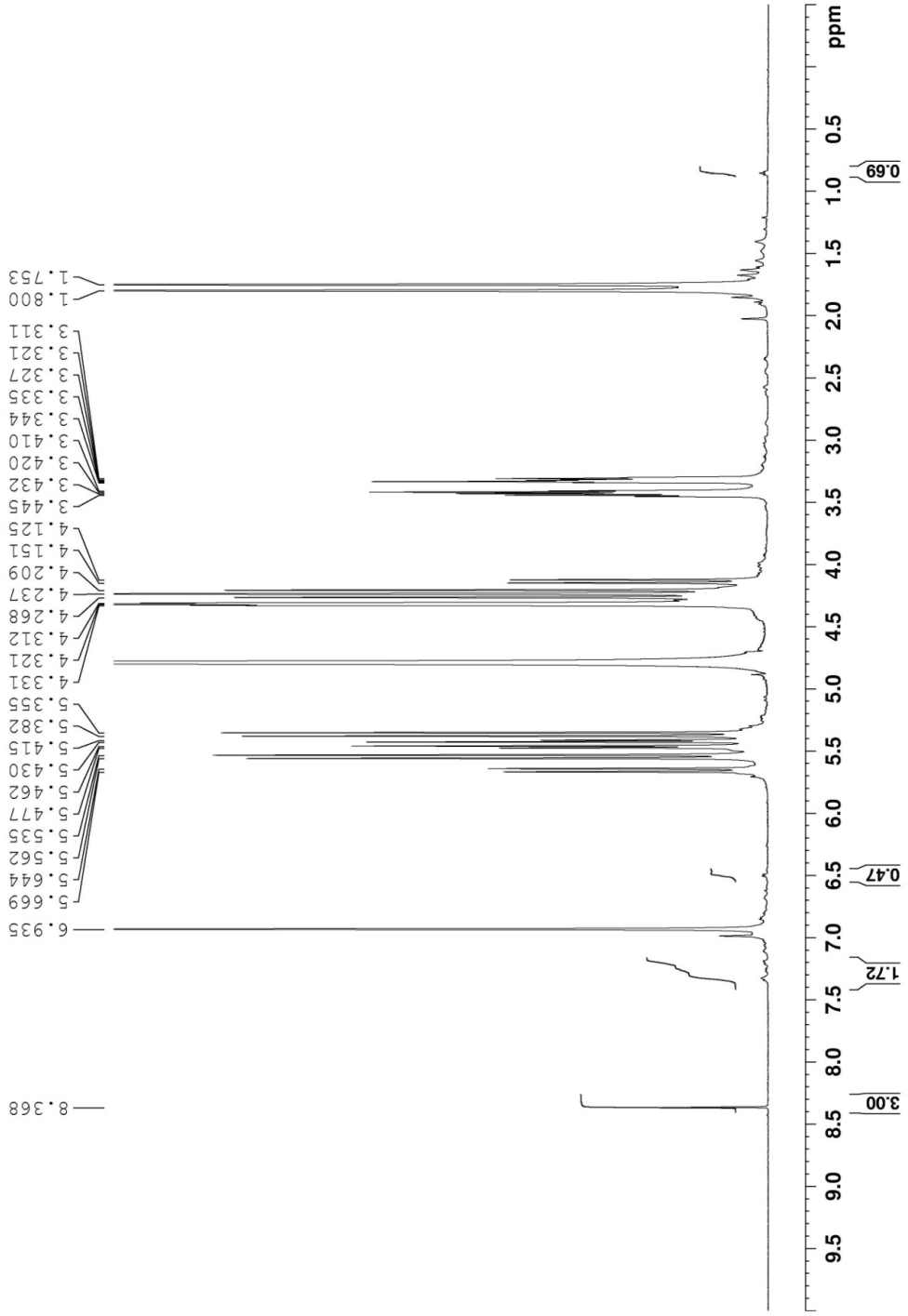

Figure S II-23 ^{1}H NMR recorded for pharmaceutical agent tamoxifen with **II-2a** (14 mM) (400 MHz, 20 mM NaD_2PO_4, pD = 7.4, RT, 1,3,5-benzenetricarboxylic acid as reference).

Determination of K_a Between Host II-2a – II-2h and Various Compounds. In this work, ^{1}H NMR and UV/Vis spectroscopic methods were used in order to determine the K_a values for various host•guest complexes. ^{1}H NMR spectroscopic method can measure K_a values up to 10^4 M^{-1} but for measurements of higher binding constants we need to use UV/Vis titration. The K_a value of hosts **II-2a** – **II-2c** with dye **II-4** was obtained from direct UV/Vis titrations of fixed concentration of the dye by fitting the change of absorbance *versus* the concentration of host to a 1:1 binding model. Then dye **II-4** was used as an indicator in the displacement assays to measure the binding constants of host **II-2a** – **II-2c** towards guest **II-5a**, **II-5b** and guest **II-6** by fitting the change of absorbance *versus* the concentration of guest to a competitive binding model. Similarly, the binding constant between host **II-2h** and dye **II-8** was determined by direct UV/Vis titration and K_a values between host **II-2h** and guest **II-6** was determined by indicator displacement assays with dye **II-8** as the indicator. Binding constants of **II-2a, II-2h and II-2f** toward guest **II-5c** , **II-2b** toward **II-5b**, and **II-2h** toward **II-5a** and **II-5b** are determined by direct ^{1}H NMR titration and the chemical shift change versus the change of concentration was fitted to a 1:1 binding model to give K_a values. The binding constant between **II-2f** and **II-5c** was also determined by ^{1}H NMR methods. The host•guest complex has a slow exchange on ^{1}H NMR, and the concentrations of free host, free guest, binding host, binding guest can be determined by the ratio of the integrals of their own NMR signals. The concentration was then used to calculate the binding constant of **II-2f** towards guest **II-5c**

Binding Models Used to Determine Values of Ka with Micromath Scientist

1:1 Binding Model (NMR).

// Micromath Scientist Model File

// 1:1 Host:Guest binding model for NMR

//This model assumes the guest concentration is fixed and host concentration is varied

IndVars: ConcHostTot

DepVars: Deltaobs

Params: Ka, ConcGuestTot, Deltasat, Deltazero

Ka = ConcHostGuest/(ConcHostFree*ConcGuestFree)

ConcHostTot=ConcHostFree + ConcHostGuest

ConcGuestTot=ConcGuestFree + ConcHostGuest

Deltaobs = Deltazero + (Deltasat - Deltazero) * (ConcHostGuest/ConcGuestTot)

//Constraints

0 < ConcHostFree < ConcHostTot

0 < Ka

0 < ConcGuestFree < ConcGuestTot

0 < ConcHostGuest < ConcHostTot

1:1 Binding Model (UV/Vis).

// Micromath Scientist Model File

// 1:1 Host:Guest binding model

//This model assumes the guest concentration is fixed and host concentration is varied

IndVars: ConcHostTot

DepVars: SpectroscopicSignal

Params: Ka, ConcGuestTot, SpectroscopicSignalMin, SpectroscopicSignalMax

Ka = ConcHostGuest/(ConcHostFree*ConcGuestFree)

ConcHostTot=ConcHostFree + ConcHostGuest

ConcGuestTot=ConcGuestFree + ConcHostGuest

SpectroscopicSignal = SpectroscopicSignalMin + (SpectroscopicSignalMax -

SpectroscopicSignalMin) * (ConcHostGuest/ConcGuestTot)

//Constraints

0 < ConcHostFree < ConcHostTot

0 < Ka

0 < ConcGuestFree < ConcGuestTot

0 < ConcHostGuest < ConcHostTot

Competitive Binding (Indicator Displacement) Model.

// MicroMath Scientist Model File

IndVars: ConcAntot

DepVars: Absorb

Params: ConcHtot, ConcGtot, Khg, Kha, AbsorbMax, AbsorbMin

Khg = ConcHG / (ConcH * ConcG)

Kha = ConcHAn / (ConcH * ConcAn)

Absorb = AbsorbMin + (AbsorbMax-AbsorbMin)*(ConcHG/ConcGtot)

ConcHtot = ConcH + ConcHG + ConcHAn

ConcGtot = ConcHG + ConcG

ConcAntot = ConcAn + ConcHAn

0 < ConcHG < ConcHtot

0 < ConcH < ConcHtot

0 < ConcG < ConcGtot

0 < ConcAn < ConcAntot

(A)

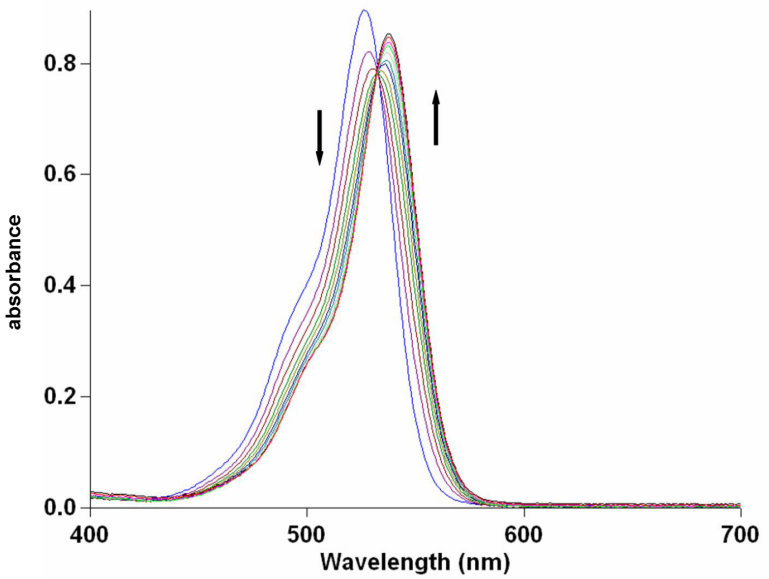

(B)

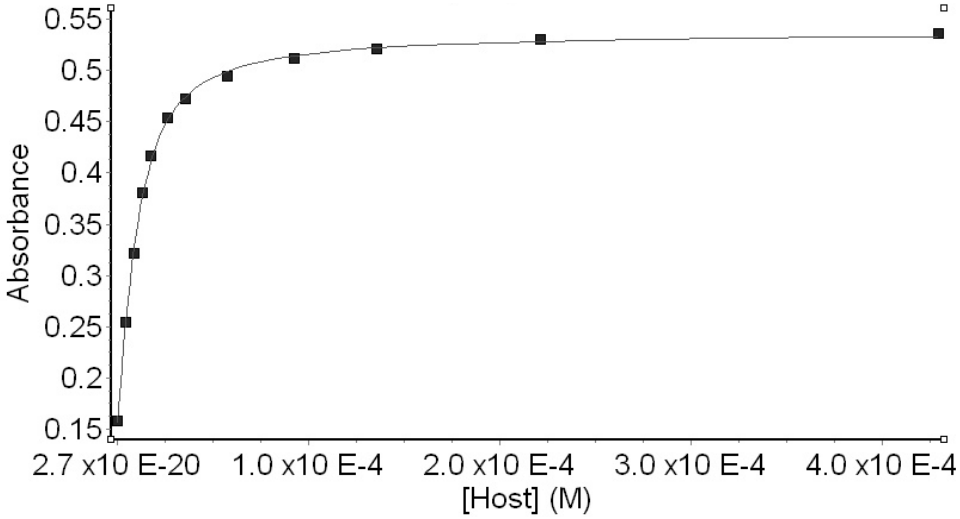

Figure S II-24. (A) UV/Vis spectra from the titration of dye **4** (10.0 μM) with **II-2a** (0 – 480 μM) in 20 mM NaH_2PO_4 buffer (pH 7.4); (B) plot of the ΔA550 as a function of **II-2a** concentration. The solid line represents the best non-linear fit of the data to a 1:1 binding model (K_a = 1.83 (± 0.08) × 10^5 M^{-1}).

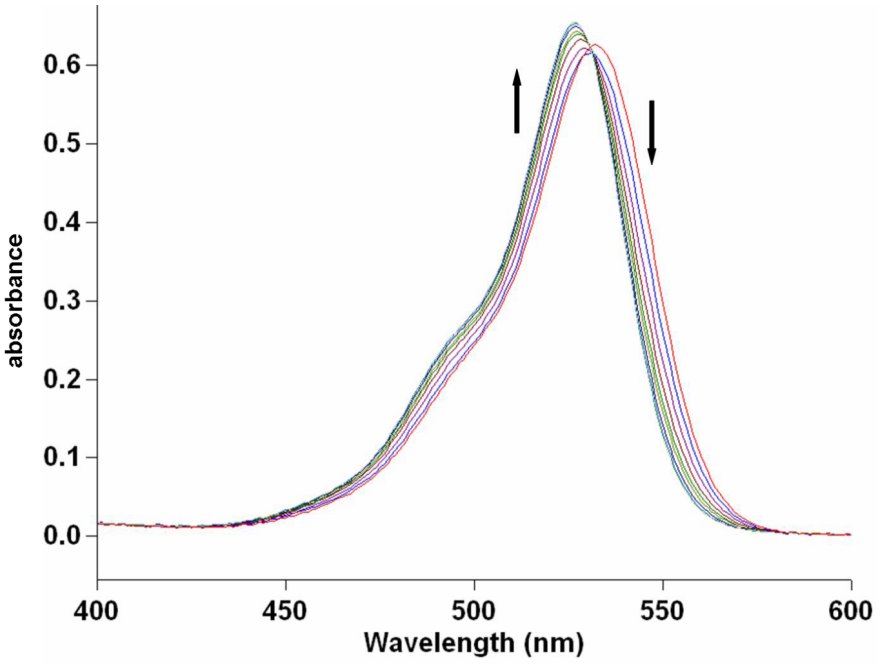

(A)

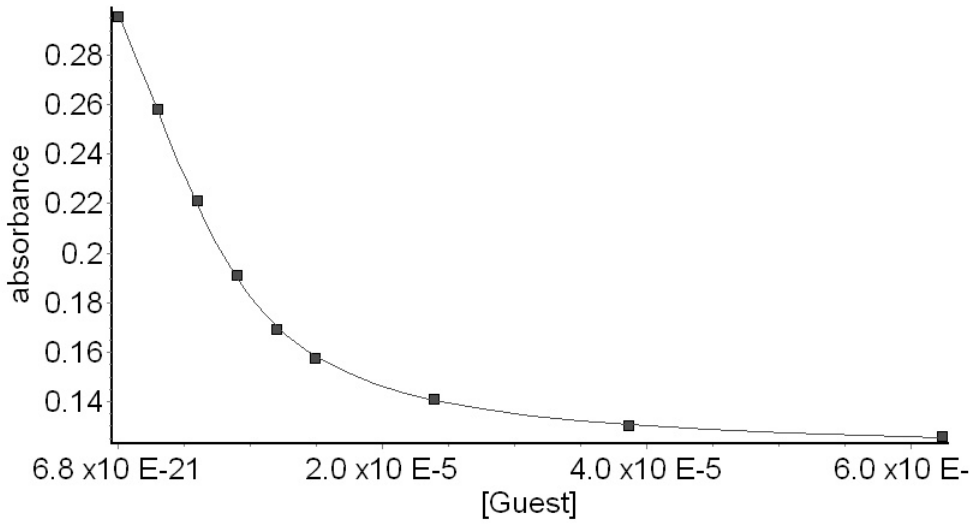

(B)

Figure S II-25. (A) Displacement titration of a solution of dye **II-4** (10.0 μM) and host **II-2a** (9.15 μM) solution with **II-5a** (0 – 65 μM) (20 mM NaH_2PO_4 buffer, pH 7.4). (B) Non-linear fitting plot of absorbance at 550 nm *versus* concentration for the displacement titration of **II-5a** using a model implemented in Scientist™. K_a was evaluated as 1.68 (± 0.09) × 10^6 M^{-1}.

(A)

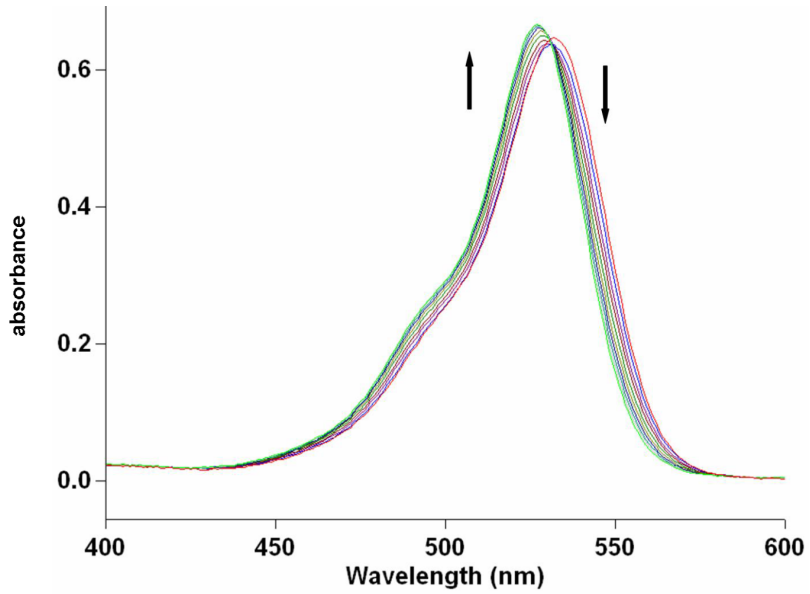

(B)

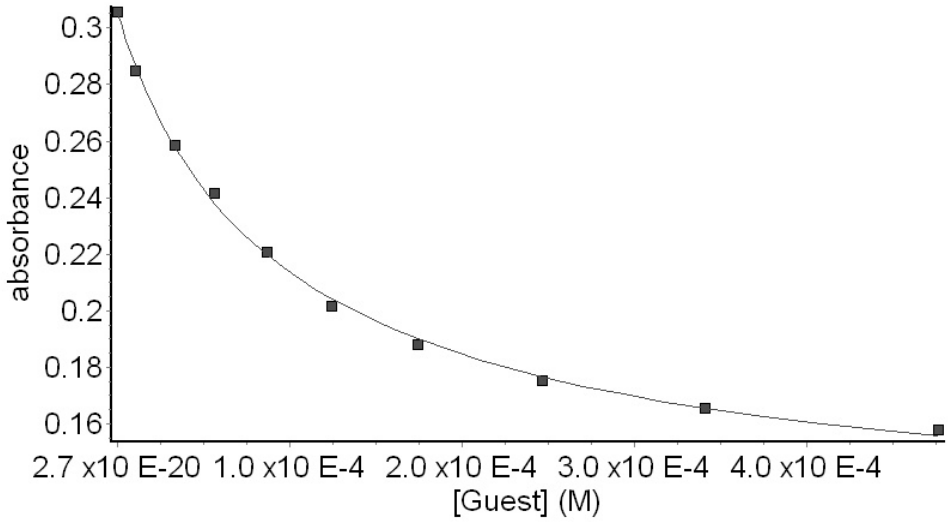

Figure S II-26. (A) Displacement titration of a solution of dye **II-4** (10.0 μM) and host **II-2a** (9.15 μM) solution with **II-5b** (0 – 480 μM) (20 mM NaH_2PO_4 buffer, pH 7.4). (B) Non-linear fitting plot of absorbance 550 nm *versus* concentration for the displacement titration of **II-5b** using a model implemented in Scientist™. K_a was evaluated as 4.47 (± 0.34) × 10^4 M^{-1}.

(A)

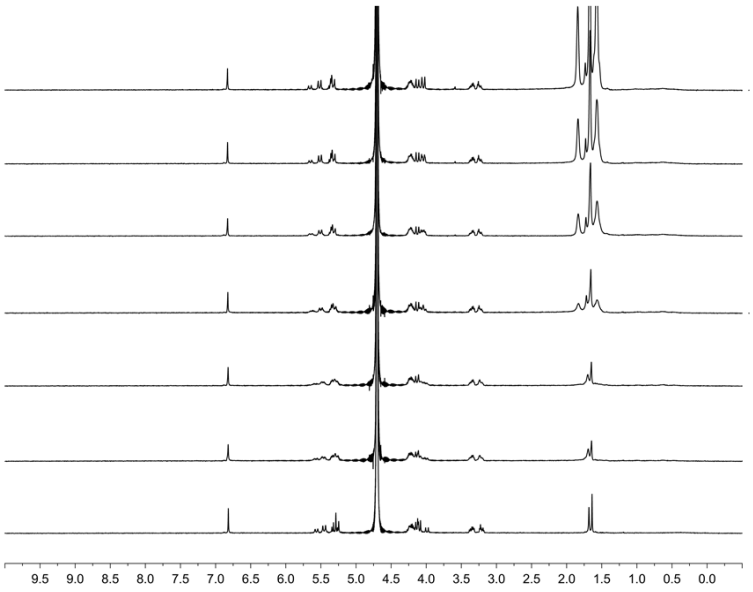

(B)

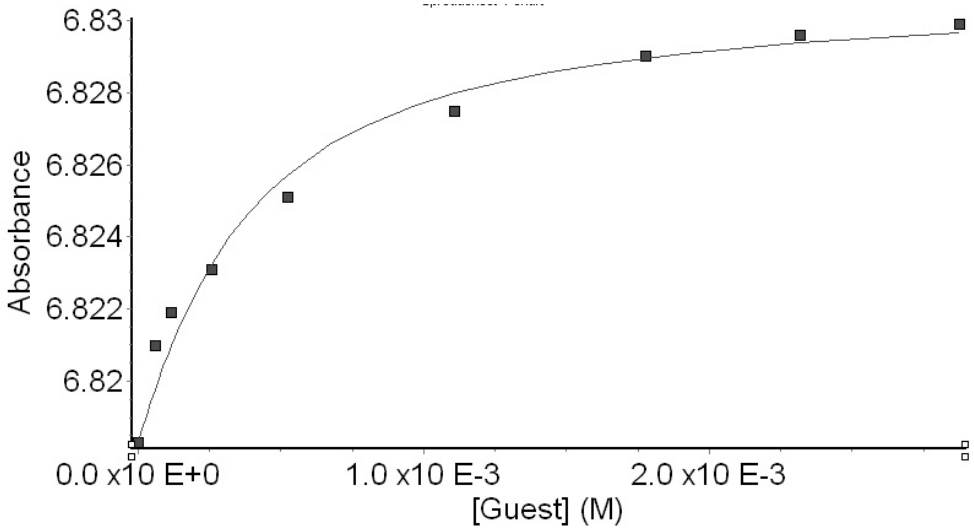

Figure S II-27. (A) ^{1}H NMR spectra (400 MHz, 20 mM sodium phosphate buffer, pD = 7.4) recorded for a solution of **II-2a** (181 μM) and **II-5c** of variable concentrations (0 – 3.1 mM). (B) Plot of the chemical shift of the aromatic proton of **II-2a** as a function of **II-5c** concentration. The solid line represents the best non-linear fitting of the data to a 1:1 binding model (K_a = 3.50 (± 0.83) × 10^3 M^{-1}).

(A)

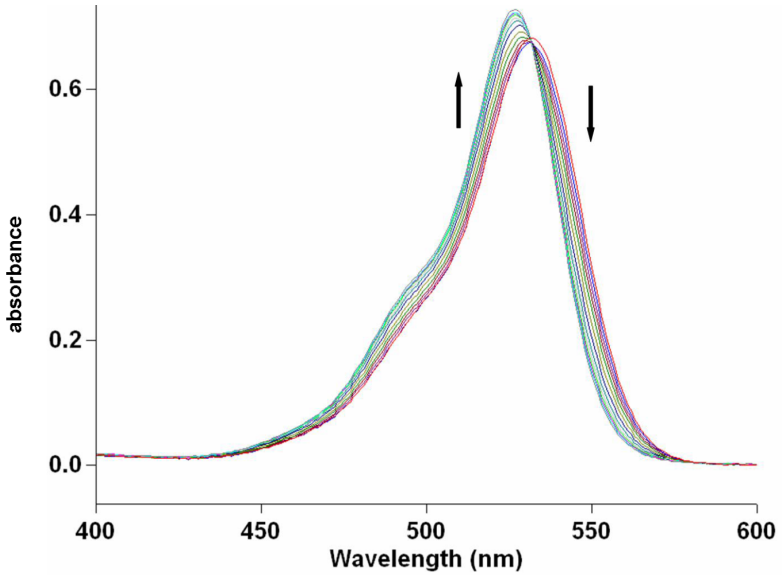

(B)

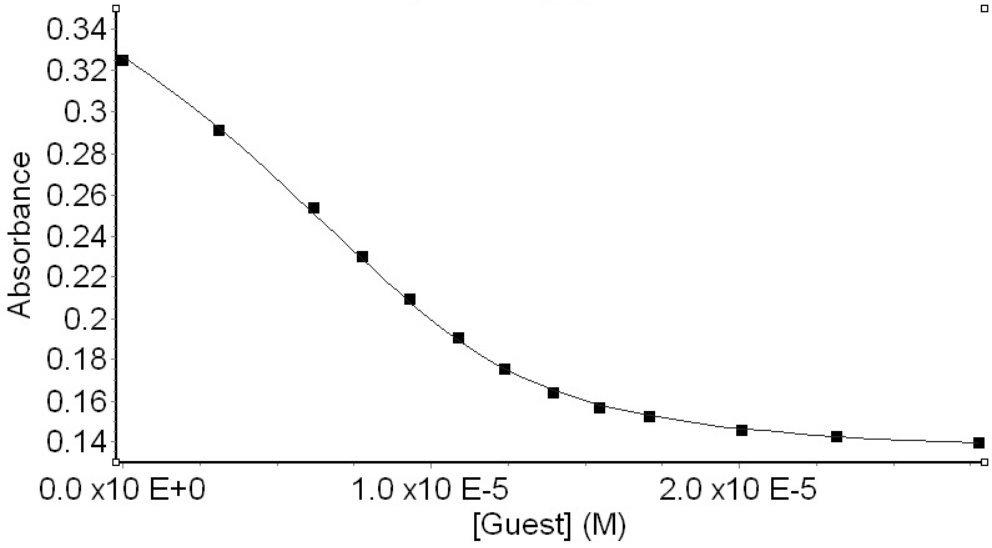

Figure S II-28. (A) Displacement titration of a solution of dye **II-4** (10.0 μM) and host **II-2a** (9.15 μM) solution with **II-6** (0 – 32 μM) (20 mM NaH_2PO_4 buffer, pH 7.4). (B) Non-linear fitting plot of absorbance at 550 nm *versus* concentration for the displacement titration of **II-6** using a model implemented in Scientist™. K_a was evaluated as 4.59 (± 0.44) × 10^6 M^{-1}.

(A)

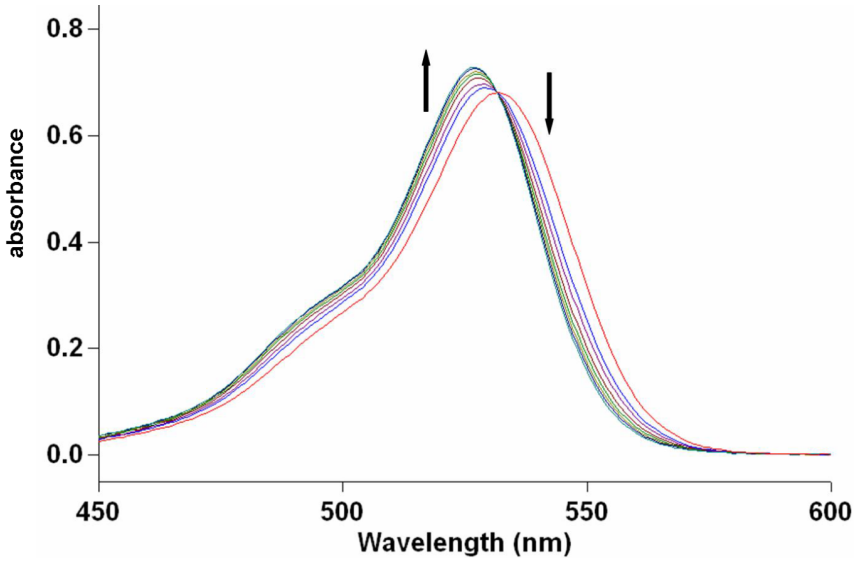

(B)

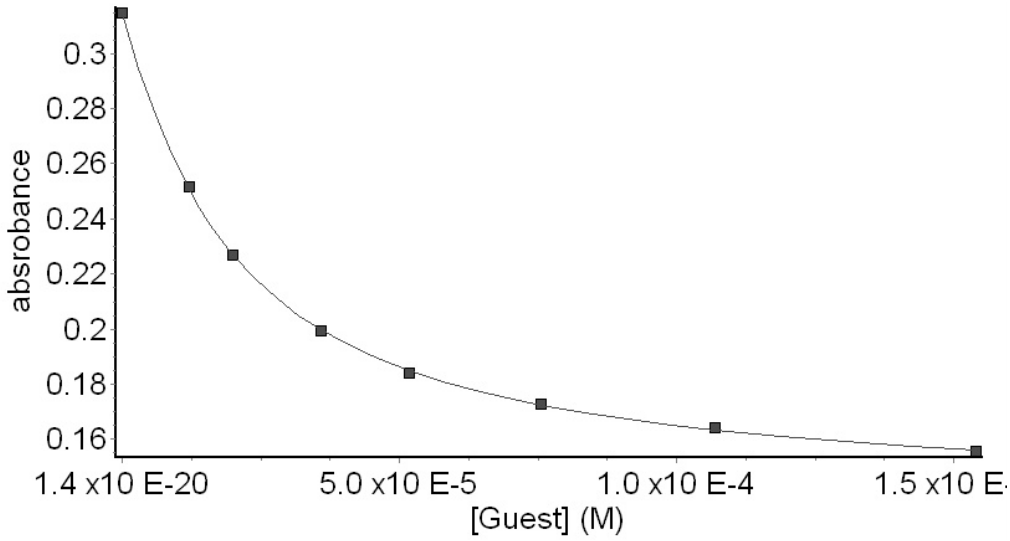

Figure S II-29. (A) Displacement titration of a solution of dye **II-4** (10.0 μM) and host **II-2a** (9.15 μM) solution with **7** (0 – 32 μM) (20 mM NaH_2PO_4 buffer, pH 7.4). (B) Non-linear fitting plot of absorbance at 550 nm *versus* concentration for the displacement titration of **II-7** using a model implemented in Scientist™. K_a was evaluated as 2.74 (± 0.06) × 10^5 M^{-1}.

(A)

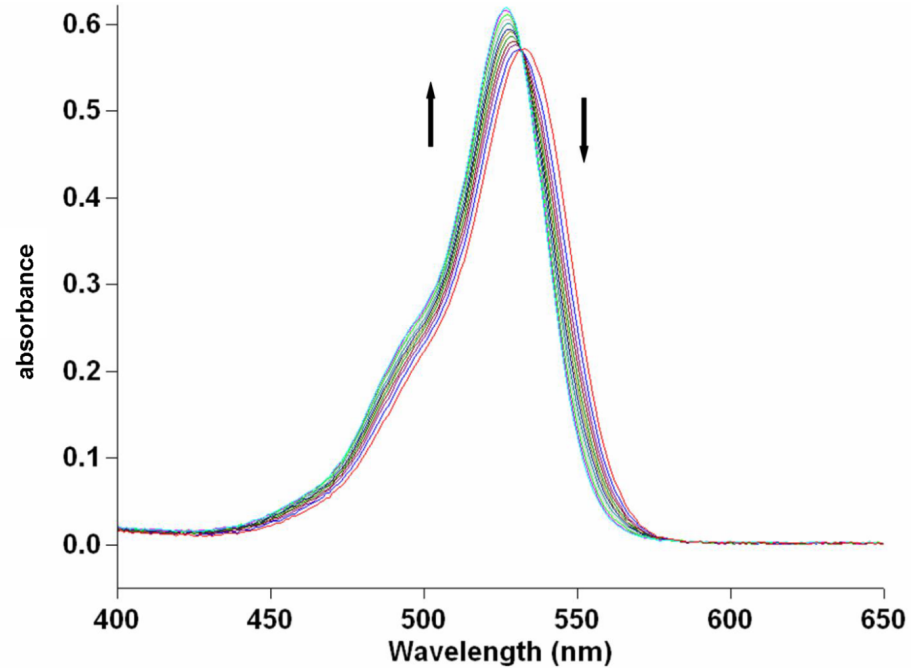

(B)

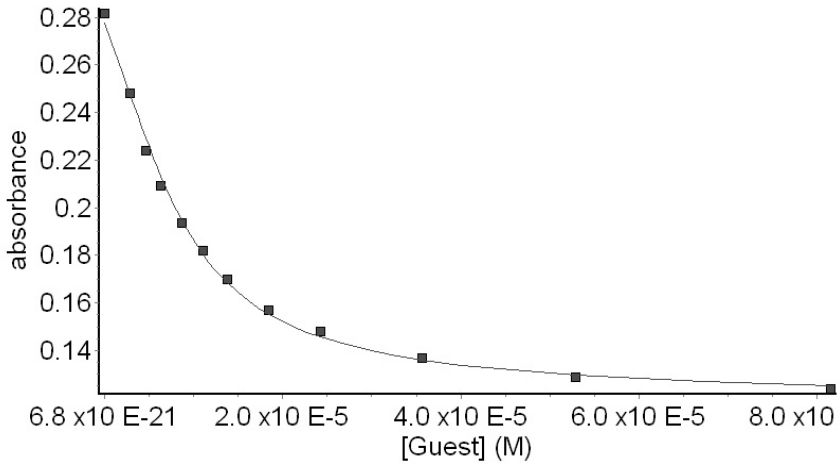

Figure S II-30. (A) Displacement titration of a solution of dye **II-4** (10.0 μM) and host **II-2b** (9.18 μM) solution with **II-5a** (0 – 32 μM) (20 mM NaH_2PO_4 buffer, pH 7.4). (B) Non-linear fitting plot of absorbance at 550 nm *versus* concentration for the displacement titration of **II-5a** using a model implemented in Scientist™. K_a was evaluated as 1.78 (± 0.21) × 10^6 M^{-1}.

(A)

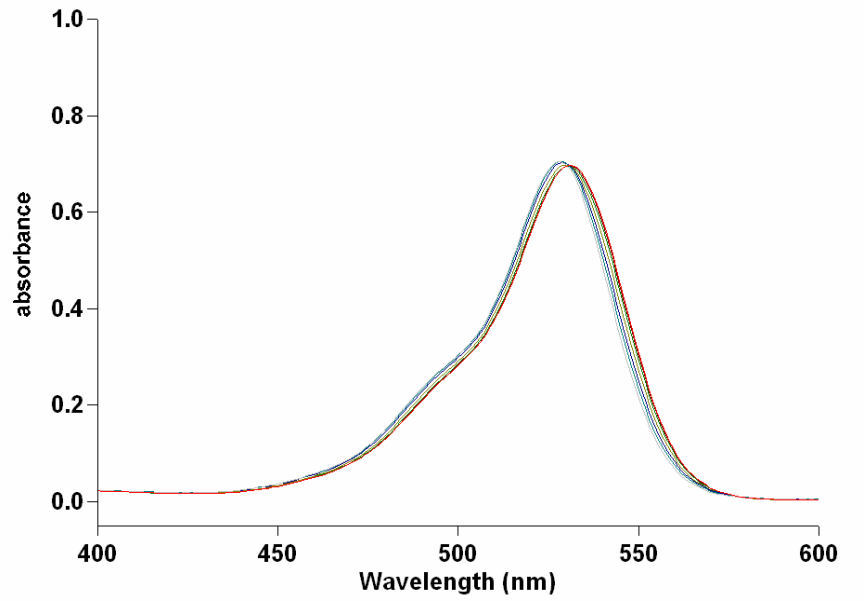

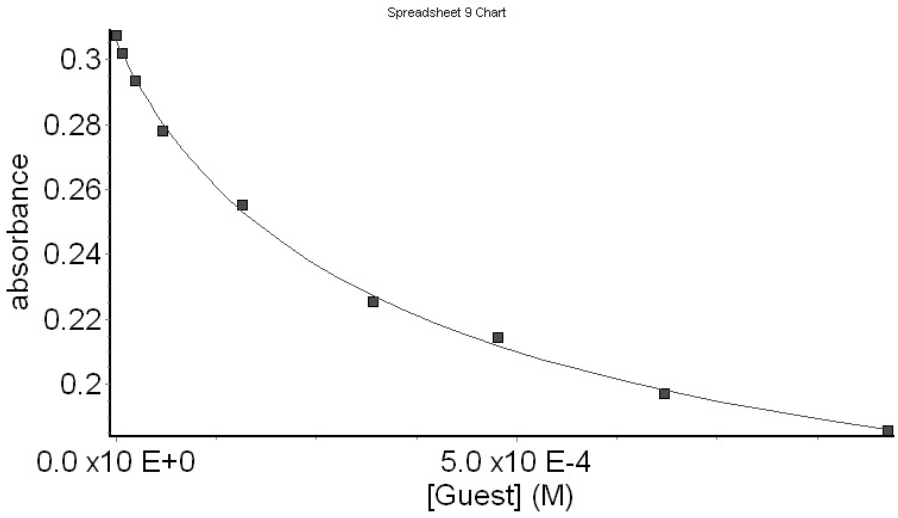

(B)

Figure S II-31. (A) Displacement titration of a solution of dye **II-4** (10.0 μM) and host **II-2b** (9.15 μM) solution with **II-5b** (0 – 32 μM) (20 mM NaH_2PO_4 buffer, pH 7.4). (B) Non-linear fitting plot of absorbance at 550 nm *versus* concentration for the displacement titration of **II-5b** using a model implemented in Scientist™. K_a was evaluated as 1.67 (± 0.18) × 10^3 M^{-1}

(A)

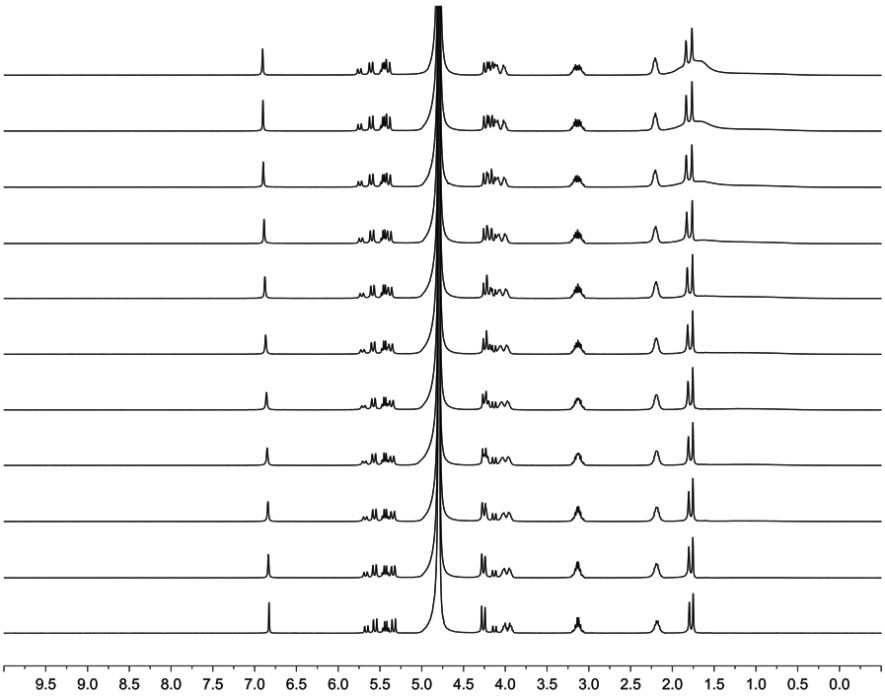

(B)

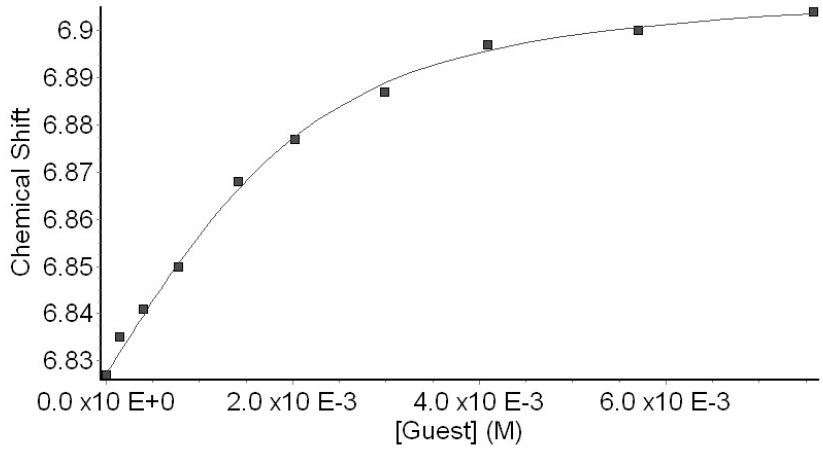

Figure S II-32. (A) ^{1}H NMR spectra (400 MHz, 20 mM sodium phosphate buffer, pD = 7.4) recorded for a solution of **II-2b** (2.0 mM) and **II-5c** of variable concentrations (0 – 8.0 mM). (B) Plot of the chemical shift of the aromatic proton of **II-2b** as a function of **II-5c** concentration. The solid line represents the best non-linear fitting of the data to a 1:1 binding model (K_a = 1.87 (± 0.31) × 10^3 M^{-1}).

(A)

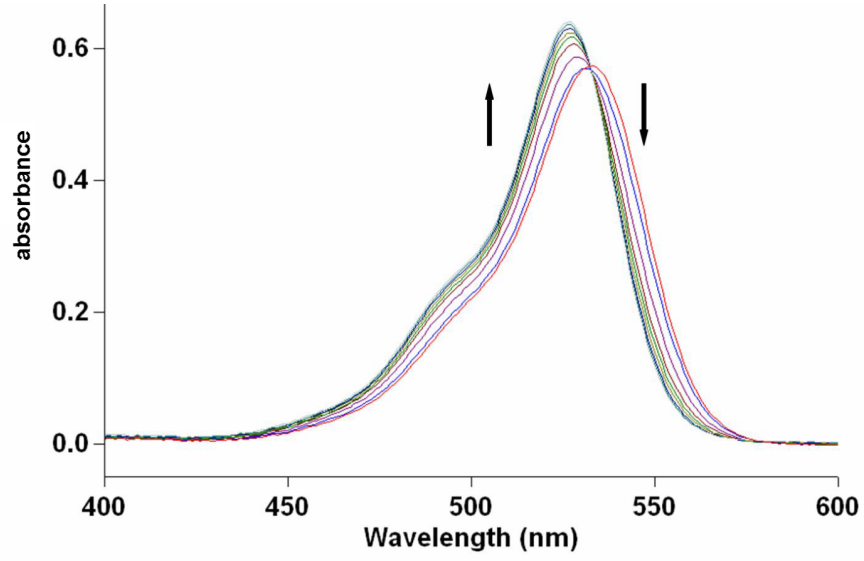

(B)

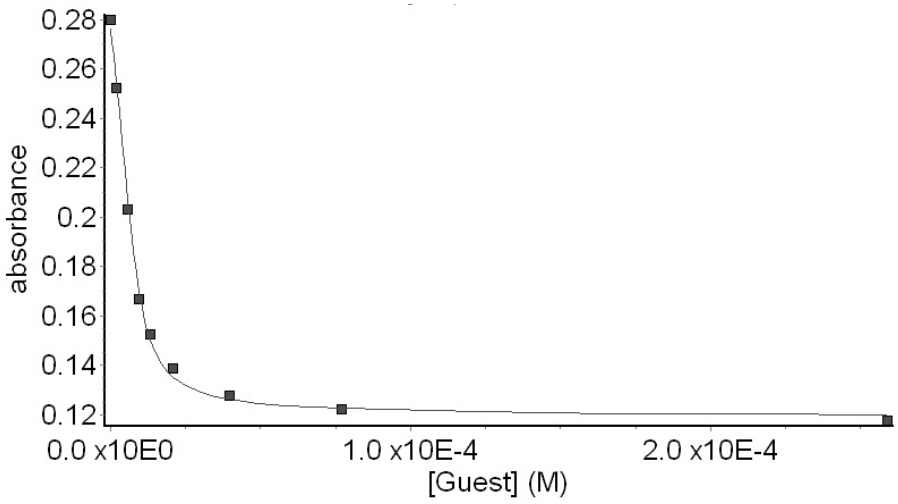

Figure S II-33. (A) Displacement titration of a solution of dye **II-4** (10.0 μM) and host **II-2b** (9.18 μM) solution with **II-6** (0 – 270 μM) (20 mM NaH_2PO_4 buffer, pH 7.4). (B) Non-linear fitting plot of absorbance at 550 nm *versus* concentration for the displacement titration of **II-6** using a model implemented in Scientist™. K_a was evaluated as 4.37 (± 0.46) × 10^6 M^{-1}.

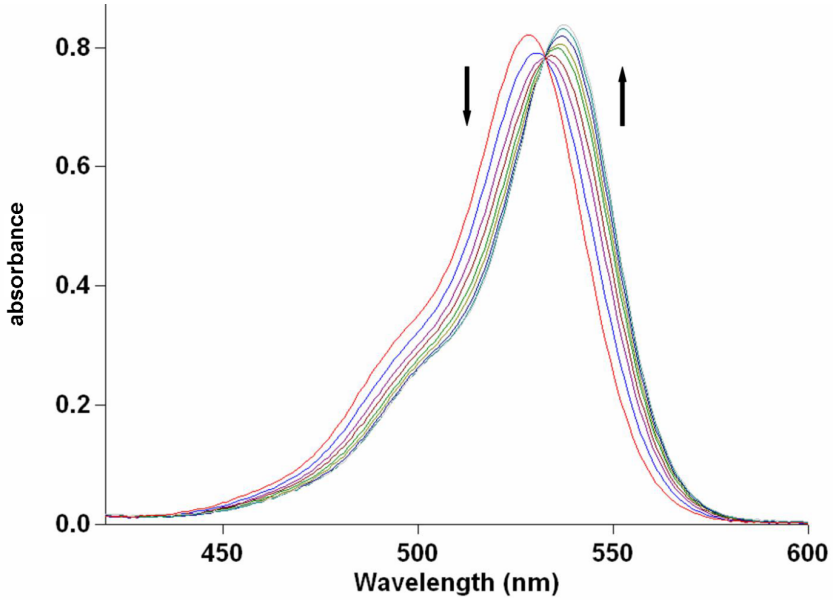

(A)

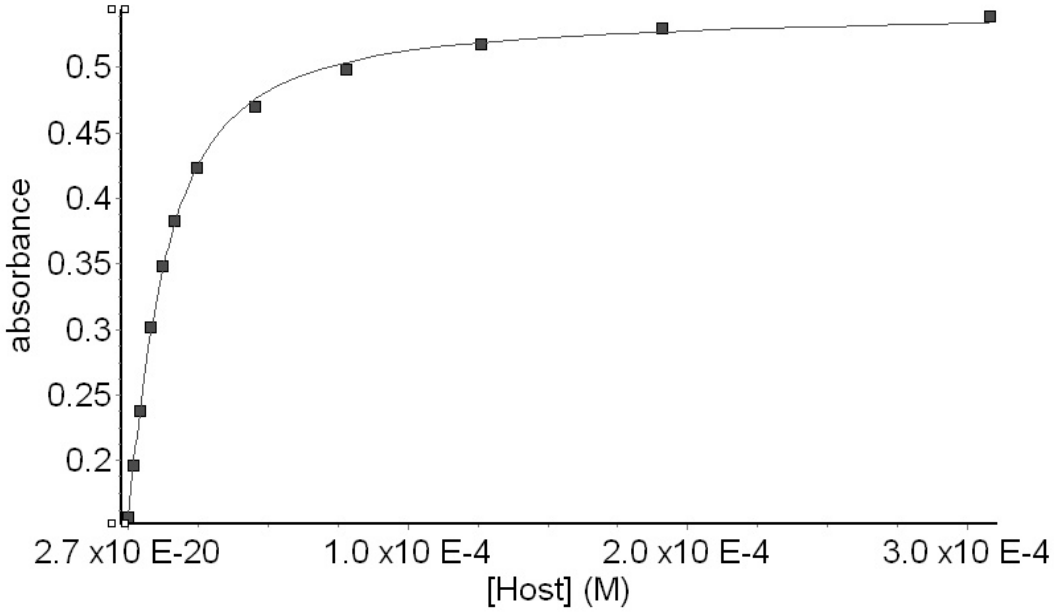

(B)

Figure S II-34. (A) UV/Vis spectra from the titration of dye **II-4** (10.0 μM) with **II-2c** (0 – 400 μM) in 20 mM NaH_2PO_4 buffer (pH 7.4); (B) plot of the ΔA550 as a function of **II-2c** concentration. The solid line represents the best non-linear fit of the data to a 1:1 binding model (K_a = 1.29 (± 0.05) × 10^5 M^{-1}).

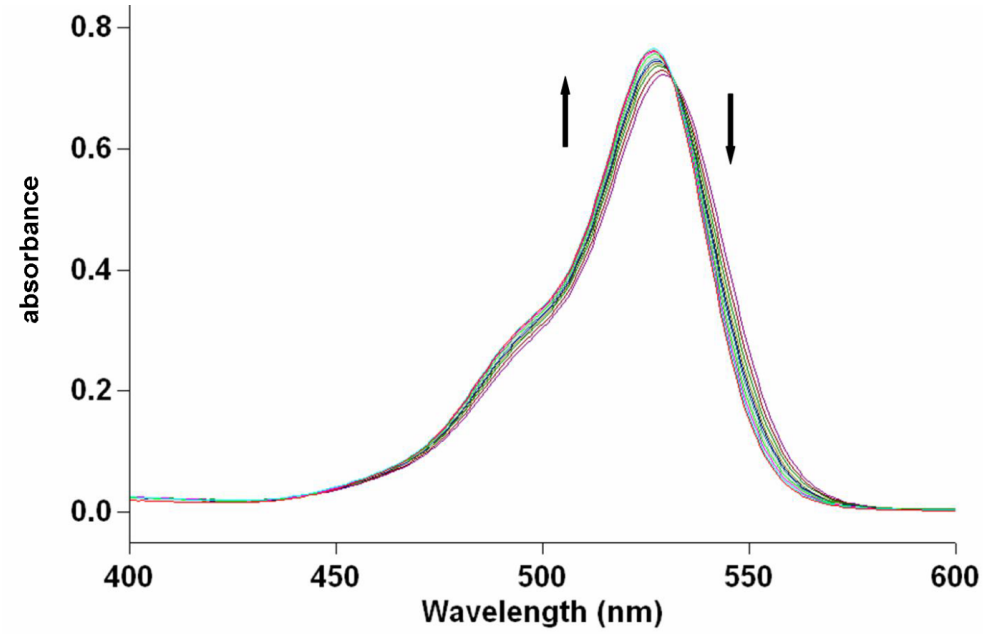

(A)

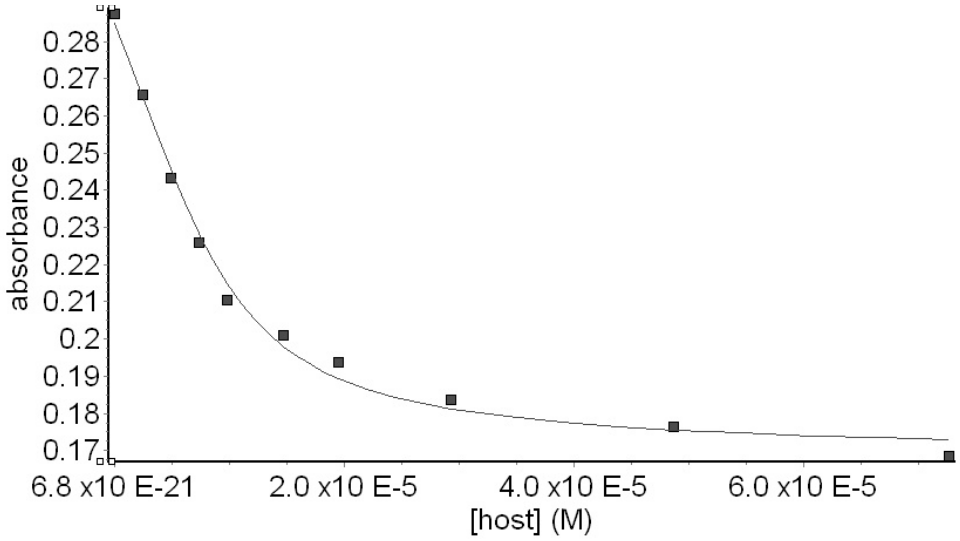

(B)

Figure S II-35. (A) Displacement titration of a solution of dye **II-4** (10.0 μM) and host **II-2c** (9.19 μM) solution with **II-6** (0 – 74 μM) (20 mM NaH_2PO_4 buffer, pH 7.4). (B) Non-linear fitting plot of absorbance at 550 nm *versus* concentration for the displacement titration of **6** using a model implemented in Scientist™. K_a was evaluated as 1.12 (± 0.24) × 10^6 M^{-1}.

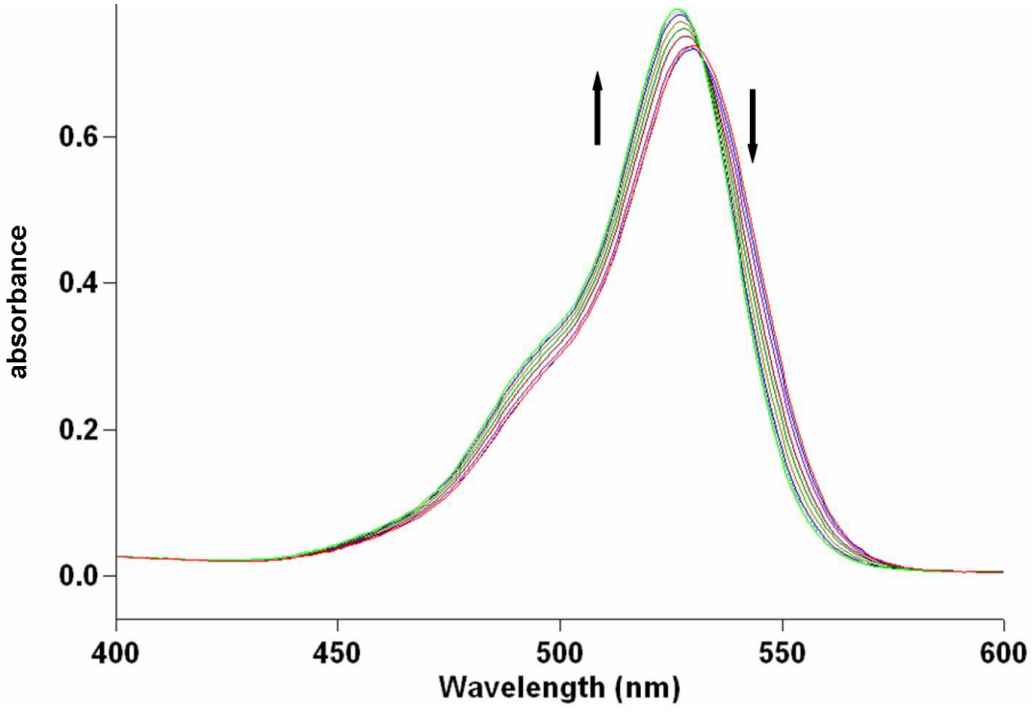

(A)

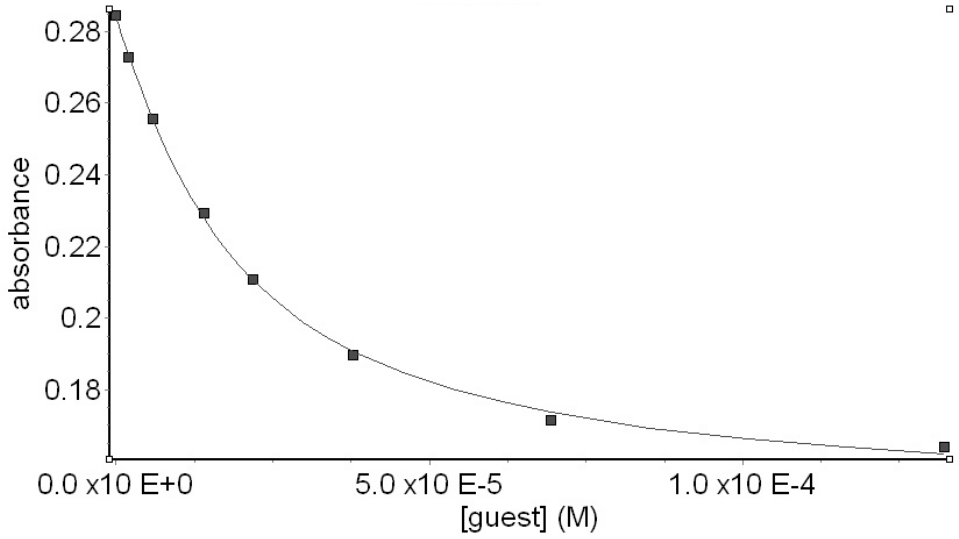

(B)

Figure S II-36. (A) Displacement titration of a solution of dye **II-4** (10.0 μM) and host **II-2c** (9.19 μM) solution with **II-5a** (0 – 130 μM) (20 mM NaH_2PO_4 buffer, pH 7.4). (B) Non-linear fitting plot of absorbance at 550 nm *versus* concentration for the displacement titration of **II-5a** using a model implemented in Scientist™. K_a was evaluated as 1.94 (± 0.18) × 10^5 M^{-1}.

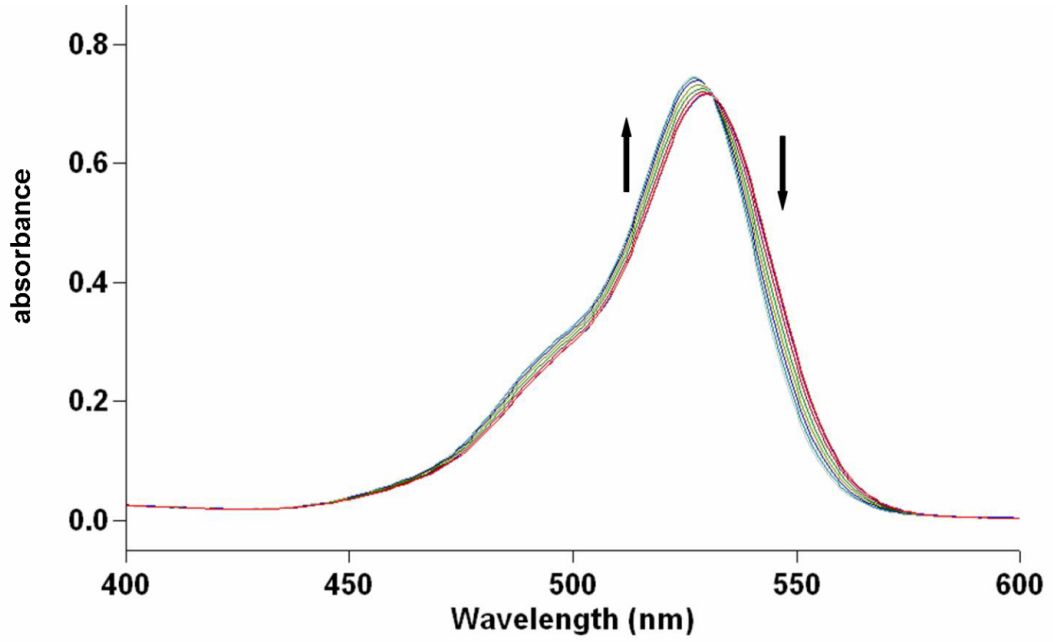

(A)

(B)

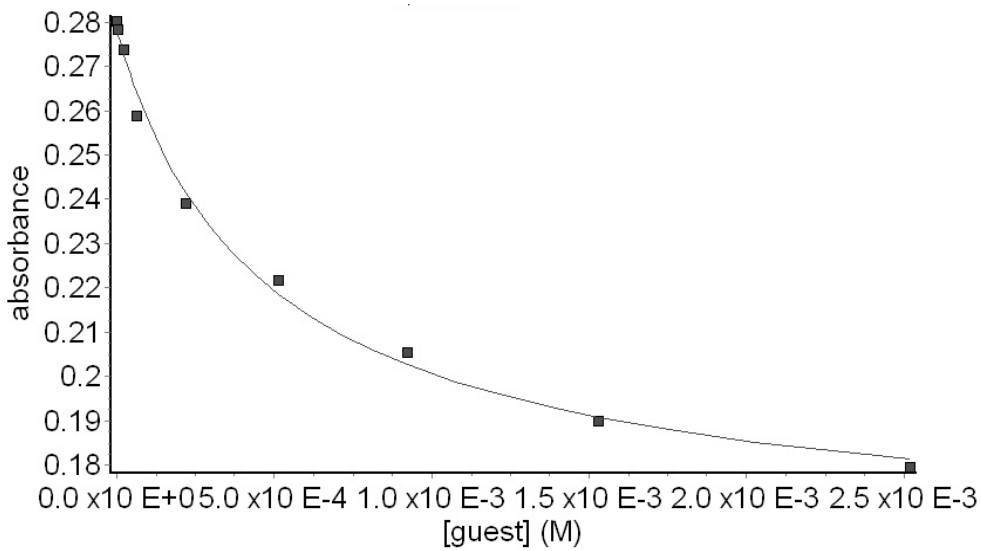

Figure S II-37. (A) Displacement titration of a solution of dye **II-4** (10.0 μM) and host **II-2c** (9.19 μM) solution with **II-5b** (0 – 2.6 mM) (20 mM NaH_2PO_4 buffer, pH 7.4). (B) Non-linear fitting plot of absorbance at 550 nm *versus* concentration for the displacement titration of **II-5b** using a model implemented in Scientist™. K_a was evaluated as 5.54 (± 0.83) × 10^4 M^{-1}.

(A)

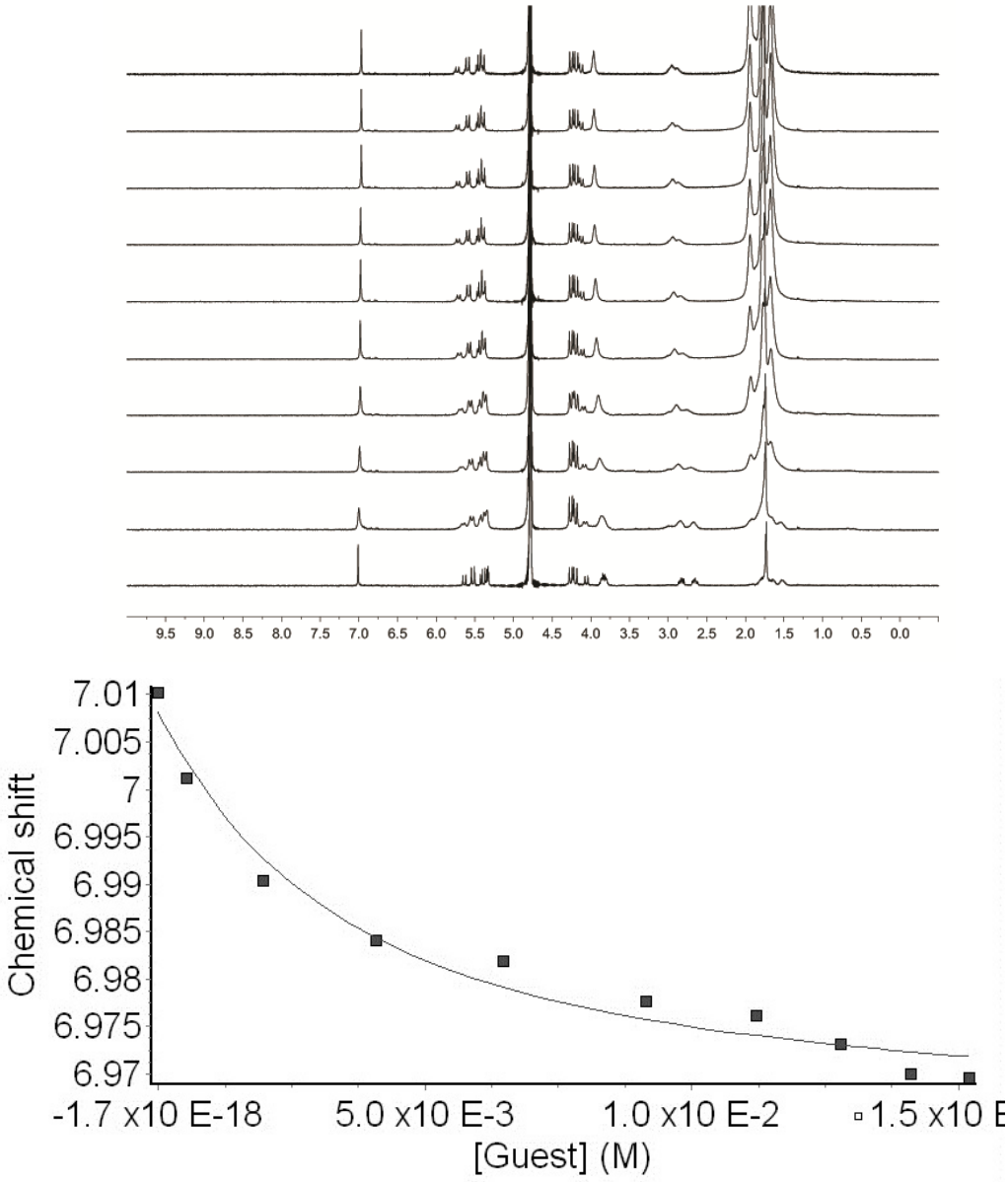

(B)

Figure S II-38. (A) ^{1}H NMR spectra (400 MHz, 20 mM sodium phosphate buffer, pD = 7.4) recorded for a solution of **II-2c** (1.055 mM) and **II-5c** of variable concentrations (0 – 16 mM). (B) Plot of the chemical shift of the aromatic proton of **II-2c** as a function of **II-5c** concentration. The solid line represents the best non-linear fitting of the data to a 1:1 binding model (K_a = 345 ± 118 M^{-1})

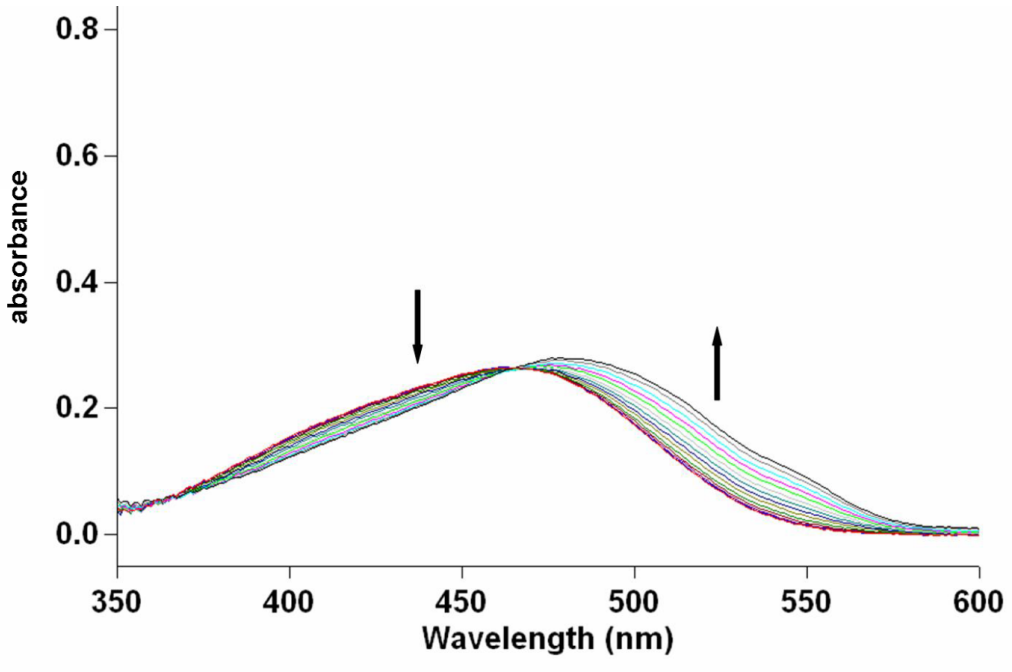

(A)

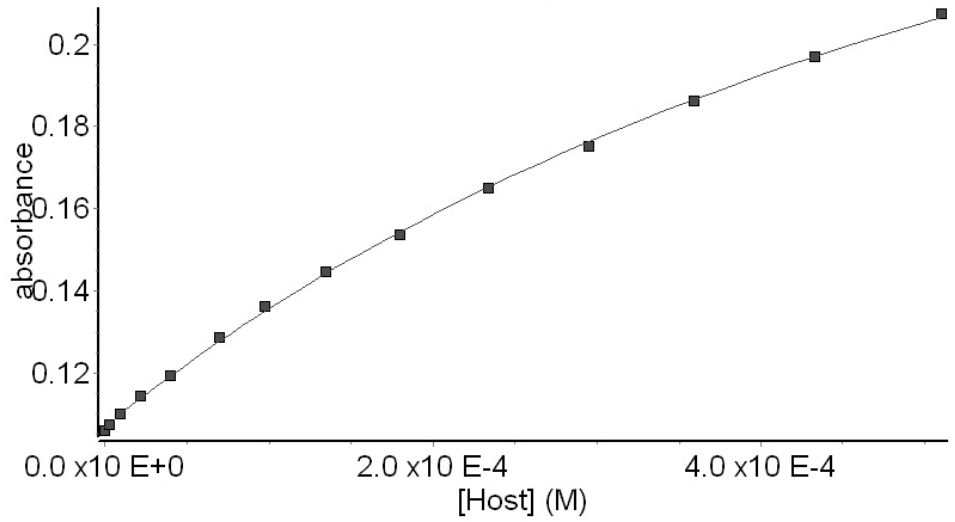

(B)

Figure S II-39. (A) UV/Vis spectra from the titration of dye **II-8** (11.0 μM) with **II-2h** (0 – 500 μM) in 20 mM NaH_2PO_4 buffer (pH 7.4); (B) plot of the ΔA550 as a function of **II-2h** concentration. The solid line represents the best non-linear fit of the data to a 1:1 binding model (K_a = 1.32 (± 0.01) × 10^3 M^{-1}).

(A)

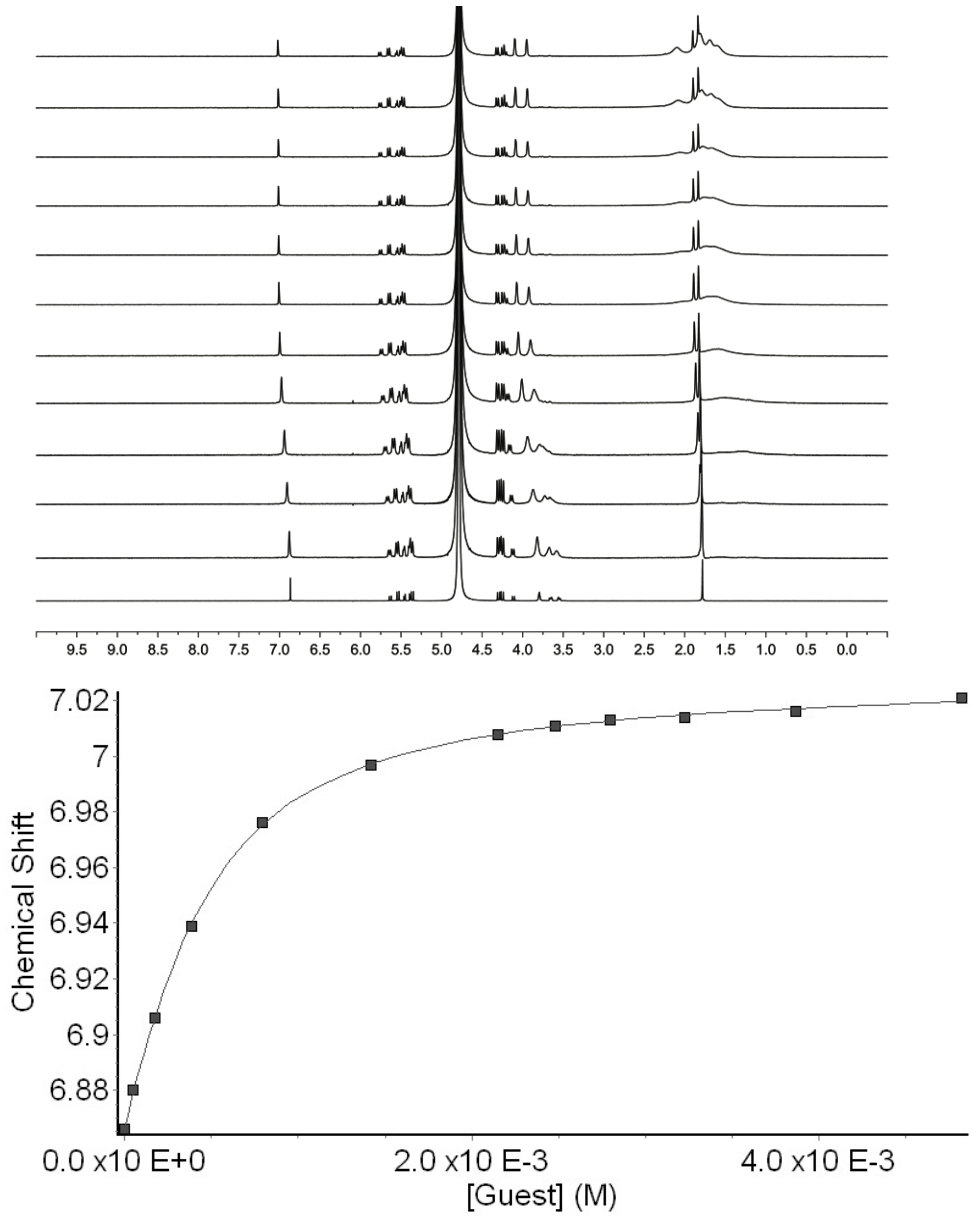

(B)

Figure S II-40. (A) ^{1}H NMR spectra (400 MHz, 20 mM sodium phosphate buffer, pD = 7.4) recorded for a solution of **II-2h** (0.350 mM) and **II-5a** of variable concentrations (0 – 5.0 mM). (B) Plot of the chemical shift of the aromatic proton of **II-2h** as a function of **II-5a** concentration. The solid line represents the best non-linear fitting of the data to a 1:1 binding model (K_a = 3.64 (± 0.10) × 10^3 M^{-1}).

(A)

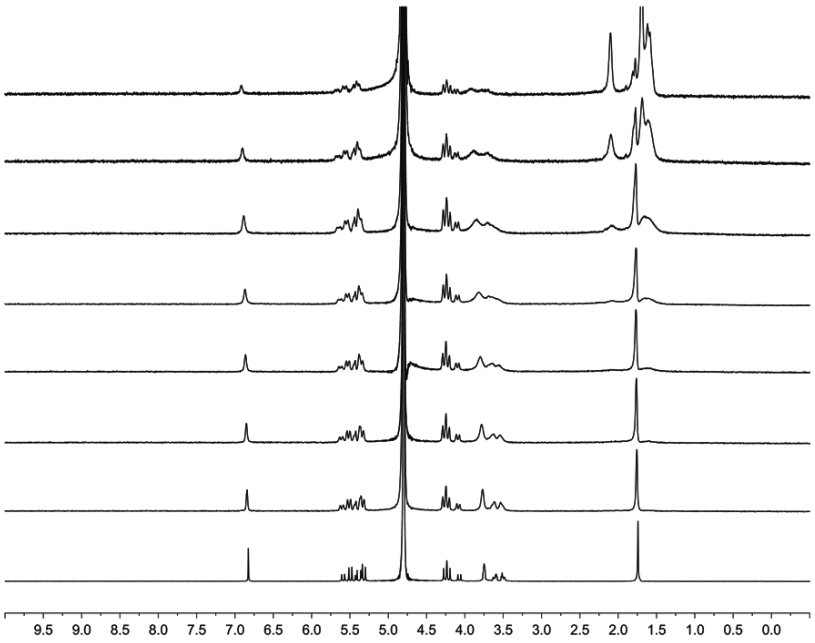

(B)

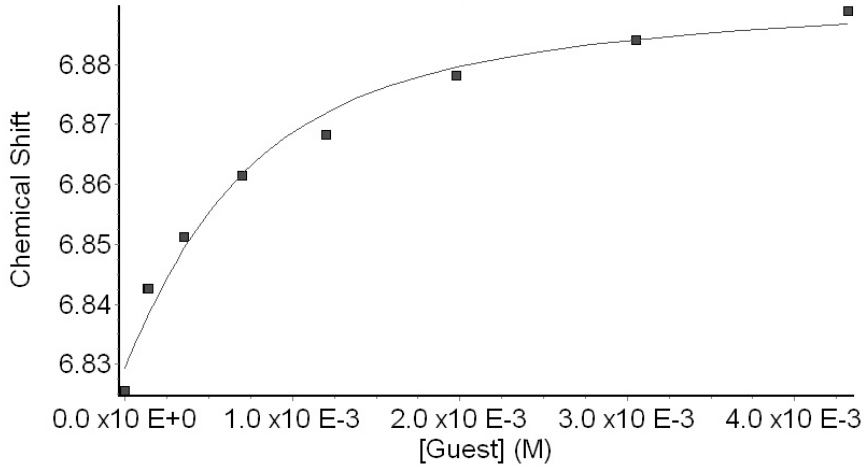

Figure S II-41. (A) ^{1}H NMR spectra (400 MHz, 20 mM sodium phosphate buffer, pD = 7.4) recorded for a solution of **II-2h** (0.350 mM) and **II-5b** of variable concentrations (0 – 5.0 mM). (B) Plot of the chemical shift of the aromatic proton of **II-2h** as a function of **II-5b** concentration. The solid line represents the best non-linear fitting of the data to a 1:1 binding model ($K_a = 2.36 \pm 0.41 \times 10^3\ M^{-1}$).

(A)

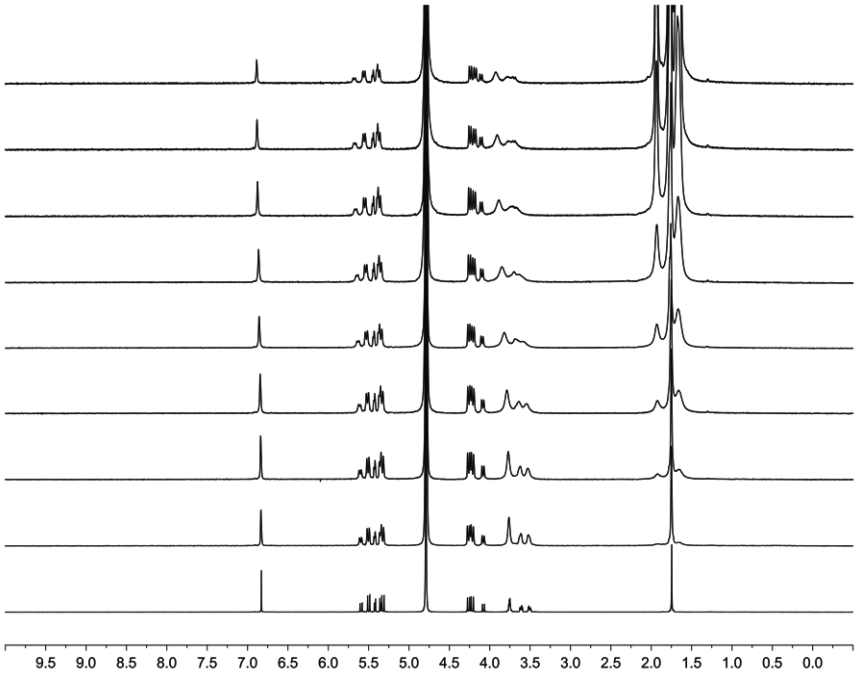

(B)

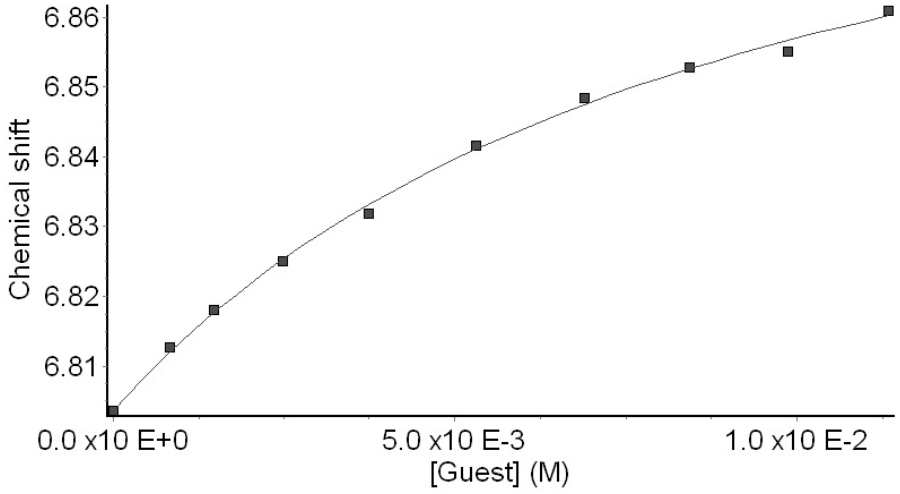

Figure S II-42. (A) ^{1}H NMR spectra (400 MHz, 20 mM sodium phosphate buffer, pD = 7.4) recorded for a solution of **II-2h** (0.350 mM) and **II-5c** of variable concentrations (0 – 11 mM). (B) Plot of the chemical shift of the aromatic proton of **II-2h** as a function of **II-5c** concentration. The solid line represents the best non-linear fitting of the data to a 1:1 binding model (K_a = 108 ± 8.3 M^{-1}).

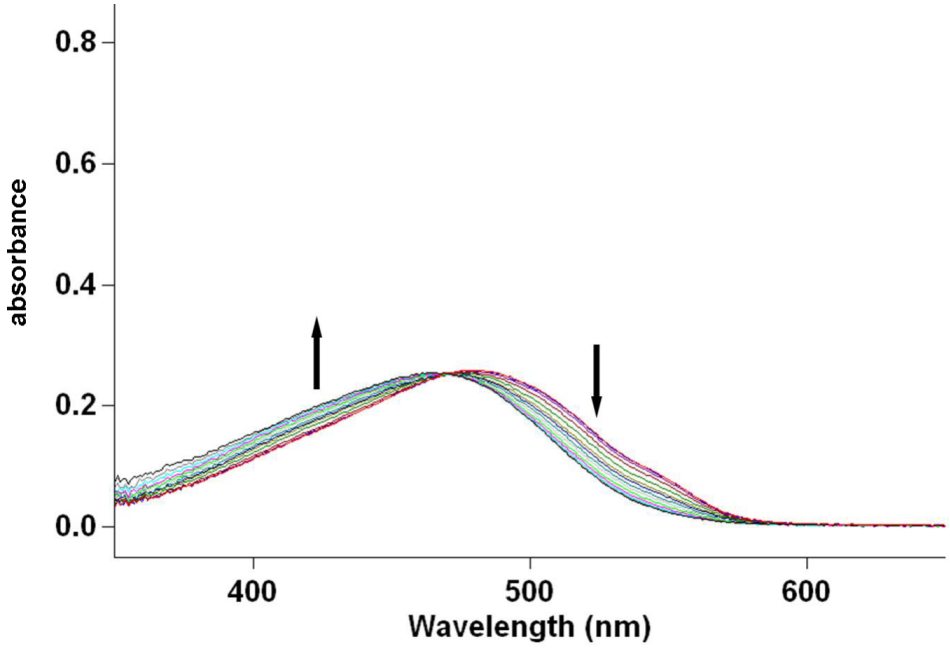

(A)

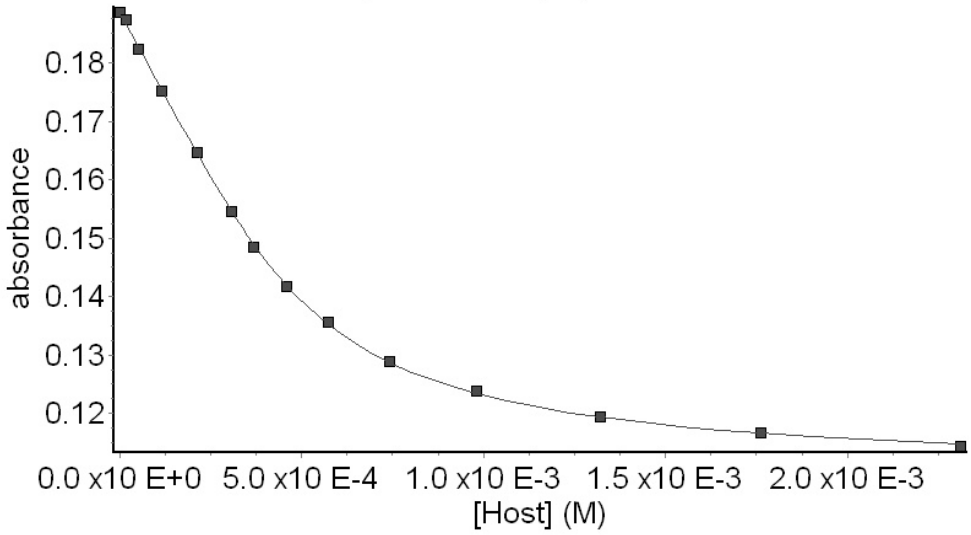

(B)

Figure S II-43. (A) Displacement titration of a solution of dye **II-8** (11.0 μM) and host **II-2h** (385 μM) solution with **II-6** (0 – 2.6 mM) (20 mM NaH_2PO_4 buffer, pH 7.4). (B) Non-linear fitting plot of absorbance at 510 nm *versus* concentration for the displacement titration of **II-6** using a model implemented in Scientist™. K_a was evaluated as $1.13 \pm 0.10 \times 10^4$ M^{-1}.

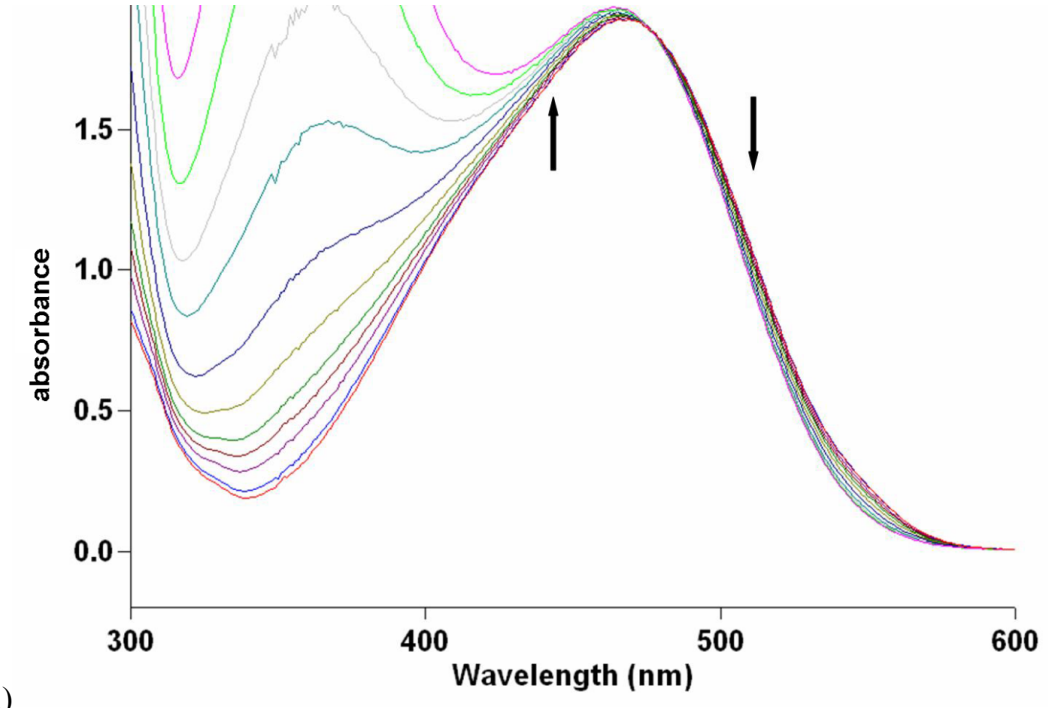

(A)

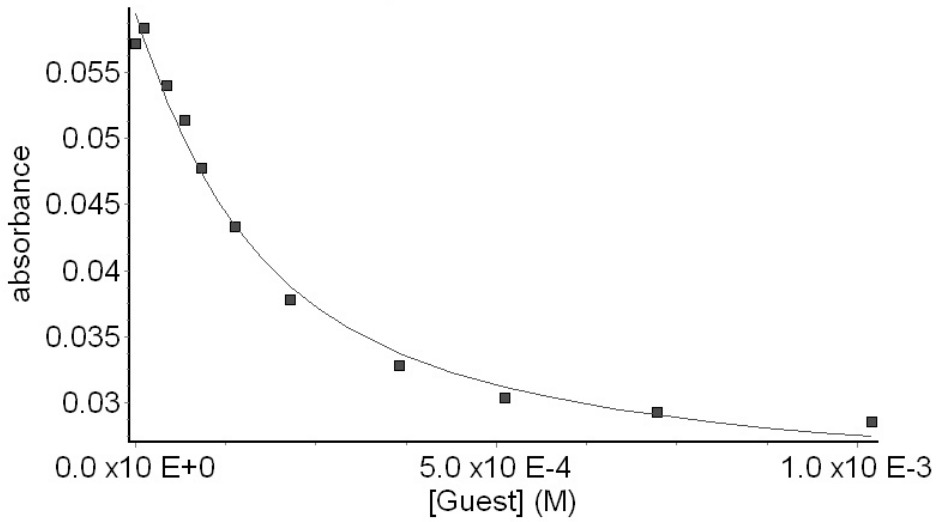

(B)

Figure S II-44. (A) Displacement titration of a solution of dye **II-8** (76.5 μM) and host **II-2h** (83.2 μM) solution with **II-7** (0 – 1.2 mM) (20 mM NaH_2PO_4 buffer, pH 7.4). (B) Non-linear fitting plot of absorbance at 550 nm *versus* concentration for the displacement titration of **II-7** using a model implemented in Scientist™. K_a was evaluated as $9.59 \pm 1.2 \times 10^3$ M^{-1}.

(A)

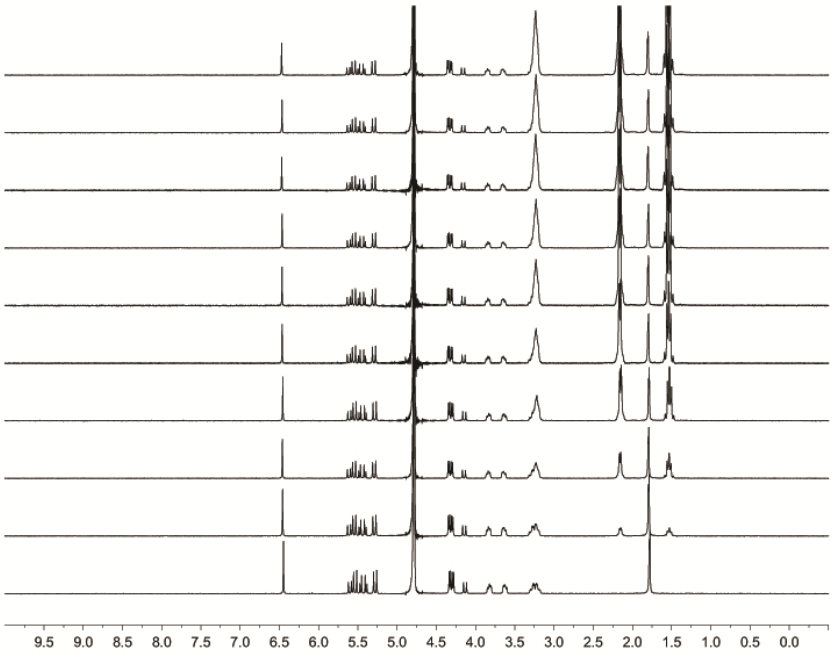

(B)

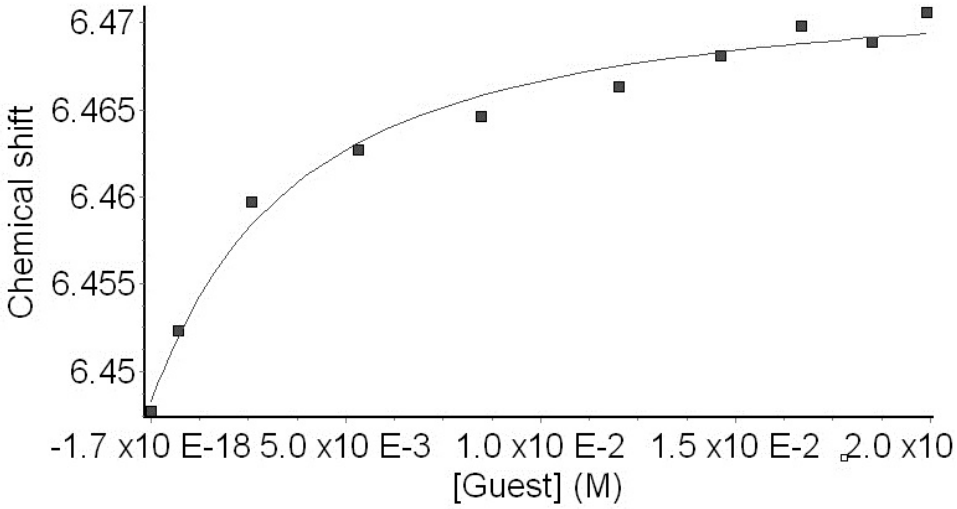

Figure S II-45. (A) ^{1}H NMR spectra (400 MHz, 20 mM sodium phosphate buffer, pD = 7.4) recorded for a solution of **II-2f** (1.055 mM) and **II-6** of variable concentrations (0 – 22 mM). (B) Plot of the chemical shift of the aromatic proton of **II-2f** as a function of **II-6** concentration. The solid line represents the best non-linear fitting of the data to a 1:1 binding model (K_a = 327 (± 82) M^{-1})

(A)

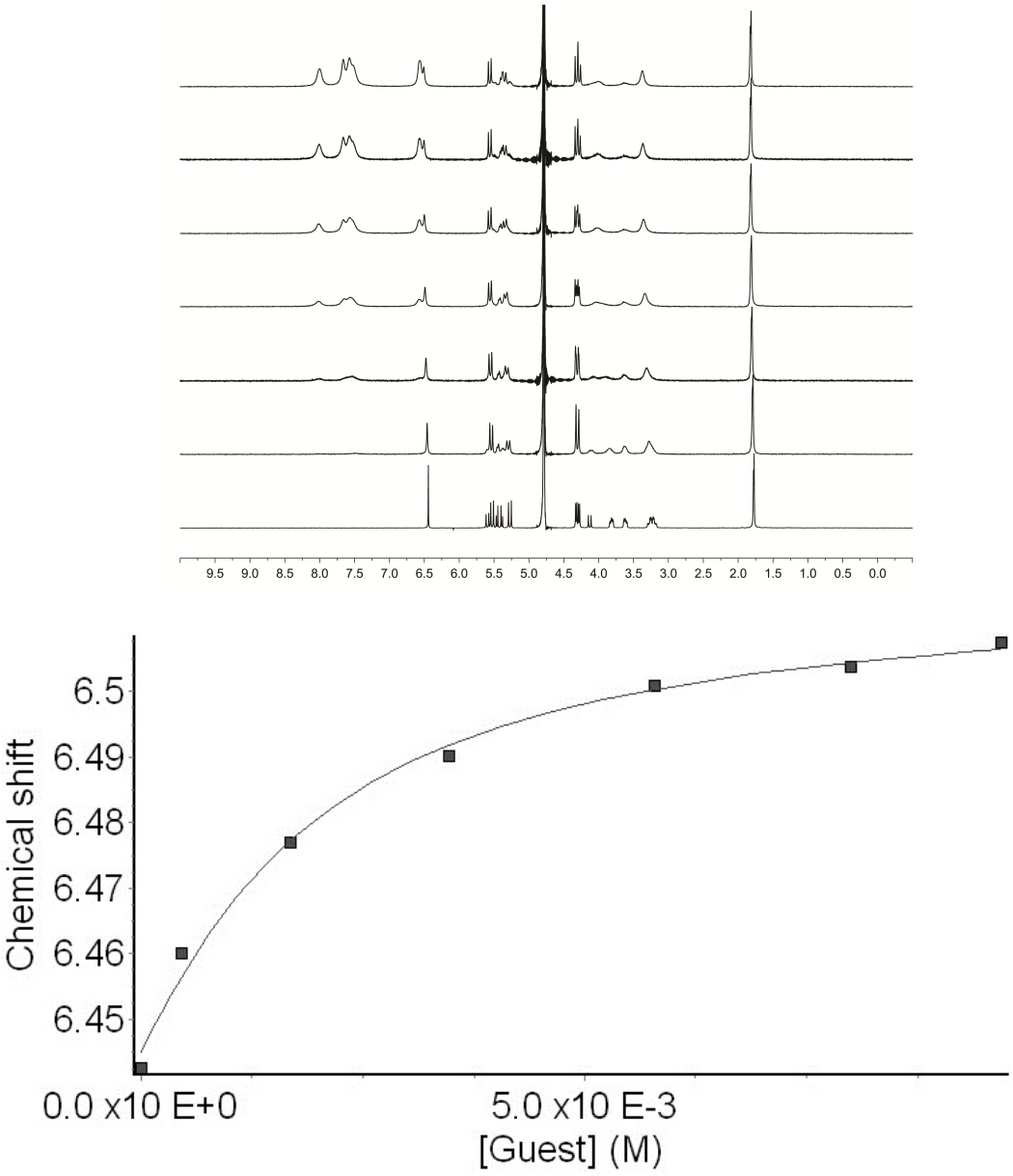

(B)

Figure S II-46. (A) ^{1}H NMR spectra (400 MHz, 20 mM sodium phosphate buffer, pD = 7.4) recorded for a solution of **II-2f** (1.055 mM) and **7** of variable concentrations (0 – 11 mM). (B) Plot of the chemical shift of the aromatic proton of **II-2f** as a function of **II-7** concentration. The solid line represents the best non-linear fitting of the data to a 1:1 binding model (K_a = 678 ± 171 M^{-1}).

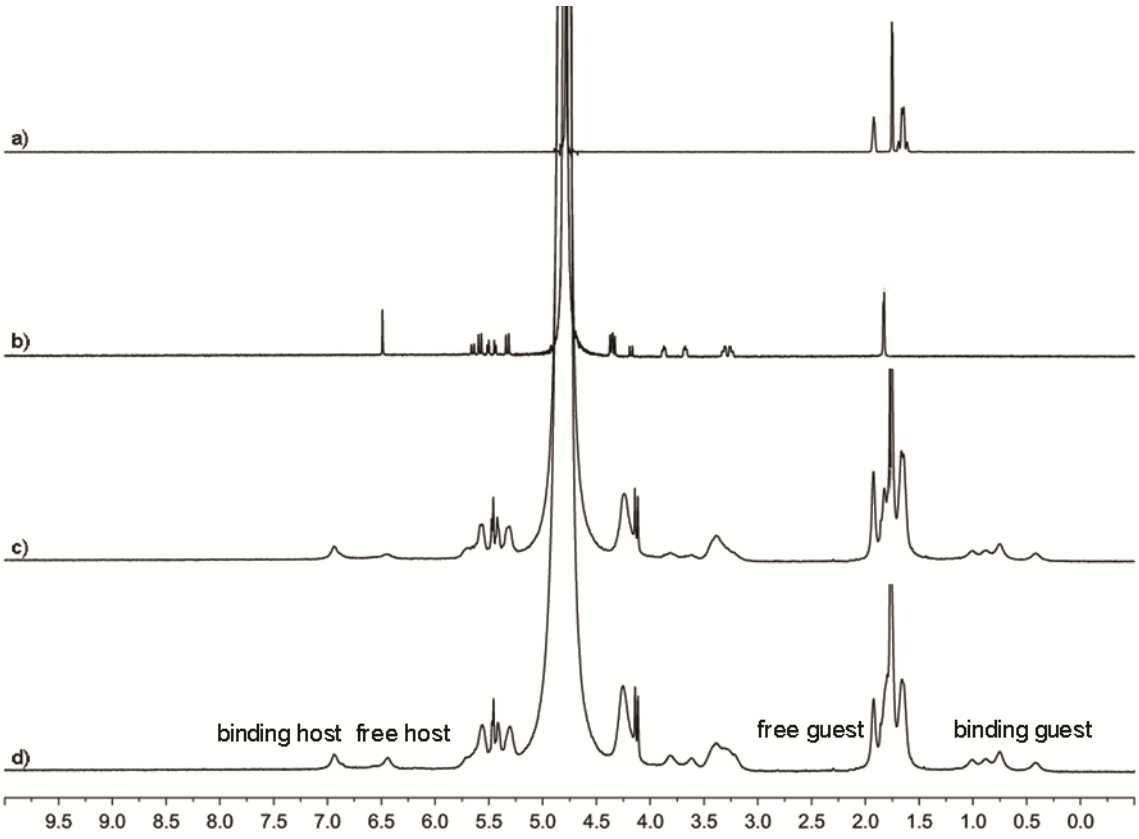

Figure S II-47. ^{1}H NMR spectra recorded (D_2O, 400 MHz, RT) for: a) **II-5c** (0.5 mM), b) **II-2f** (0.5 mM), c) a mixture of **II-2f** (0.5 mM) and **II-5c** (4.0 mM), and d) a mixture of **II-2f** (0.5 mM) and **II-5c** (2.5 mM).

Determination of pK_a shift of guest II-7 when forming complexes with II-2a, II-2f and II-2h UV/Vis spectroscopy was used in this work to determine the pK_a values. The direct pH titration of fixed concentrations of UV/Vis dye **7** and different hosts allowed us to determine their values of pK_a by fitting to a pK_a model.

pK_a Models Used to Determine Values of K_a with Micromath Scientist

// Micromath Scientist Model File

IndVars: pH

DepVars: Iobs

Params: Imax, Imin, pKa

Iobs=Imax/(1+10^(pH-pKa))+Imin/(1+10^(pKa-pH))

0<pKa<14

0<pH

0<Imax

0<Imin

***

(A)

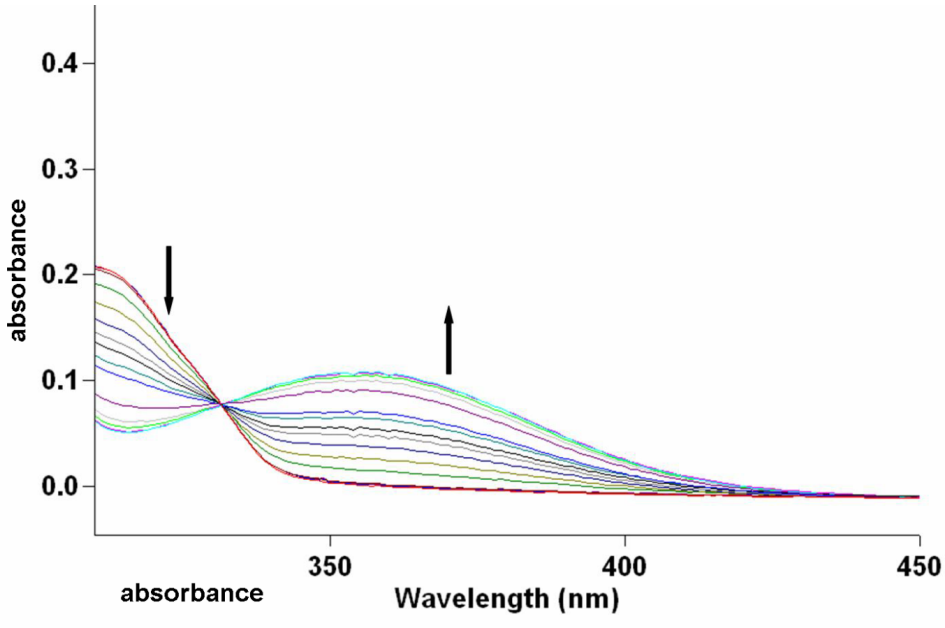

(B)

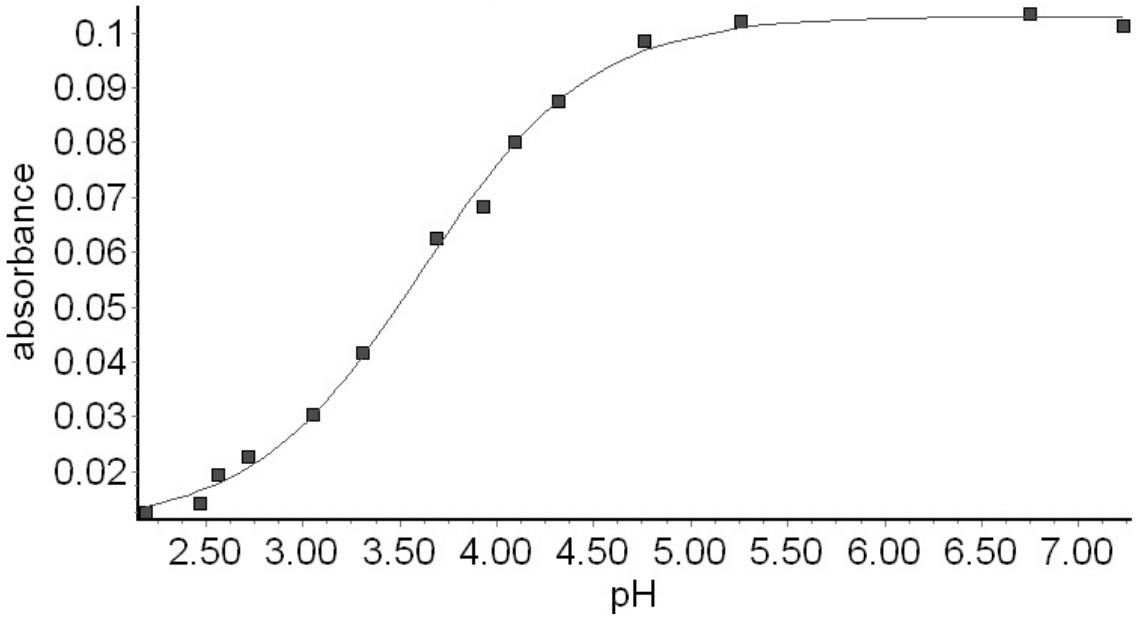

Figure S II-48. (A) pH titration of a solution of dye **II-7** (36.5 μM) solution (B) Non-linear fitting plot of absorbance *versus* pH for the pH titration of **II-7** with using a model implemented in Scientist™. pK_a was evaluated as 3.6.

(A)

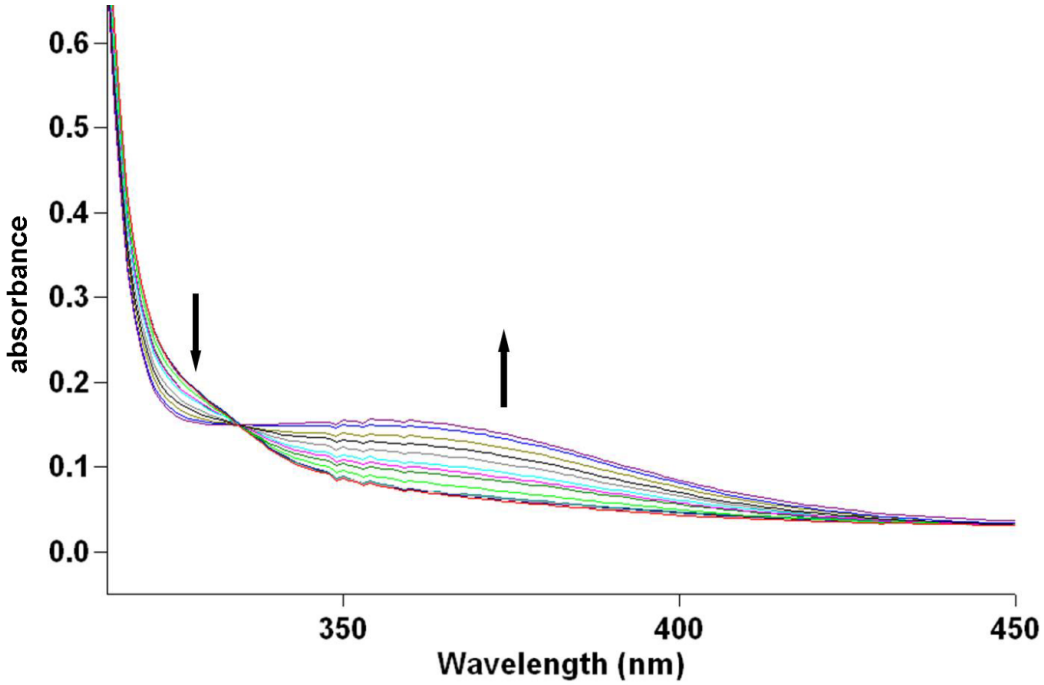

(B)

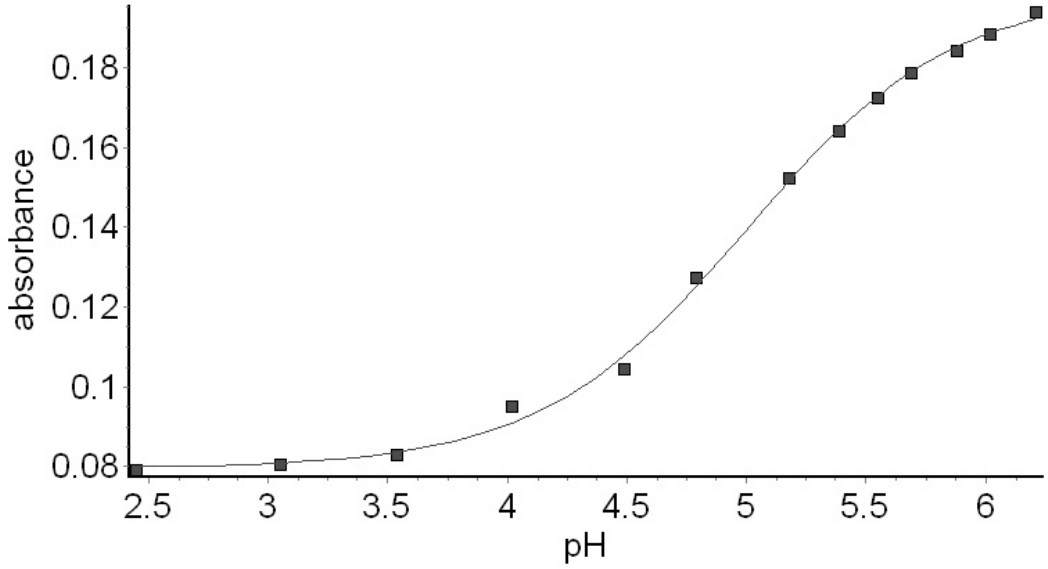

Figure S II-49. (A) pH titration of a solution of dye **II-7** (36.5 µM) solution with **II-2a** (1.5 mM) (B) Non-linear fitting plot of absorbance *versus* pH for the pH titration of **II-7** with using a model implemented in Scientist™. pK_a was evaluated as 4.9.

(A)

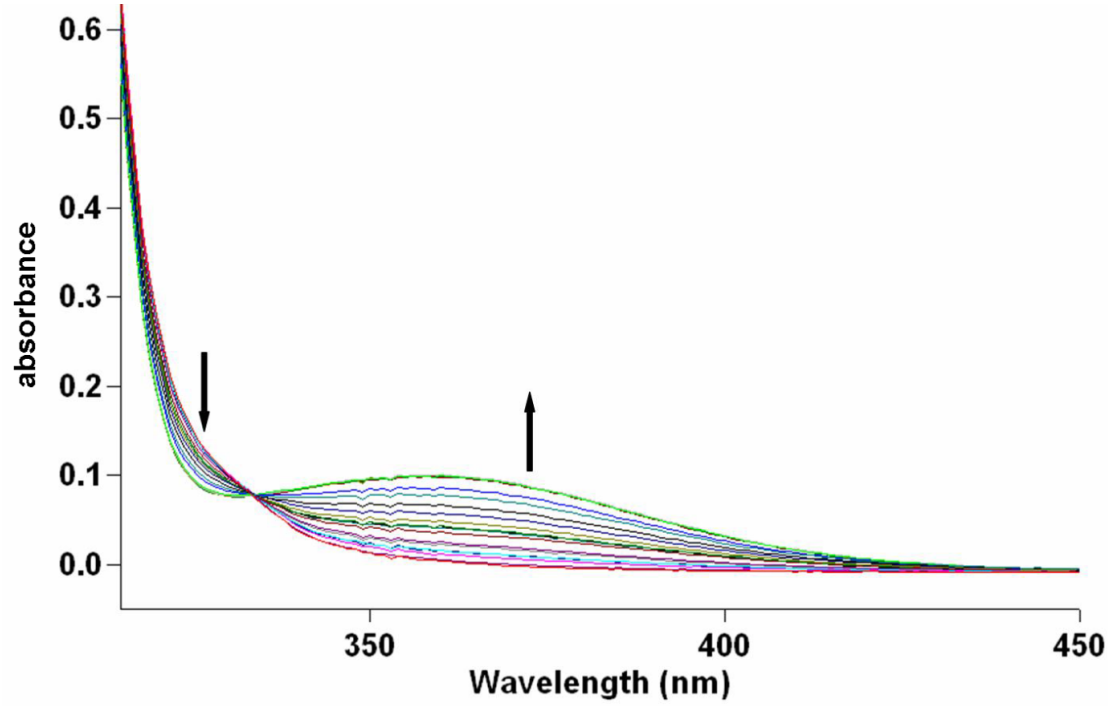

(B)

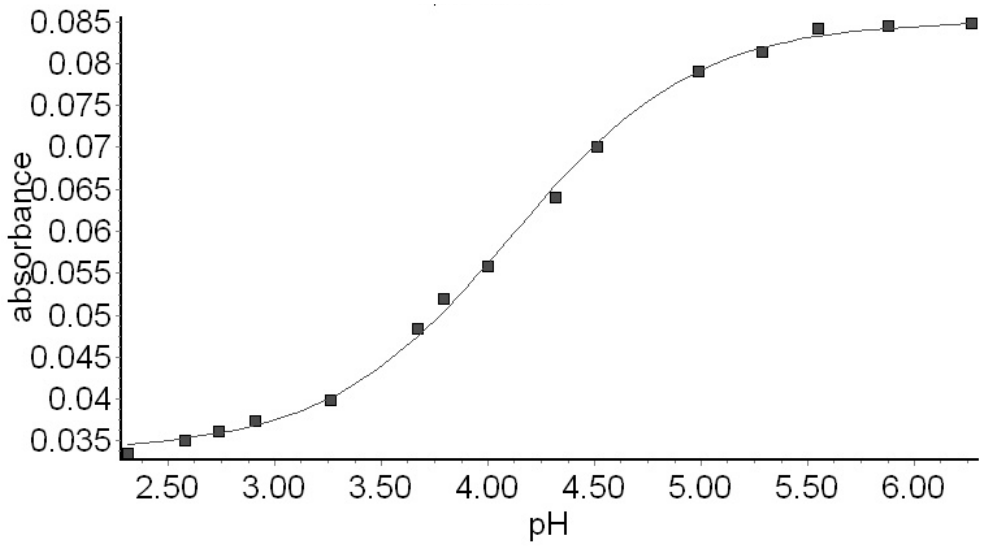

Figure S II-50. (A) pH titration of a solution of dye **II-7** (36.5 µM) solution with **II-2h** (1.5 mM) (B) Non-linear fitting plot of absorbance *versus* pH for the pH titration of **II-7** with using a model implemented in Scientist™. pK_a was evaluated as 4.1.

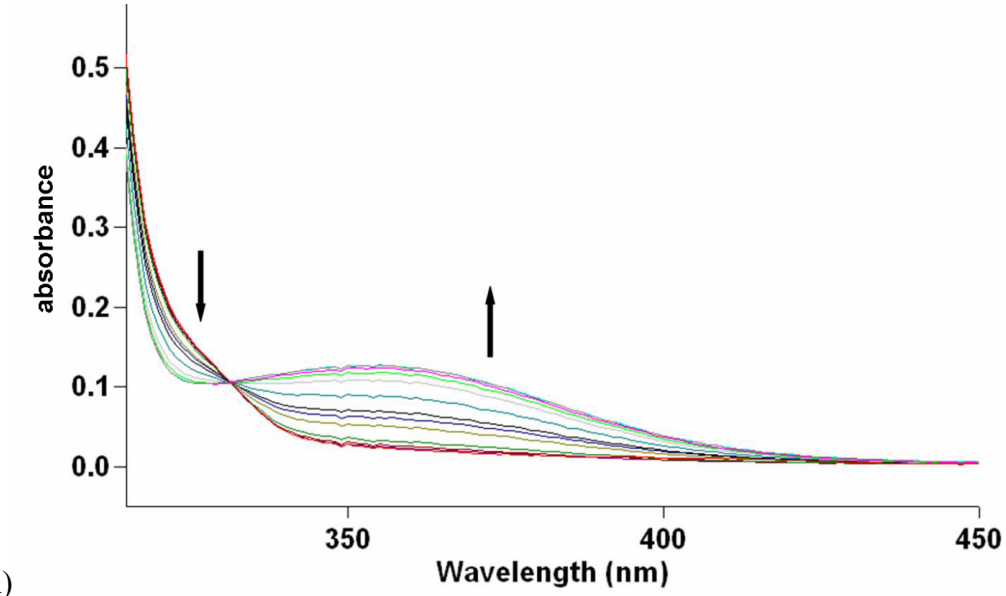

(A)

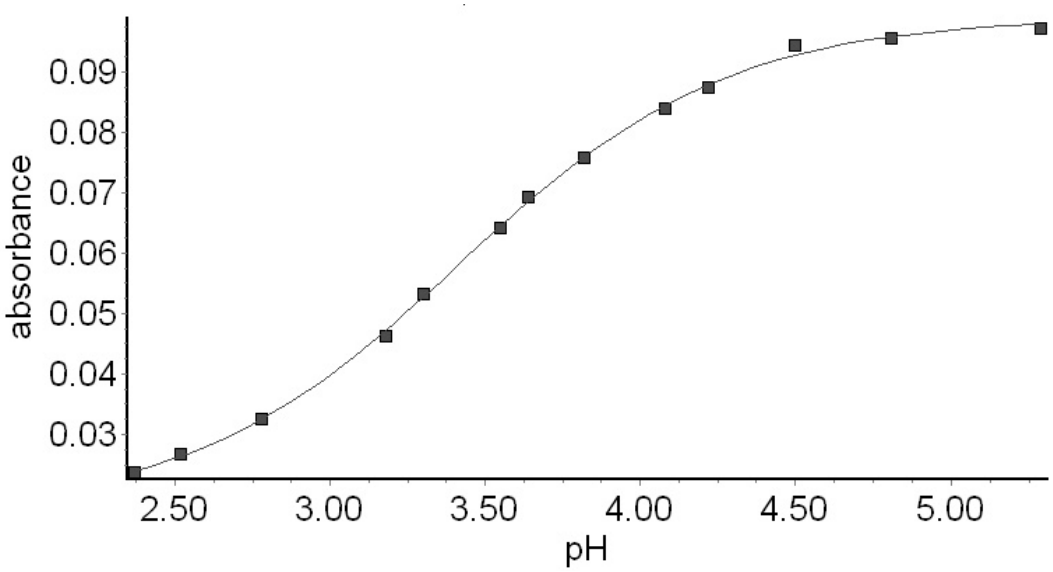

(B)

Figure S II-51. (A) pH titration of a solution of dye **II-7** (36.5 μM) solution with **II-2f** (1.5 mM) (B) Non-linear fitting plot of absorbance *versus* pH for the pH titration of **II-7** using a model implemented in Scientist™. pK_a was evaluated as 3.4.

Details of the X-ray crystallographic structure of II-2h. A colorless prism-like specimen of $C_{100}H_{155}N_{32}O_{49.50}$, approximate dimensions 0.21 mm × 0.30 mm × 0.42 mm, was used for the X-ray crystallographic analysis. The X-ray intensity data were measured on a Bruker APEX-II CCD system equipped with a graphite monochromator and a MoKα sealed tube (λ = 0.71073 Å). Data collection temperature was 150 K.

The total exposure time was 16.72 hours. The frames were integrated with the Bruker SAINT software package using a narrow-frame algorithm. The integration of the data using a monoclinic unit cell yielded a total of 116519 reflections to a maximum θ angle of 25.00° (0.84 Å resolution), of which 21005 were independent (average redundancy 5.547, completeness = 99.9%, R_{int} = 3.15%, R_{sig} = 2.19%) and 16835 (80.15%) were greater than $2\sigma(F^2)$. The final cell constants of *a* = 29.339(3) Å, *b* = 13.8631(13) Å, *c* = 29.715(3) Å, β = 99.2288(16)°, *V* = 11930.(2) $Å^3$, are based upon the refinement of the XYZ-centroids of 9901 reflections above 20 σ(I) with 4.649° < 2θ < 56.33°. Data were corrected for absorption effects using the multi-scan method (SADABS). The calculated minimum and maximum transmission coefficients (based on crystal size) are 0.9526 and 0.9759.

The structure was solved and refined using the Bruker SHELXTL Software Package, using the space group P 1 21/n 1, with Z = 4 for the formula unit, $C_{100}H_{155}N_{32}O_{49.50}$. The final anisotropic full-matrix least-squares refinement on F^2 with 1867 variables converged at R_1 = 5.88%, for the observed data and wR_2 = 12.11% for all data. The goodness-of-fit was 1.008. The largest peak in the final difference electron density synthesis was 0.798 $e^-/Å^3$ and the largest hole was -0.470 $e^-/Å^3$ with an RMS deviation of 0.057 $e^-/Å^3$. On the basis of the final model, the calculated density was 1.446 g/cm^3 and F(000), 5500 e^-

APEX2 Version 2010.11-3 (Bruker AXS Inc.)

SAINT Version 7.68A (Bruker AXS Inc., 2009)

SADABS Version 2008/1 (G. M. Sheldrick, Bruker AXS Inc.)

XPREP Version 2008/2 (G. M. Sheldrick, Bruker AXS Inc.)

XS Version 2008/1 (G. M. Sheldrick, *Acta Cryst.* (2008). A**64**, 112-122)

XL Version 2008/4 (G. M. Sheldrick, *Acta Cryst.* (2008). A**64**, 112-122)

Platon (A. L. Spek, *Acta Cryst.* (1990). A**46**, C-34)

Table 1. Sample and crystal data for UM2316a.

Identification code	2316a	
Chemical formula	$C_{100}H_{155}N_{32}O_{49.50}$	
Formula weight	2597.56	
Temperature	150(2) K	
Wavelength	0.71073 Å	
Crystal size	0.21 × 0.30 × 0.42 mm	
Crystal habit	colorless prism	
Crystal system	monoclinic	
Space group	P 1 21/n 1	
Unit cell dimensions	a = 29.339(3) Å	α = 90°
	b = 13.8631(13) Å	β = 99.2288(16)°
	c = 29.715(3) Å	γ = 90°

Volume	11930.(2) $Å^3$
Z	4
Density (calculated)	1.446 Mg/cm^3
Absorption coefficient	0.117 mm^{-1}
F(000)	5500

Table 2. Data collection and structure refinement for UM2316a.

Diffractometer	Bruker APEX-II CCD
Radiation source	sealed tube, MoKα
Theta range for data collection	2.07 to 25.00°
Index ranges	$-34 \leq h \leq 34, -16 \leq k \leq 16, -35 \leq l \leq 35$
Reflections collected	116519
Independent reflections	21005 [R(int) = 0.0315]
Coverage of independent reflections	99.9%
Absorption correction	multi-scan
Max. and min. transmission	0.9759 and 0.9526
Structure solution technique	direct methods
Structure solution program	SHELXS-97 (Sheldrick, 2008)
Refinement method	Full-matrix least-squares on F^2

Refinement program	SHELXL-97 (Sheldrick, 2008)
Function minimized	$\Sigma\, w(F_o^2 - F_c^2)^2$
Data / restraints / parameters	21005 / 440 / 1867
Goodness-of-fit on F^2	1.008
Δ/σ_{max}	0.009
Final R indices	16835 data; $I>2\sigma(I)$: $R_1 = 0.0588$, $wR_2 = 0.1160$
	all data: $R_1 = 0.0737$, $wR_2 = 0.1211$
Weighting scheme	$w=1/[\sigma^2(F_o^2)+(0.0100P)^2+26.5000P]$, $P=(F_o^2+2F_c^2)/3$
Extinction coefficient	0.0002(0)
Largest diff. peak and hole	0.798 and -0.470 eÅ^{-3}
R.M.S. deviation from mean	0.057 eÅ^{-3}

$R_{int} = \Sigma|F_o^2 - F_o^2(\text{mean})| / \Sigma[F_o^2]$

$R_1 = \Sigma||F_o| - |F_c|| / \Sigma|F_o|$

$\text{GOOF} = S = \{\Sigma[w(F_o^2 - F_c^2)^2] / (n - p)\}^{1/2}$

$wR_2 = \{\Sigma[w(F_o^2 - F_c^2)^2] / \Sigma[w(F_o^2)^2]\}^{1/2}$

Details of the X-ray crystallographic structure of II-2f. A colorless plate-like specimen of $C_{50}H_{94.28}Cl_4N_{20}O_{25.14}$, approximate dimensions 0.18 mm × 0.44 mm × 0.48 mm, was used for the X-ray crystallographic analysis. The X-ray intensity data were measured on a Bruker APEX-II CCD system equipped with a graphite monochromator and a MoKα sealed tube (λ = 0.71073 Å). Data collection temperature was 150 K.

The total exposure time was 22.73 hours. The frames were integrated with the Bruker SAINT software package using a narrow-frame algorithm. The integration of the data using a monoclinic unit cell yielded a total of 118279 reflections to a maximum θ angle of 30.00° (0.71 Å resolution), of which 39291 were independent (average redundancy 3.010, completeness = 99.5%, R_{int} = 4.30%, R_{sig} = 4.63%) and 34631 (88.14%) were greater than $2\sigma(F^2)$. The final cell constants of *a* = 13.7177(10) Å, *b* = 27.048(2) Å, *c* = 18.9817(14) Å, β = 92.5526(12)°, *V* = 7035.9(9) $Å^3$, are based upon the refinement of the XYZ-centroids of 9755 reflections above 20 σ(I) with 4.685° < 2θ < 61.03°. Data were corrected for absorption effects using the multi-scan method (SADABS). The calculated minimum and maximum transmission coefficients (based on crystal size) are 0.8858 and 0.9549.

The structure was solved and refined using the Bruker SHELXTL Software Package, using the space group P 1 21 1, with Z = 4 for the formula unit, $C_{50}H_{94.28}Cl_4N_{20}O_{25.14}$. The final anisotropic full-matrix least-squares refinement on F^2 with 1686 variables converged at R_1 = 5.29%, for the observed data and wR_2 = 12.34% for all data. The goodness-of-fit was 1.011. The largest peak in the final difference electron density synthesis was 0.689 $e^-/Å^3$ and the largest hole was -0.916 $e^-/Å^3$ with an RMS deviation of 0.071 $e^-/Å^3$. On the basis of the final model, the calculated density was 1.435 g/cm^3 and F(000), 3214 e^-.

APEX2 Version 2010.11-3 (Bruker AXS Inc.)

SAINT Version 7.68A (Bruker AXS Inc., 2009)

SADABS Version 2008/1 (G. M. Sheldrick, Bruker AXS Inc.)

XPREP Version 2008/2 (G. M. Sheldrick, Bruker AXS Inc.)

XS Version 2008/1 (G. M. Sheldrick, *Acta Cryst.* (2008). A**64**, 112-122)

XL Version 2012/4 (G. M. Sheldrick, (2012) University of Gottingen, Germany)

Platon (A. L. Spek, *Acta Cryst.* (1990). A**46**, C-34)

Table 1. Sample and crystal data for UM2349.

Identification code	2349	
Chemical formula	$C_{50}H_{94.28}Cl_4N_{20}O_{25.14}$	
Formula weight	1519.77	
Temperature	150(2) K	
Wavelength	0.71073 Å	
Crystal size	0.18 × 0.44 × 0.48 mm	
Crystal habit	colorless plate	
Crystal system	monoclinic	
Space group	P 1 21 1	
Unit cell dimensions	a = 13.7177(10) Å	α = 90°
	b = 27.048(2) Å	β = 92.5526(12)°
	c = 18.9817(14) Å	γ = 90°

Volume	7035.9(9) $Å^3$
Z	4
Density (calculated)	1.435 Mg/cm^3
Absorption coefficient	0.259 mm^{-1}
F(000)	3214

Table 2. Data collection and structure refinement for UM2349.

Diffractometer	Bruker APEX-II CCD
Radiation source	sealed tube, MoKα
Theta range for data collection	2.28 to 30.00°
Index ranges	$-19 \leq h \leq 19$, $-36 \leq k \leq 38$, $-26 \leq l \leq 26$
Reflections collected	118279
Independent reflections	39291 [R(int) = 0.0430]
Coverage of independent reflections	99.5%
Absorption correction	multi-scan
Max. and min. transmission	0.9549 and 0.8858
Structure solution technique	direct methods
Structure solution program	SHELXS-97 (Sheldrick, 2008)
Refinement method	Full-matrix least-squares on F^2

Refinement program	SHELXL-97 (Sheldrick, 2008)
Function minimized	$\Sigma\, w(F_o^2 - F_c^2)^2$
Data / restraints / parameters	39291 / 31 / 1686
Goodness-of-fit on F^2	1.011
Δ/σ_{max}	0.001
Final R indices	34631 data; R_1 = 0.0529, wR_2 = I>2σ(I) 0.1210
	R_1 = 0.0583, wR_2 = all data 0.1234
Weighting scheme	$w=1/[\sigma^2(F_o^2)+(0.0100P)^2+9.0000P]$, $P=(F_o^2+2F_c^2)/3$
Absolute structure parameter	0.5(0)
Largest diff. peak and hole	0.689 and -0.916 eÅ^{-3}
R.M.S. deviation from mean	0.071 eÅ^{-3}

$R_{int} = \Sigma|F_o^2 - F_o^2(\text{mean})| / \Sigma[F_o^2]$

$R_1 = \Sigma||F_o| - |F_c|| / \Sigma|F_o|$

$\text{GOOF} = S = \{\Sigma[w(F_o^2 - F_c^2)^2] / (n - p)\}^{1/2}$

$wR_2 = \{\Sigma[w(F_o^2 - F_c^2)^2] / \Sigma[w(F_o^2)^2]\}^{1/2}$

Chapter 3. Acyclic Cucurbit[n]uril-Type Molecular Containers: Influence of Aromatic Walls on their Function as Solubilizing Excipients for Insoluble Drugs

3.1 Introduction

In chapter 2, we studied the influence of the nature of the solubilizing groups (e.g. SO_3^- vs. OH vs NH_3^+) on the ability of acyclic CB[n] type containers to act as solubilizing agents for insoluble drugs and found that sulfonate groups are particularly well suited for this application because they impart high solubility in water and do not promote self-folding and complexation (e.g. as NH_3^+ does).[80] In this chapter we explore the influence of the nature of the aromatic sidewalls on the ability of the acyclic CB[n]-type containers (**III-1a** – **III-1e**, Scheme III-1) to act as solubilizing agents for insoluble drugs.

3.2 Results and discussion.

This results and discussion section is organized as follows. First, we describe the synthesis and solubility of two new acyclic CB[n]-type receptors **III-1d** and **III-1e**. Next, we investigate the self-association properties of **III-1a** – **III-1e**. Subsequently, we create phase solubility diagrams for **III-1a** – **III-1e** toward a range of well-known poorly soluble pharmaceutical agents (Figure III-2) and analyze trends in the solubilization data.

3.2.1 Design and Synthesis of Acyclic CB[n]-Type Containers III-1a – III-

1e.

Previously, we reported the synthesis and application of acyclic CB[n] type containers **III-1a** – **III-1c** by the double electrophilic aromatic substitution reaction of glycoluril tetramer bis(cyclic ether) building block **III-2** with the corresponding dialkoxyaromatic sidewalls **III-3** in hot CF_3CO_2H.[30,35,80] Compounds **III-1a** – **III-1e** differ in the nature of their aromatic sidewalls (e.g. benzene vs naphthalene) which impact the structure of the uncomplexed container and therefore their ability to act as a host and solubilizing agent for insoluble drugs. For example, the x-ray crystal structures of **III-1a** shows that the tips of the substituted benzene sidewalls are in close contact with one another.[35] Therefore, to accommodate the longer naphthalene sidewalls of **III-1b**, the glycoluril tetramer backbone of **III-1b** flexes which results in a larger cavity which is defined in larger part by the aromatic naphthalene sidewalls.[35] Compound **III-1c** is an isomer of **III-1b**; in this case the sidewalls are shorter and deeper by virtue of the attachment at the naphthalene 1,8 positions.[30] To prepare new acyclic CB[n] type receptors **III-1d** and **III-1e** we needed to prepare aromatic sidewalls **III-3d** and **III-3e**. Accordingly, we reacted 2,3-dimethylhydroquinone with 1,3-propanesultone (**III-4**) under basic conditions (NaOH) in dioxane at room temperature to give **III-3d** in 73% yield (Scheme III-1a). Sidewall **III-3e** was prepared by a multistep procedure (Scheme III-1b). First, we performed the Diels-Alder reaction between benzoquinone and 1,3-butadiene in toluene to give **III-5** in 92% yield.[124] Next, we aromatized **III-5** by treatment with HBr to give **III-6** in 82% yield.[124] Subsequently, we reduced the double bond of **III-6** under standard conditions to give **III-7** in 85% yield.[125] Finally, **III-7** was reacted with **III-4** under basic conditions to give the required aromatic wall **III-3e** in 60% yield. The reaction of

glycoluril tetramer **III-2** with sidewall **III-3d** (4 equiv.) in a 1:1 (v:v) mixture of TFA:Ac_2O at 70 ˚C gave acyclic CB[n] type container **III-1d** in 43% yield. Similarly, the reaction of **III-2** with **III-3e** (4 equiv.) gave container **III-1e** in 30% yield.

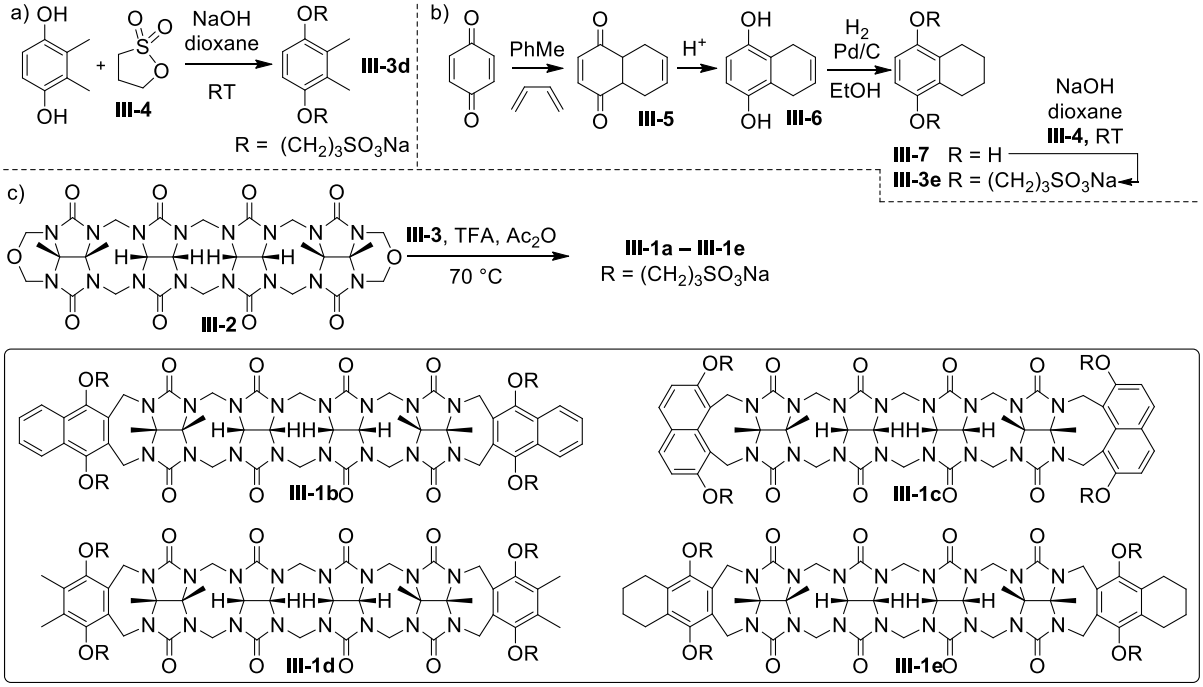

Scheme III-1. Structures of known acyclic CB[n] solubilizing excipients **III-1b** and **III-1c** and synthesis of **III-1d** and **III-1e.**

3.2.2 Solubility Properties of the Acyclic CB[n] Type Containers III-1a – III-1e.

An important property of a container that is to be used as a solubilizing excipient for insoluble drugs is the inherent solubility of the container alone. Previously, we have reported the solubility of **III-1a** and **III-1b** in 20 mM sodium phosphate buffered D_2O at pD 7.4 as 105 mM and 14 mM, respectively. We used the methodology reported previously[35,80] – ^{1}H NMR assay in the presence of 1,3,5-benzene tricarboxylic acid as internal standard of known concentration – to determine the inherent solubilities of **III-1c** (115 mM), **III-1d** (353

mM), and **III-1e** (145 mM). The high solubilities of **III-1a**, **III-1c**, **III-1d**, and **III-1e** make them particularly attractive as solubilizing excipients for insoluble drugs.

3.2.3 Self-Association Properties of Acyclic CB[n] Type Containers III-1a – III-1e.

Previously, we have investigated the self-association of **III-1a** and **III-1b** by dilution experiments monitored by ^{1}H NMR spectroscopy. We found that the observed changes in chemical shift for each container fit well to a 2-fold self association model and extracted the corresponding self-association constants (**III-1a**, K_s = 47 M^{-1}; **III-1b**, K_s = 624 M^{-1}).[35,117] Because **III-1a** and **III-1b** have a low propensity to self-associate they are well suited to act as solubilizing excipients for insoluble drugs. In a similar manner, we performed the ^{1}H NMR dilution experiment (15 mM – 0.1 mM) for **III-1d** and measured the corresponding value of K_s for **III-1d** as 130 M^{-1}. When we performed similar ^{1}H NMR dilution experiments for **III-1c** we unexpectedly observed two sets of resonances that were in slow exchange on the chemical shift timescale. We measured the diffusion coefficients for these two species by DOSY NMR spectroscopy (D = 2.058 and 1.751 x 10^{-10} m^2/s, Supporting Information) which allows us to conclude that the two species correspond to monomer **III-1c** and dimer (**III-1c**)$_2$. Accordingly, we integrated the resonances for the two species at several different concentrations and determined the value of K_s (372 M^{-1}) in the usual manner.[94] Finally, we performed a dilution experiment for **III-1e** (35 mM – 0.2 mM) and observed both broadening and changes in ^{1}H NMR chemical shifts. Unfortuantely, the changes in chemical shift could not be fitted to the standard 2-fold self- association model and we belive that **III-1e**

undergoes more complex higer order aggregation. The generally weak self-association observed for **III-1a** – **III-1e** are advantageous toward their use as solubilizing excipients for insoluble drugs because the container is free to associate with drug without having to overcome strong self-assocation.

3.2.4 Theoretical Treatment of Phase Solubility Diagrams.

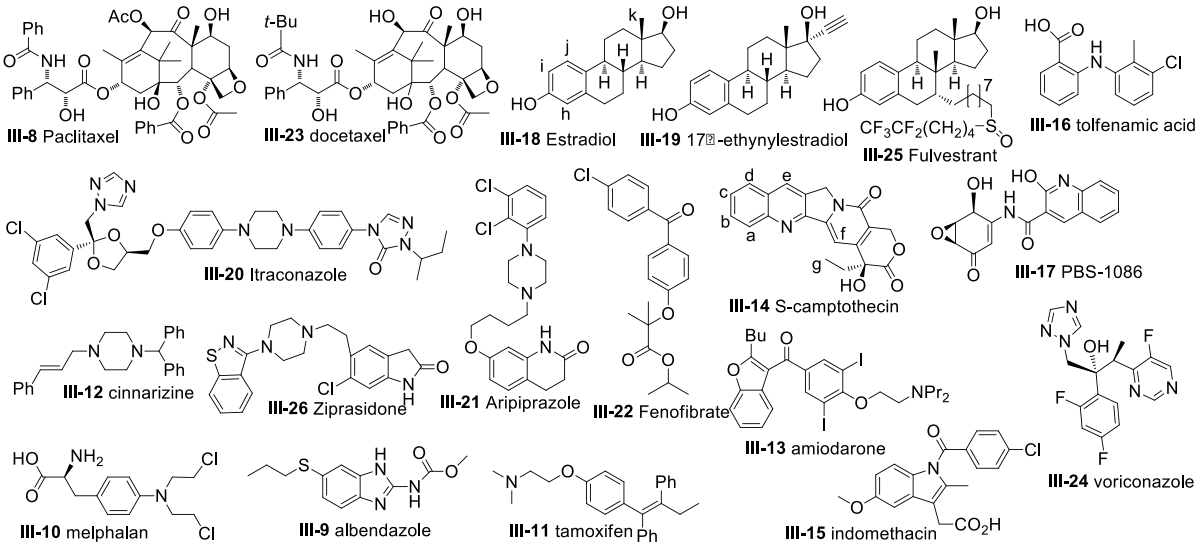

Figure III-1. Chemical structures of drugs used in this study.

Phase solubility diagrams (PSD) – plots of [Drug] as a function of [Container] are commonly used to study the ability of molecular containers to increase the solubility of insoluble drugs.[52,117] These phase solubility diagrams can assume a variety of shapes, but linear PSDs (A_L type) are most common and occur when container and guest form well defined 1:1 container•guest complexes. Such PSDs behave according to equation III-1 where S_0 is the solubility of drug alone, K_a is the binding constant for the container•drug complex, and slope is the slope of the PSD. Figure III-3 shows the results of two simulations that were

performed on a hypothetical container•drug system that obeys equation III-1 to stimulate the discussion and analysis of the experimental PSDs created for containers **III-1a**– **III-1e** and HP-β-CD with drugs **III-8** – **III-26** shown in Figure III-2. Figure III-3a shows the calculated PSDs for five different containers and a single drug with $S_0 = 1 \times 10^{-6}$ M which form well defined 1:1 container•drug complexes of high solubility. The different K_a values for the different container•drug complexes translate into PSDs with different slopes. For example, a change in slope from 0.1 to 0.5 and from 0.5 to 0.9 each correspond to a 9-fold increase of K_a. Importantly, a precise knowledge of S_0 is not necessary in order to calculate relative K_a values ($K_{rel} = K_{a,C1•D1} / K_{a,C2•D1}$) from the PSDs obtained with two different containers (e.g. C1 and C2) toward a common drug (e.g. D1) because the S_0 values cancel as shown in equation III-2. If S_0 is known precisely, then absolute K_a values can be calculated using equation III-1. Figure III-3b shows a plot of the slope of the PSD as a function of the K_a for the container•drug complex for five different values of S_0 (1 mM, 100 μM, 10 μM, 1 μM, 100 nM). Clearly, the lower the inherent solubility of the drug (S_0), the higher the value of K_a needed to result in a PSD of comparable slope. As a special case of equation III-1, consider the situation when $(K_a)(S_0) = 1$; under this constraint, then slope = 0.5 (Figure III-3b) From a practical point of view this means that to efficiently solubilize an insoluble drug (e.g. slope of PSD = 0.5) with an inherent solubility of 10 mM (100 nM) requires a K_a value of 10^5 M^{-1} (10^7 M^{-1}). In theory, the high values of K_a that are typically observed for CB[n]-type receptors promise to enable the solubilization of drugs whose solubilities are too low to be solubilized by lower affinity hosts (e.g. cyclodextrins).

$$K_a = \frac{\text{slope}}{S_0\,(1\text{-slope})} \qquad \text{(III-1)}$$

$$K_{rel} = \frac{K_{a,C1\bullet D1}}{K_{a,C2\bullet D1}} = \frac{\dfrac{slope_{C1\bullet D1}}{S_{0,D1}\,(1\text{-}slope_{C1\bullet D1})}}{\dfrac{slope_{C2\bullet D1}}{S_{0,D1}\,(1\text{-}slope_{C2\bullet D1})}} = \frac{(slope_{C1\bullet D1})\,(1\text{-}slope_{C2\bullet D1})}{(slope_{C2\bullet D1})\,(1\text{-}slope_{C1\bullet D1})} \qquad \text{(III-2)}$$

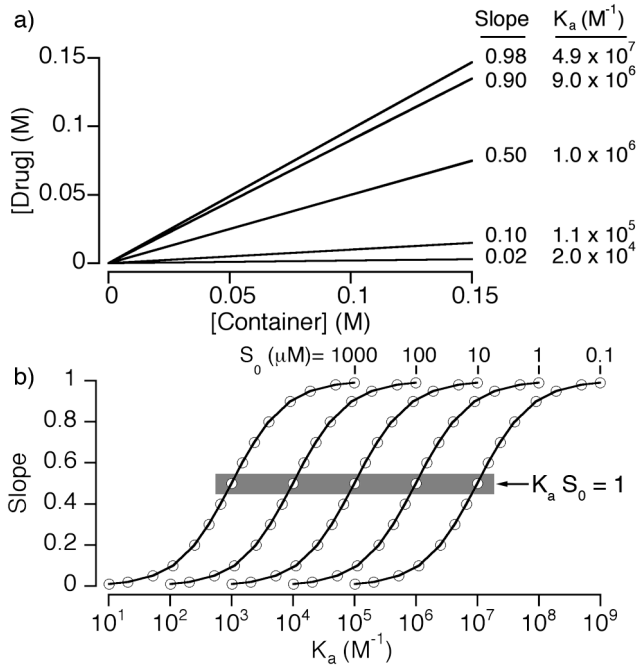

Figure III-2. Simulations of the phase solubility behavior of hypothetical container•drug 1:1 systems that obey equation III-1. a) Plot of [Drug] versus [Container] for a system with S_0 = 1 μM and five different K_a values. B) Plot of slope of the PSD versus K_a (M^{-1}) for five different values of S_0 (1 mM, 100 μM, 10 μM, 1 μM, 100 nM).

3.2.5 Use of III-1a – III-1e as Solubilizing Agents for Insoluble Drugs.

Table III-1. Inherent solubility (S_0) of selected drugs and values of slope calculated from the linear region of the PSDs for containers **III-1a** – **III-1e** and HP- β-CD with drugs **III-8** – **III-26**. The corresponding K_a (M^{-1}) and K_{rel} values were calculated using equations **III-**1 and **III-**2.

		III-1a		**III-1b**		**III-1c**		**III-1d**		**III-1e**		**HPCD**	
	S_0 (mM)	Slope	K_{rel} K_a	Slope	K_{rel} K_a	Slope	K_{rel} K_a	Slope	K_{rel} K_a	Slope	K_{rel} K_a	Slope	K_{rel} K_a
III-8	n.d.	n.l.	–	0	–	0	–	0	–	0	–	0	–
III-9	2.74	0.122	9.385 5.06×10^4	0.479	62.169 3.35×10^5	0.026	1.827 9.84×10^3	0.105	7.953 4.29×10^4	0	– –	0.015	1 5.39×10^3
III-10	n.d.	0.774	27.055	1.053	TL	0.814	34.549	0.801	31.686	0.467	6.898	0.113	1
III-11	12.97	0.040	1.461 3.21×10^3	0.101	3.944 8.67×10^3	0.461	29.993 6.60×10^4	0.060	2.238 4.92×10^3	0	– –	0.028	1 2.20×10^3
III-12	n.d.	0.588	632.642	0	–	0	–	0	–	0.057	26.580	0.002	1
III-13	n.d.	0.080	0.890	1.032	TL	0.138	1.634	0.125	1.455	0.132	1.557	0.089	1
III-14	58.71	0.137	0.996 2.70×10^3	1.147	TL TL	0.255	2.152 5.84×10^3	0.505	6.403 1.74×10^4	0.137	1 2.71×10^3	0	– –
III-15	n.d.	0.024	1.846	0.473	66.589	0.022	1.694	0.017	1.269	0	–	0.013	1
III-16	2.15	0.043	5.756 2.09×10^4	0.543	151.885 5.52×10^5	0.052	6.953 2.53×10^4	0.033	4.414 1.61×10^4	0	– –	0.008	1 3.64×10^3
III-17	n.d.	0.711	14.761	0.919	67.764	0.143	1	0.517	6.434	0.159	1.132	0	–
III-18	9.33	0.354	2.417 5.86×10^4	0.920	50.631 1.23×10^6	0.409	3.059 7.42×10^4	0.607	6.834 1.66×10^5	0.517	4.728 1.15×10^5	0.185	1 2.43×10^4
III-19	n.d.	0.353	1	1.085	TL	0.405	1.247	0.383	1.138	0.439	1.437	0.469	1.620
III-20	n.d.	0	–	0	–	0.121	8.569	0.016	1	0.021	1.317	0	–
III-21	26.69	0.066	2.015 2.63×10^3	0.309	12.824 1.67×10^4	0.034	1 1.30×10^3	0	– –	0	– –	0	– –
III-22	n.d.	0	–	n.l.	–	0	–	0	–	0	–	0	–
III-23	n.d.	0.079	1	0	–	0	–	0	–	0	–	0	–
III-24	36.49	0.496	3.419 2.70×10^4	0.893	28.845 2.28×10^5	0.395	2.264 1.79×10^4	0.834	17.392 1.37×10^5	0.895	29.706 2.34×10^5	0.224	1 7.89×10^3
III-25	n.d.	0	–	0.104	1	0	–	0	–	0	–	0	–
III-26	63.54	1.077	TL	0.432	28.786 1.19×10^4	0.178	8.220 3.41×10^3	0.388	24.075 9.99×10^3	0.458	32.066 1.33×10^4	0.026	1 4.15×10^2

n.d. = not determined, n.l. = non-linear PSD; – = could not be determined because PSD is non-linear or slope = 0; TL = too large to be determined from PSD.

In order to more fully understand the correlation between container structure (e.g. **III-1a** – **III-1e**), drug structure and properties, and the ability of the containers to solubilize insoluble drugs we created phase solubility diagrams (PSD) for containers **III-1a** – **III-1e** and HP- β-CD with the 19 insoluble drugs (**III-8** – **III-26**) shown in Figure III-2. Of these, 18 are drugs

currently used in practice along with PBS-1086 which is a developmental compound with documented anti-cancer activity.[126] To create these PSDs we stir an excess of insoluble drug with a known concentration of container until equilibrium is achieved, then remove remaining insoluble drug by filtration or centrifugation, and measure the concentration of drug in the supernatant by ^{1}H NMR spectroscopy. Our ^{1}H NMR assay relies on the addition of a known concentration of 1,3,5-benzene tricarboxylic acid as a non-binding internal standard of known concentration which allows us to use the ratio of the integrals for drug versus internal standard to measure drug concentration. We have measured full PSDs for all 19 drugs with the six containers (Supporting Information). In nearly all cases, linear PSDs were observed at low [container] indicative of well defined 1:1 complex formation, although some of the PSDs display plateau regions at higher [container] which indicates that the solubility of the container•drug complex is lower than that of uncomplexed container. Table III-1 gives the initial slopes of the PSDs determined by linear regression for all container-drug combinations. Table III-1 also presents the K_{rel} values calculated using equation III-2 referenced to the weakest bind host (usually HP-β-CD). Figure III-4 presents the PSDs measured for three drugs (Estradiol, PBS-1086, Camptothecin) with the 6 different containers. In the sections below, we analyze the data presented in Table III-1 to ascertain key features of the use of acyclic CB[n]-type containers as solubilizing excipients for insoluble drugs.

*Container **III-1b** is the Most Potent Solubilizing Agent.* Of the 19 drugs tested, compound **III-1b** is most efficient solubilizing agent (e.g. largest slope, highest K_{rel}) for 12 drugs, and is

nearly the best for two additional drugs (slopes for voriconazole: **III-1b** = 0.893 versus **III-1e** = 0.895; slopes for ziprasidone: **III-1b** = 0.432 versus **III-1e** = 0.458). For four drugs (melphalan, amiodarone, camptothecin, 17a-ethynylestradiol), **III-1b** forms such tight complexes (slope ≈ 1) that it is not possible to calculate a K_{rel} value using equation III-1. To understand the superior binding properties of **III-1b** we performed MMFF minimizations of the complexes between truncated versions of **III-1a** – **III-1e** (OMe instead of $O(CH_2)_3SO_3Na$ arms) and *trans*-1,4-cyclohexane diammonium ion (Figure III-5) to assess the geometrical features of the complexes. As can readily be seen, container **III-1a** features the smallest cavity (distances between opposing glycoluril methine C-atoms = 10.90 and 10.38 Å) whereas the corresponding distances for **III-1b – III-1e** are substantially longer. Container **III-1b** features the largest cavity (opposing C-atom distance = 12.34 and 11.42 Å) and its naphthalene walls engage in a perfect edge-to-face p-p interaction which provides a large hydrophobic p-surfaces to engage in π–π interactions with aromatic drugs. Although the cavity size of containers **III-1d** and **III-1e** are comparable to that of **III-1b** they are partly shaped by the CH_3 groups and fused cyclohexyl rings reduce the available p-surface area. We surmise these are the reasons behind the superior binding abilities of **III-1b**.

Solubilization of Steroids. The test panel of insoluble drugs contained three steroids (estradiol, 17-a-ethynylestradiol, and fulvestrant). Steroids can often be solubilized with HP-β-CD, which allows a head-to-head comparison with our acyclic CB[n]-type containers. Figure III-4a shows the PSDs measured for all six containers toward estradiol which is illustrative. All five acyclic CB[n]-type containers **III-1a** – **III-1e** solubilize estradiol more

efficiently (slope = 0.354 to 0.92; K_{rel} from 2.4 to 50.5) than HP-β-CD (slope = 0.185; K_{rel} = 1). Figure III-6a-c shows the ^{1}H NMR spectra recorded for estradiol alone in DMSO-d_6 and in the presence of **III-1a** and **III-1b** in buffered D_2O. The large upfield shifts observed for the axial Me-group (H_k) and the protons on the sp^3-hydridized C-atoms of the steroidal skeleton indicate that the containers bind preferentially to this region of the steroids. Container **III-1b** solubilizes 17-a-ethynylestradiol with 1:1 stoichiometry which is indicative of a very large association constant K_a for this complex. Only container **III-1b** was capable of solubilizing fulvestrant which is both highly hydrophobic and fluorinated. Previously, we have established that **III-1b** binds to the neuromuscular blocking agents rocuronium and vecuronium which are steroidal diammoniums with $K_a > 10^9$ M^{-1}.[112] In combination, these results allow us to conclude that acyclic CB[n]-type containers – but especially **III-1b** – are better receptors for steroids than HP-β-CD.

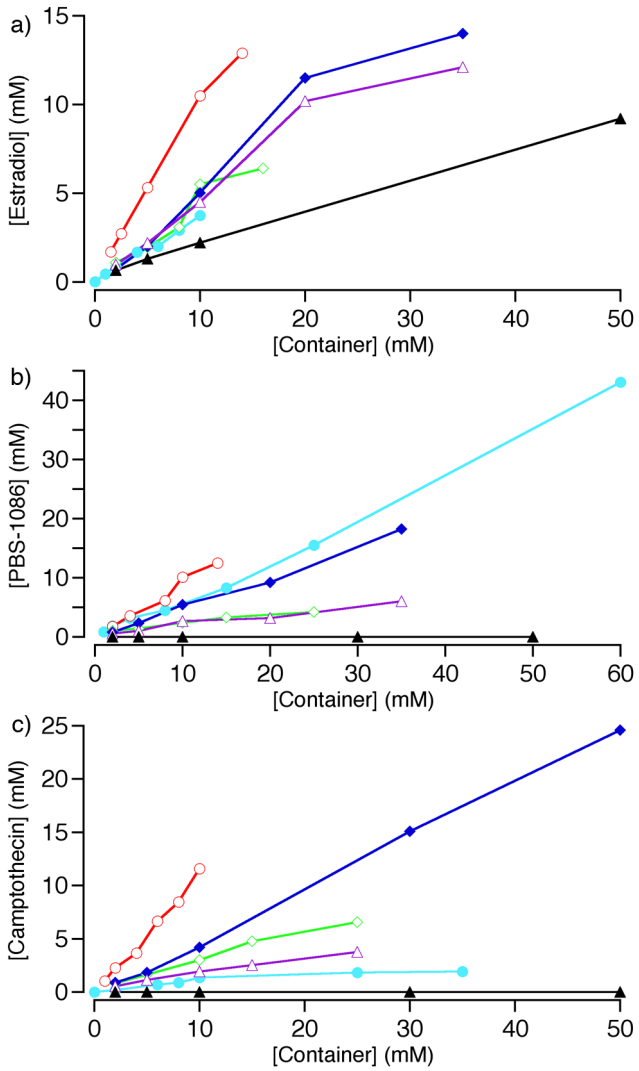

Figure III-3. Phase solubility diagrams constructed for mixtures of containers (**III-1a**, ●; **III-1b**, o; **III-1c**, ◊; **III-1d**, ◆; **III-1e**, △; HP-β-CD,▲) with selected insoluble drugs: a) Estradiol, b) PBS-1086, c) Camptothecin. Conditions: 20 mM sodium phosphate buffered D_2O (pH = 7.4, RT).

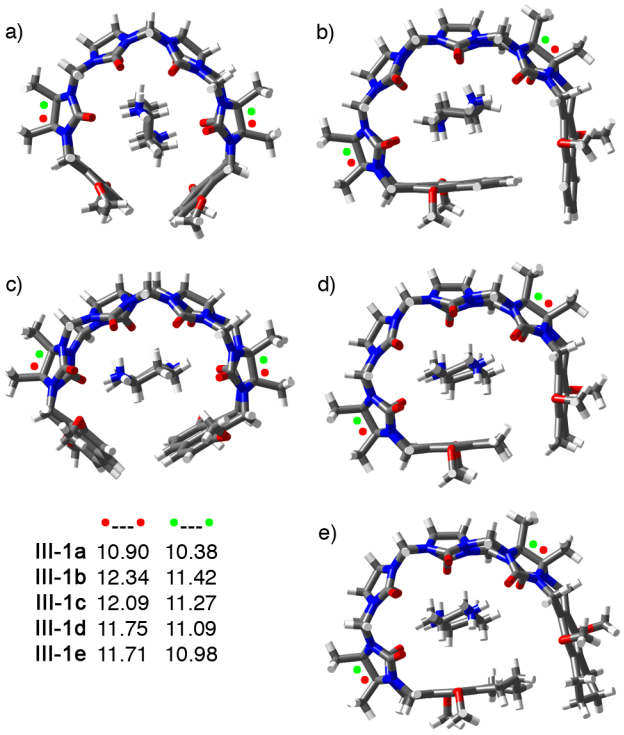

Figure III-4. MMFF minimized models of the trans-1,4-cyclohexanediammonium ion complexes of truncated versions (OMe rather than $O(CH_2)_3SO_3Na$ arms) of: a) **III-1a**, b) **III-1b**, c) **III-1c**, d) **III-1d**, e) **III-1e**. The distances between the labeled (• and •) glycoluril quaternary C-atoms are given in Å.

Developmental Anticancer Agent PBS-1086. PBS-1086 is a developmental drug with documented *in vivo* anticancer activity using a DMSO formulation, but which could not be formulated in water using the standard techniques including cyclodextrins.[126] Accordingly, we decided to investigate the formulation of PBS-1086 using container **III-1a** – **III-1e** (Table III-1 and Figure III-4b). All five acyclic CB[n]-type containers solubilize PBS-1086 (slope = 0.143 to 0.919) whereas HP-β-CD is incapable of solubilizing this drug. Interestingly, although PBS-1086 is most efficiently solubilized by **III-1b** (slope = 0.919), container **III-1a** (slope = 0.711) generates a solution with the highest concentration of PBS-1086 because of

the higher inherent solubility of **III-1a**. PBS-1086 is also nicely solubilized by **III-1d** which is perhaps unsurprising given that the Me-substituted sidewalls of **III-1d** makes it intermediate in size (Figure III-5) between **III-1a** and **III-1b**.

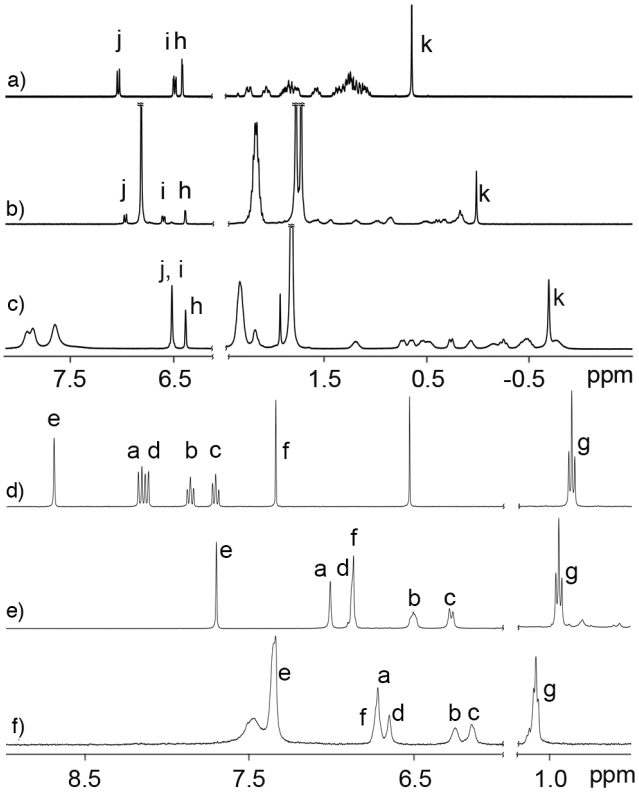

Figure III-5. ^{1}H NMR recorded (400 MHz, RT, 20 mM sodium phosphate buffered D_2O, pH 7.4) for: a) estradiol (in DMSO-d_6), b) **III-1a** (10 mM) with estradiol, c) **III-1b** (10 mM) with estradiol, d) camptothecin (in DMSO-d_6), e) **III-1d** (15 mM) with camptothecin, and f) **III-1b** (10 mM) with camptothecin.

Acyclic CB[n]-type Containers are Good Solubilizing Agents for Insoluble Drugs Containing Aromatic Rings. The molecular models of **III-1a** – **III-1e** show that the aromatic sidewalls are oriented at approximately right angles to one another which defines a hydrophobic box. Accordingly, it would be expected that insoluble drugs that contain aromatic rings would be

good guests for acyclic CB[n]-type containers. The majority of drugs studied in this paper contain aromatic rings within their structure and we generally observed upfield shifting of the ^{1}H NMR resonances of these aromatic rings upon complexation with **III-1a** – **III-1e**. Those aromatic rings with attached ammonium functional groups (e.g. anilines, benzimidazoles, N-arylpiperazines) constitute preferred binding sites. In only one case (amiodarone, **III-13**) was complexation at an aliphatic ammonium (Pr_2NHR^+) moiety predominant. The observed upfield shifting of the aromatic protons confirms that the aromatic residues of the drugs are encapsulated within the hydrophobic box that is defined by the two aromatic walls and the methylene bridged glycoluril tetramer backbone. For example, Figure III-6d-f shows the ^{1}H NMR spectra recorded for camptothecin alone in DMSO-d_6 and in water in the presence of containers **III-1d** and **III-1b**. Obviously, the protons on the aromatic rings of camptothecin (H_a – H_f) undergo substantial upfield shifts upon complexation. Larger upfield shifts are observed upon complexation with **III-1b** probably because of the larger anisotropic effect of the naphthalene walls of **III-1b** relative to the *o*-xylylene walls of **III-1d**. Figure III-4c shows the PSDs created for mixtures of camptothecin with containers **III-1a** – **III-1e** and HP-β-CD which display A_L-type PSDs indicative of 1:1 complexation. All five acyclic CB[n]-type containers (**III-1a** – **III-1e**) solubilize camptothecin nicely, with **III-1b** doing so in equimolar amounts whereas HP-β-CD is unable to solubilize camptothecin under these conditions. We believe that the strategic merging of the structural features of CB[n] receptors (to deliver strong hydrophobic binding and ammonium binding) with the aromatic walls of cyclophanes to impart affinity toward the wide variety of insoluble aromatic drugs positions acyclic CB[n]-type receptors **III-1a** – **III-1e** as a powerful alternative to

cyclodextrins that expands the scope of insoluble drugs that can be formulated with molecular container technology.

Some Drugs are Solubilized by a Narrow Set of Containers. Four drugs are solubilized by only one acyclic CB[n]-type container: paclitaxel and docetaxel by **III-1a**, fenofibrate and fulvestrant by **III-1b**. Cinnarizine is only solubilized by two containers; it is best solubilized by **III-1a** and less well by **III-1e**. Based on this data we believe that containers **III-1a** and **III-1b** are the most versatile and general purpose solubilizing agents and that these containers are best positioned for further development as novel solubilizing excipients for practical applications.

*Container **III-1d** is Structurally and Functionally Intermediate Between **III-1a** and **III-1b**.* The dimethyl substituted *o*-xylylene walls of container **III-1d** are intermediate in length between **III-1a** and **III-1b** which feature benzene and napthalene derived sidewalls. Compound **III-1d** is also intermediate between **III-1a** and **III-1b** in terms of its self-association properties but possesses superior solubility characteristics (353 mM) in buffered water. Figure III-5 shows that the difference in length of the aromatic walls of **III-1d** also results in a cavity that is intermediate between those of **III-1a** and **III-1b**. Accordingly, and perhaps unsurprisingly, we find that **III-1d** exhibits solubilization abilities that are similar to those of **III-1a** and **III-1b**. For example, for albendazole, melphalan, amiodarone, indomethacin, and tolfenamic acid the slopes and K_{rel} values for **III-1d** are comparable to those of **III-1a** but significantly smaller than the corresponding values measured for **III-1b**.

For other drugs, namely voriconazole and ziprasidone, the slope and K_{rel} values measured for **III-1d** are more comparable to those of **III-1b** than **III-1a**.

3.2.6 Comparison of the Binding Affinity of III-1a – III-1e with HP-β-CD Toward Insoluble Drugs.

It is also possible to determine the absolute K_a value for container•drug complexes from the PSDs if the solubility of the uncomplexed drug (S_0) is known. Accordingly, we measured the inherent solubility for 8 drugs (albendazle, tamoxifen, camptothecin, tolfenamic acid, estradiol, aripiprazole, voriconazole, and ziprasidone) and used these S_0 values to determine the absolute K_a values for this selection of drugs as given in Table III-1. The binding constants for these eight drugs toward HP-β-CD span the range of 415 to 24300 M^{-1} which is in line with the well-known low affinity (log K_a = 2.5 ± 1.1 M^{-1}) and low selectivity of cyclodextrins toward their guests.[127,128] In contrast, the K_a values measured for these 8 drugs toward **III-1a** – **III-1e** fall in the range of 1300 to 1.2 x 10^6 M^{-1} with two additional complexes being too tight to measure using the PSD. The best acyclic container (e.g. **III-1a – III-1e**) always forms significantly stonger container•drug complexes (29 to 152-fold stronger). In many cases the acyclic containers bind to and solubilize drugs (e.g. camptothecin and aripiprazole) that cannot be solubilized at all with HP- β-CD. The ability of **III-1a** – **III-1e** to solubilize drugs that cannot be solubilized with HP- β-CD and to do so more efficiently (larger slope and K_a) suggests that acyclic CB[n]-type containers will become an important tool to formulate insoluble pharmaceutical agents.

3.3 Conclusion.

In summary, we have compared the ability of **III-1a** – **III-1e** to solubilize insoluble drugs relative to HP- β-CD. Compounds **III-1a – III-1e** do not undergo strong self-association ($K_s \leq 624\ M^{-1}$) in buffered water and possess good solubility characteristics. We created phase solubility diagrams for mixtures of containers **III-1a** – **III-1e** and HP- β-CD with 19 drugs. We find that the solubilizing ability of the best container (**III-1a** – **III-1e**) is superior to HP-β-CD in all cases; **III-1a** – **III-1e** even solubilize 8 drugs that are completely insoluble with HP- β-CD. The superior solubilizing ability can be traced to the 29 to 152-fold higher binding affinity of the best acyclic CB[n]-type container toward the drugs compared to HP-β-CD. Less container is needed, therefore, to achieve a given [drug]. A notable achievement was the solubilization of the developmental anticancer agent PBS-1086. The acyclic CB[n]-type containers display an affinity for the steroid ring system, aromatic moieties of insoluble drugs, and cationic ammonium groups. Compound **III-1b** is generally the most potent (K_a up to and exceeding $10^6\ M^{-1}$) container whereas both **III-1a** and **III-1b** display excellent solubility enhancement toward a broad range of insoluble drugs. The broad scope of insoluble drugs that can be formulated with **III-1a** and **III-1b –** in many cases where HP- β-CD fails completely – makes acyclic CB[n]-type containers particularly attractive alternatives to cyclodextrins as solubilizing excipients for practical applications.

3.4 Experimental Section.

General Experimental. Starting materials were purchased from commercial suppliers and were used without further purification or were prepared by literature procedures.

Compounds **III-1a – III-1c**, **III-2**, **III-5** and **III-6** were prepared according to literature procedures.[30,35,124] Melting points were measured on a Meltemp apparatus in open capillary tubes and are uncorrected. IR spectra were measured on a JASCO FT/IR 4100 spectrometer and are reported in cm^{-1}. NMR spectra were measured at 400 MHz or 600 MHz for ^{1}H and 125 MHz for ^{13}C. Mass spectrometry was performed using a JEOL AccuTOF electrospray instrument using the electrospray ionization (ESI) technique.

Compound III-3d. A solution of **III-4** (18.409 g, 150 mmol) in 1,4-dioxane (130 mL) was added into a solution of 2,3-dimethylhydroquinone (8.005 g, 57.9 mmol) in aqueous NaOH solution (1.00 M, 100 mL). The mixture was stirred at RT for 12 h then filtered to collect the crude solid. The solid was stirred with acetone (200 mL) then dried under high vacuum to yield **III-3d** as a pale red solid (18.007 g, 73%). M.p. > 280 ˚C. IR (ATR, cm^{-1}): 2938w, 2869w, 1625m, 1489m, 1472m, 1205s, 1157s, 1112s, 1059s, 801m, 624m, 551m. ^{1}H NMR (400 MHz, D_2O): δ 6.88 (s, 2H), 4.10 (t, J = 5.6, 4H), 3.10 (t, J = 7.2, 4H), 2.15 - 2.05 (m, 8H), 1.71 (s, 6H). ^{13}C NMR (125 MHz, D_2O, 1, 4-dioxane as internal reference): δ 150.5, 127.6, 111.8, 68.2, 47.6, 24.1, 11.1. High-Res MS (ESI): *m/z* 381.0694 ($[M - 2Na + H]^-$, $C_{14}H_{21}O_8S_2$, calculated for 381.0678).

Compound III-7. A solution of **III-6** (5.315 g, 32.8 mmol) in EtOH (160 mL) was mixed with palladium on activated carbon (3.510 g, 10 wt. %, 3.3 mmol). The mixture was stirred under H_2 gas (15 Psi) for 3 days at RT. The slurry was then filtered and the filtrate was concentrated under reduced pressure. After the residual solvent was removed under high

vacuum, the product was obtained as a light purple solid (4.57 g, 85%). Characterization data matches the literature report.[19]

Compound III-3e. A solution of **III-4** (8.580 g, 69.8 mmol) in 1,4-dioxane (60 mL) was added into a solution of **III-7** (4.000 g, 27.9 mmol) in aqueous NaOH solution (1.00 M, 45 mL). The mixture was stirred at RT for 12 h then filtered to collect the crude solid. The crude solid was stirred with acetone (100 mL) then dried under high vacuum to yield **III-3e** as a white solid (7.570 g, 60%). M.p. > 280 ˚C. IR (ATR, cm^{-1}): 2946w, 2846w, 1652w, 1471w, 1256m, 1194s, 1094m, 1045s, 791w, 604w, 521w. ^{1}H NMR (400 MHz, D_2O): δ 6.83 (s, 2H), 4.09 (t, J = 6.0, 4H), 3.08 (t, J = 6.2, 4H), 2.65 - 2.55 (m, 4H), 2.35 – 2.15 (m, 4H), 1.75 – 1.60 (m, 4H). ^{13}C NMR (125 MHz, D_2O, 1, 4-dioxane as internal reference): δ 150.0, 128.1, 110.2, 67.4, 47.6, 24.0, 22.7, 21.2. High-Res MS (ESI): *m/z* 407.0842 ($[M - 2Na + H]^-$, $C_{16}H_{23}O_8S_2$, calculated for 407.0834).

Container III-1d. Compound **III-3d** (0.658 g, 1.55 mmol) was added into a solution of **III-2** (0.300 g, 0.38 mmol) in TFA/Ac_2O (3.0 mL, v/v = 1:1). The mixture was stirred and heated at 70 ˚C for 3 h. The solvent was removed with under reduced pressure and the solid was further dried under high vacuum. The solid was recrystallized with the mixture of water and EtOH (1:2, v/v, 20 mL) twice and then dissolved in water and adjusted to pH = 7 with 1 M aqueous NaOH. The solvent was removed under reduced pressure and then the solid was further dried under high vacuum to yield **III-1d** as a white solid (0.262 g, 43%). M.p. > 300 ^{o}C. IR (ATR, cm^{-1}): 2999w, 2952w, 2875w, 1733s, 1652s, 1474s, 1368m, 1321m, 1233s,

1185s, 1093m, 1044s, 960w, 823w, 800m, 795m. ^{1}H NMR (400 MHz, D_2O): δ 5.68 (d, *J* = 15.3, 2H), 5.59 (d, *J* = 15.7, 4H), 5.43 (d, *J* = 7.8, 2H), 5.36 (d, *J* = 7.8, 2H), 5.17 (d, *J* = 16.1, 4H), 4.35 (d, *J* =16.1, 4H), 4.25 (d, *J* = 15.7, 4H), 4.07 (d, *J* = 15.3, 2H), 4.00 – 3.80 (m, 4H), 3.75 – 3.55 (m, 4H), 3.25 -3.05 (m, 8H), 2.25 – 2.15 (m, 8H), 1.82 (s, 12H), 1.78 (s, 6H), 1.74 (s, 6H). ^{13}C NMR (125 MHz, D_2O, 1,4-dioxane as internal reference): δ 156.1, 155.5, 149.7, 130.9, 127.6, 78.0, 76.9, 72.1, 70.7, 70.5, 52.1, 47.8, 47.3, 35.6, 24.3, 15.8, 14.8, 11.8. High-Res MS (ESI): *m/z* 753.1997 ($[M - 4Na + 2H]^{2-}$, $C_{58}H_{74}N_{16}O_{24}S_4$, calculated for 753.1972).

Container III-1e. Compound **III-3e** (1.160 g, 2.56 mmol) was added into a solution of **III-2** (0.500 g, 0.64 mmol) in TFA/Ac_2O (5.0 mL, v:v = 1:1). The mixture was stirred and heated at 70 ˚C for 3 h. The solvent was removed under reduced pressure and the solid was further dried under high vacuum. The solid was recrystallized with the mixture of water and EtOH (1:2, v/v, 300 mL) twice and then dissolved in water and adjusted to pH = 7 by adding 1 M aqueous NaOH. The solvent was removed under reduced pressure and then the solid was further dried under high vacuum to yield **III-1e** as a white solid (0.301 g, 30%). M.p. > 300 ^{o}C. IR (ATR, cm^{-1}): 2930w, 2875w, 1724s, 1471s, 1375m, 1320m, 1233s, 1171s, 1084m, 1041s, 824w, 801m, 759w. ^{1}H NMR (400 MHz, D_2O, with added *p*-xylenediamine): δ 5.64 (d, *J* = 15.8, 4H), 5.49 (d, *J* = 15.5, 2H), 5.45 (d, *J* = 8.8, 2H), 5.28 (d, *J* = 8.8, 2H), 5.23 (d, *J* = 16.4, 4H), 4.38 (d, *J* =16.4, 4H), 4.29 (d, *J* = 15.8, 4H), 3.97 (d, *J* = 15.5, 2H), 4.00 – 3.80 (m, 4H), 3.75 – 3.65 (m, 4H), 3.25 -3.15 (m, 8H), 2.65 – 2.50 (m, 4H), 2.30 – 2.15 (m, 12H), 1.88 (s, 6H), 1.83 (s, 6H), 1.60 – 1.55 (m, 4H), 1.35 – 1.20 (m, 4H). ^{13}C NMR (125 MHz,

D_2O, with added *p*-xylenediamine and 1,4-dioxane as internal reference): δ 156.5, 155,7, 149.7, 132.0, 131.6, 127.8, 126.7, 78.3, 77.2, 71.7, 71.2, 71.0, 52.7, 48.4, 47.6, 41.6, 35.6, 24.7, 22.9, 21.0, 15.5, 14.8. High-Res MS (ESI): 779.2154 ($[M-4Na+2H]^{2-}$, $C_{62}H_{78}N_{16}O_{24}S_4$, calculated for 779.2129).

3.4 Supporting Information

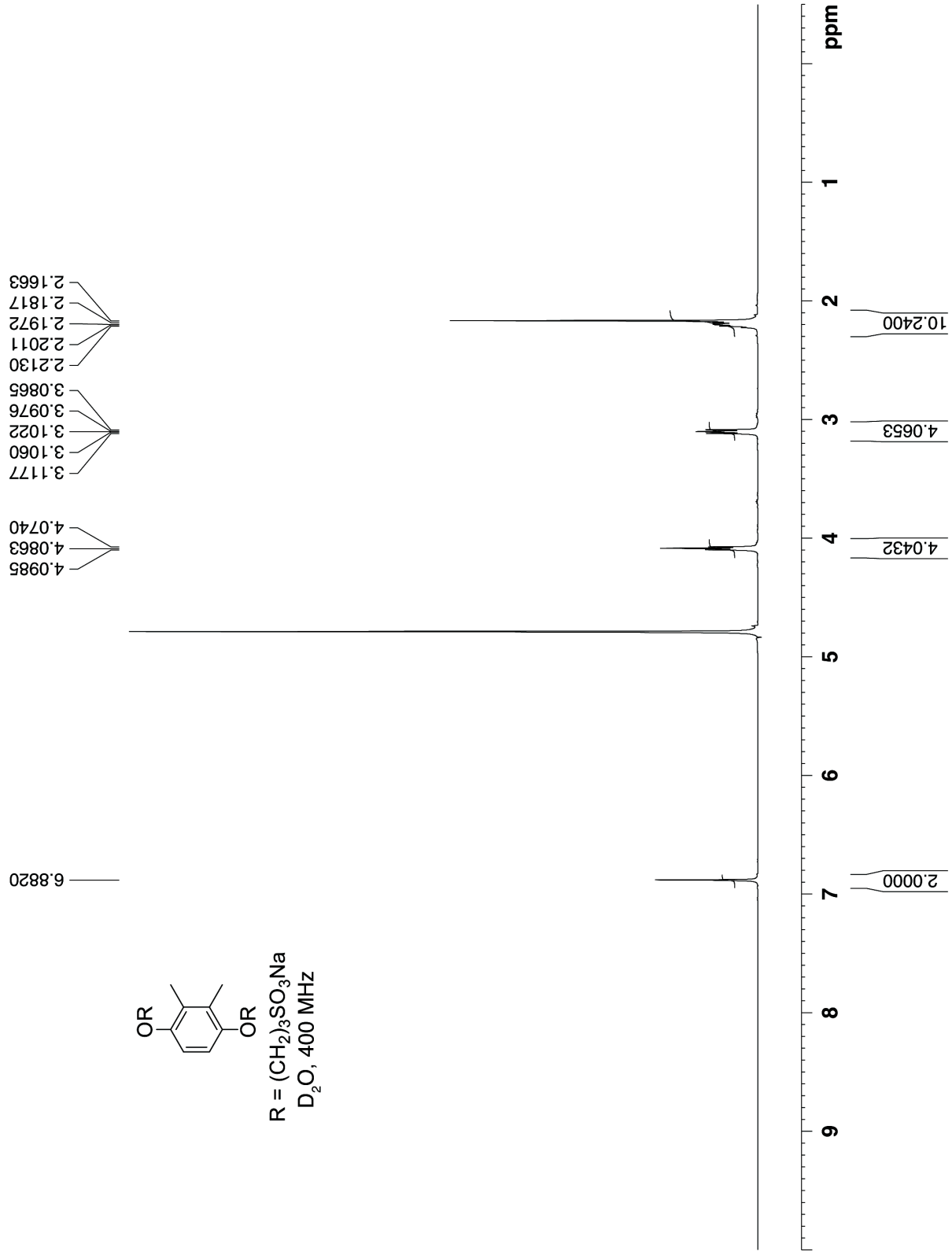

Figure S III-1. ^{1}H NMR spectra (400 MHz, D_2O, RT) recorded for **III-3d**.

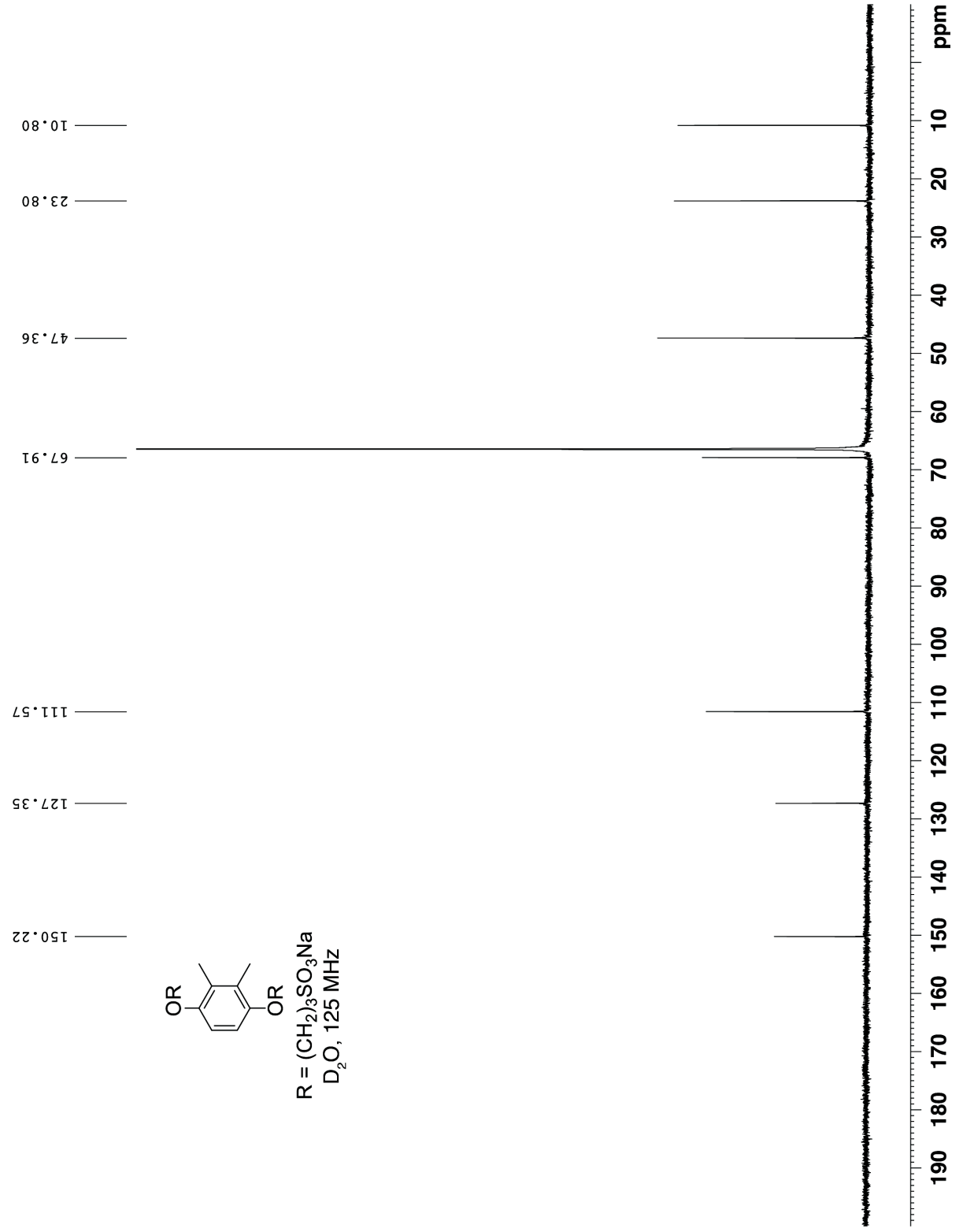

Figure S III-2. ^{13}C NMR spectra (125 MHz, D_2O, RT, 1,4-dioxane as internal reference) recorded for **III-3d**.

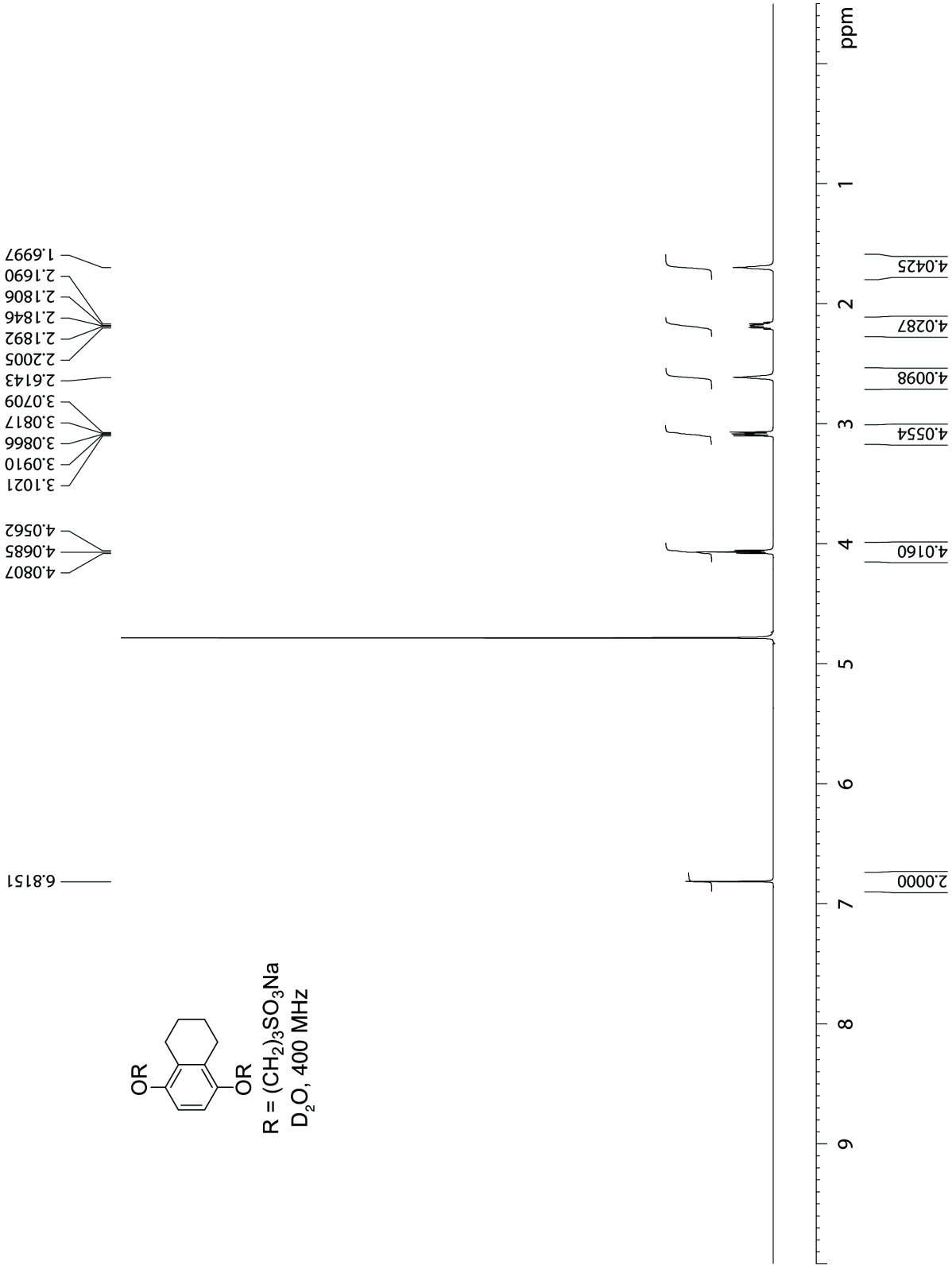

Figure S III-3. ^{1}H NMR spectra (400 MHz, D_2O, RT) recorded for **III-3e**.

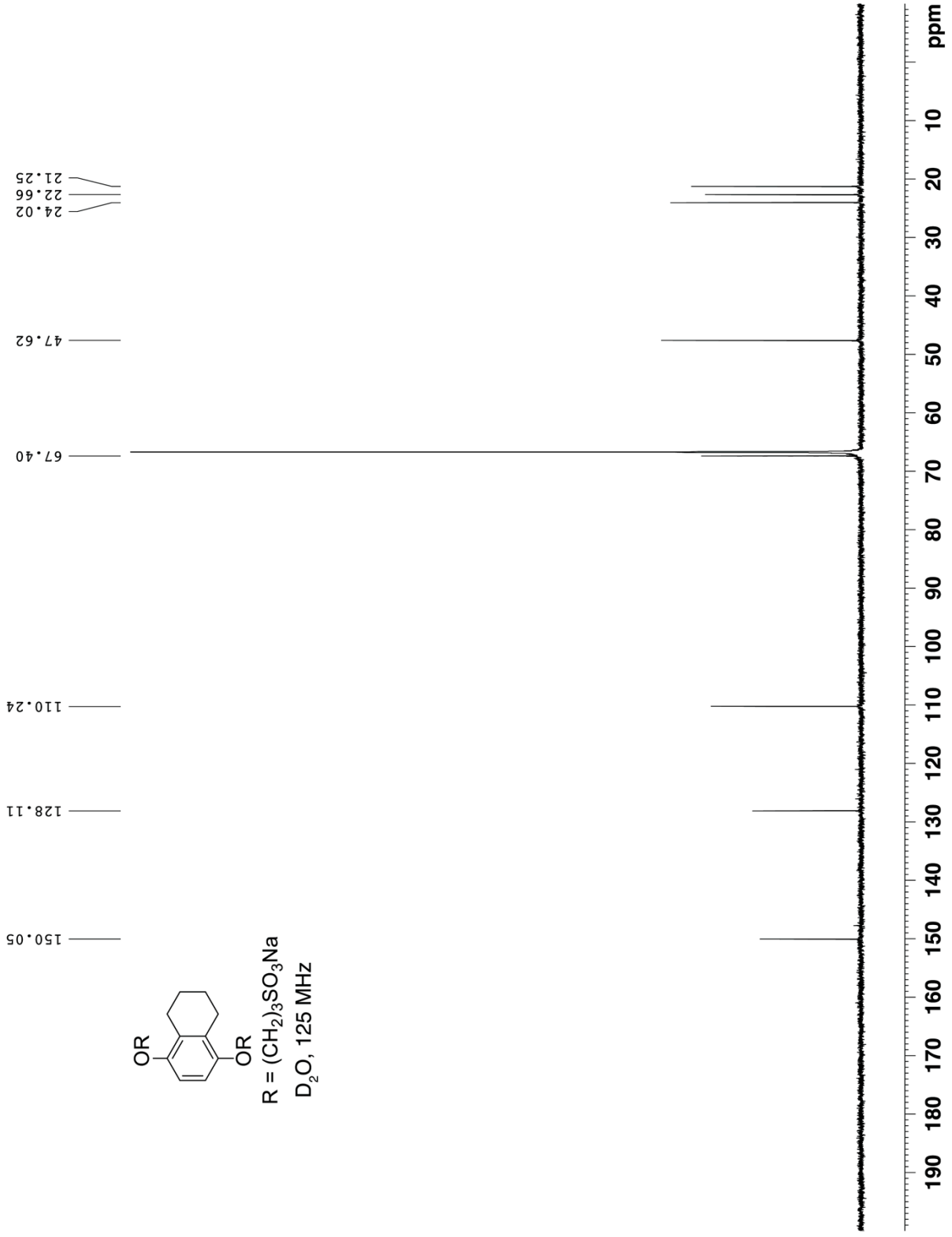

Figure S III-4. ^{13}C NMR spectra (125 MHz, D_2O, RT, 1,4-dioxane as internal reference) recorded for **III-3e**.

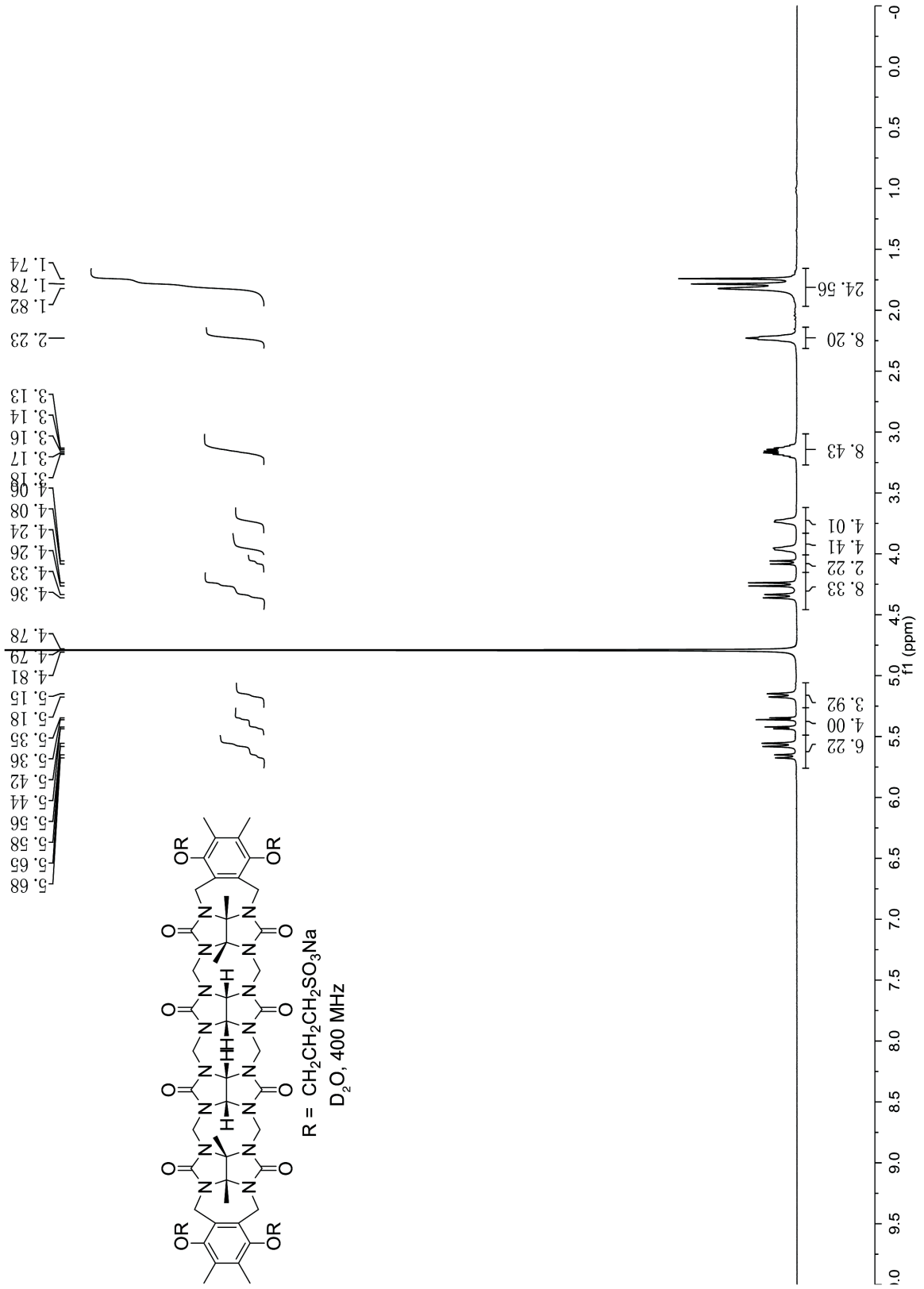

Figure S III-5. ^{1}H NMR spectra (400 MHz, D_2O, RT) recorded for **III-1d**

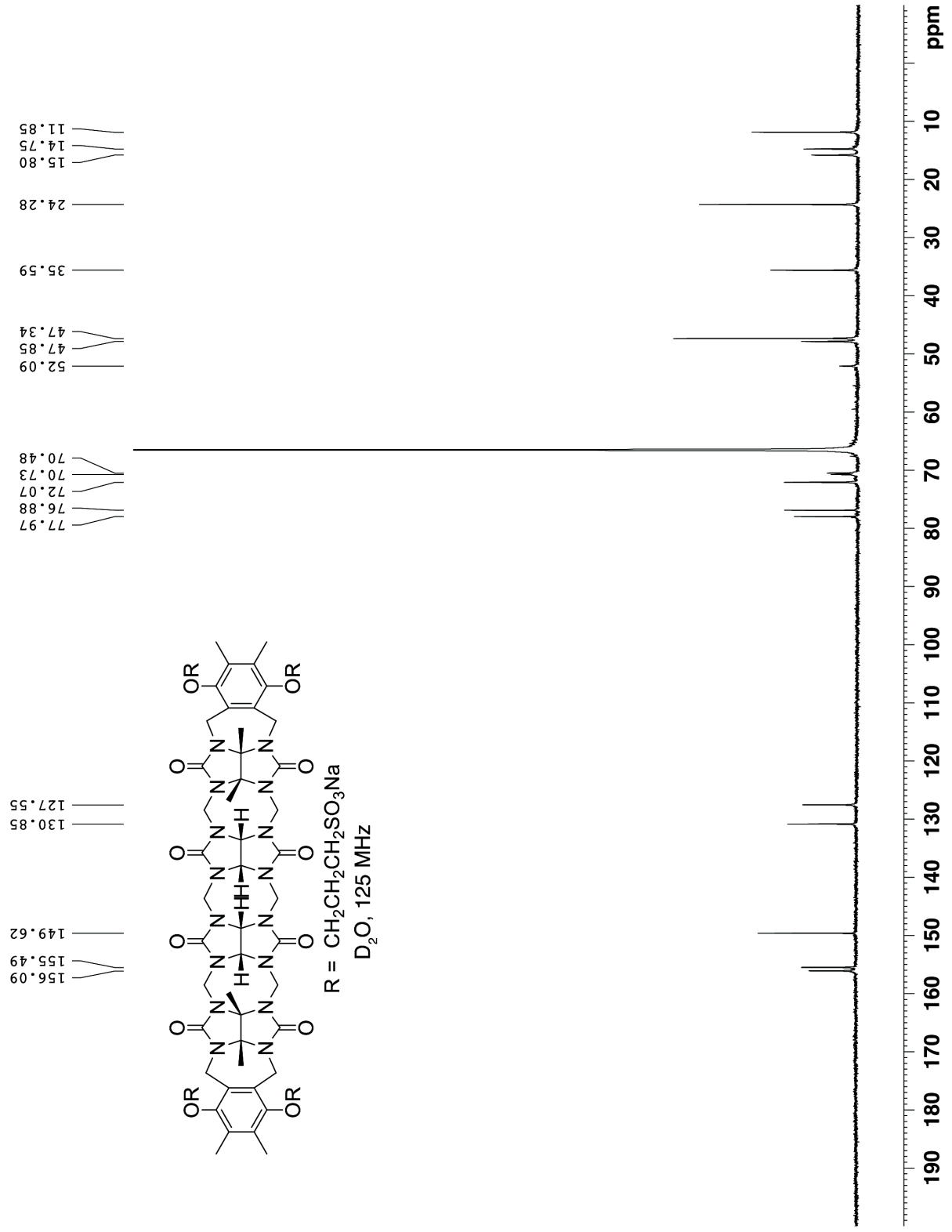

Figure S III-6. ^{13}C NMR spectra (125 MHz, D_2O, RT, 1,4-dioxane as internal reference) recorded for **III-1d**.

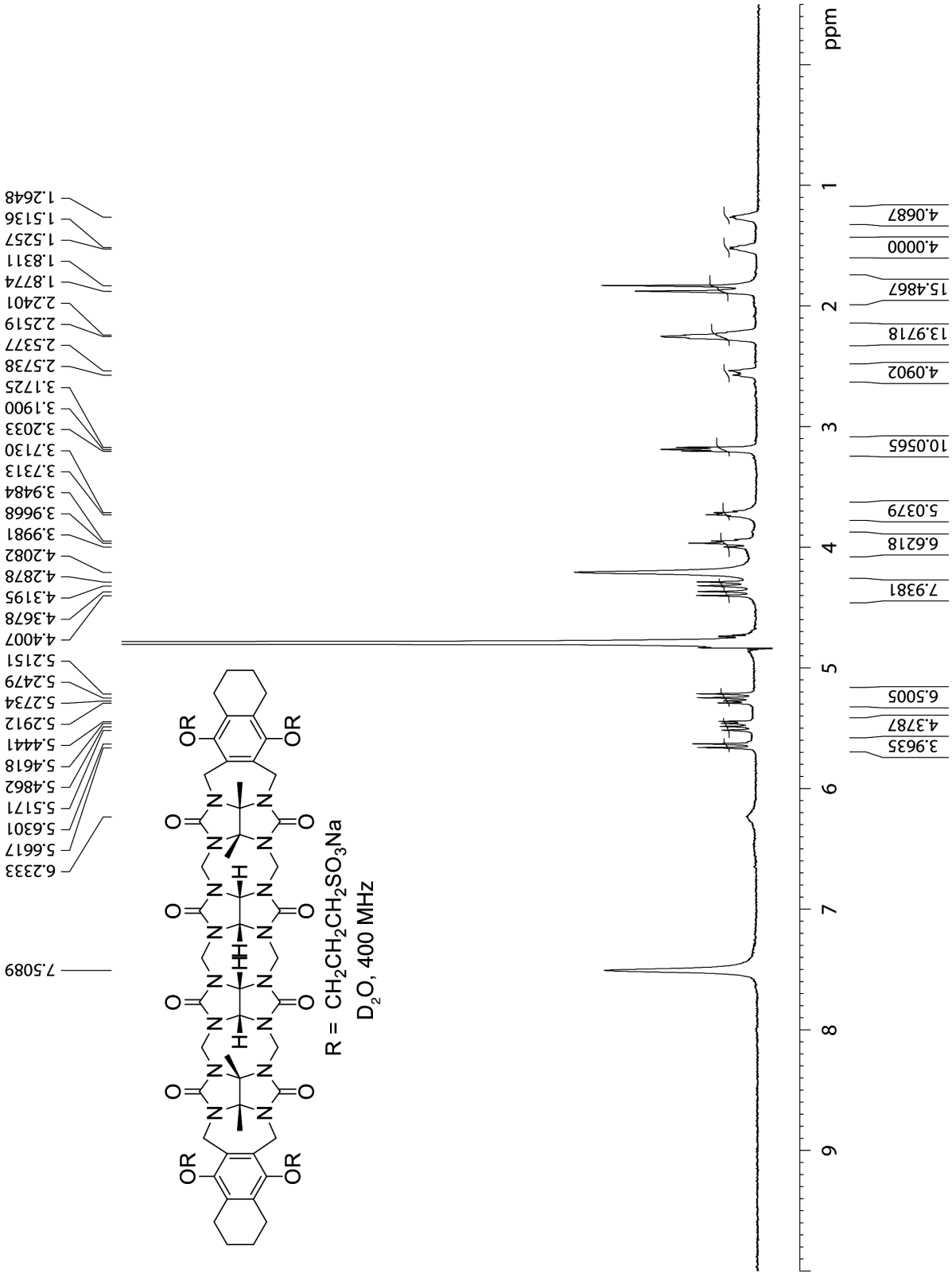

Figure S III-7. ^{1}H NMR spectra (400 MHz, D_2O, RT, excess *p*-xylenediammonium ion as guest) recorded for **III-1e.**

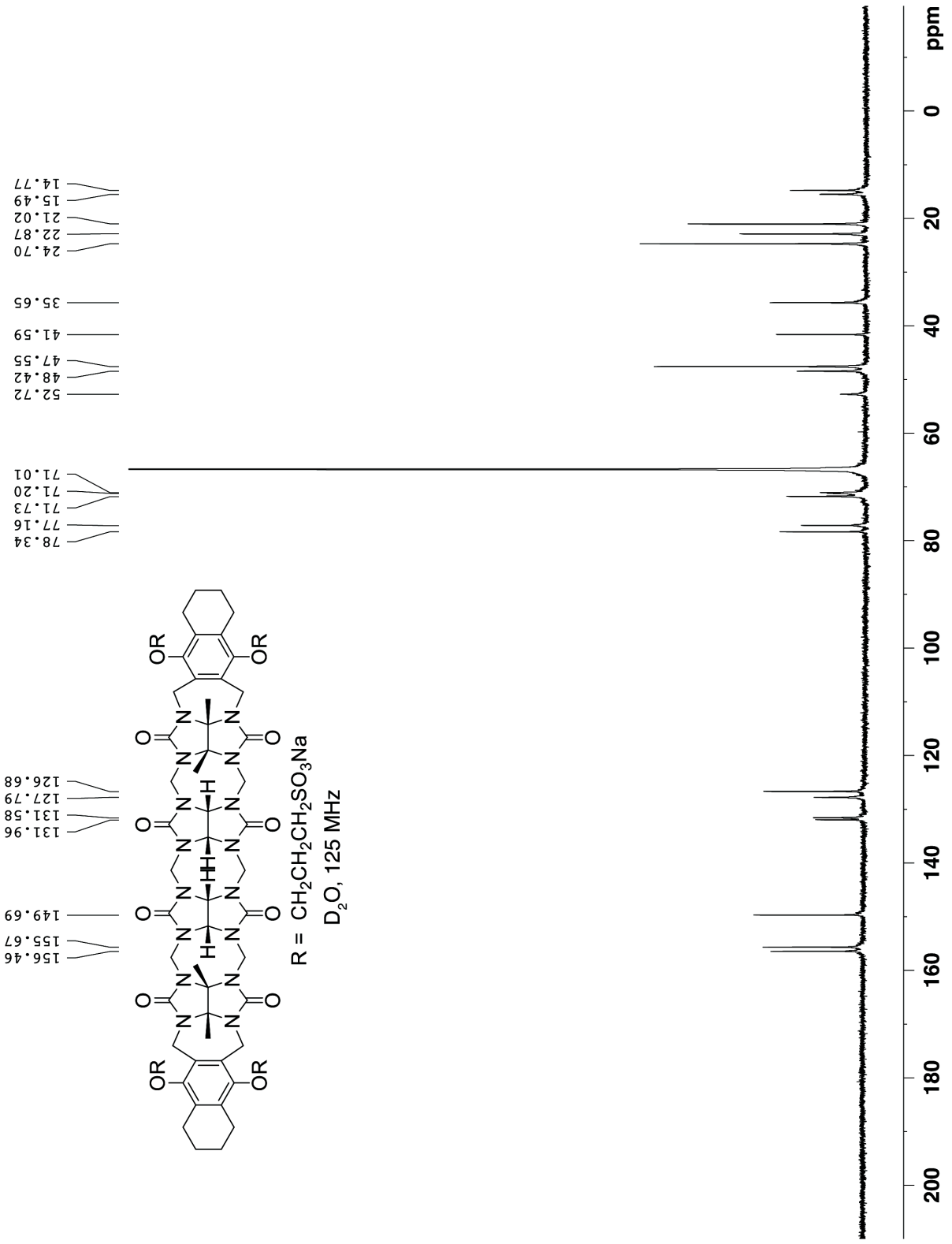

Figure S III-8. ^{13}C NMR spectra (125 MHz, D_2O, RT, 1,4-dioxane as internal reference, excess *p*-xylenediammonium ion as guest) recorded for **III-1e**.

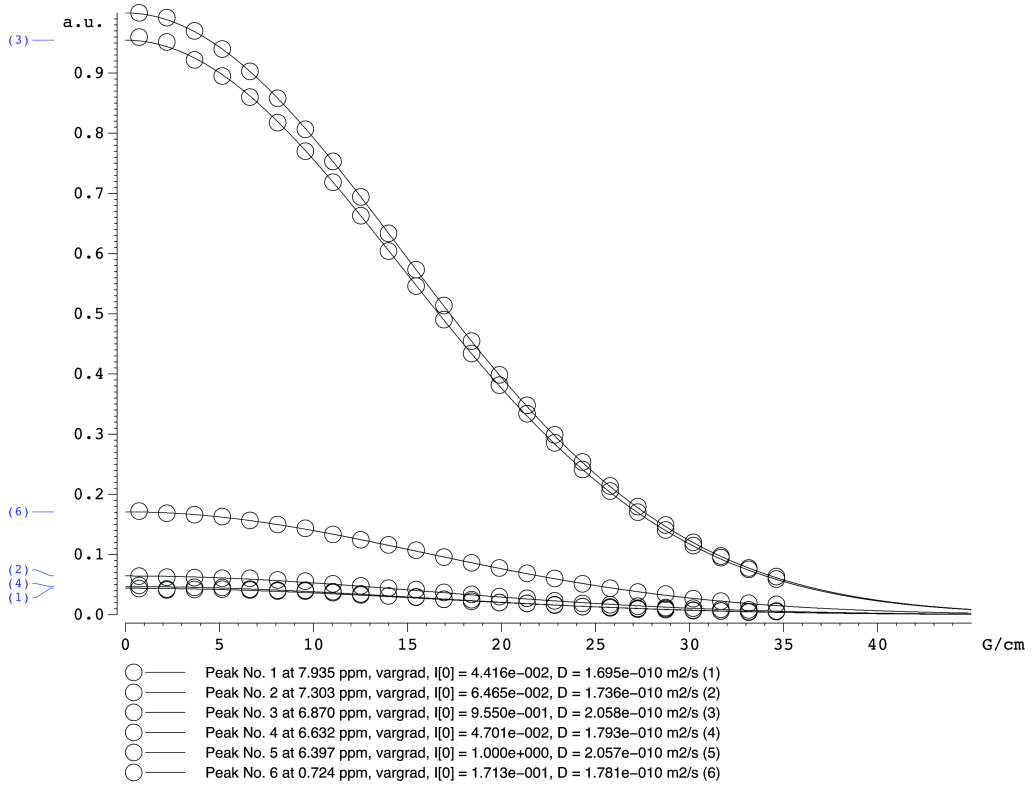

Figure S III-9. Plots of the change in intensity of the indicated NMR resonances in the DOSY spectra as a function of magnetic field gradient recorded (600 MHz, D_2O, 298K) for host **III-1c** and (**III-1c**)$_2$.

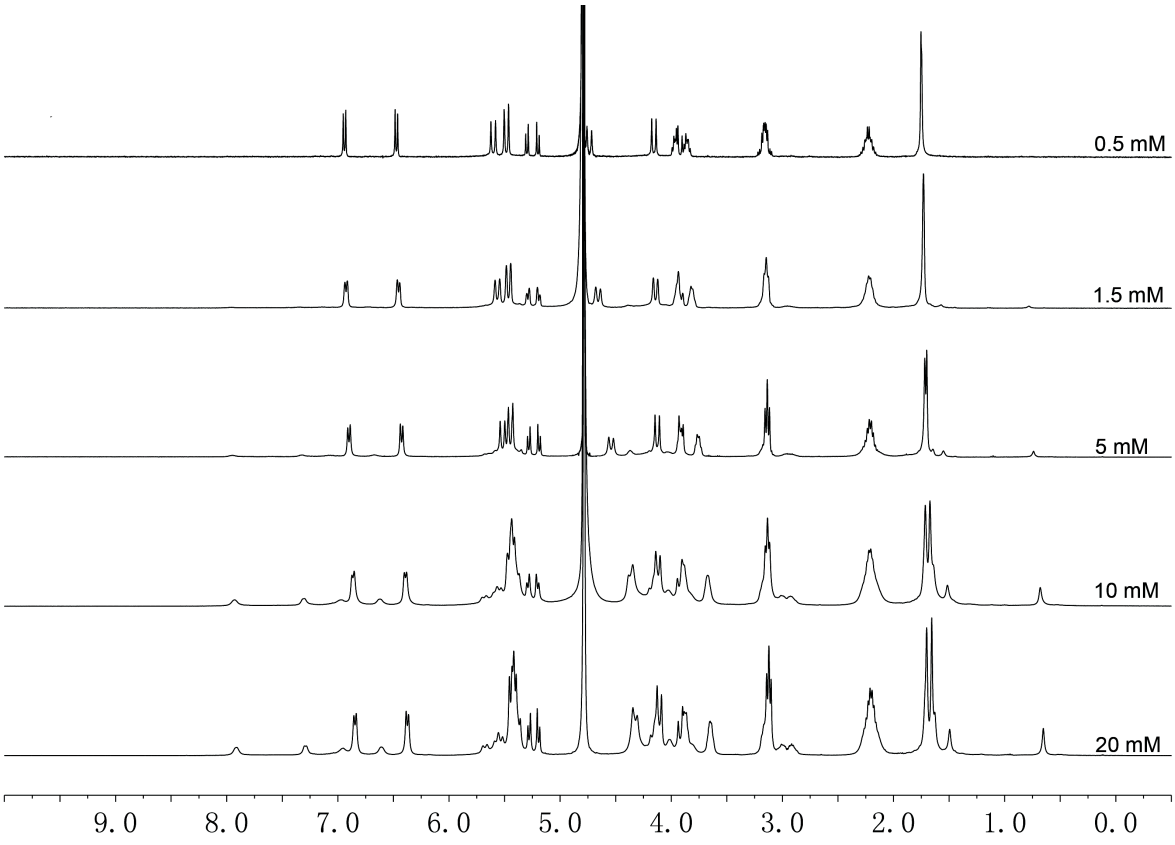

Figure S III-10. ^{1}H NMR recorded (400 MHz, 20 mM NaD_2PO_4, pD = 7.4) for **III-1c** at varied concentration (0.5 – 20 mM) for self-association study, K_s calculated to be 372 M^{-1}.

[1].

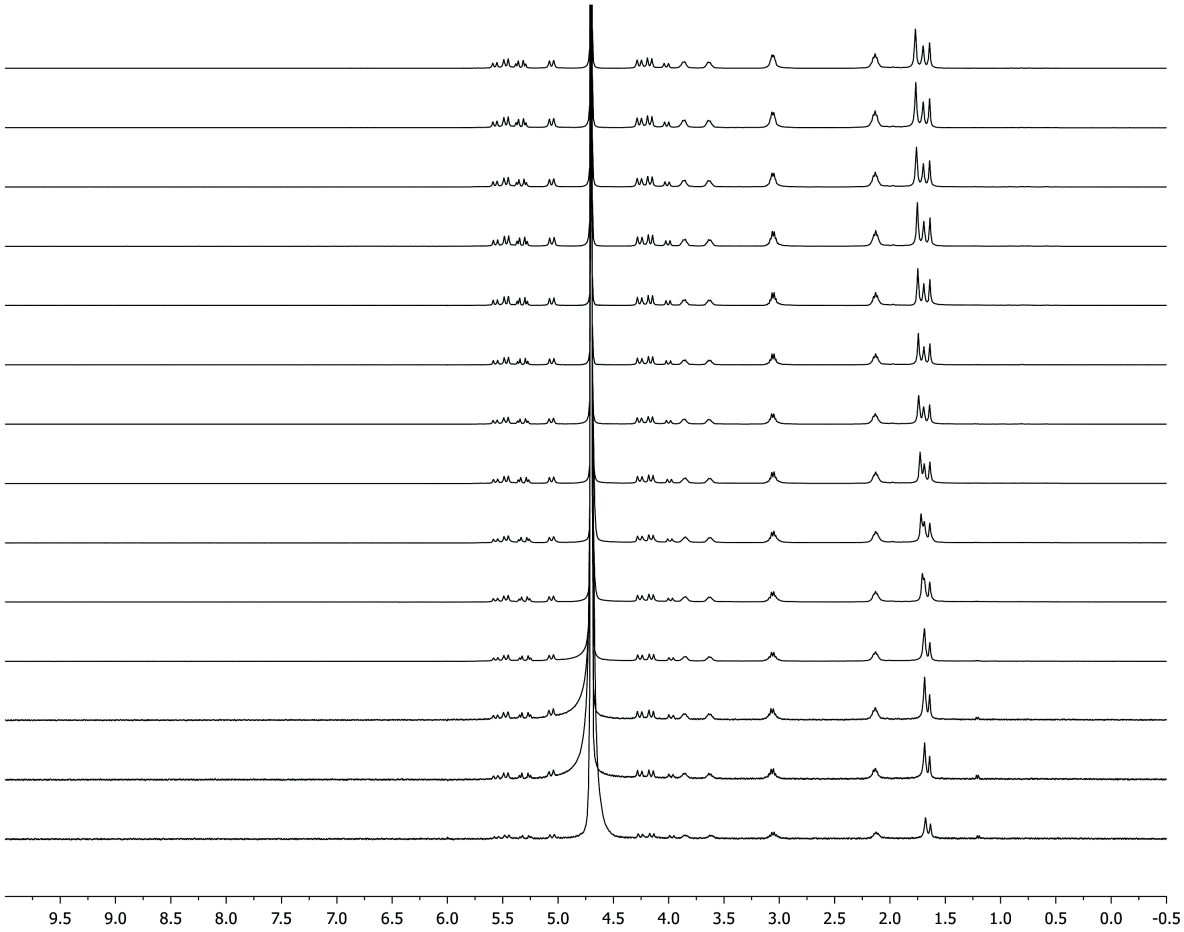

Figure S III-11. ^{1}H NMR recorded (400 MHz, 20 mM NaD_2PO_4, pD = 7.4) for for **III-1d** at varied concentration (0.1 – 15 mM) self-association study.

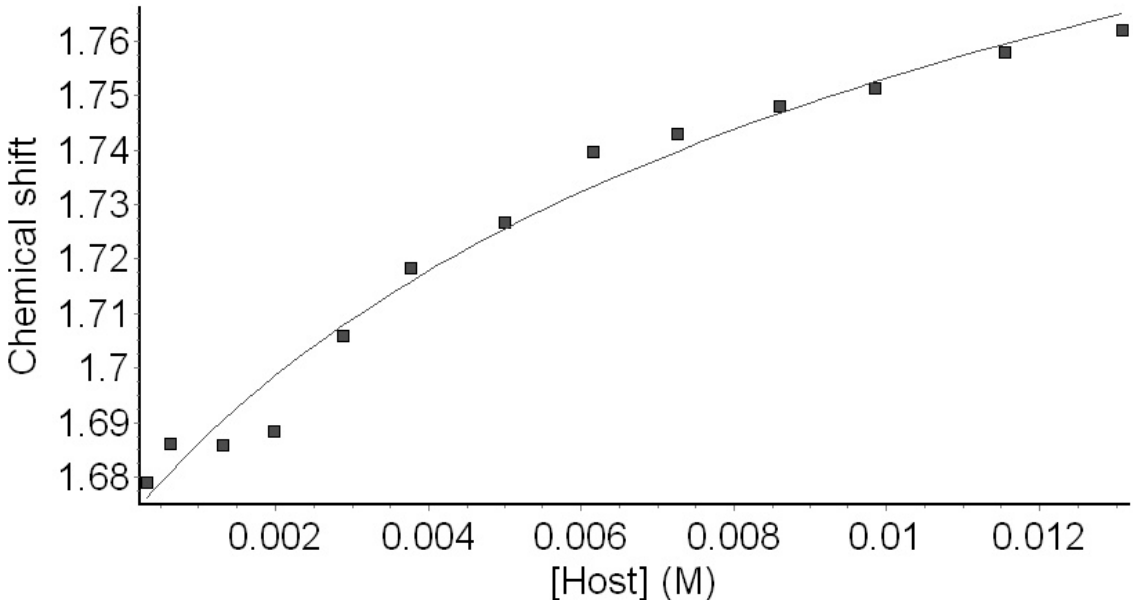

Figure S III-12. Plot of chemical shift of **III-1d** versus [**III-1d**]. The solid line represents the best non-linear fitting of the data to a two-fold self-assocation model with K_s = 130 M^{-1}.

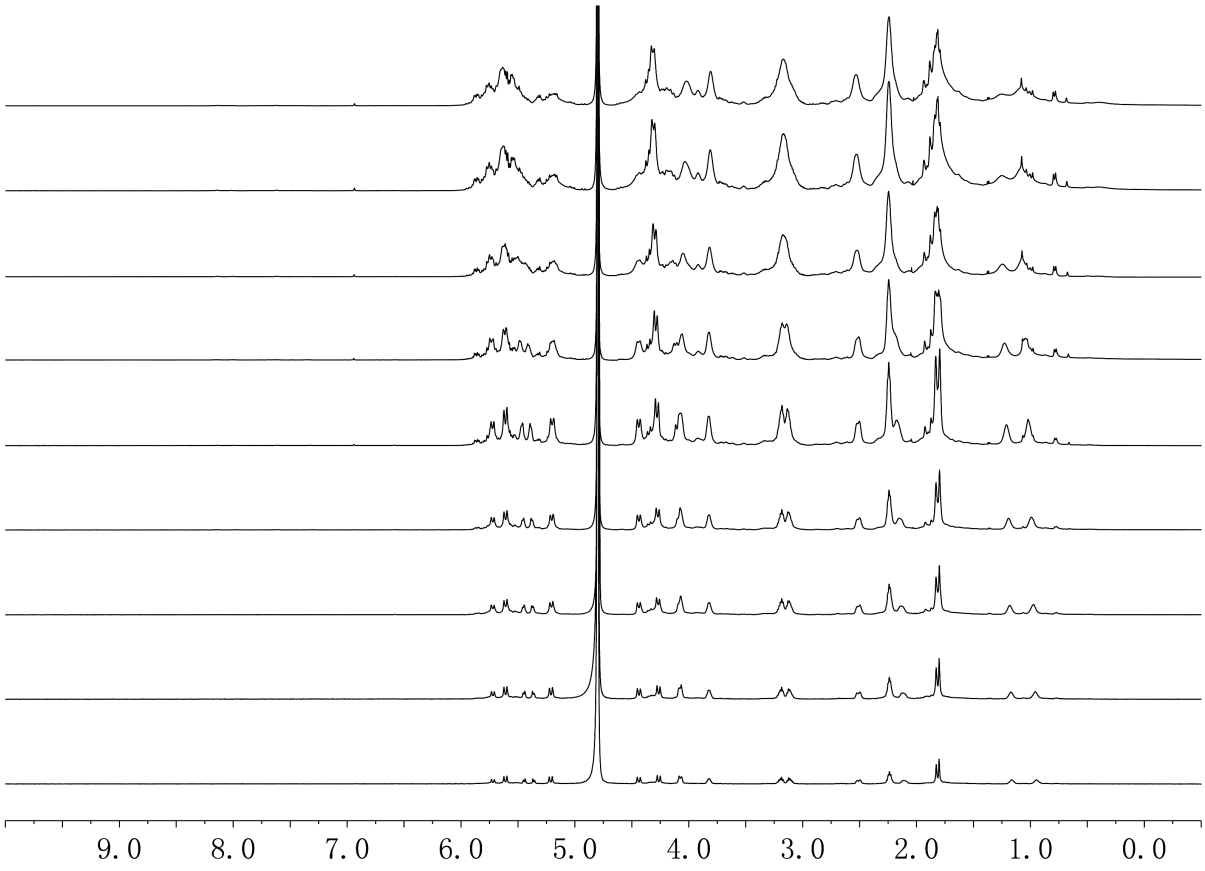

Figure S III-13. ^{1}H NMR recorded (400 MHz, 20 mM NaD_2PO_4, pD = 7.4) for **III-1e** at varied concentration (0.2 – 35 mM)for self-association study.

Procedure to measure the solubility of drugs with Host III-1a – III-1e. Excess amount of drug was added into a solution of host (**III-1a – III-1e)** of known concentration in deuterated sodium phosphate buffer (20 mM, pD = 7.4). The suspended mixture was magnetically stirred at room temperature for 6 h. During this period, the pD value of the solution was monitored and adjusted back to 7.4 if it changed. The mixture was then filtered. The ^{1}H NMR spectrum of the supernatant was measured (400 MHz) with 1,3,5-benzenetricarboxylic acid (1.00 mM) as internal standard. The signal for the reference shows up at 8.35 ppm (s, 3H). Diagnostic signals for the dissolved drug were also integrated. From the ratio of integrations of reference peak relative to the drug peak, and the concentration of reference, the concentration of the drug can be calculated.

Procedure to measure the solubility of drugs with Host III-1c. Excess amount of drug was added into a solution of host **III-1c** of known concentration in deuterated sodium phosphate buffer (1.0 mL, 20 mM, pD = 7.4). The suspended mixture was magnetically stirred at room temperature for 6 h. During this period, the pD value of the solution was monitored and adjusted back to 7.4 if it changed. The mixture was then filtered, and 5 equivalents of spermine tetrahydrochloride salt was added as an aqueous solution. The solvent was then removed from the mixture under reduced pressure, and the residue solid was extracted with EtOH (3.0 mL × 3). The EtOH extracts was combined and solvent was removed under reduced pressure. The residue was then dissolved in 1.0 mL deuterated DMSO, and the 1H NMR spectrum of the solution was measured (400 MHz) with 1,3,5-benzenetricarboxylic acid (1.00 mM) as internal standard. The signal for the reference shows up at 8.35 ppm (s,

3H). Diagnostic signals for the dissolved drug were also integrated. From the ratio of integrations of reference peak relative to the drug peak, and the concentration of reference, the concentration of the drug can be calculated. The chemical structures of drugs used in this study are shown below.

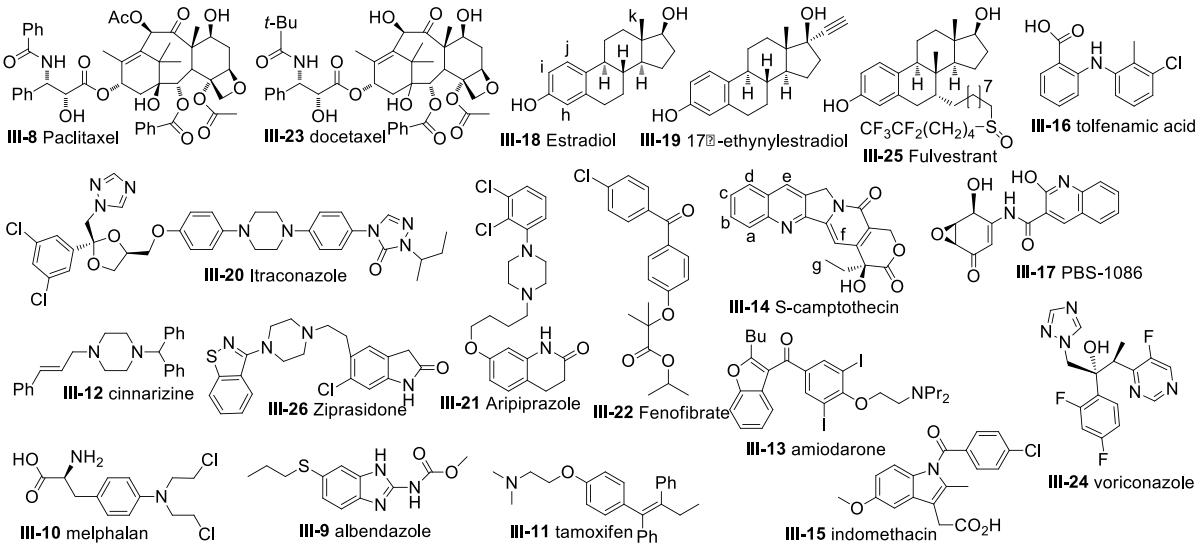

Table SIII-1. Solubility enhancement of water-insoluble drugs (mM) with hosts **III-1a** – **III-1c**.

	III-1a		**III-1b**		**III-1c**	
	[Host]	[Drug]	[Host]	[Drug]	[Host]	[Drug]
Taxol	10	0.41	14	0	20	0
	15	0.66				
	22	1.56				
	33	2.24				
	50	4.34				
	90	11				
Albendazole	10	1.87	1	0.62	2	0.17
	15	2.56	2	1.97	5	0.34
	22	3.54	4	2.22	10	0.51
	33	4.91	6	3.02	15	0.55
	50	6.74	8	4.48	25	0.82
Melphalan	6.6	9.2	4	5.6	2	0.3
	10	16.9	6	8.3	5	4.4
	15	24.1	8	9.7	10	8.2
	22	27	10	12.9	15	11.2
	33	31.5	14	16.1	25	13.5
	50	32				
	90	36				
Tamoxifen	1	0.04	1	0.22	2	1.44
	2	0.08	2	0.46	5	3.12
	3.5	0.14	4	0.54	10	5.18
	6.5	0.18	6	0.81	15	7.77
	12	0.21	8	0.98	25	12.1
	24	0.23	10	1.18		
Cinnarizine	0.65	0.32	14	0	2	0
	1.3	0.72			5	0

	2.6	1.47			10	0

	III-1a		III-1b		III-1c	
	[Host]	[Drug]	[Host]	[Drug]	[Host]	[Drug]
Cinnarizine	7.9	3.3			15	0
	23	4.4			25	0
	42	4.5				
	69	4.6				
Amiodarone	6.6	0.54	1	0.50	2	0.33
	10	0.75	2	1.15	5	0.63
	15	1.14	4	4.25	10	1.54
	22	2.28	6	5.31	15	1.93
	33	2.88	8	4.95	25	3.51
	50	3.9	10	5.1		
	90	4				
Camptothecin	2	0.21	1	1.04	2	0.82
	6	0.71	2	2.28	5	1.63
	8	0.89	4	3.68	10	2.99
	10	1.36	6	6.65	15	4.77
	25	1.82	8	8.47	25	6.56
	35	1.94	10	11.6		
Indomethacin	2	0.11	1	2.35	2	0.11
	5	0.21	2	3.28	5	0.15
	10	0.33	4	4.44	10	0.22
	20	0.69	6	5.19	15	0.43
	50	1.28	8	6.15	25	0.51
			10	6.70	35	0.87
Tolfenamic acid	2	0.07	1	0.7	2	0.05
	5	0.32	2	1.14	5	0.18

	10	0.51	4	2.58	10	0.52
	25	1.11	6	3.4	15	0.76

	III-1a		**III-1b**		**III-1c**	
	[Host]	[Drug]	[Host]	[Drug]	[Host]	[Drug]
Tolfenamic acid	50	1.52	8	4.47	25	1.22
			10	5.6		
PBS-1086	1	0.89	2	1.77	2	1.03
	2	1.86	4	3.61	5	1.41
	4	3.2	8	6.11	10	2.4
	8	4.5	10	10.1	15	3.28
	15	8.29	14	12.5	25	4.21
	25	15.5				
	60	43.1				
β-estradiol	1	0.45	1.5	1.71	2	1.10
	2	0.85	2.5	2.73	5	1.96
	4	1.69	5	5.32	8	3.08
	6	2.01	10	10.5	10	5.52
	8	2.91	14	12.9	16	6.4
	10	3.75				
17α - ethynylestradiol	1	0.51	1	0.85	2	1.12
	2	0.95	2	2.11	5	2.76
	4	1.77	4	3.67	8	3.22
	6	2.21	6	5.84	10	5.56
	8	3.17	8	8.78	15	6.22
	10	3.69	10	10.5		
Itraconazole	20	0	14	0	2	0.45
					5	0.66
					10	1.52

	20	2.92
	30	3.65

	III-1a		III-1b		III-1c	
	[Host]	[Drug]	[Host]	[Drug]	[Host]	[Drug]
Aripiprazole	2	0.18	2	0.55	2	0.08
	5	0.31	4	1.45	5	0.21
	10	0.68	6	1.82	10	0.32
	15	1.01	8	2.32	15	0.57
	25	1.13	10	3.20	25	0.85
Fenofibrate	25	0	2	0.07	25	0
			4	0.11		
			6	0.15		
			8	0.31		
			10	0.46		
Docetaxel	2	0.55	14	0	25	0
	4	0.72				
	6	1.02				
	8	1.11				
	10	1.36				
	15	1.55				
Voriconazole	2	0.82	2	1.94	2	0.67
	4	1.72	4	3.21	4	1.18
	6	2.31	6	5.88	6	2.52
	8	3.44	8	6.48	8	3.03
	10	4.92	10	9.23	10	3.69
Fulvestrant	50	0	2	0.08	25	0
			4	0.29		
			6	0.43		
			8	0.71		
			10	0.91		
Ziprasidone	2	0.72	2	1.21	2	0.22

	III-1a		III-1b		III-1c	
	[Host]	[Drug]	[Host]	[Drug]	[Host]	[Drug]
Ziprasidone	4	3.11	4	1.72	5	1.03
	6	6.88	6	2.59	10	1.82
	8	6.13	8	3.21	18	3.88
	10	9.21	10	4.78	30	5.13

Table SIII-2. Solubility enhancement of water-insoluble drugs (mM) with hosts **III-1d, III-1e, and HPCD**.

	III-1d		**III-1e**		**HPCD**	
	[Host]	[Drug]	[Host]	[Drug]	[Host]	[Drug]
Taxol	25	0	25	0	100	0
Albendazole	2	0.25	25	0	2	0.06
	5	0.53			5	0.11
	10	1.37			10	0.23
	20	2.11			50	0.71
	35	3.77			100	1.52
Melphalan	2	0.84	2	1.33	5	4.33
	5	3.61	5	2.67	10	5.58
	10	10.8	10	5.96	30	9.23
	20	14.5	20	12.3	50	10.3
	35	28.4	35	16.2	100	15.5
Tamoxifen	2	0.15	25	0	2	0.07
	5	0.33			10	0.33
	10	0.50			20	0.89
	15	0.94			30	1.17
	20	1.22			60	1.75
					100	2.90
Cinnarizine	25	0	2	0.09	5	0.06
			5	0.27	10	0.08
			10	0.57	20	0.11
			20	1.11	50	0.17
			35	1.34	100	0.28
Amiodarone	2	0.44	2	0.18	2	0.22
	5	0.87	5	0.62	5	0.41
	10	1.39	10	1.36	10	1.24
	20	2.71	20	2.57	20	2.13

	35	3.23	35	2.92	35	3.11

	III-1d		III-1e		HPCD	
	[Host]	[Drug]	[Host]	[Drug]	[Host]	[Drug]
Camptothecin	2	0.87	2	0.55	50	0
	5	1.82	5	1.13		
	10	4.22	10	1.93		
	30	15.1	15	2.52		
	50	24.6	25	3.77		
Indomethacin	2	0.06	25	0	5	0.15
	5	0.11			10	0.27
	10	0.27			30	0.55
	20	0.44			50	0.80
	35	0.61			100	1.44
Tolfenamic acid	2	0.11	25	0	5	0.07
	5	0.14			10	0.13
	10	0.20			30	0.35
	15	0.53			50	0.41
	25	0.83			100	0.64
PBS-1086	2	0.81	2	0.55	50	0
	5	2.33	5	1.01		
	10	5.48	10	2.66		
	20	9.23	20	3.21		
	35	18.22	35	6.01		
β-estradiol	2	0.75	2	0.98	2	0.67
	5	2.01	5	2.21	5	1.31
	10	5.03	10	4.51	10	2.23
	20	11.5	20	10.2	50	9.21
	35	14.0	35	12.1	100	18.9
17α -	2	0.82	2	0.88	2	1.03

ethynylestradiol	5	2.01	5	2.21	5	3.21

	III-1d		**III-1e**		**HPCD**	
	[Host]	[Drug]	[Host]	[Drug]	[Host]	[Drug]
17α - ethynylestradiol	10	4.30	10	4.84	10	5.51
	20	9.03	20	8.32	20	12.1
	35	13.2	35	15.6	35	16.3
Itraconazole	2	0.09	2	0.06	100	0
	5	0.13	5	0.14		
	10	0.32	10	0.20		
	20	0.47	20	0.44		
	30	0.51	35	0.57		
Aripriprzole	30	0	30	0	30	0
Fenofibrate	35	0	35	0	100	0
Docetaxel	35	0	35	0	100	0
Voriconazole	2	1.32	2	0.98	2	0.61
	4	2.21	4	1.77	4	0.88
	6	4.21	6	5.31	6	1.52
	8	6.38	8	6.44	8	1.77
	10	7.57	10	8.86	10	2.40
Fulvestrant	30	0	30	0	100	0
Ziprasidone	2	0.92	2	1.11	2	0.08
	5	1.97	5	2.03	5	0.17
	10	4.54	10	4.30	10	0.28
	20	8.21	20	9.21	20	0.63
	30	11.72	30	10.3	30	0.77

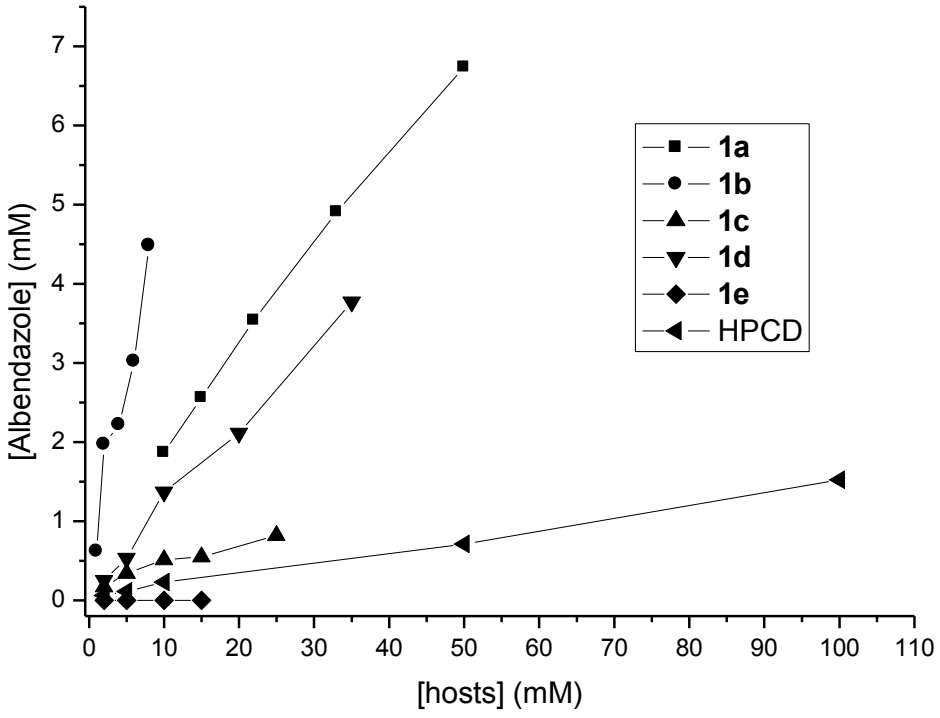

Figure S III-14. Phase solubility diagram of albendazole with different hosts in phosphate buffer (20 mM, pH 7.4, RT).

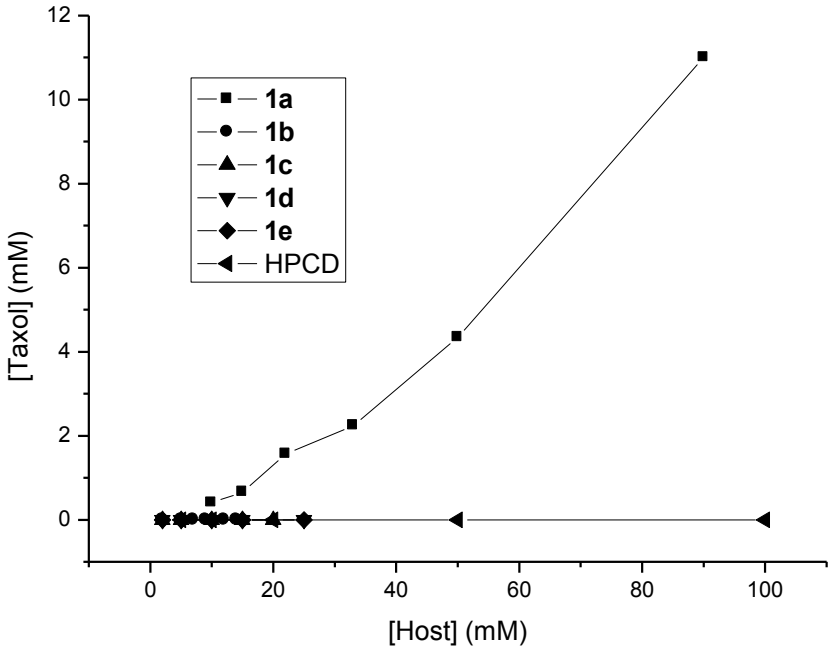

Figure S III-15. Phase solubility diagram of taxol with different hosts in phosphate buffer (20 mM, pH 7.4, RT).

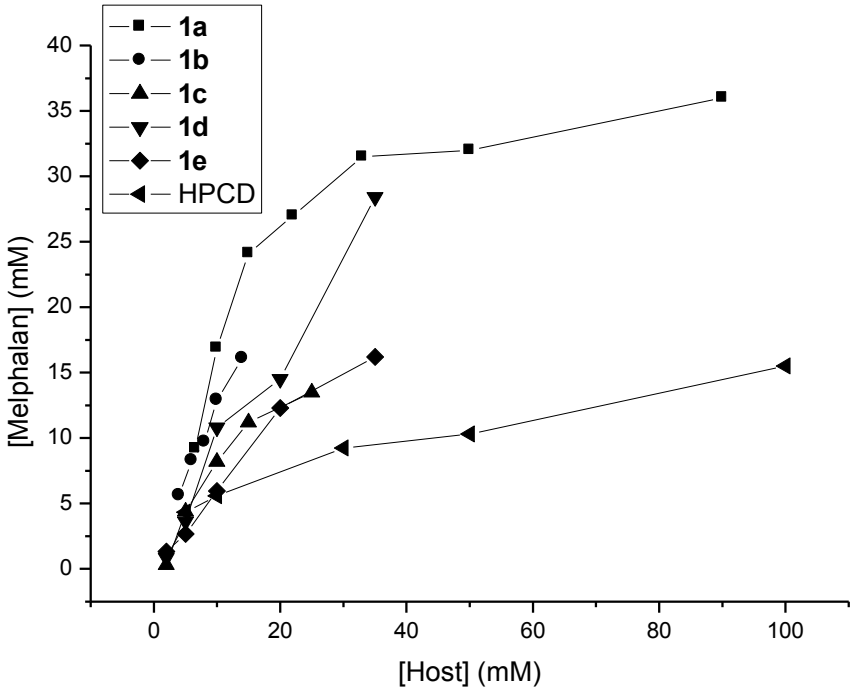

Figure S III-16. Phase solubility diagram of melphalan with different hosts in phosphate buffer (20 mM, pH 7.4, RT).

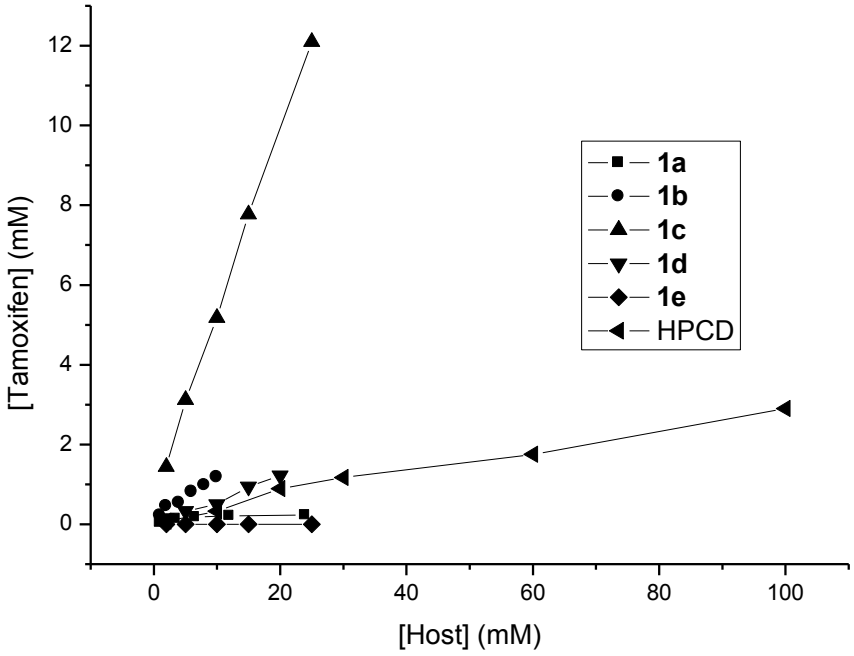

Figure S III-17. Phase solubility diagram of tamoxifen with different hosts in phosphate buffer (20 mM, pH 7.4, RT).

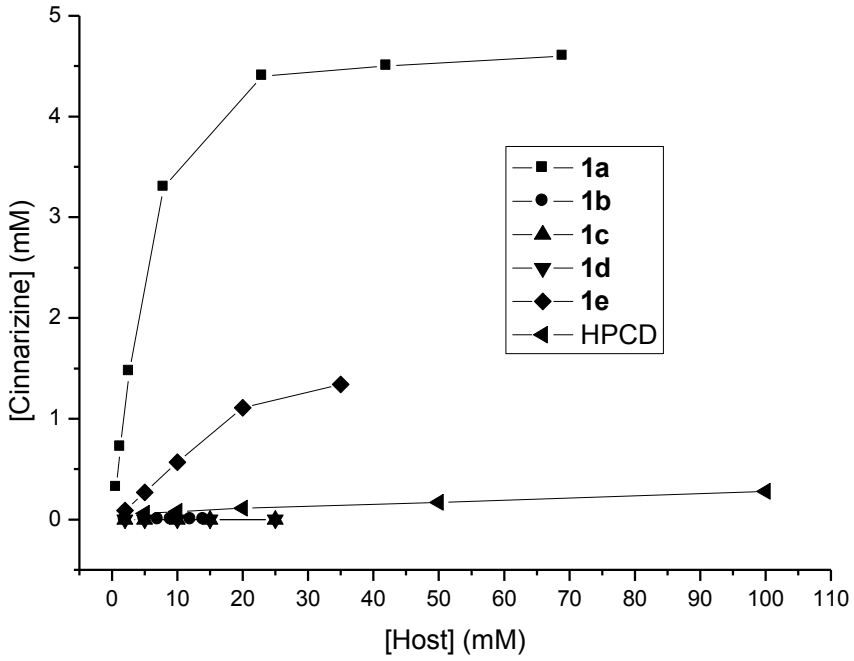

Figure S III-18. Phase solubility diagram of cinnarizine with different hosts in phosphate buffer (20 mM, pH 7.4, RT).

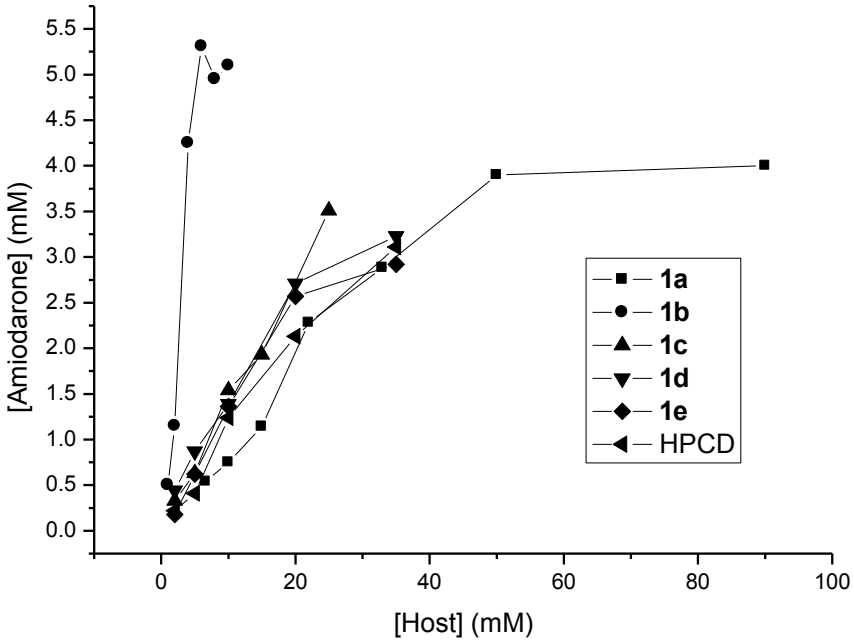

Figure S III-19. Phase solubility diagram of amiodarone with different hosts in phosphate buffer (20 mM, pH 7.4, RT).

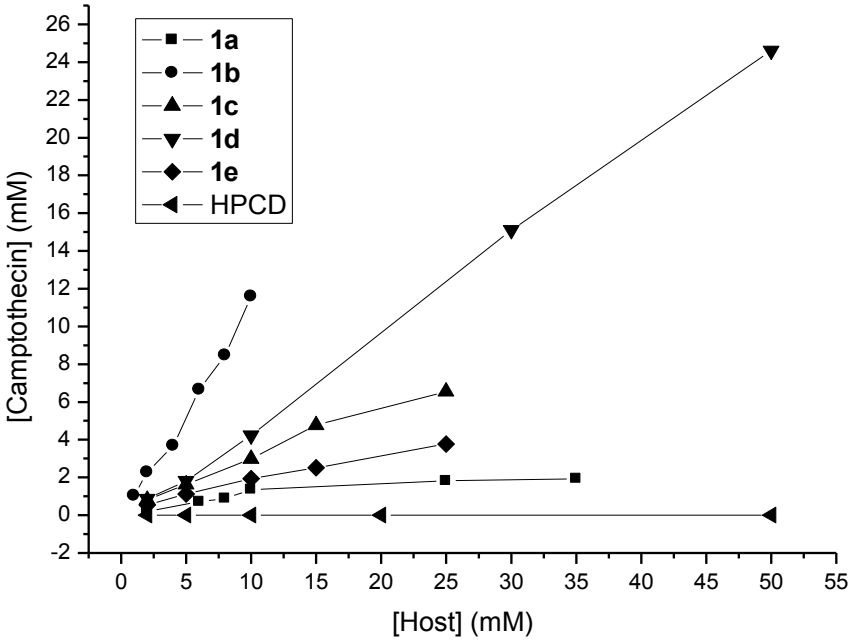

Figure S III-20. Phase solubility diagram of camptothecin with different hosts in phosphate buffer (20 mM, pH 7.4, RT).

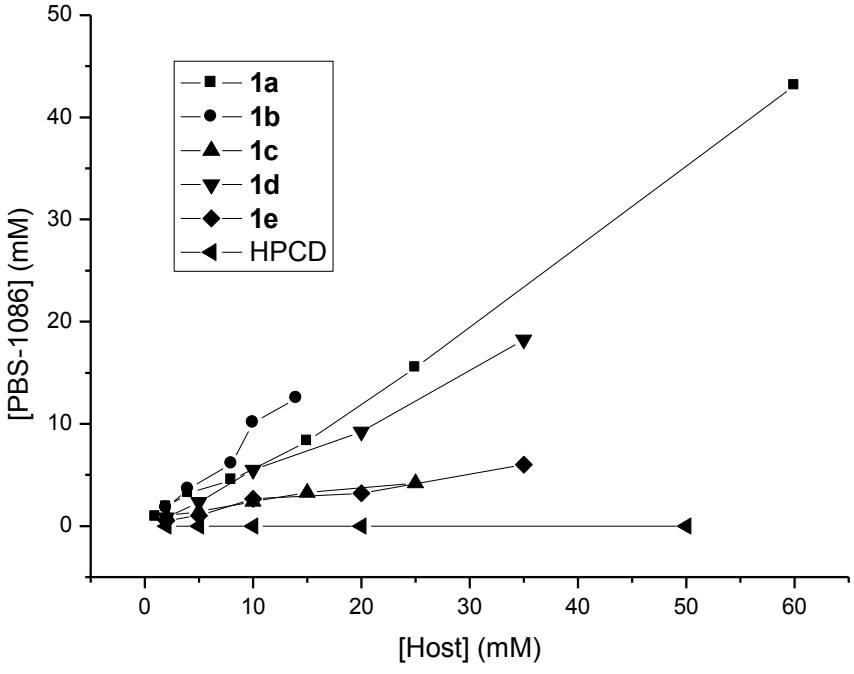

Figure S III-21. Phase solubility diagram of PBS-1086 with different hosts in phosphate buffer (20 mM, pH 7.4, RT).

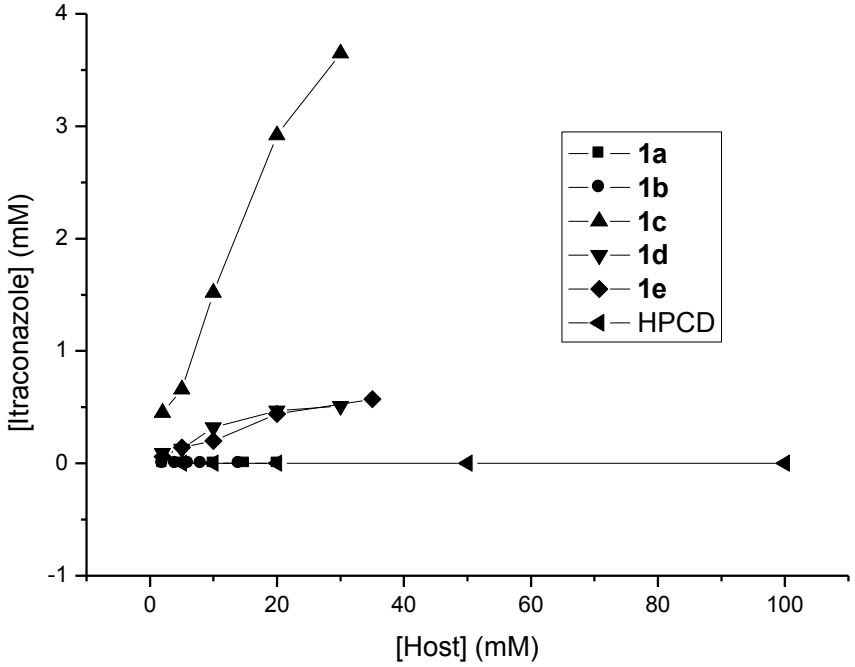

Figure S III-22. Phase solubility diagram of itraconazole with different hosts in phosphate buffer (20 mM, pH 7.4, RT).

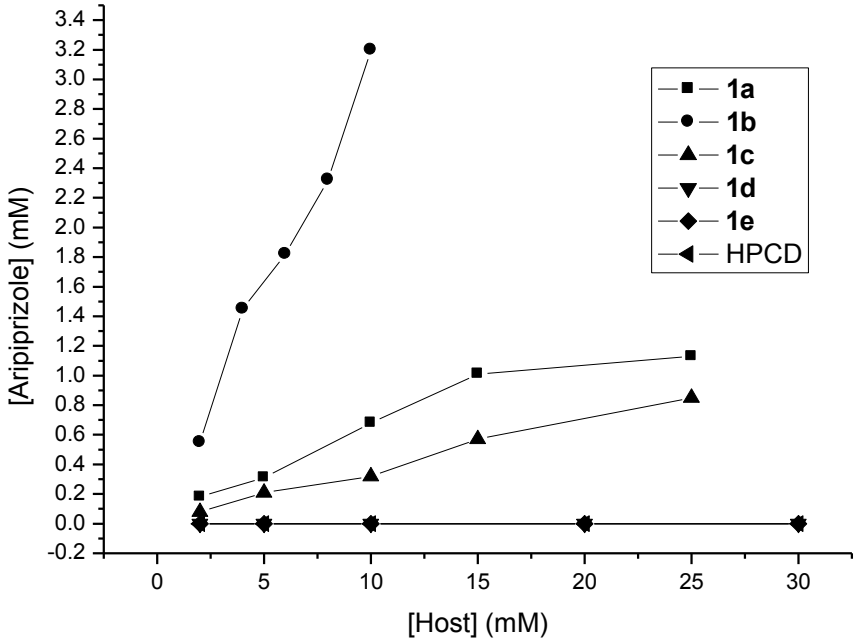

Figure S III-23. Phase solubility diagram of aripiprizole with different hosts in phosphate buffer (20 mM, pH 7.4, RT).

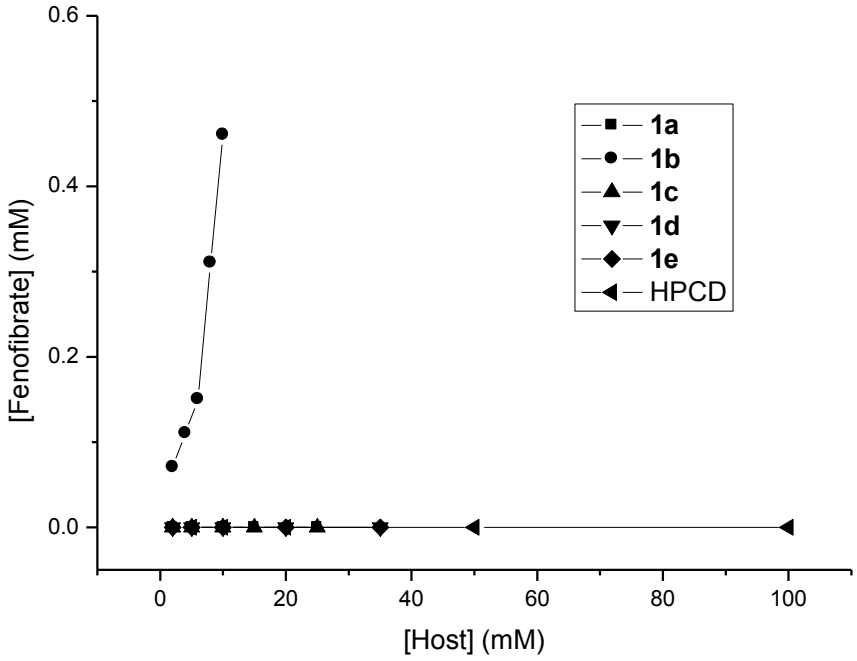

Figure S III-24. Phase solubility diagram of fenofibrate with different hosts in phosphate buffer (20 mM, pH 7.4, RT).

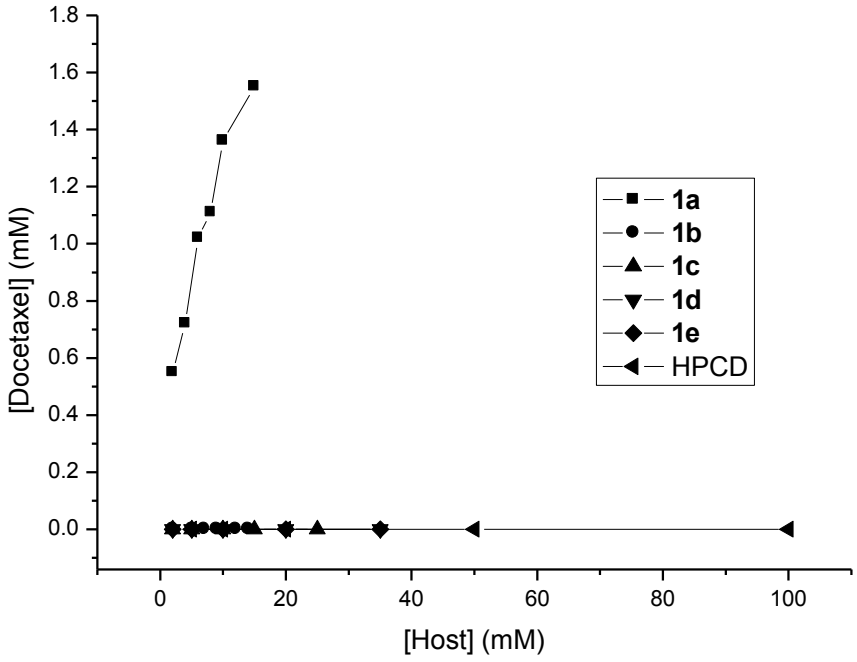

Figure S III-25. Phase solubility diagram of docetaxel with different hosts in phosphate buffer (20 mM, pH 7.4, RT).

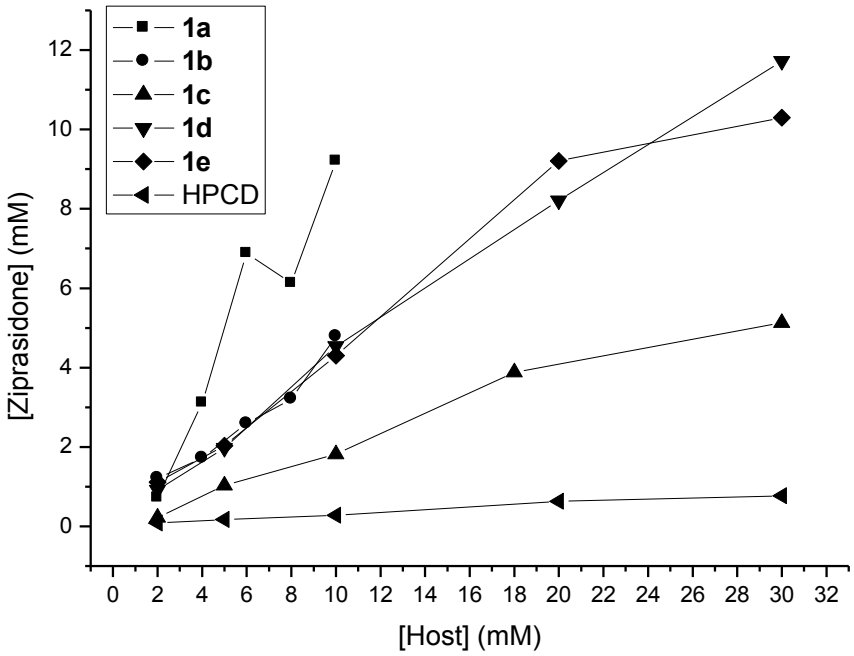

Figure S III-26. Phase solubility diagram of ziprasidone with different hosts in phosphate buffer (20 mM, pH 7.4, RT).

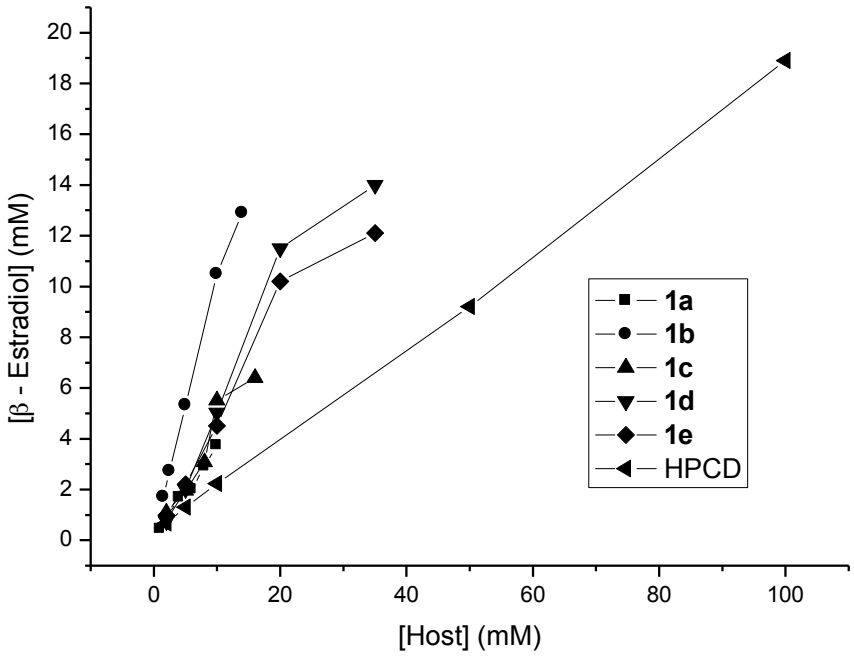

Figure S III-27. Phase solubility diagram of β - estradiol with different hosts in phosphate buffer (20 mM, pH 7.4, RT).

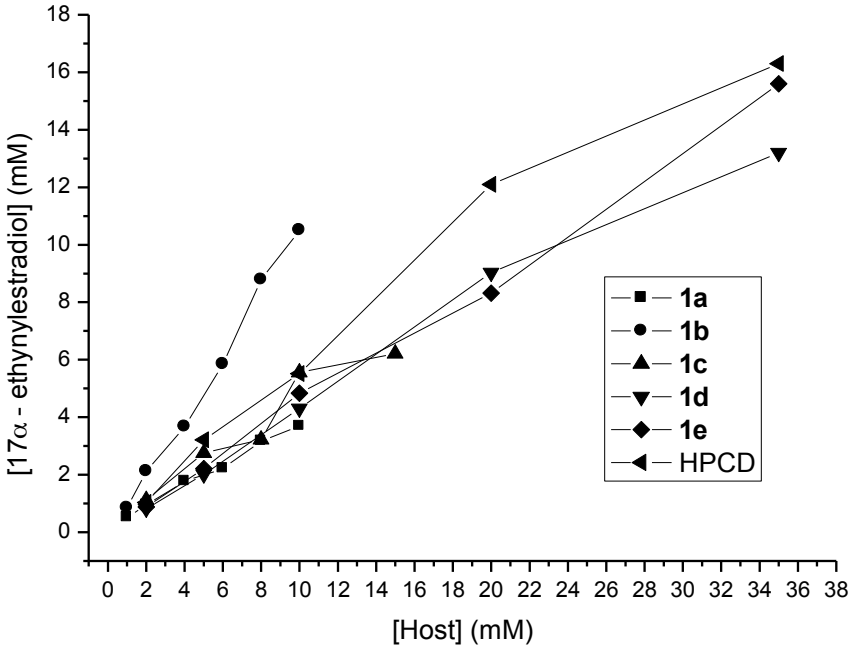

Figure S III-28. Phase solubility diagram of 17α - ethynylestradiol with different hosts in phosphate buffer (20 mM, pH 7.4, RT).

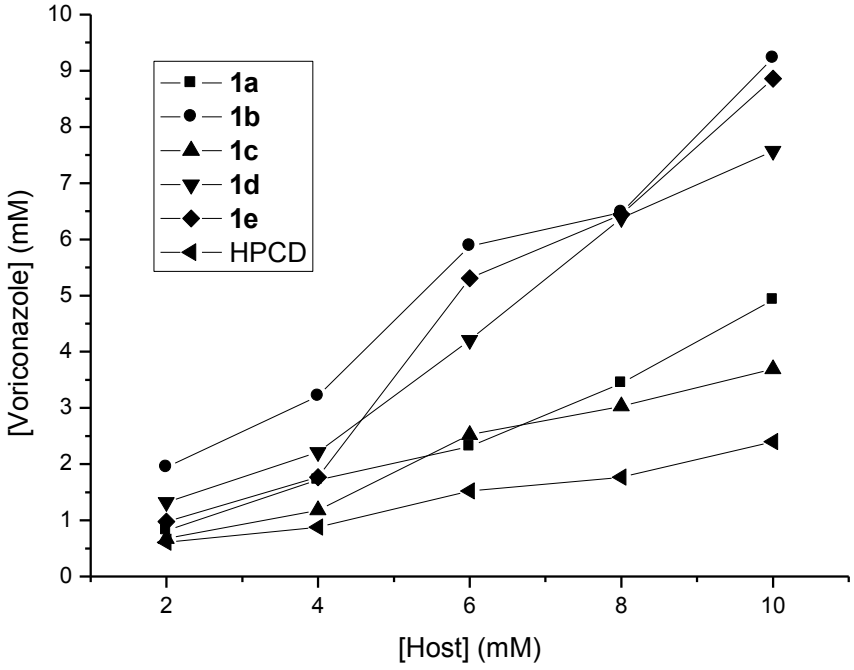

Figure S III-29. Phase solubility diagram of voriconazole with different hosts in phosphate buffer (20 mM, pH 7.4, RT).

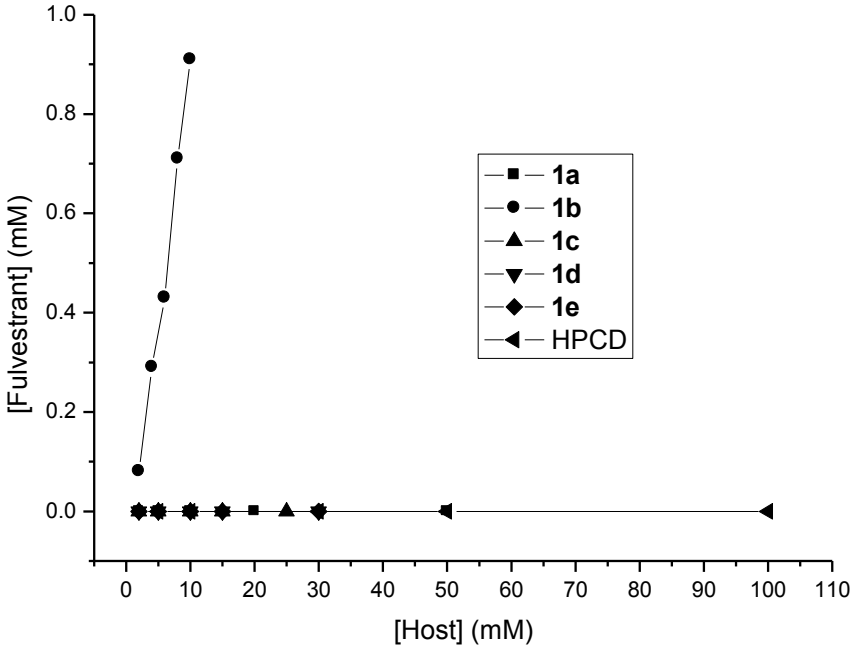

Figure S III-30. Phase solubility diagram of fulvestrant with different hosts in phosphate buffer (20 mM, pH 7.4, RT).

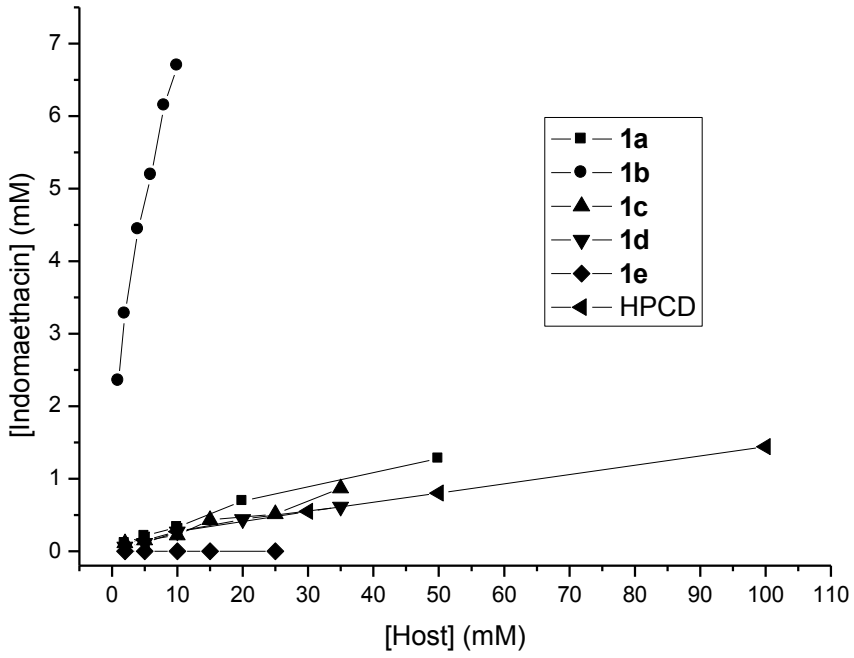

Figure S III-31. Phase solubility diagram of indomethacin with different hosts in phosphate buffer (20 mM, pH 7.4, RT).

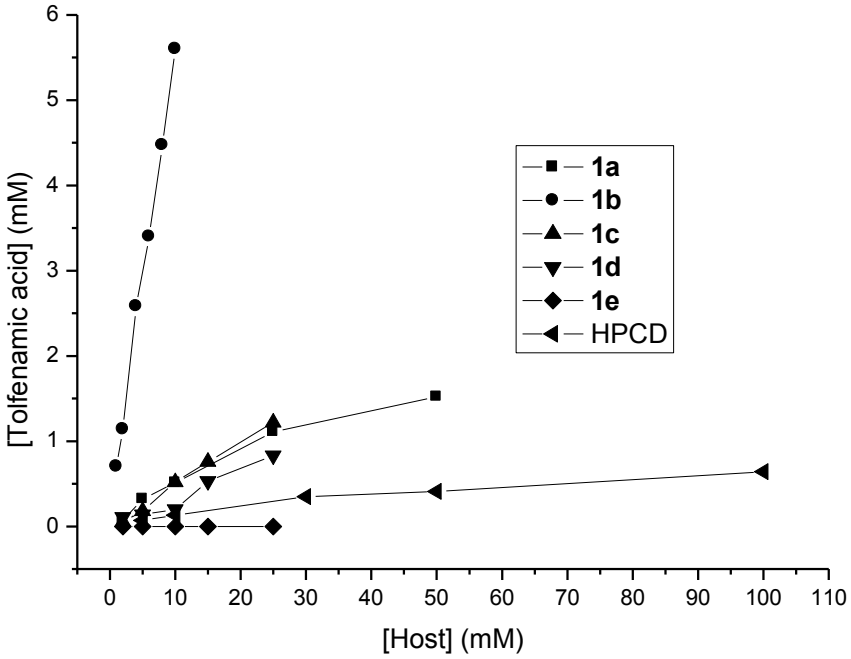

Figure S III-32. Phase solubility diagram of tolfenamic acid with different hosts in phosphate buffer (20 mM, pH 7.4, RT).

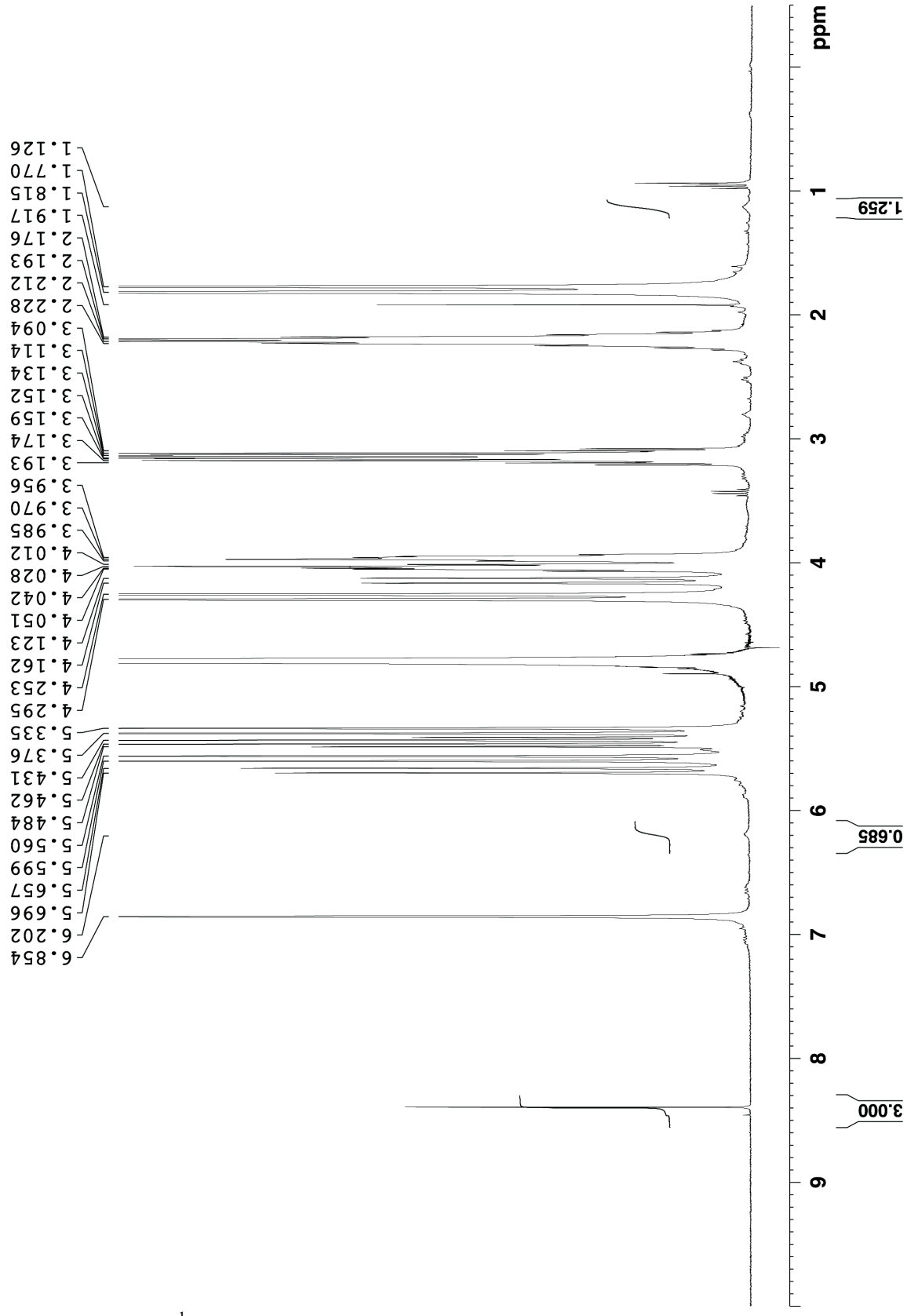

Figure S III-33. ^{1}H NMR recorded for pharmaceutical agent Aripiprazole with **III-1a** (10 mM) (400 MHz, 20 mM NaD_2PO_4, pD = 7.4, RT, 1,3,5-benzenetricarboxylic acid as reference).

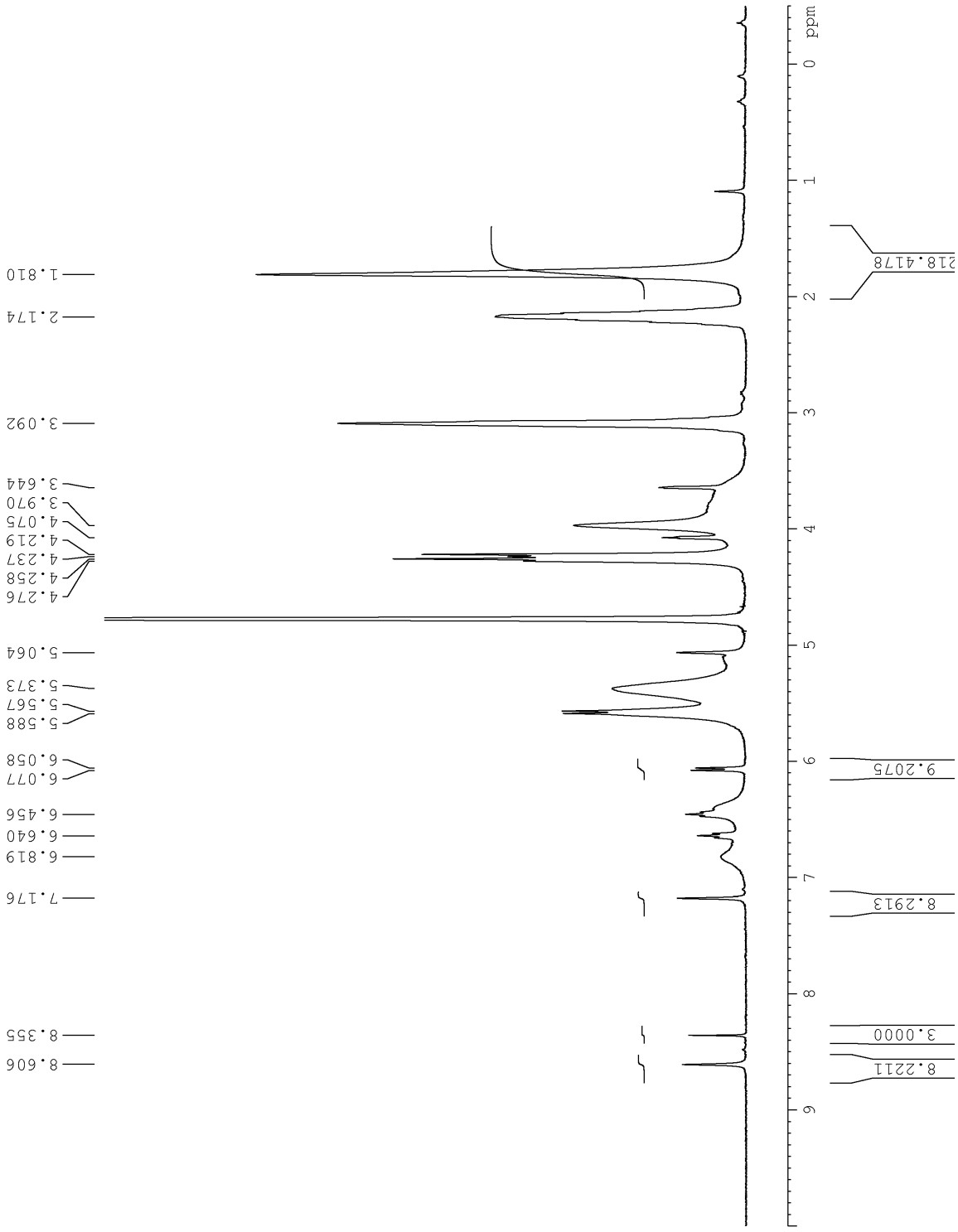

Figure S III-34. ^{1}H NMR recorded for pharmaceutical agent PBS-1086 with **III-1a** (15 mM) (400 MHz, 20 mM NaD_2PO_4, pD = 7.4, RT, 1,3,5-benzenetricarboxylic acid as reference).

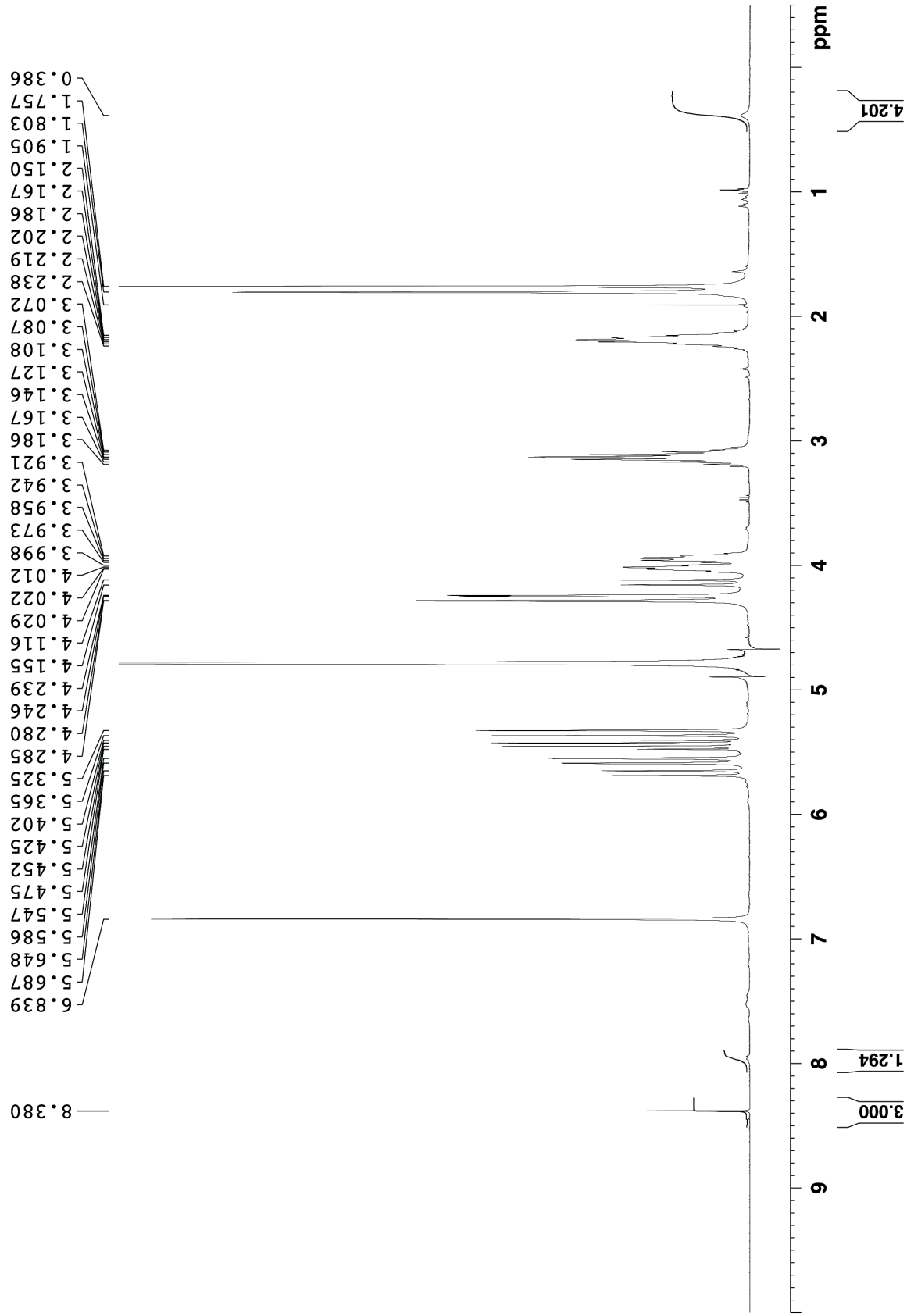

Figure S III-35. ^{1}H NMR recorded for pharmaceutical agent Docetaxel with **III-1a** (10 mM) (400 MHz, 20 mM NaD_2PO_4, pD = 7.4, RT, 1,3,5-benzenetricarboxylic acid as reference).

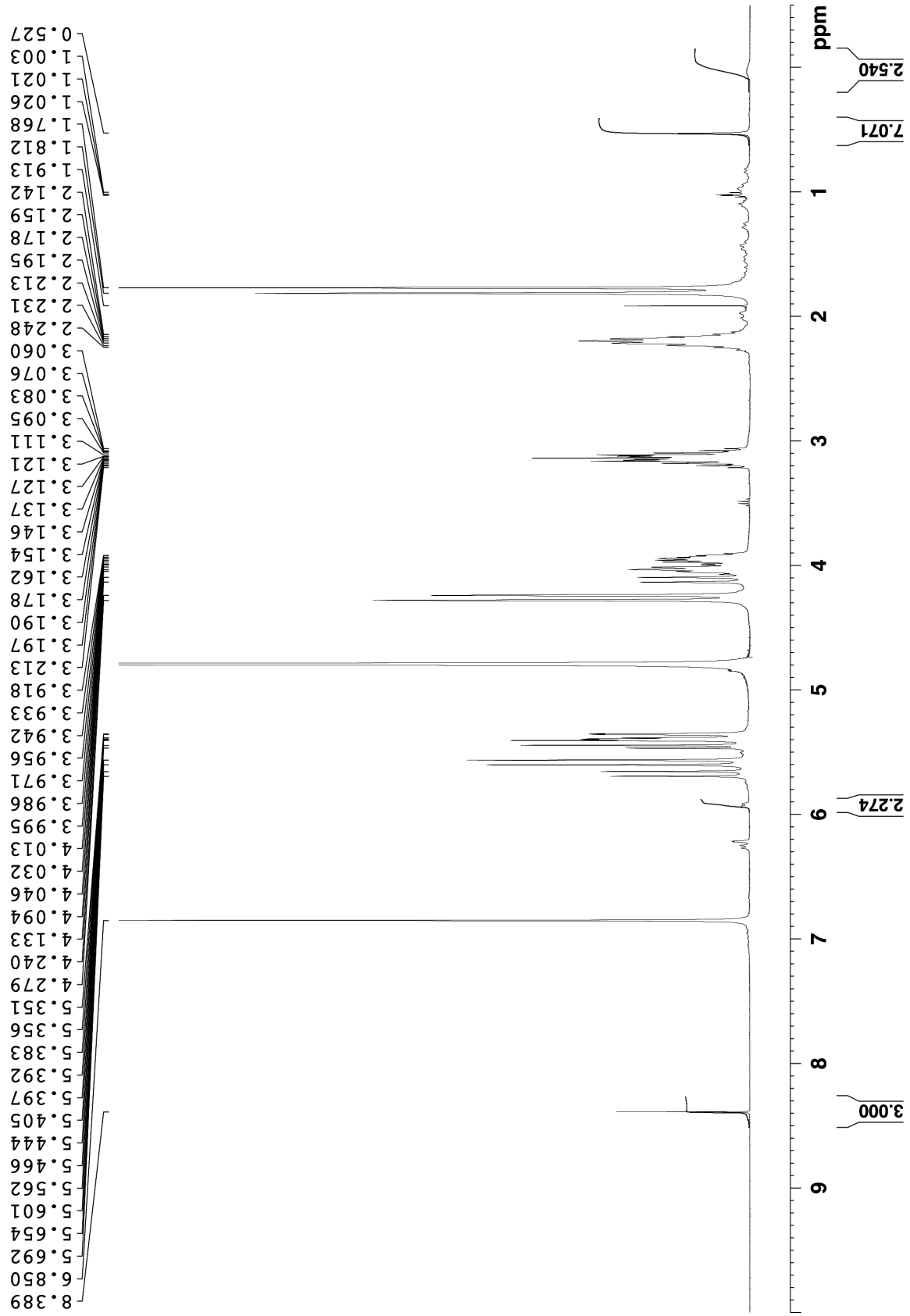

Figure S III-36. ^{1}H NMR recorded for pharmaceutical agent 17α-ethynylestradiol with **III-1a** (6 mM) (400 MHz, 20 mM NaD_2PO_4, pD = 7.4, RT, 1,3,5-benzenetricarboxylic acid as reference).

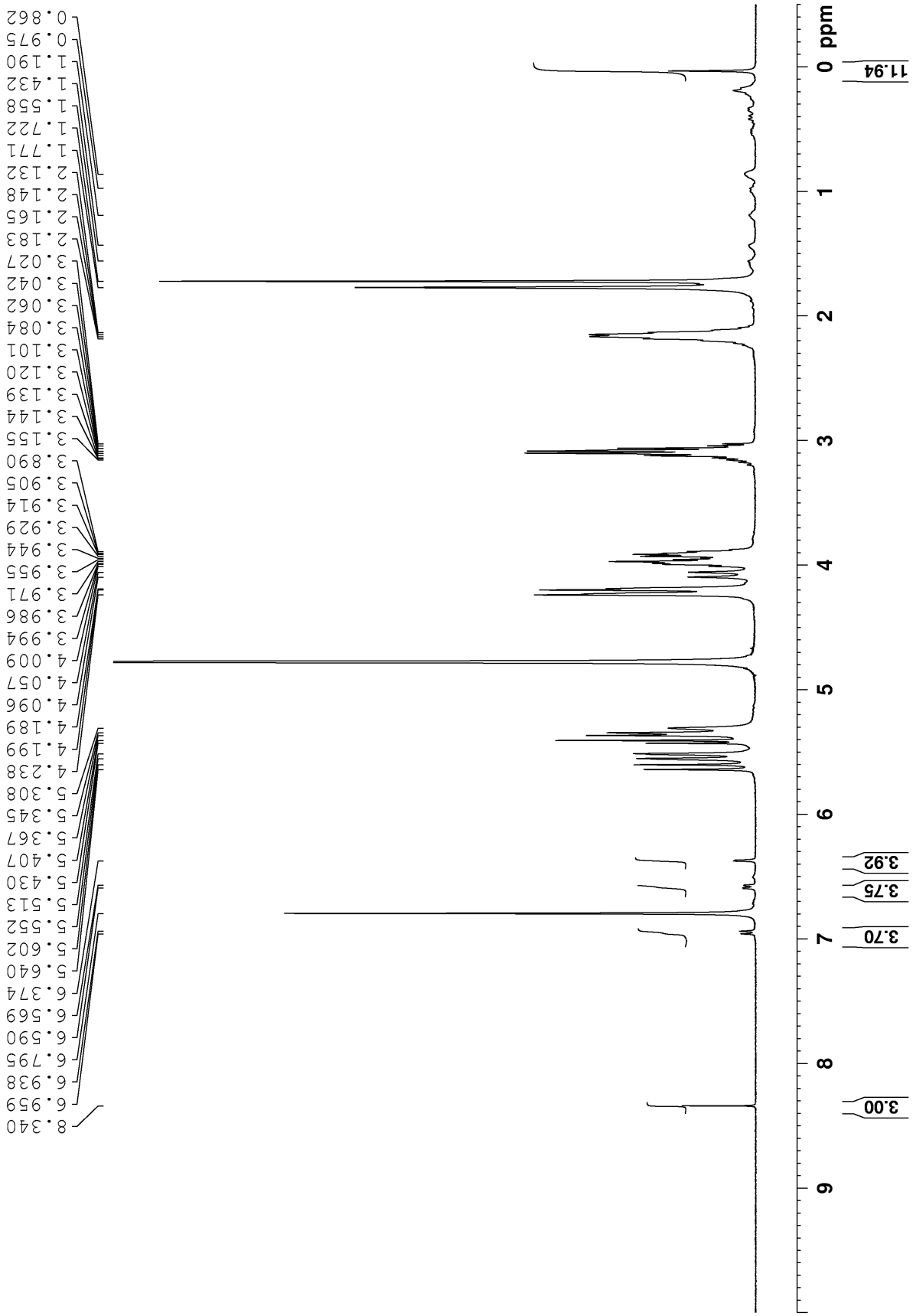

Figure S III-37. ^{1}H NMR recorded for pharmaceutical agent β-estradiol with **III-1a** (10 mM) (400 MHz, 20 mM NaD_2PO_4, pD = 7.4, RT, 1,3,5-benzenetricarboxylic acid as reference).

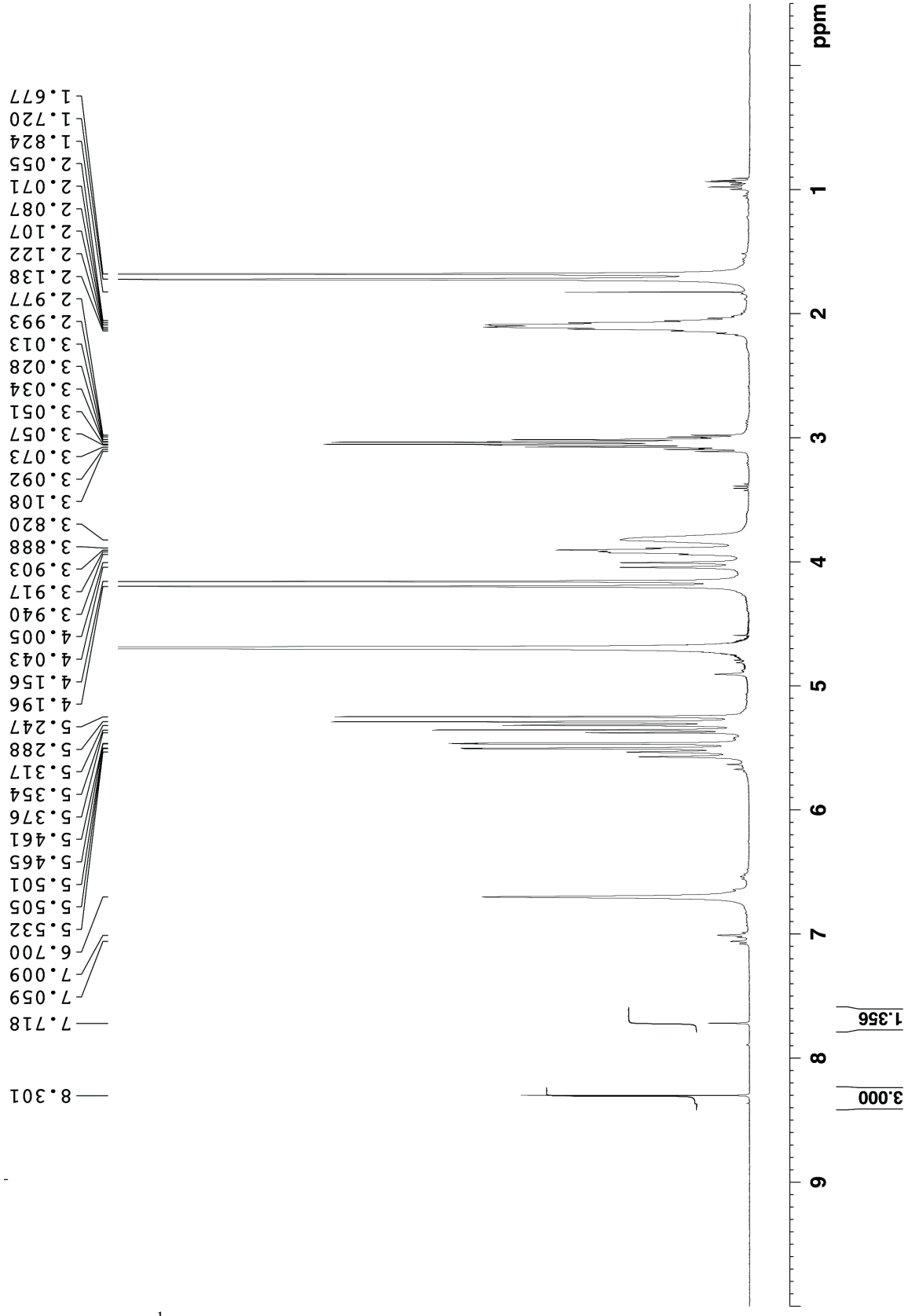

Figure S III-38. ^{1}H NMR recorded for pharmaceutical agent camptothecin with **III-1a** (10 mM) (400 MHz, 20 mM NaD_2PO_4, pD = 7.4, RT, 1,3,5-benzenetricarboxylic acid as reference).

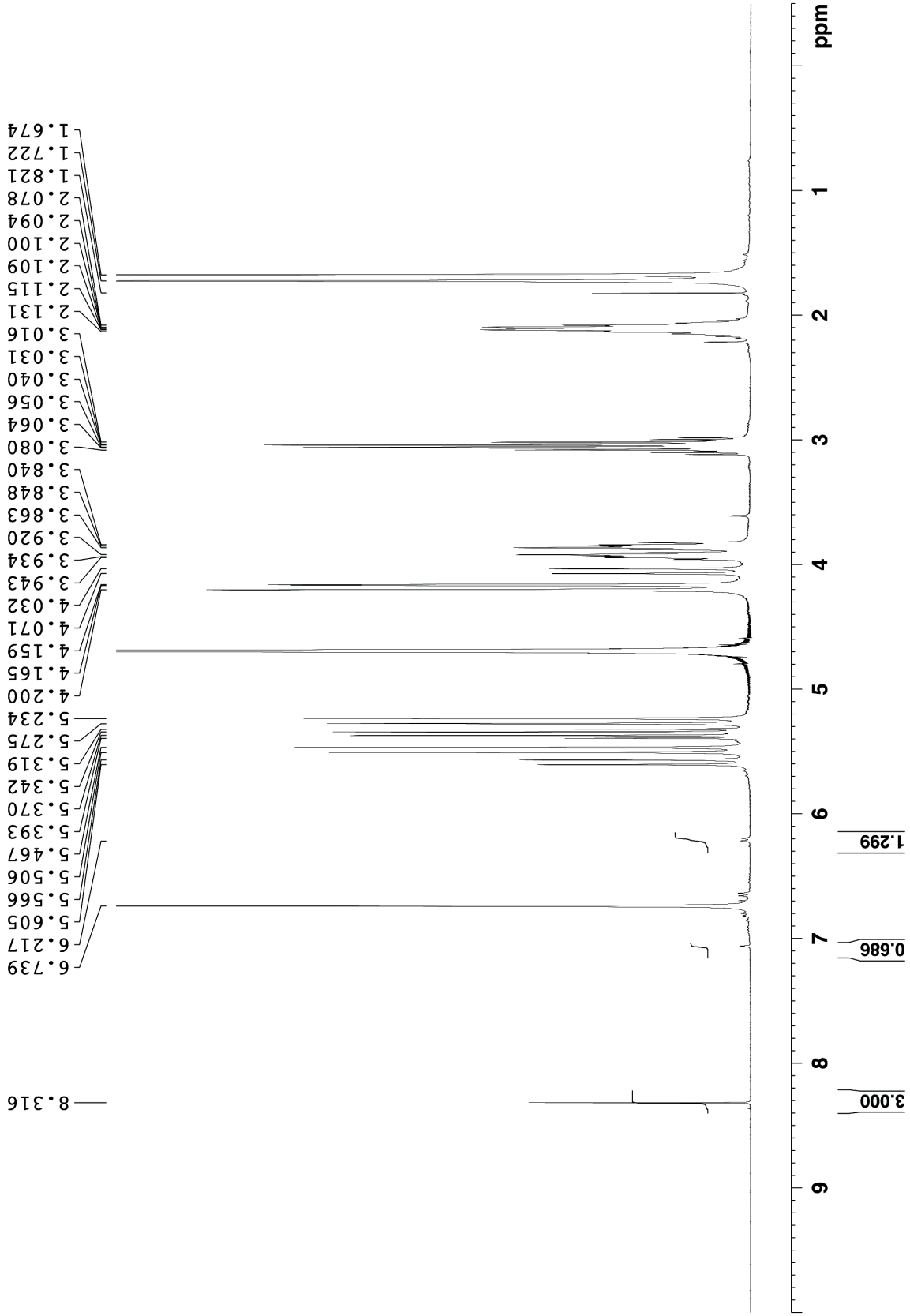

Figure S III-39. ^{1}H NMR recorded for pharmaceutical agent Indomethacin with **III-1a** (20 mM) (400 MHz, 20 mM NaD_2PO_4, pD = 7.4, RT, 1,3,5-benzenetricarboxylic acid as reference).

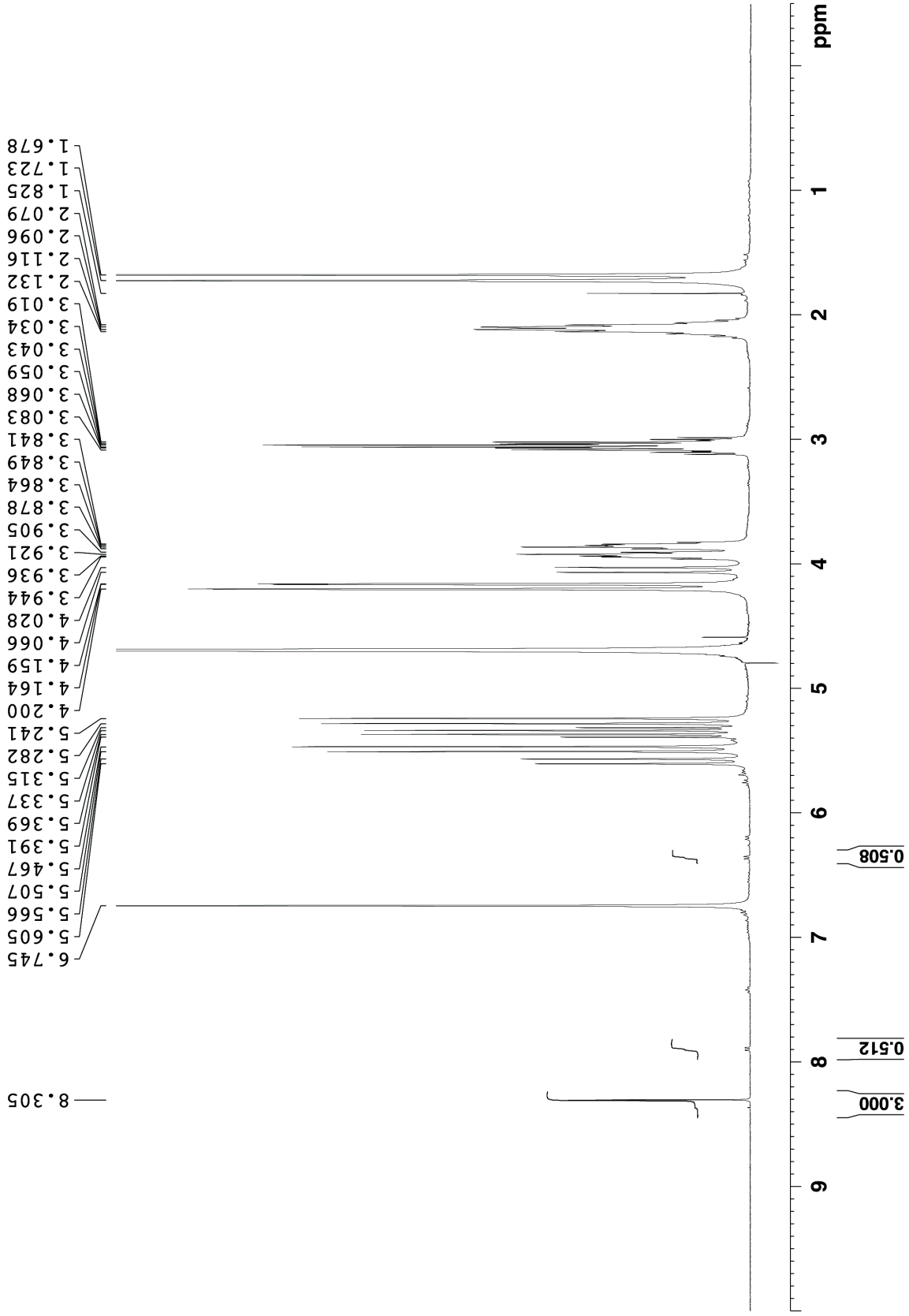

Figure S III-40. ^{1}H NMR recorded for pharmaceutical agent Tolfenamic acid with **III-1a** (10 mM) (400 MHz, 20 mM NaD_2PO_4, pD = 7.4, RT, 1,3,5-benzenetricarboxylic acid as reference).

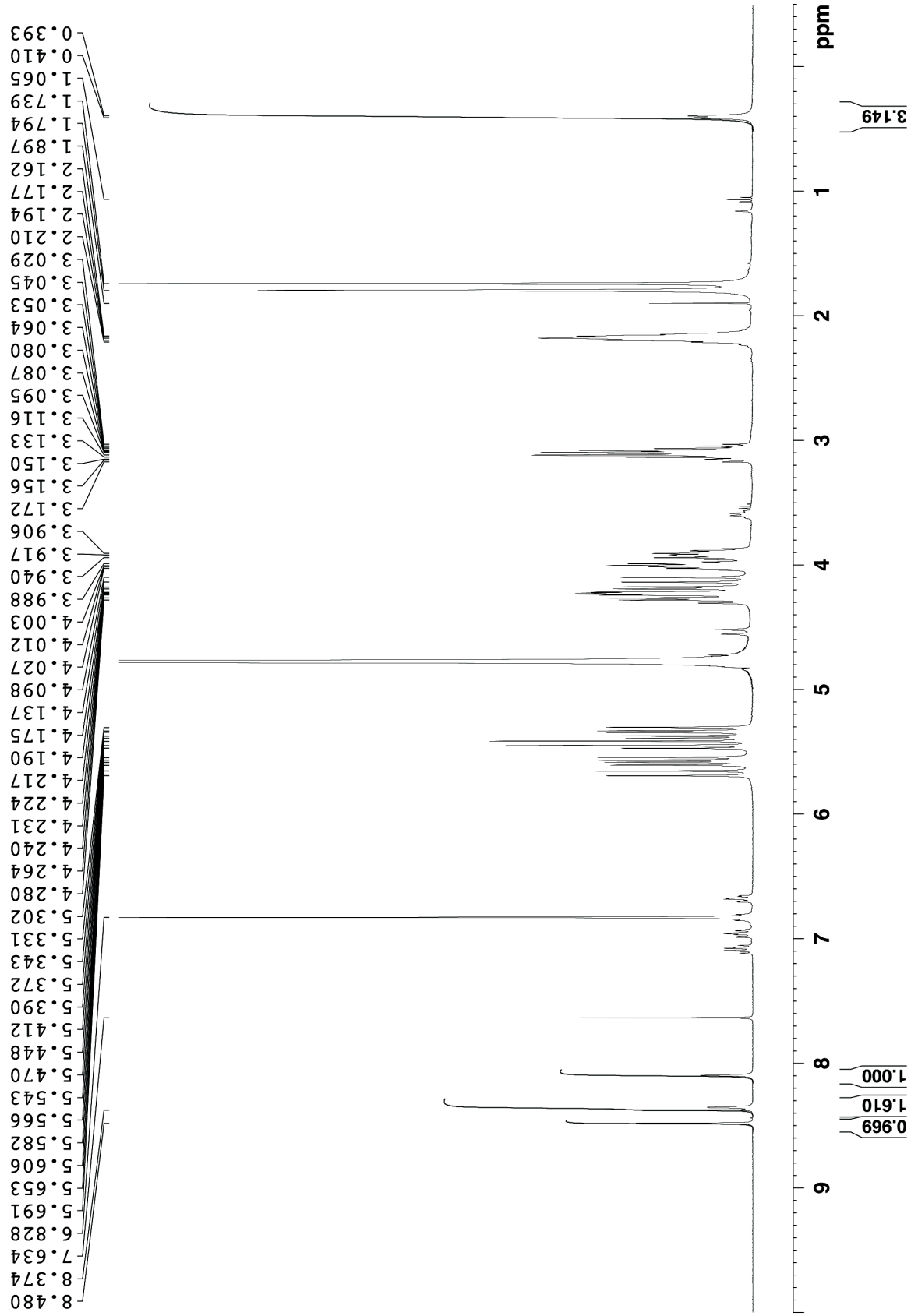

Figure S III-41. ^{1}H NMR recorded for pharmaceutical agent Voriconazole with **III-1a** (10 mM) (400 MHz, 20 mM NaD_2PO_4, pD = 7.4, RT, 1,3,5-benzenetricarboxylic acid as reference).

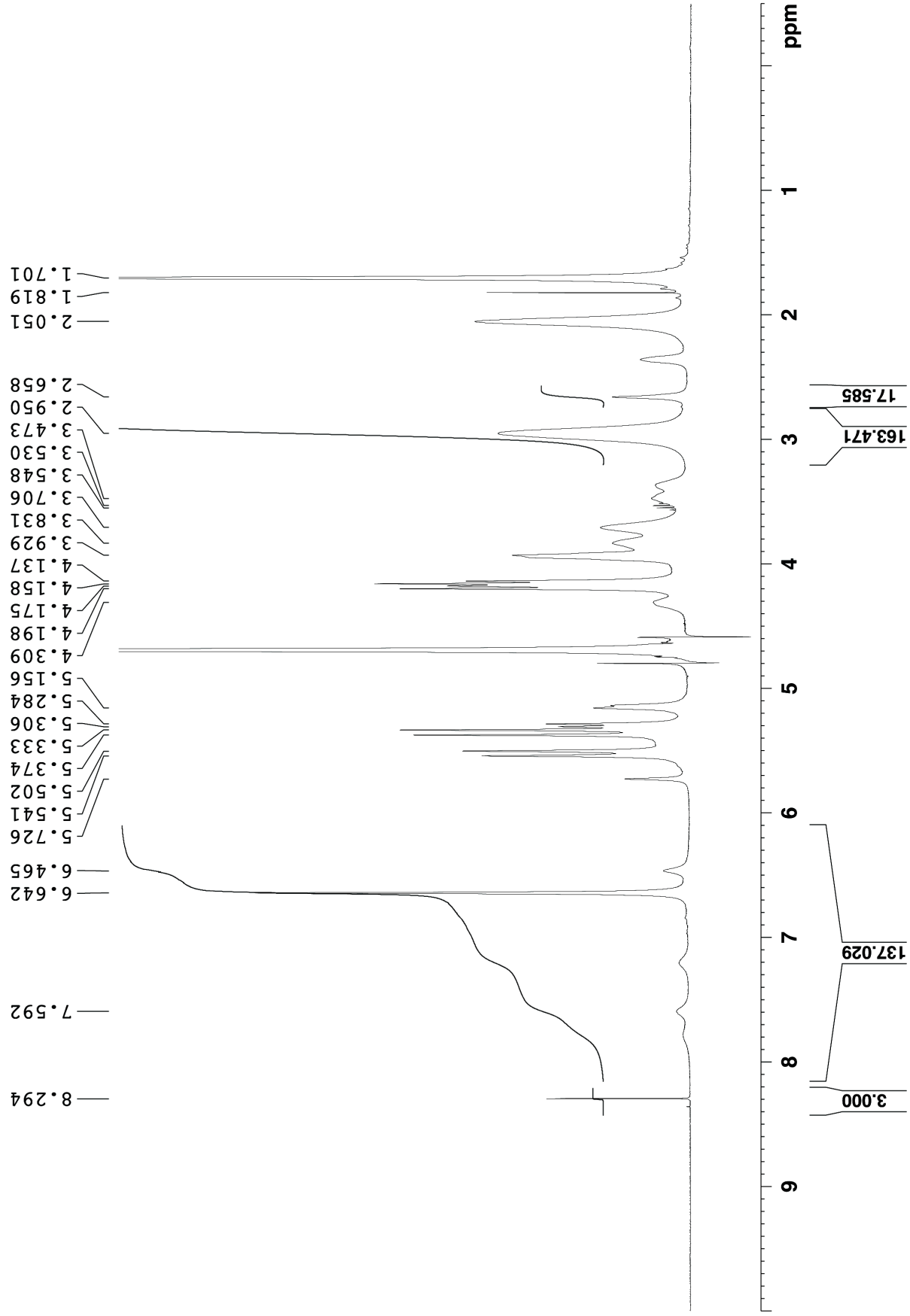

Figure S III-42. ^{1}H NMR recorded for pharmaceutical agent ziprasidone with **III-1a** (10 mM) (400 MHz, 20 mM NaD_2PO_4, pD = 7.4, RT, 1,3,5-benzenetricarboxylic acid as

reference).

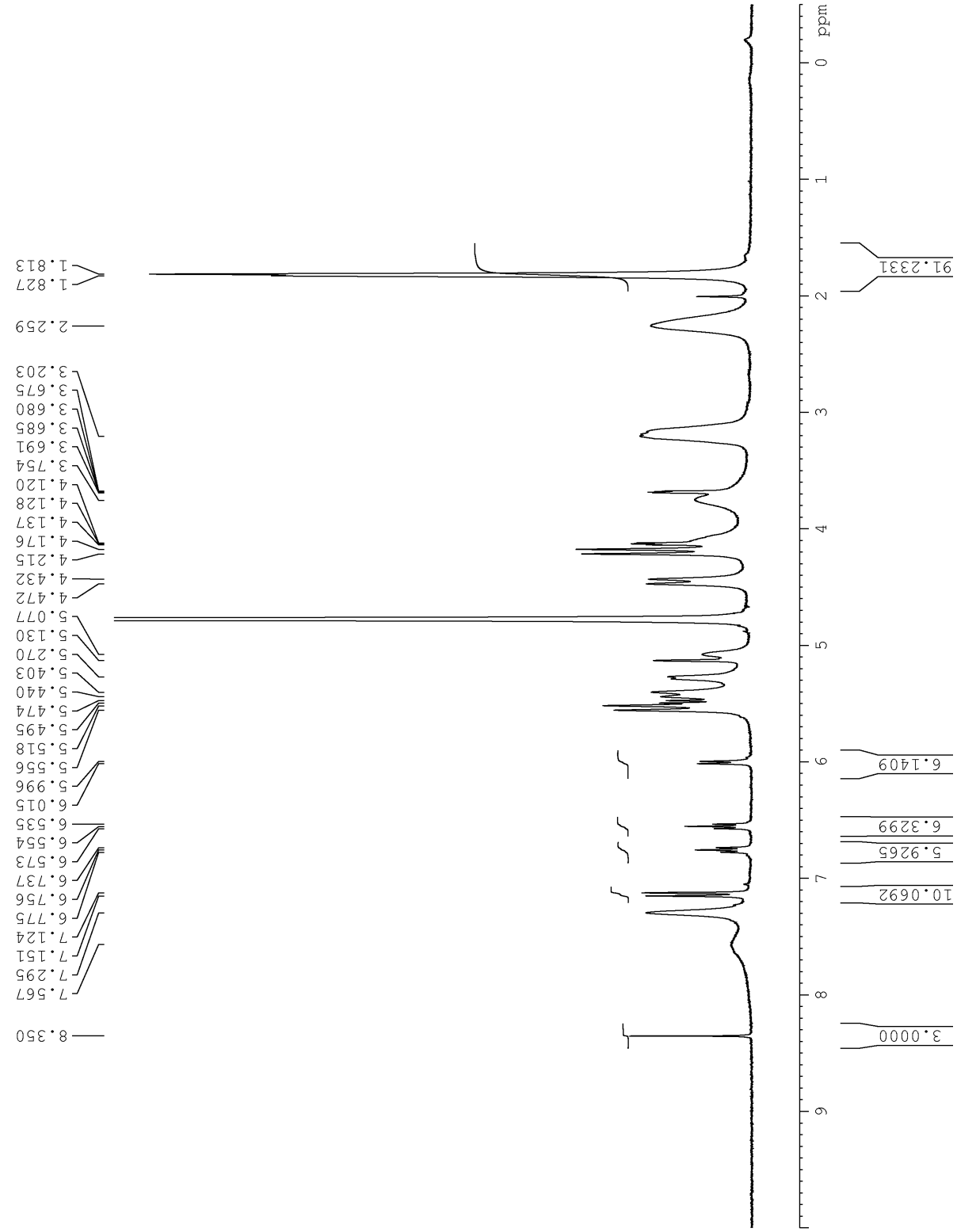

Figure S III-43. ^{1}H NMR recorded for pharmaceutical agent PBS-1086 with **III-1b** (8 mM) (400 MHz, 20 mM NaD_2PO_4, pD = 7.4, RT, 1,3,5-benzenetricarboxylic acid as reference).

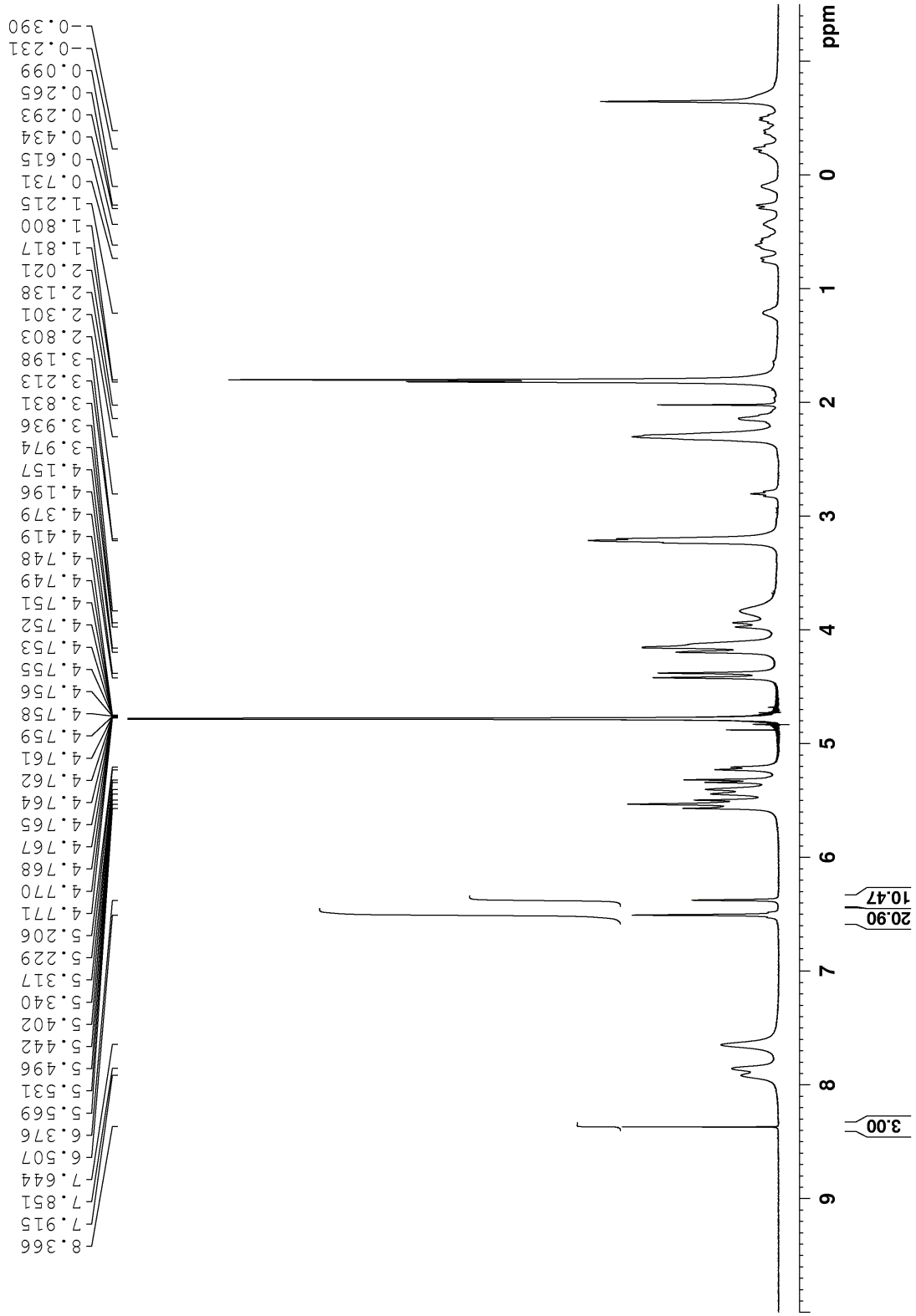

Figure S III-44. ^{1}H NMR recorded for pharmaceutical agent β-estradiol with **III-1b** (10 mM) (400 MHz, 20 mM NaD_2PO_4, pD = 7.4, RT, 1,3,5-benzenetricarboxylic acid as reference).

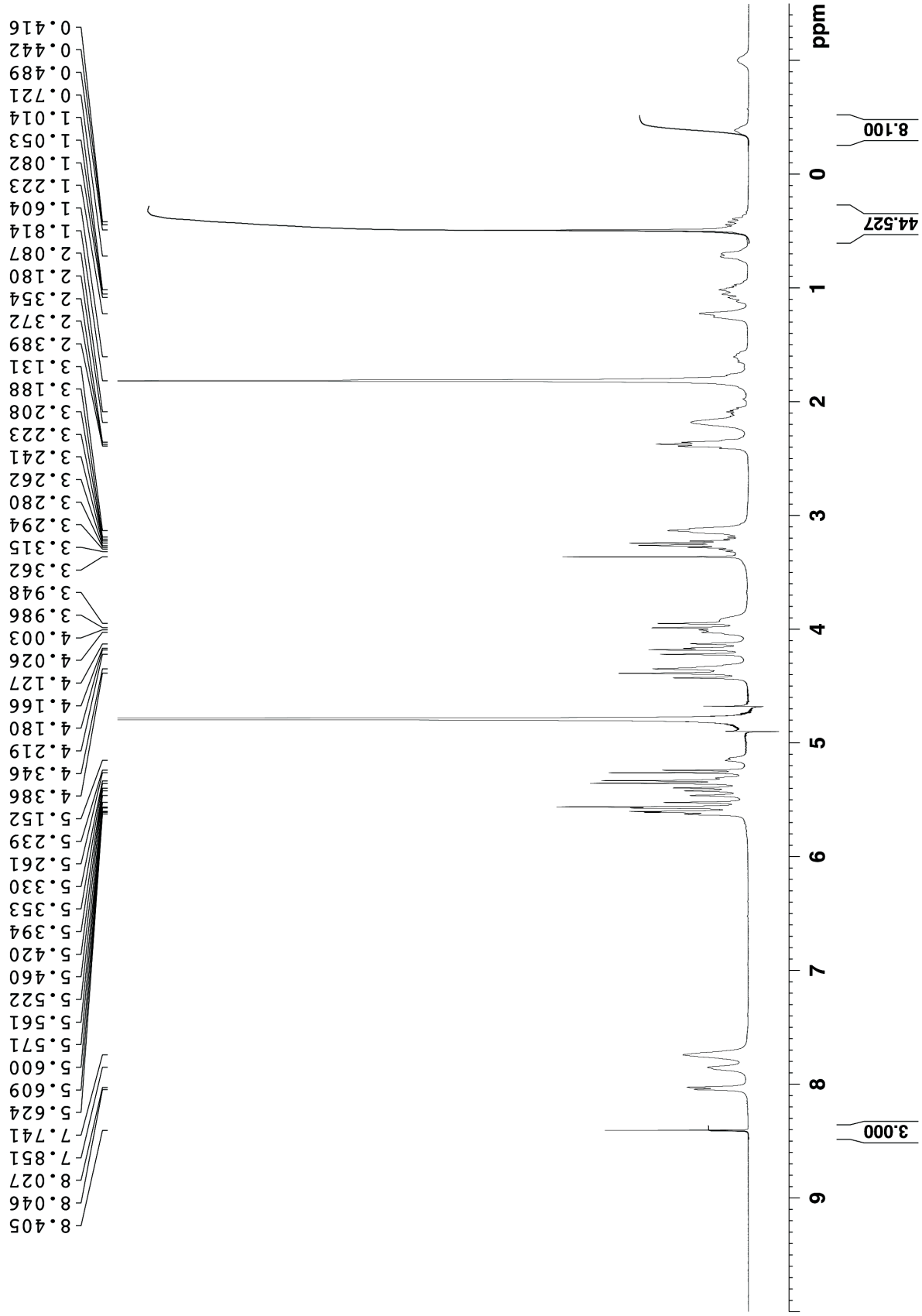

Figure S III-45. ^{1}H NMR recorded for pharmaceutical agent 17α-ethynylestradiol with **III-1b** (10 mM) (400 MHz, 20 mM NaD_2PO_4, pD = 7.4, RT, 1,3,5-benzenetricarboxylic acid as reference).

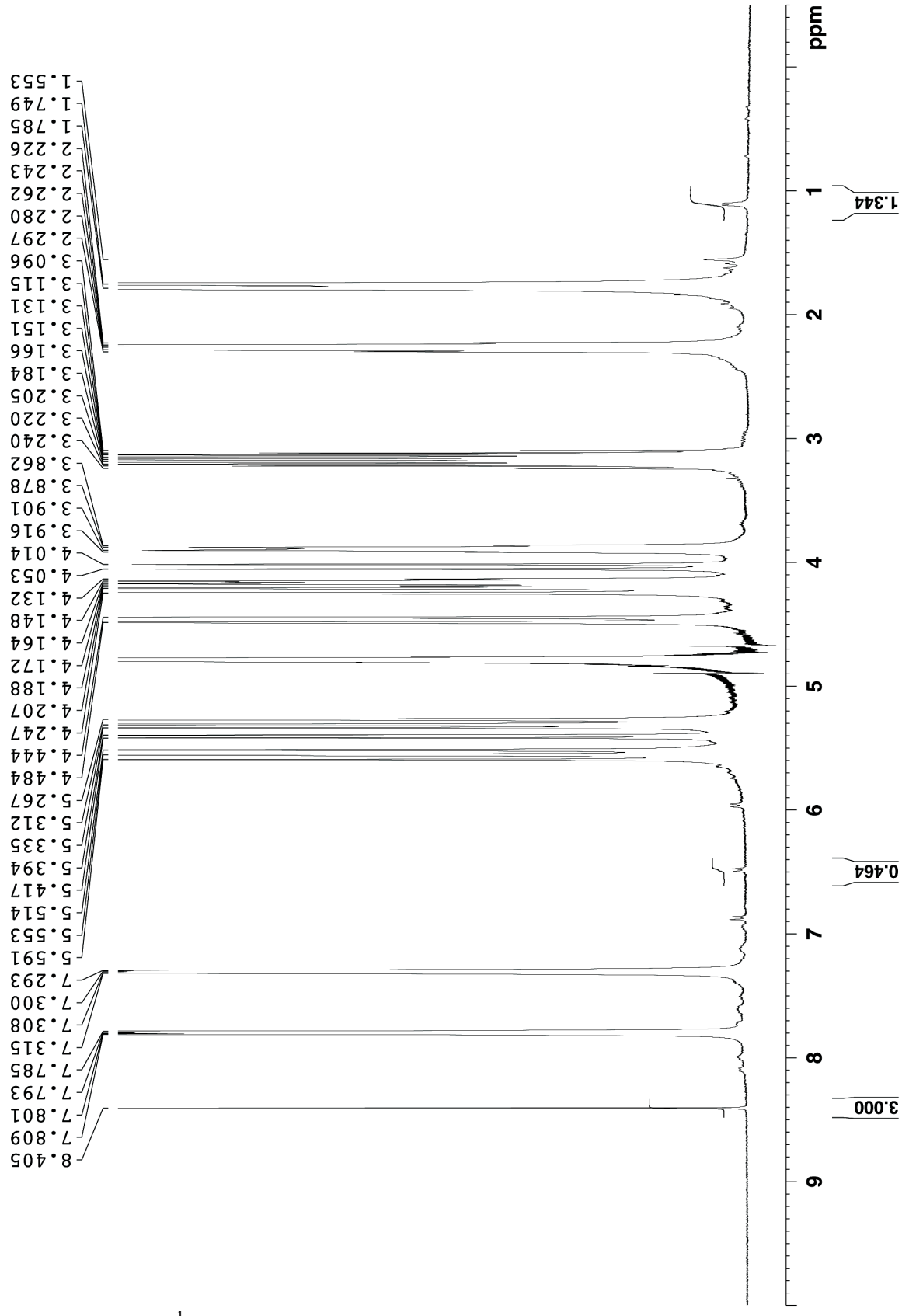

Figure S III-46. ^{1}H NMR recorded for pharmaceutical agent Fenofibrate with **III-1b** (10 mM) (400 MHz, 20 mM NaD_2PO_4, pD = 7.4, RT, 1,3,5-benzenetricarboxylic acid as reference).

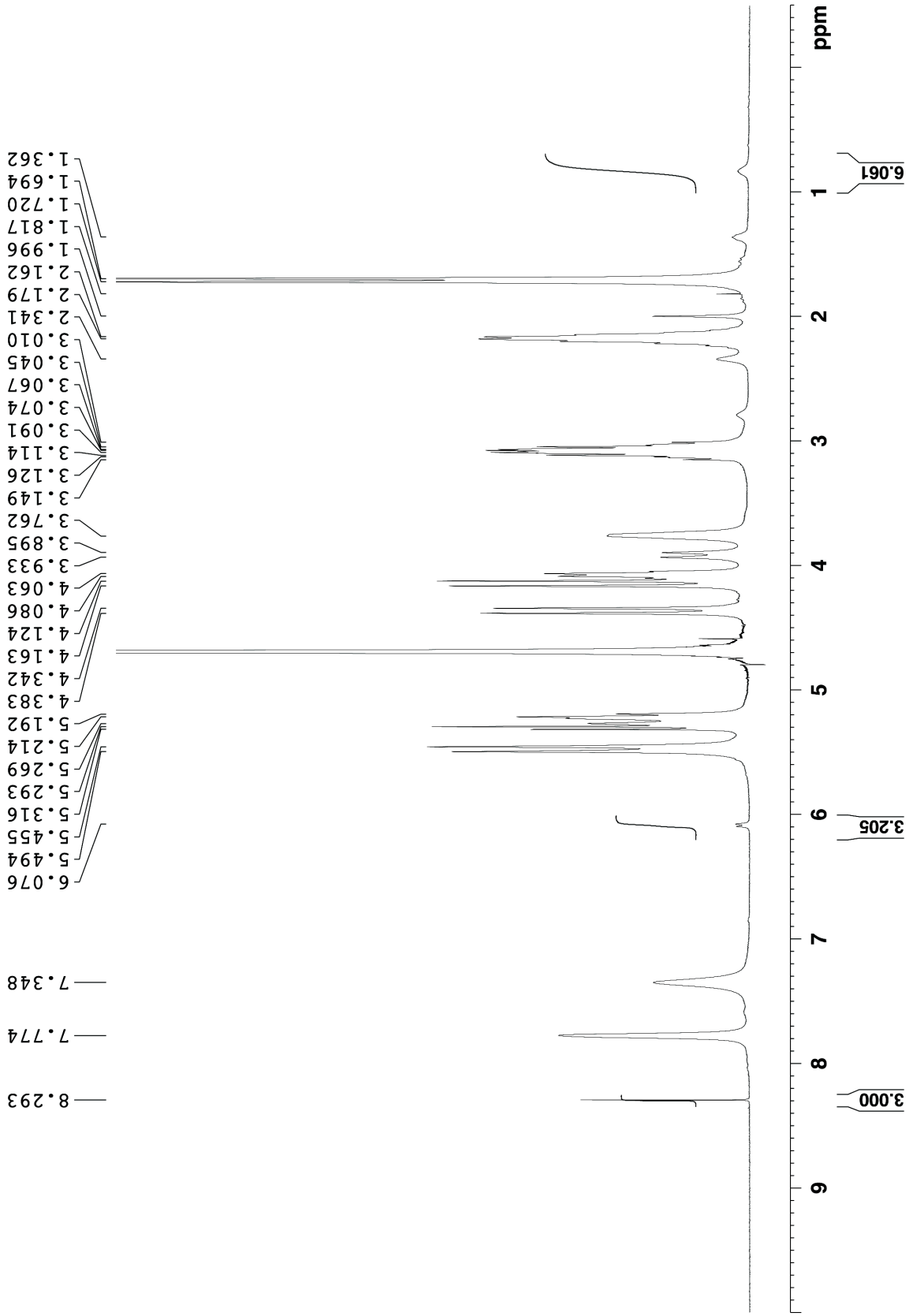

Figure S III-47. ^{1}H NMR recorded for pharmaceutical agent Aripiprazole with **III-1b** (10 mM) (400 MHz, 20 mM NaD_2PO_4, pD = 7.4, RT, 1,3,5-benzenetricarboxylic acid as reference).

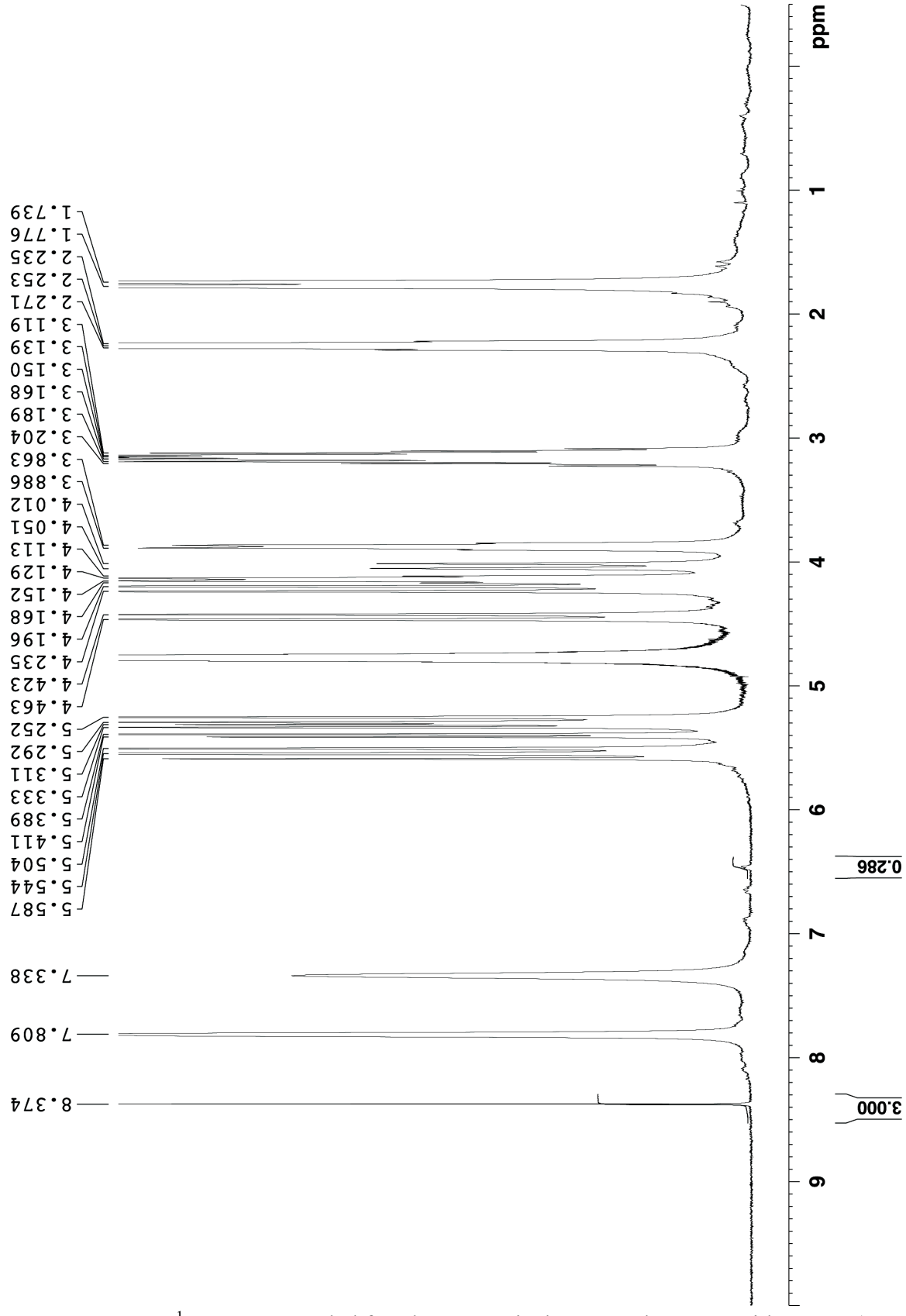

Figure S III-48. ^{1}H NMR recorded for pharmaceutical agent Fulvestrant with **III-1b** (4 mM) (400 MHz, 20 mM NaD_2PO_4, pD = 7.4, RT, 1,3,5-benzenetricarboxylic acid as reference).

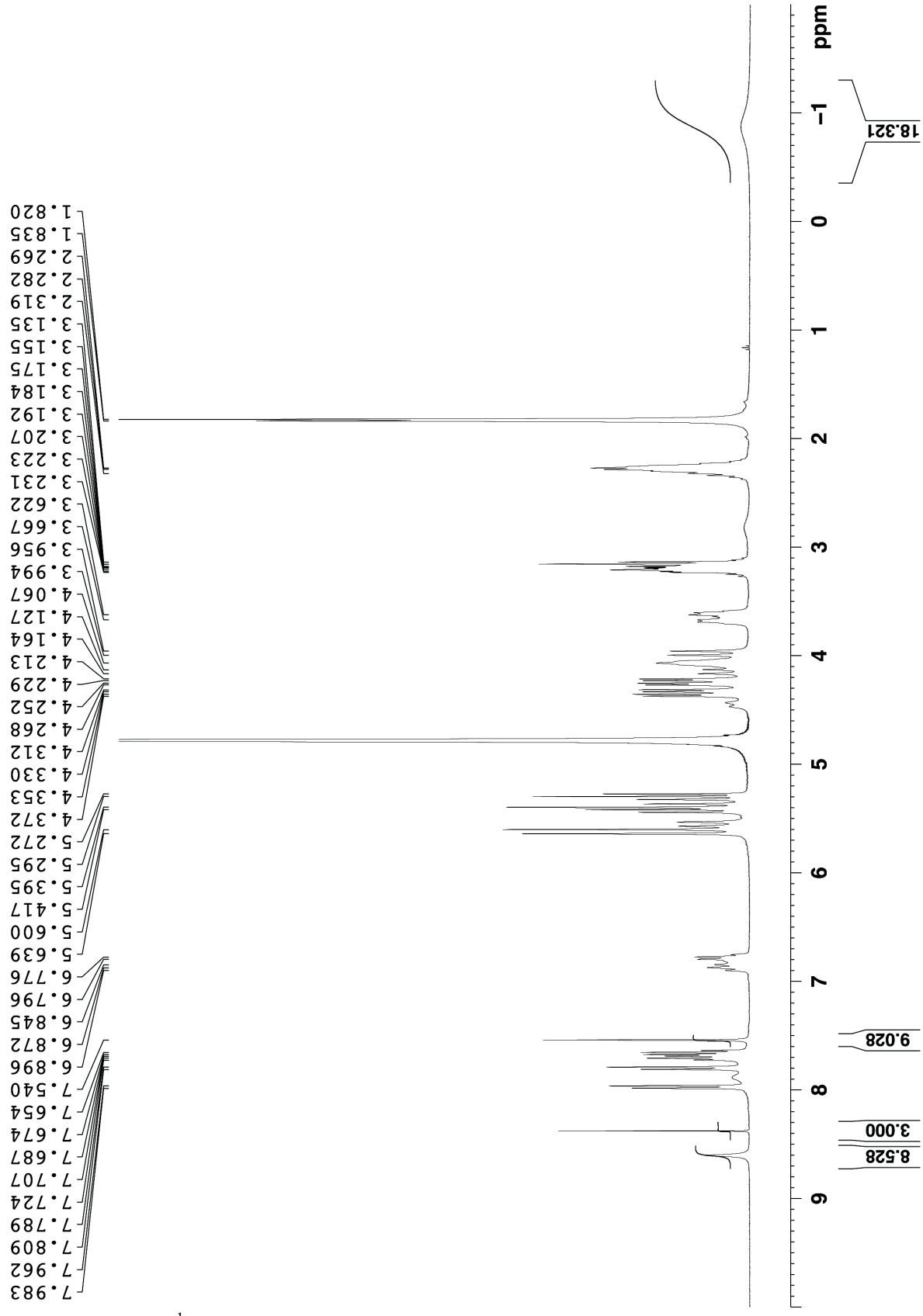

Figure S III-49. ^{1}H NMR recorded for pharmaceutical agent Voriconazole with **III-1b** (10 mM) (400 MHz, 20 mM NaD_2PO_4, pD = 7.4, RT, 1,3,5-benzenetricarboxylic acid as reference).

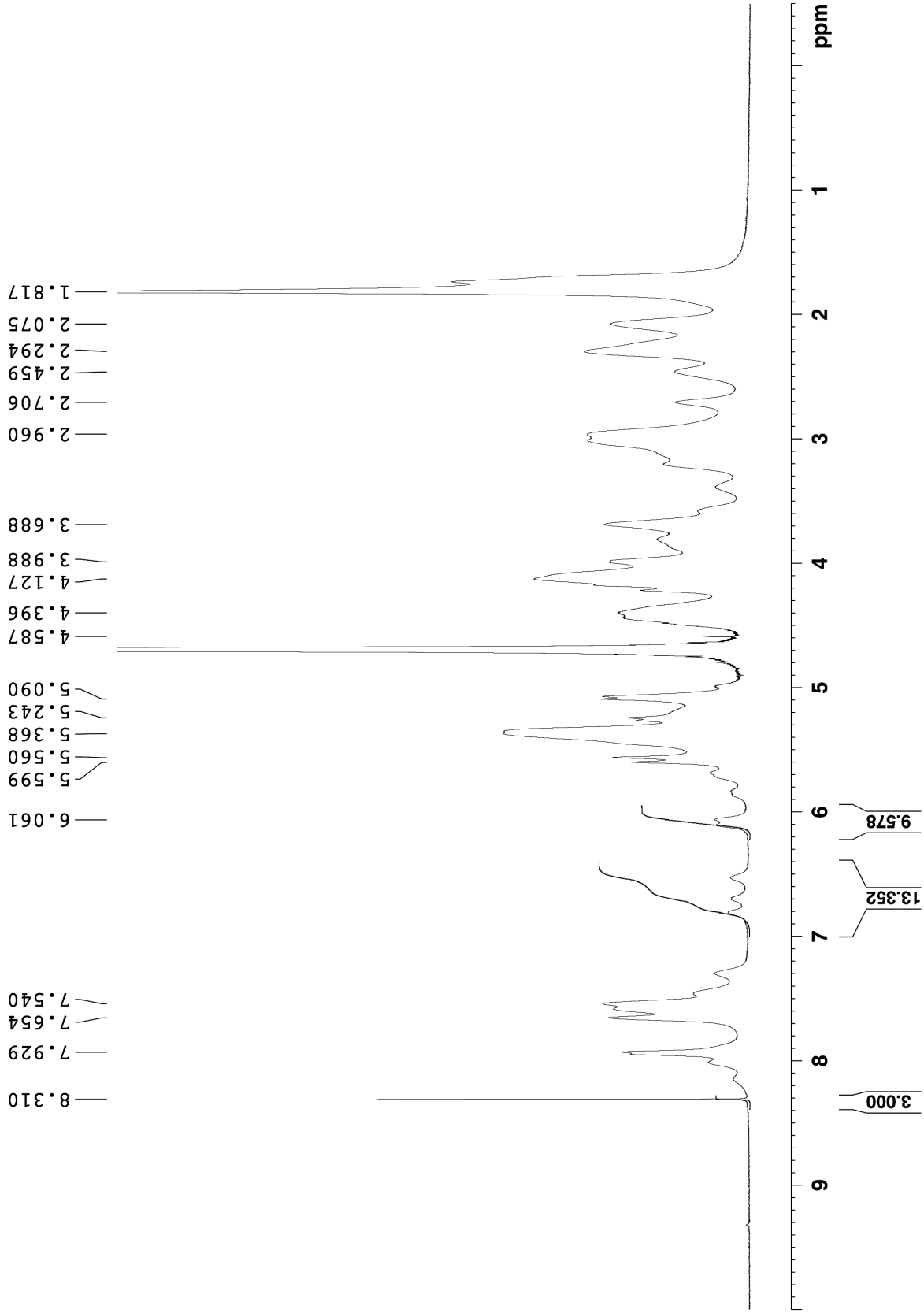

Figure S III-50. ^{1}H NMR recorded for pharmaceutical agent ziprasidone with **III-1b** (10 mM) (400 MHz, 20 mM NaD_2PO_4, pD = 7.4, RT, 1,3,5-benzenetricarboxylic acid as reference).

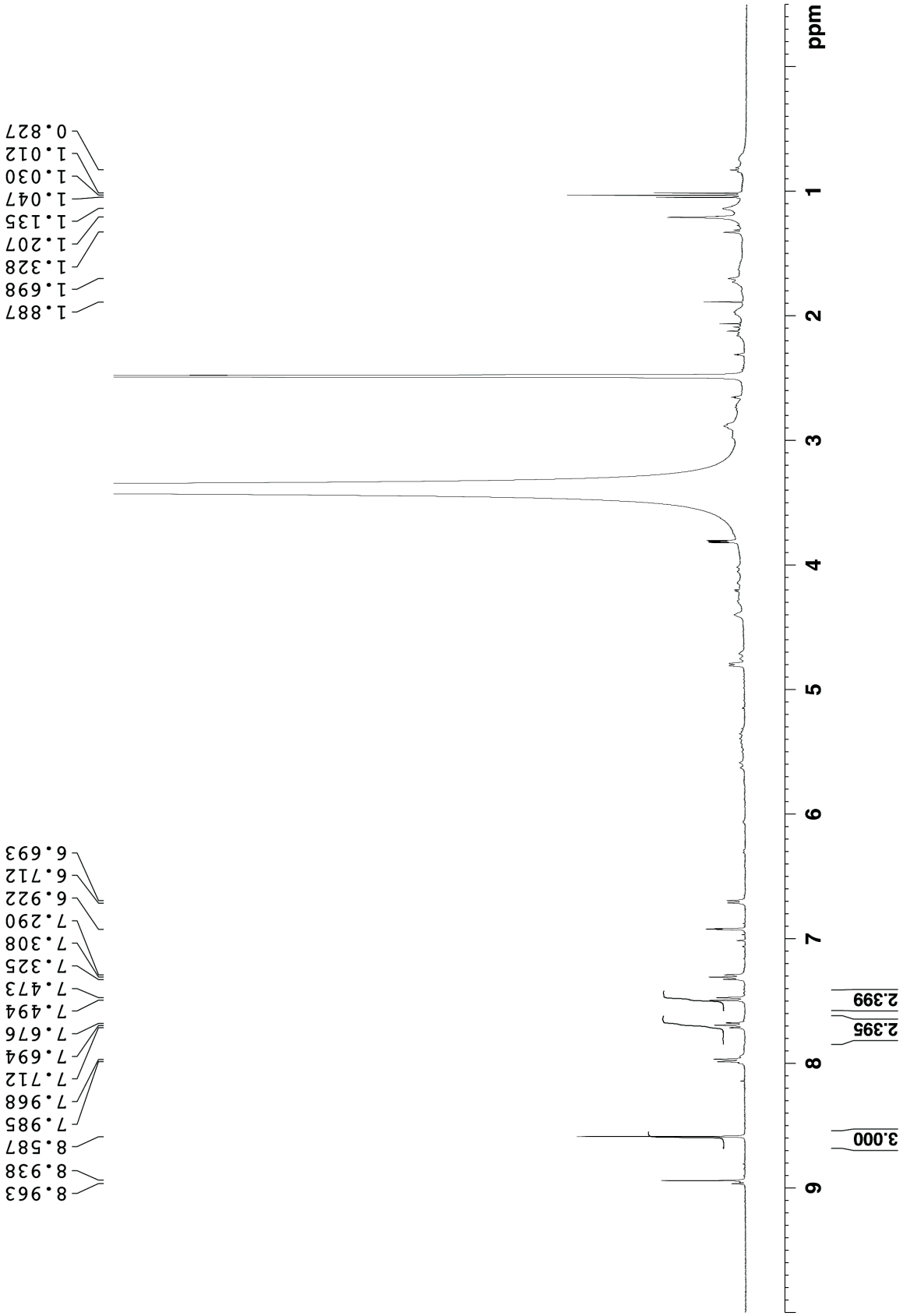

Figure S III-51. ^{1}H NMR recorded for pharmaceutical agent PBS-1086 with **III-1c** (10 mM) (400 MHz, DMSO, RT, 1,3,5-benzenetricarboxylic acid as reference).

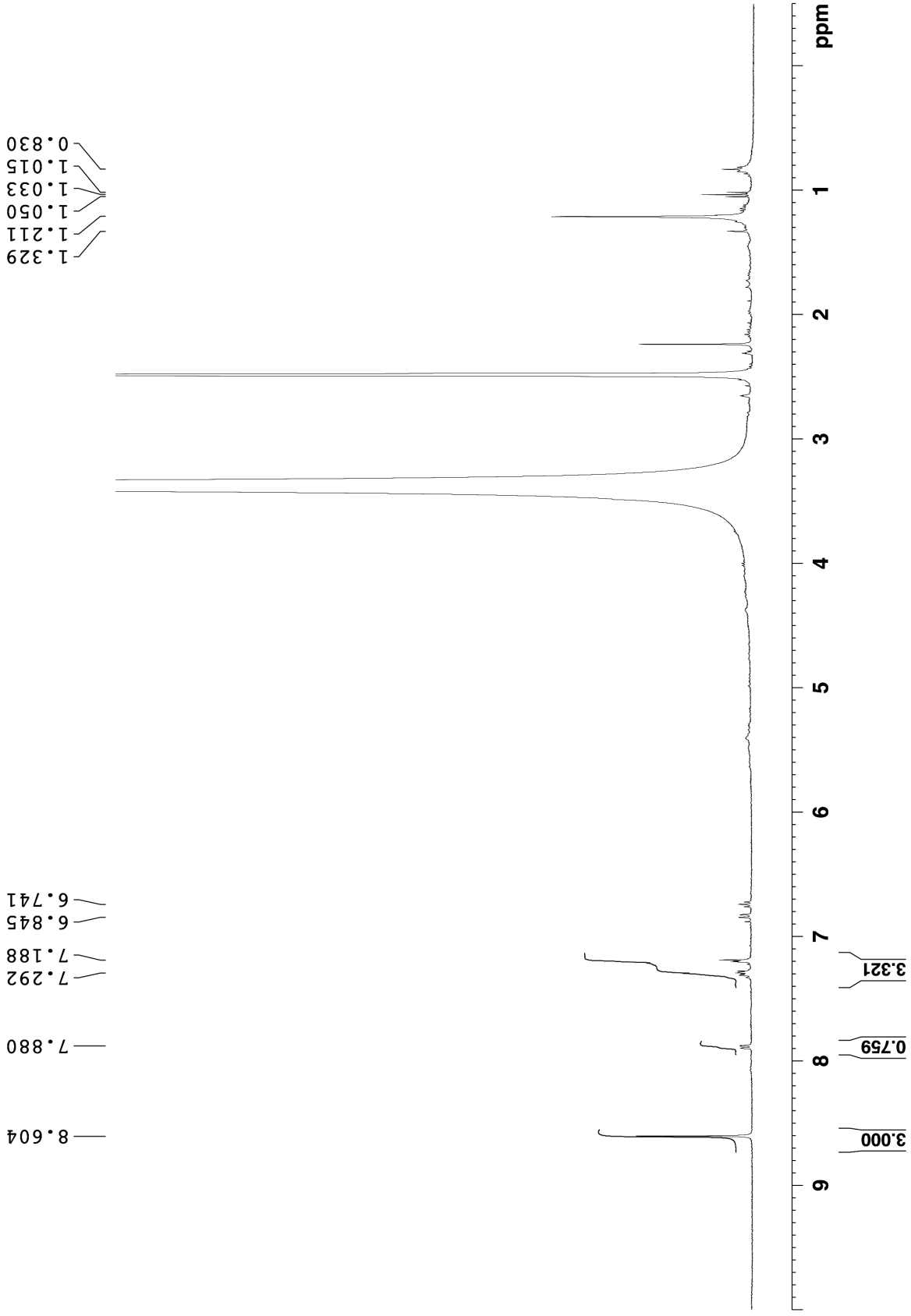

Figure S III-52. ^{1}H NMR recorded for pharmaceutical agent Tolfenamic acid with **III-1c** (15 mM) (400 MHz, DMSO, RT, 1,3,5-benzenetricarboxylic acid as reference).

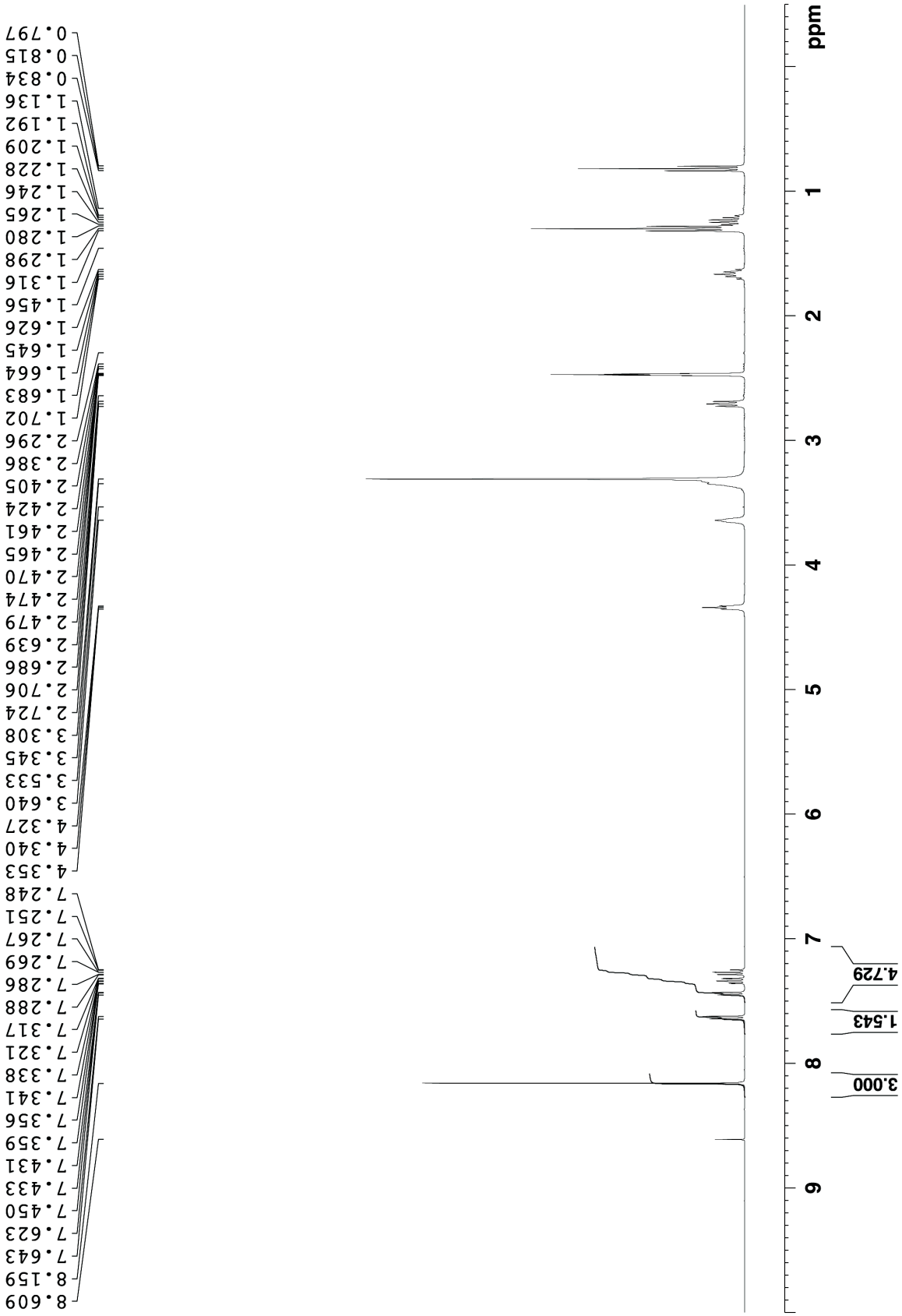

Figure S III-53. ^{1}H NMR recorded for pharmaceutical agent Amiodarone with **III-1c** (10 mM) (400 MHz, DMSO, pD = 7.4, RT, 1,3,5-benzenetricarboxylic acid as reference).

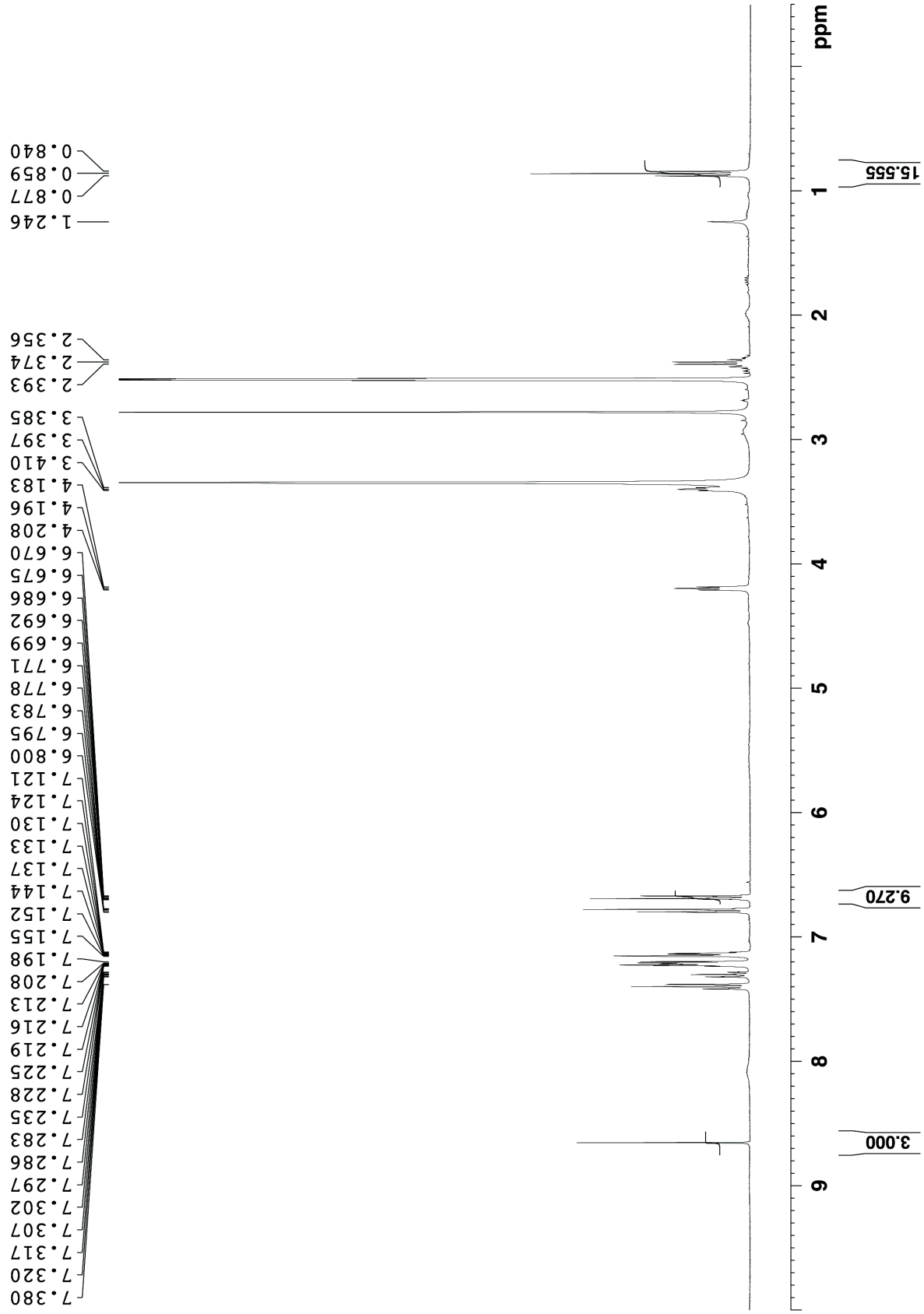

Figure S III-54. ^{1}H NMR recorded for pharmaceutical agent Tamoxifen with **III-1c** (10 mM) (400 MHz, DMSO, RT, 1,3,5-benzenetricarboxylic acid as reference).

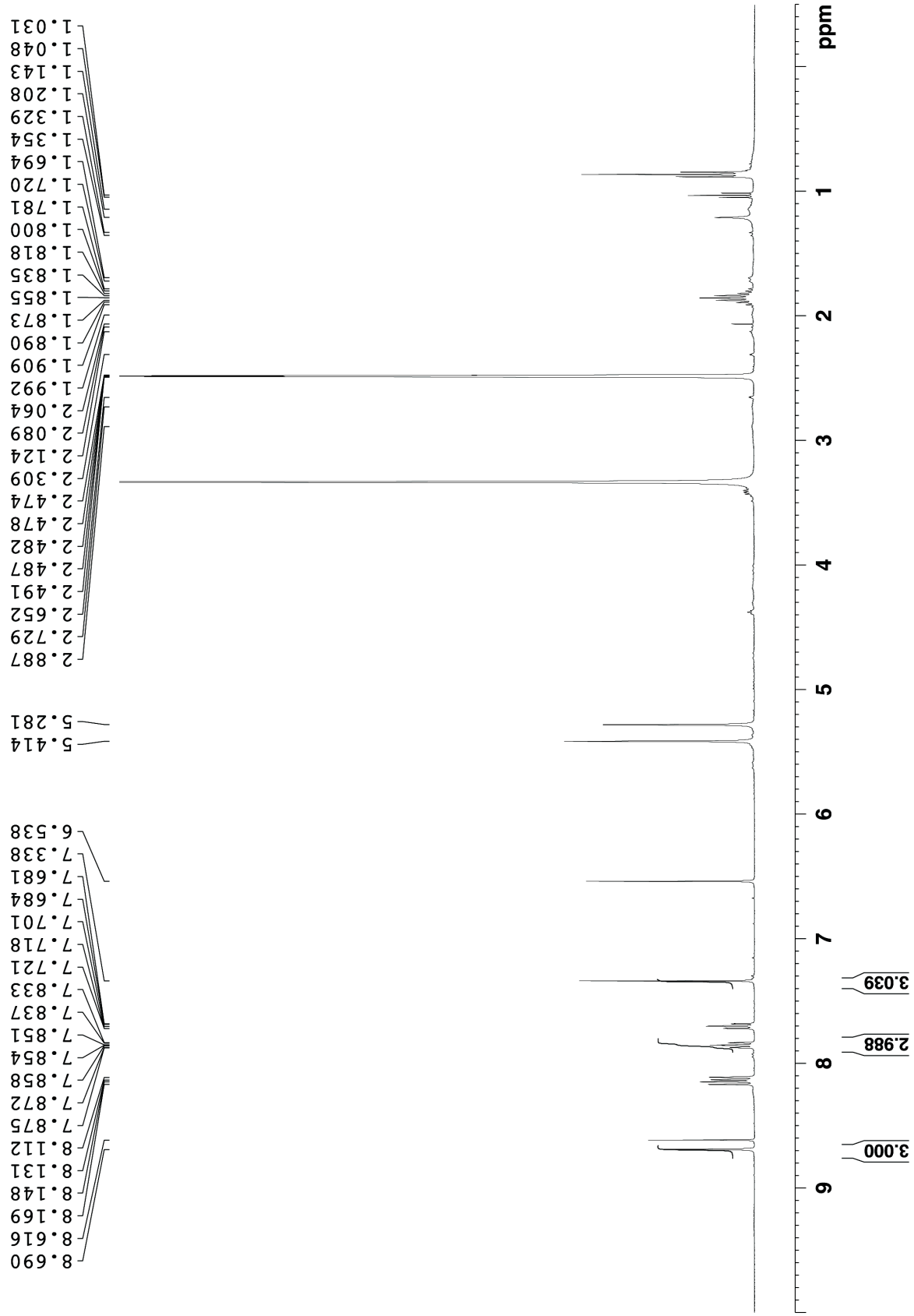

Figure S III-55. [1]H NMR recorded for pharmaceutical agent Camptothecin with **III-1c** (10 mM) (400 MHz, DMSO, RT, 1,3,5-benzenetricarboxylic acid as reference).

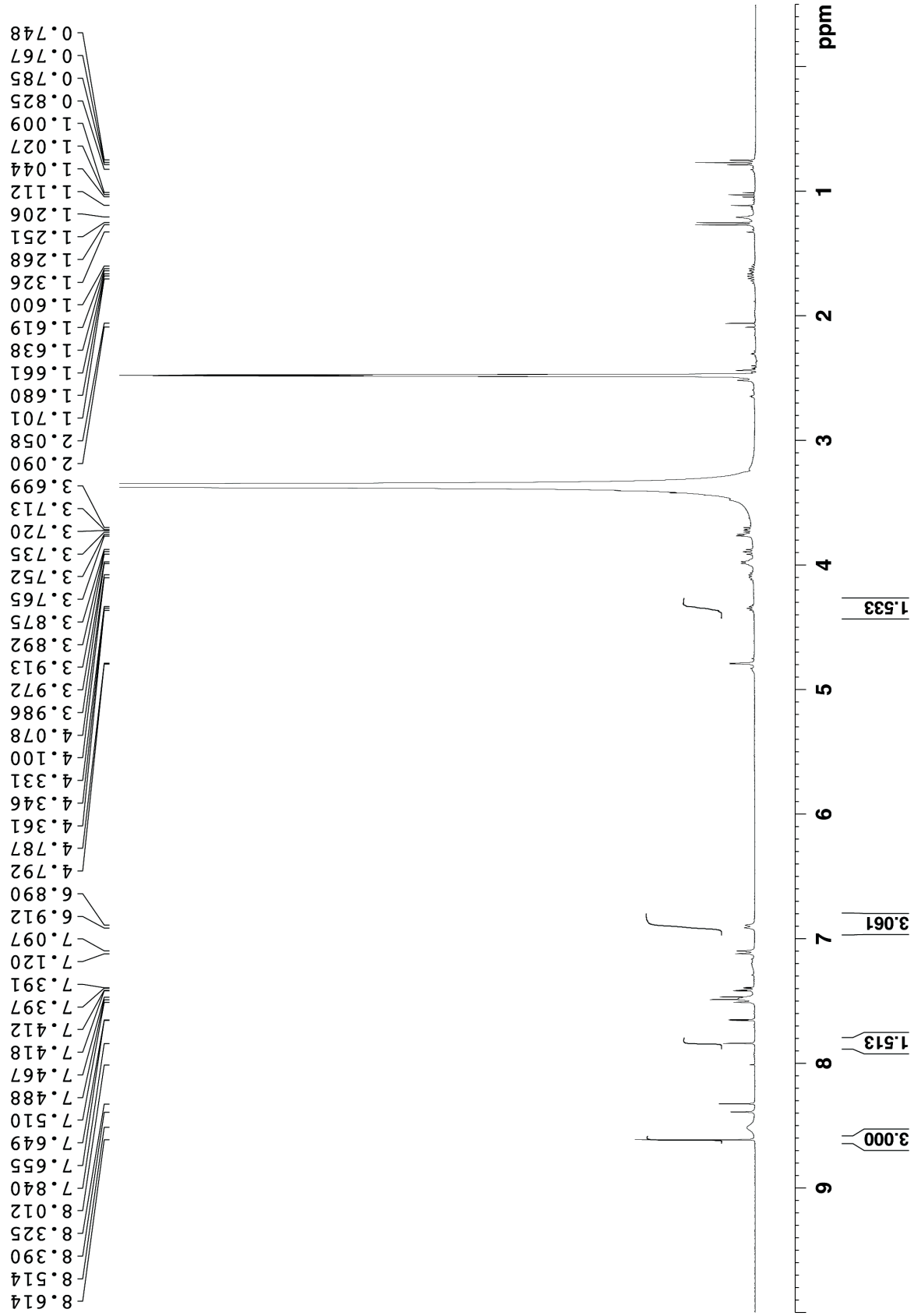

Figure S III-56. ^{1}H NMR recorded for pharmaceutical agent Itraconazole with **III-1c** (10 mM) (400 MHz, DMSO, RT, 1,3,5-benzenetricarboxylic acid as reference).

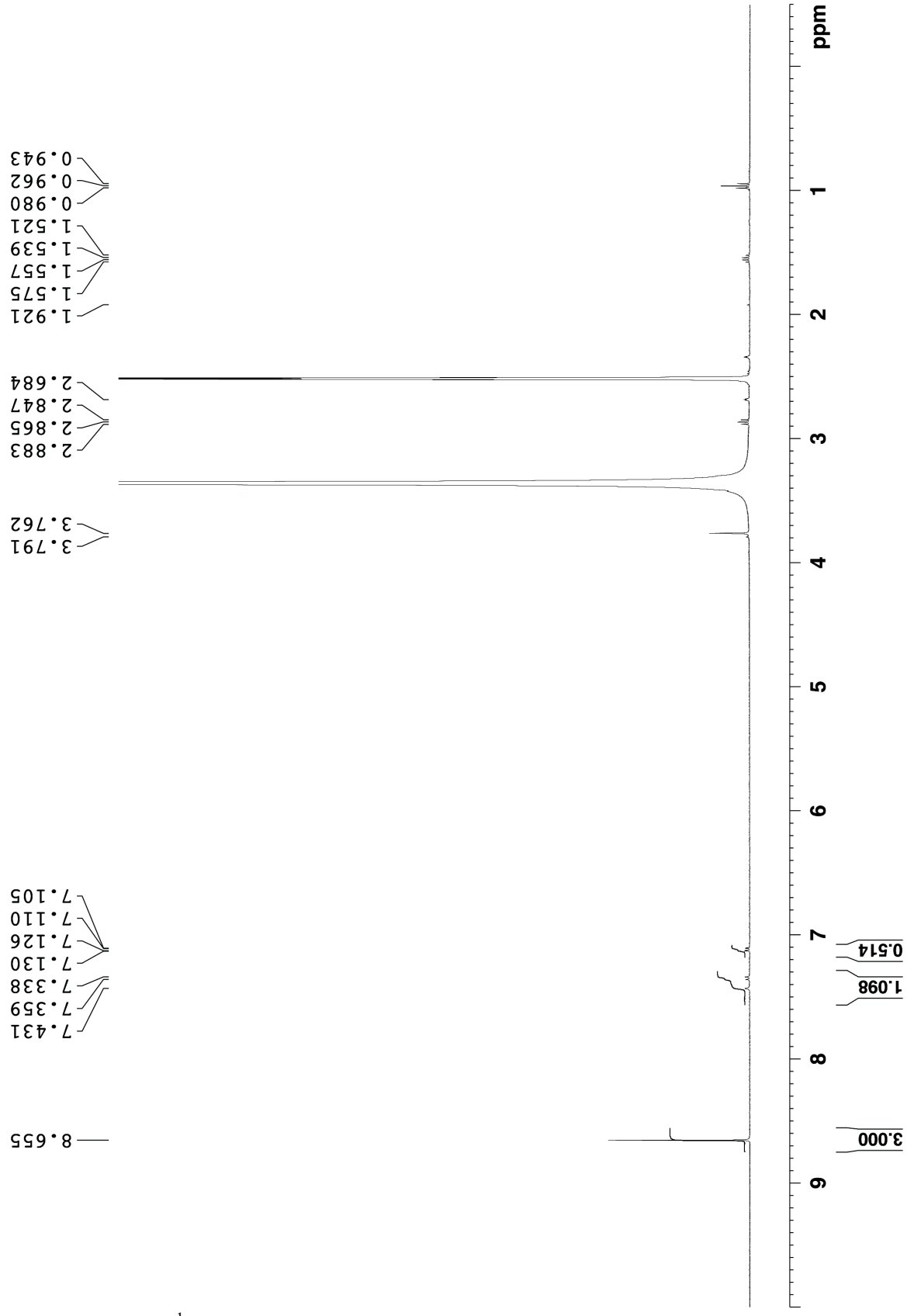

Figure S III-57. ^{1}H NMR recorded for pharmaceutical agent albendazole with **III-1c** (10 mM) (400 MHz, DMSO, RT, 1,3,5-benzenetricarboxylic acid as reference).

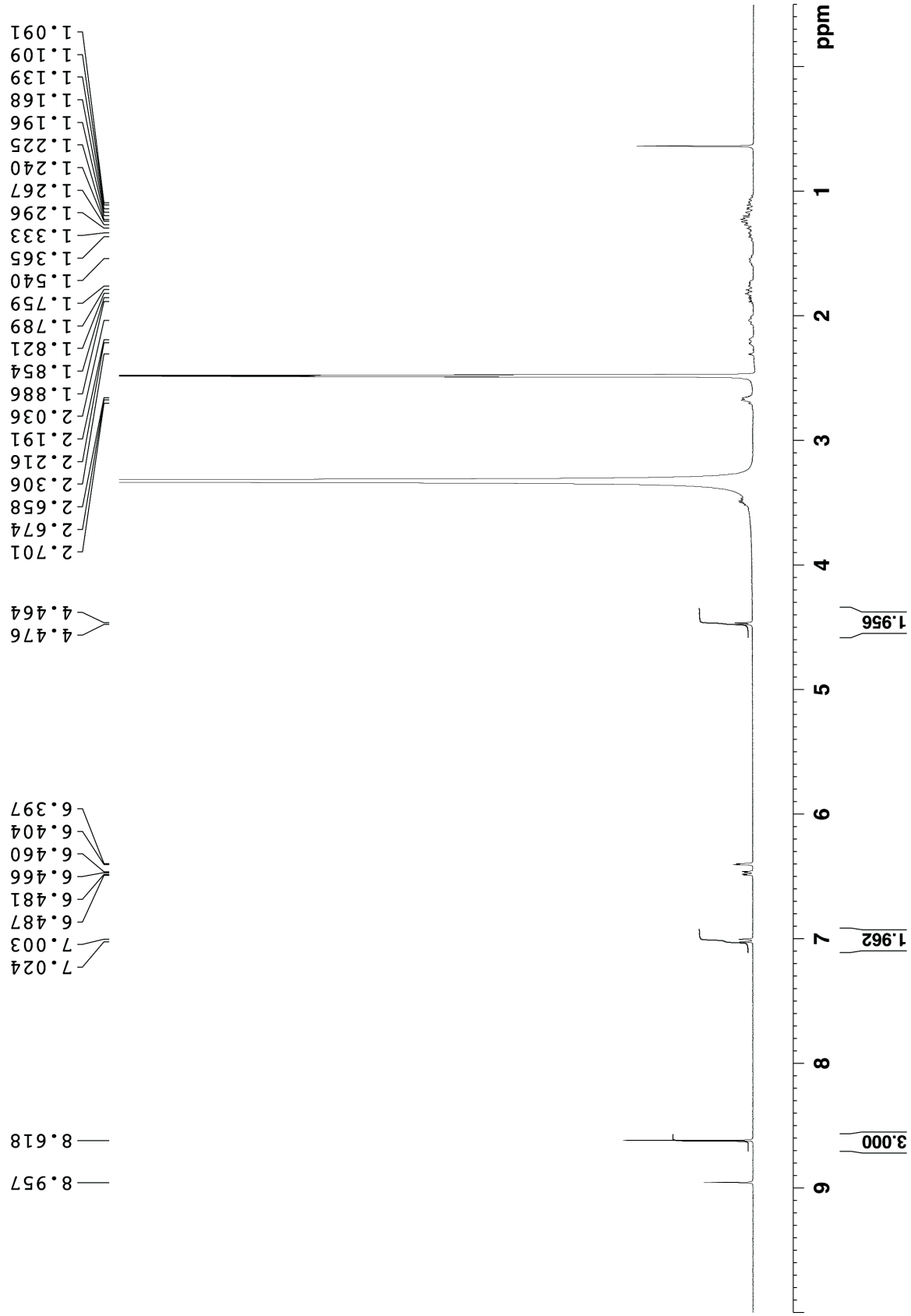

Figure S III-58. ^{1}H NMR recorded for pharmaceutical agent β-estradiol with **III-1c** (10 mM) (400 MHz, DMSO, RT, 1,3,5-benzenetricarboxylic acid as reference).

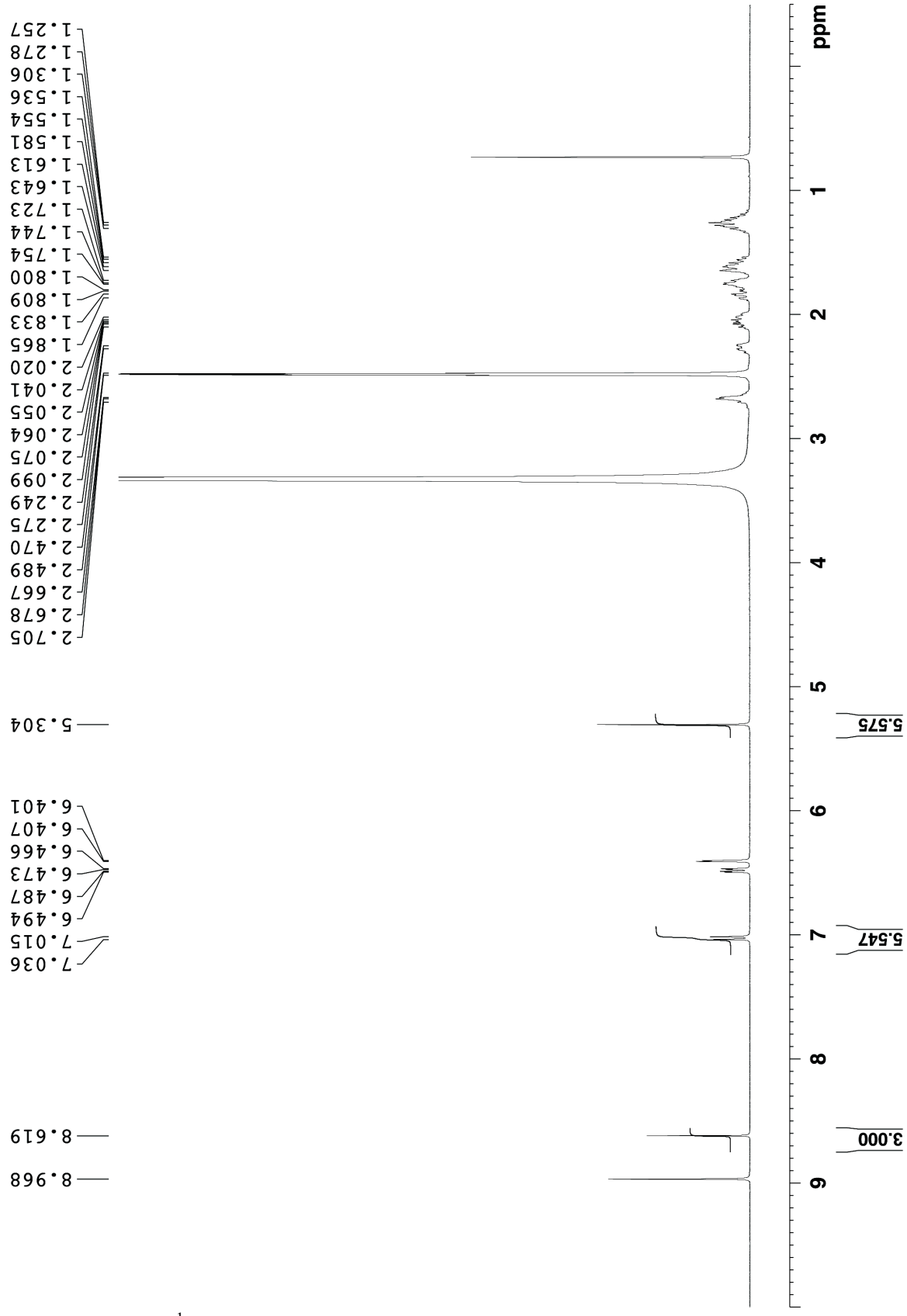

Figure S III-59. ^{1}H NMR recorded for pharmaceutical agent 17α-ethynylestradiol with **III-1c** (10 mM) (400 MHz, DMSO, RT, 1,3,5-benzenetricarboxylic acid as reference).

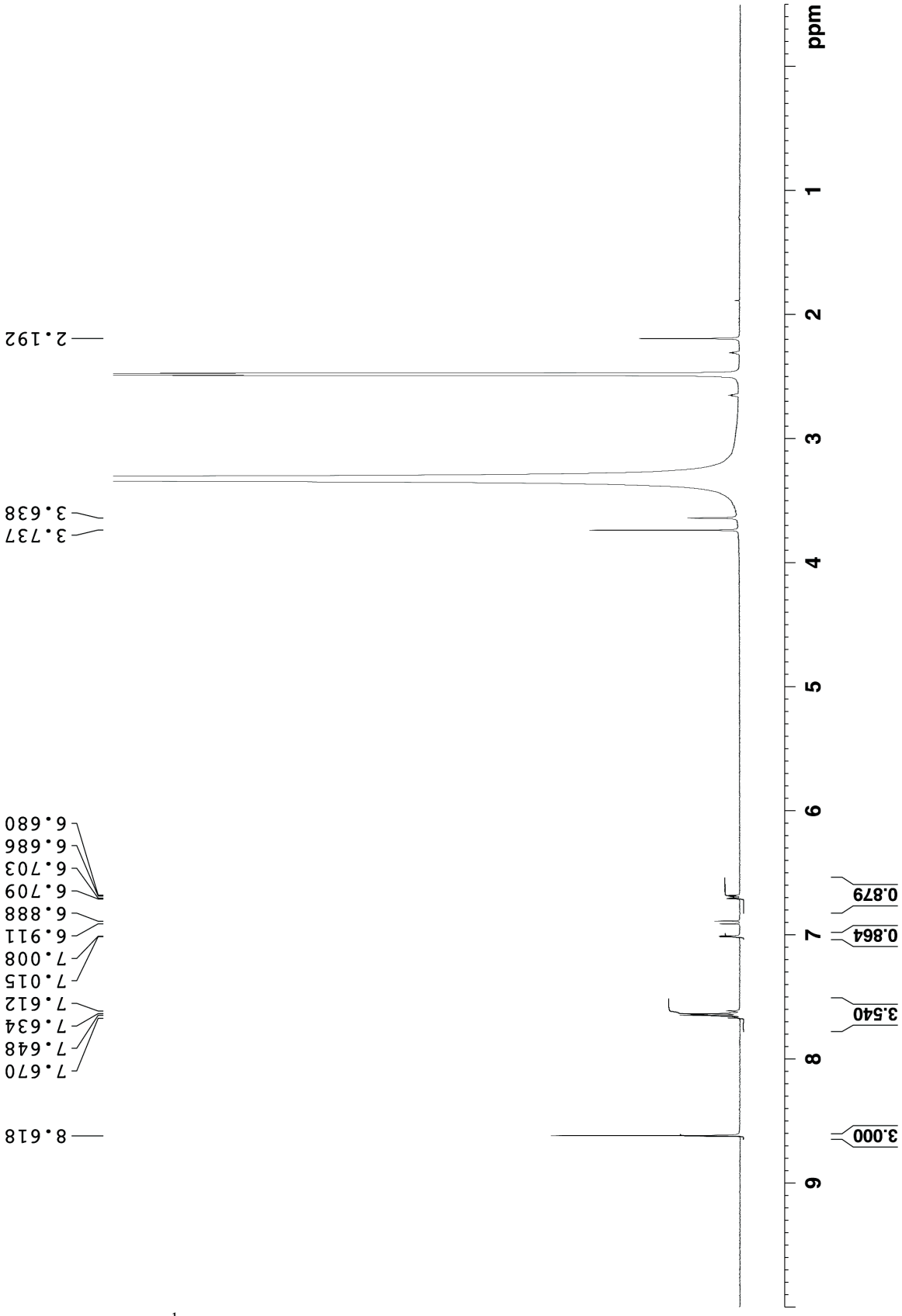

Figure S III-60. ^{1}H NMR recorded for pharmaceutical agent indomethacin with **III-1c** (35 mM) (400 MHz, DMSO, RT, 1,3,5-benzenetricarboxylic acid as reference).

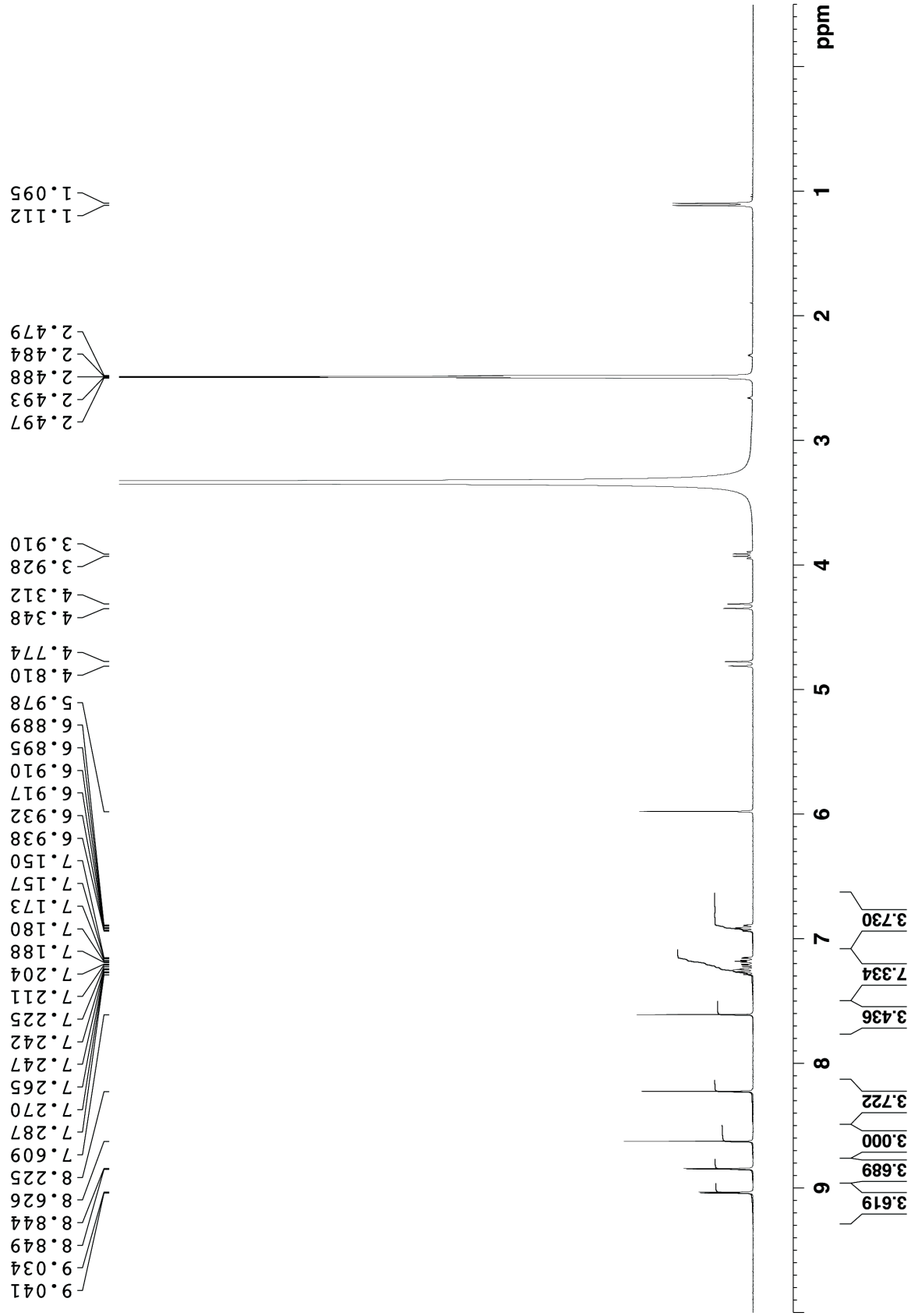

Figure S III-61. [1]H NMR recorded for pharmaceutical agent Voriconazole with **III-1c** (10 mM) (400 MHz, DMSO, RT, 1,3,5-benzenetricarboxylic acid as reference).

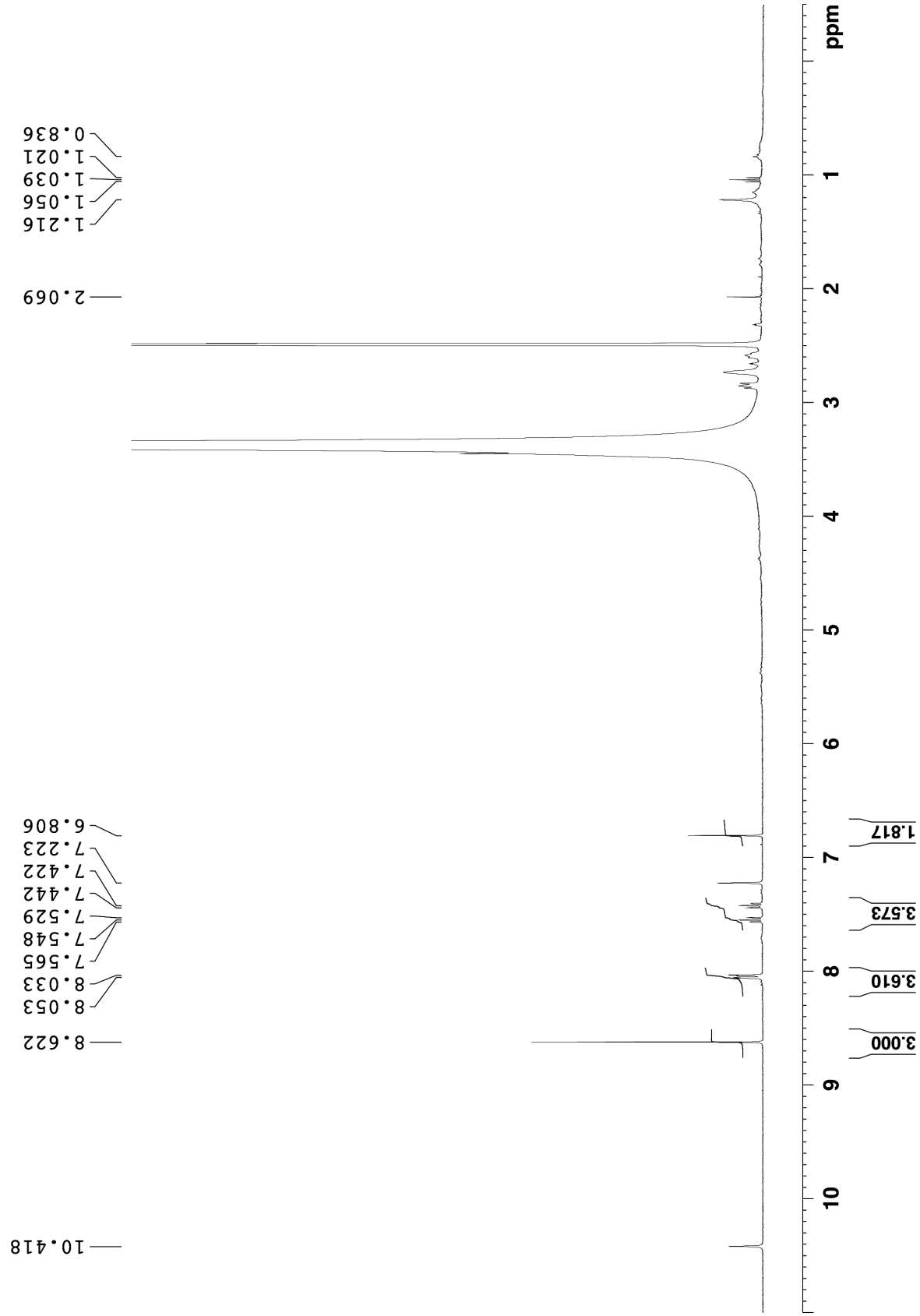

Figure S III-62. [1]H NMR recorded for pharmaceutical agent Ziprasidone with **III-1c** (10 mM) (400 MHz, DMSO, RT, 1,3,5-benzenetricarboxylic acid as reference).

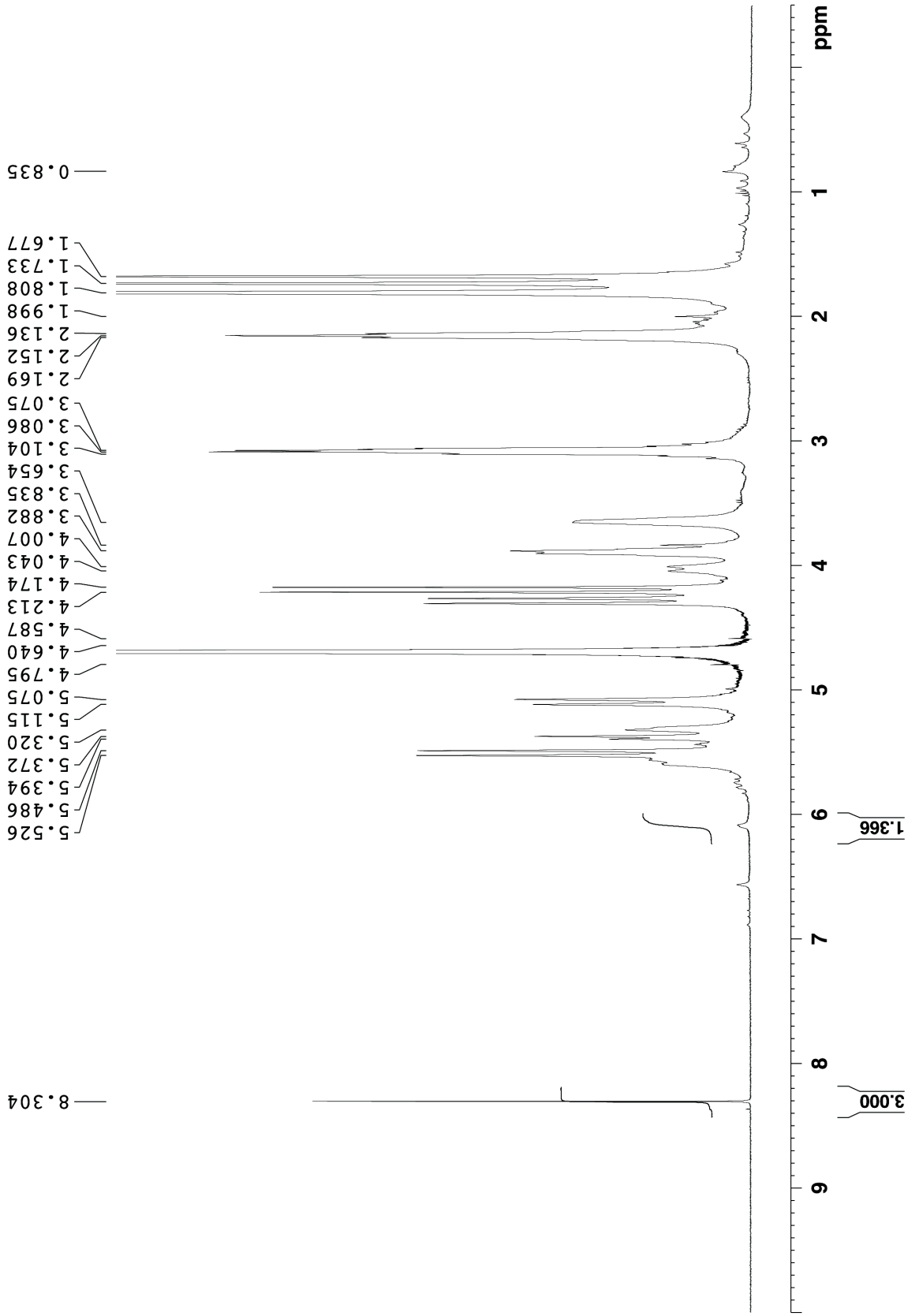

Figure S III-63. ^{1}H NMR recorded for pharmaceutical agent Albendazole with **III-1d** (10 mM) (400 MHz, 20 mM NaD_2PO_4, pD = 7.4, RT, 1,3,5-benzenetricarboxylic acid as reference).

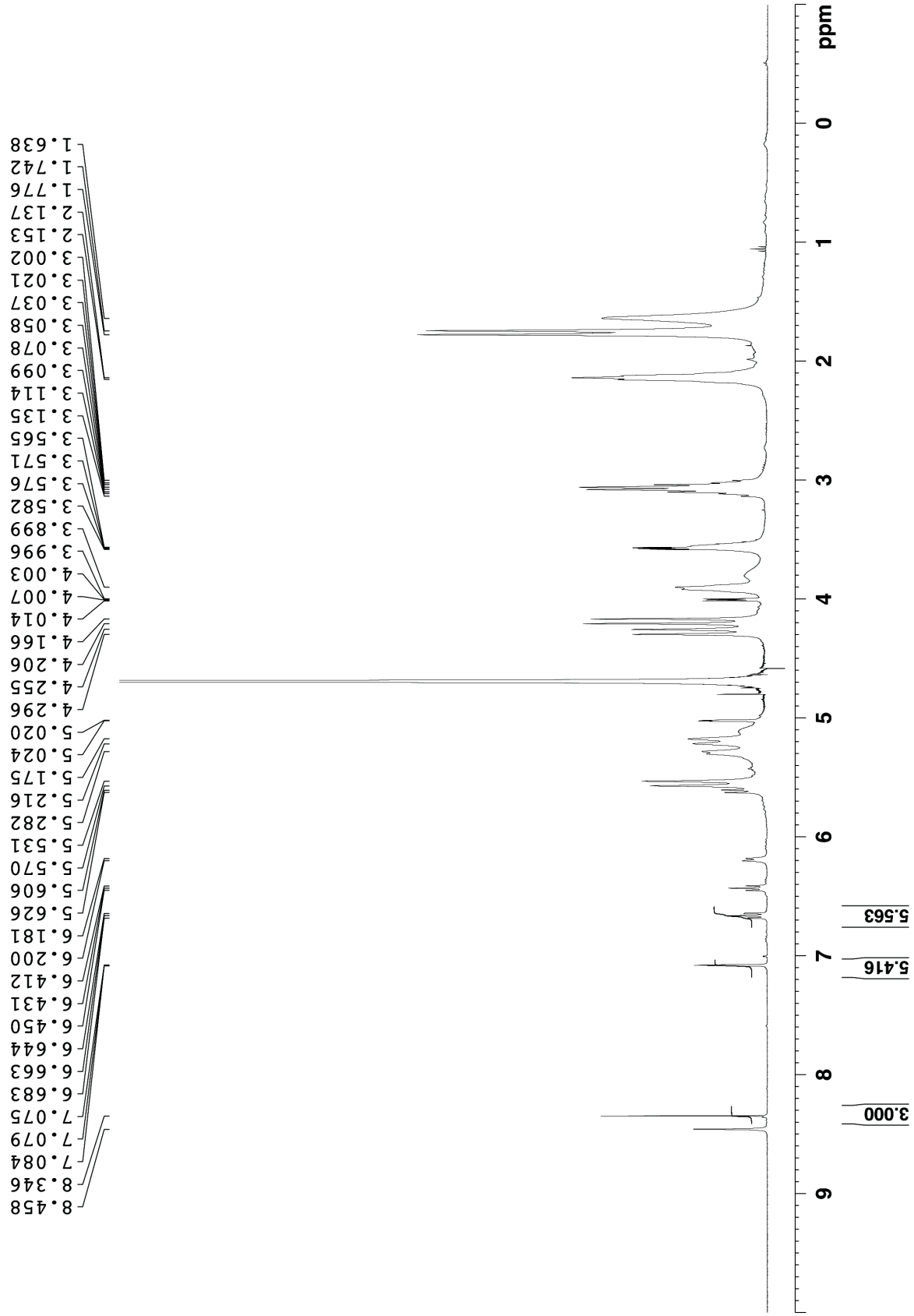

Figure S III-64. ^{1}H NMR recorded for pharmaceutical agent PBS-1086 with **III-1d** (10 mM) (400 MHz, 20 mM NaD_2PO_4, pD = 7.4, RT, 1,3,5-benzenetricarboxylic acid as reference).

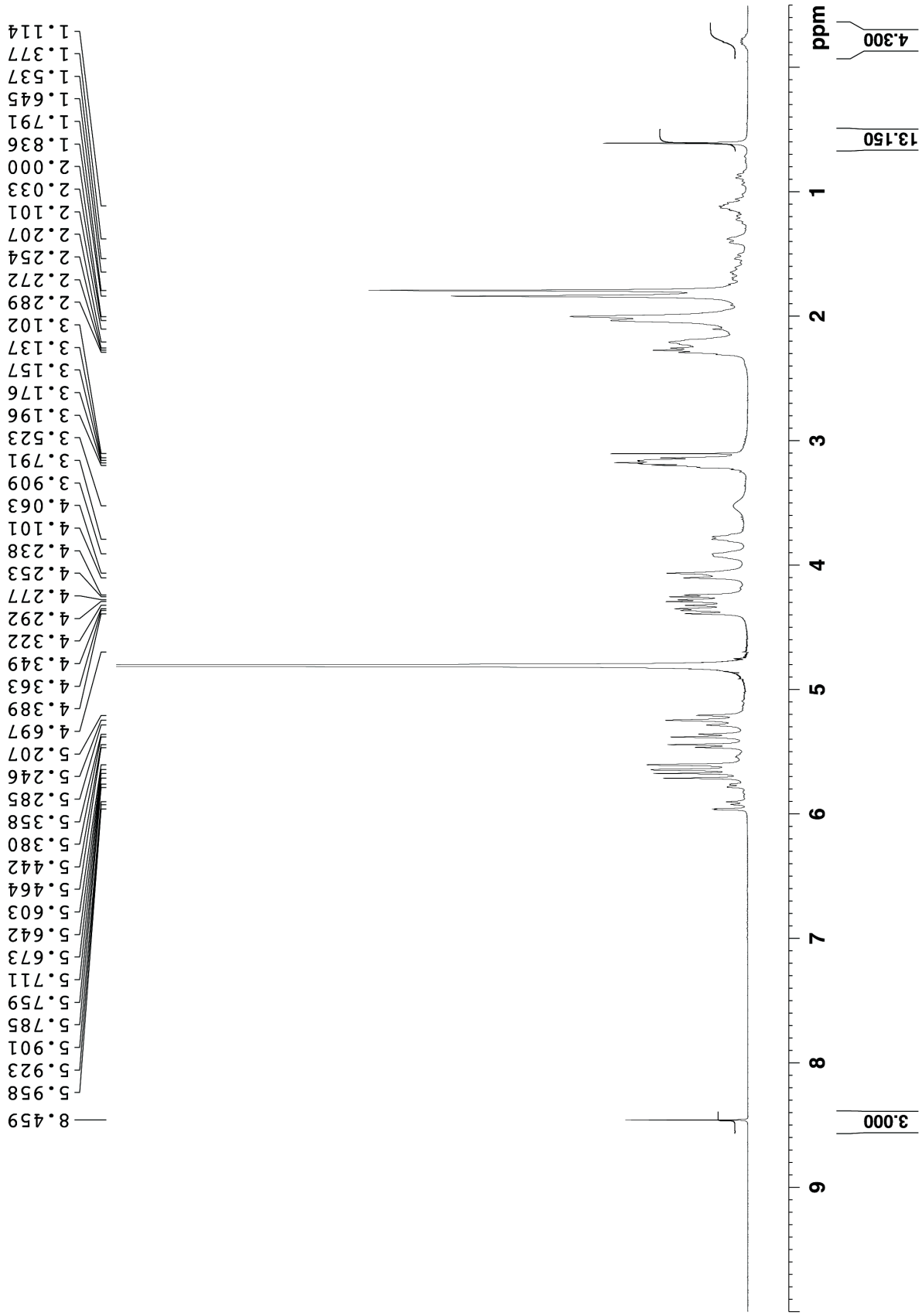

Figure S III-65. ^{1}H NMR recorded for pharmaceutical agent 17α-ethynylestradiol with **III-1d** (10 mM) (400 MHz, 20 mM NaD_2PO_4, pD = 7.4, RT, 1,3,5-benzenetricarboxylic acid as reference).

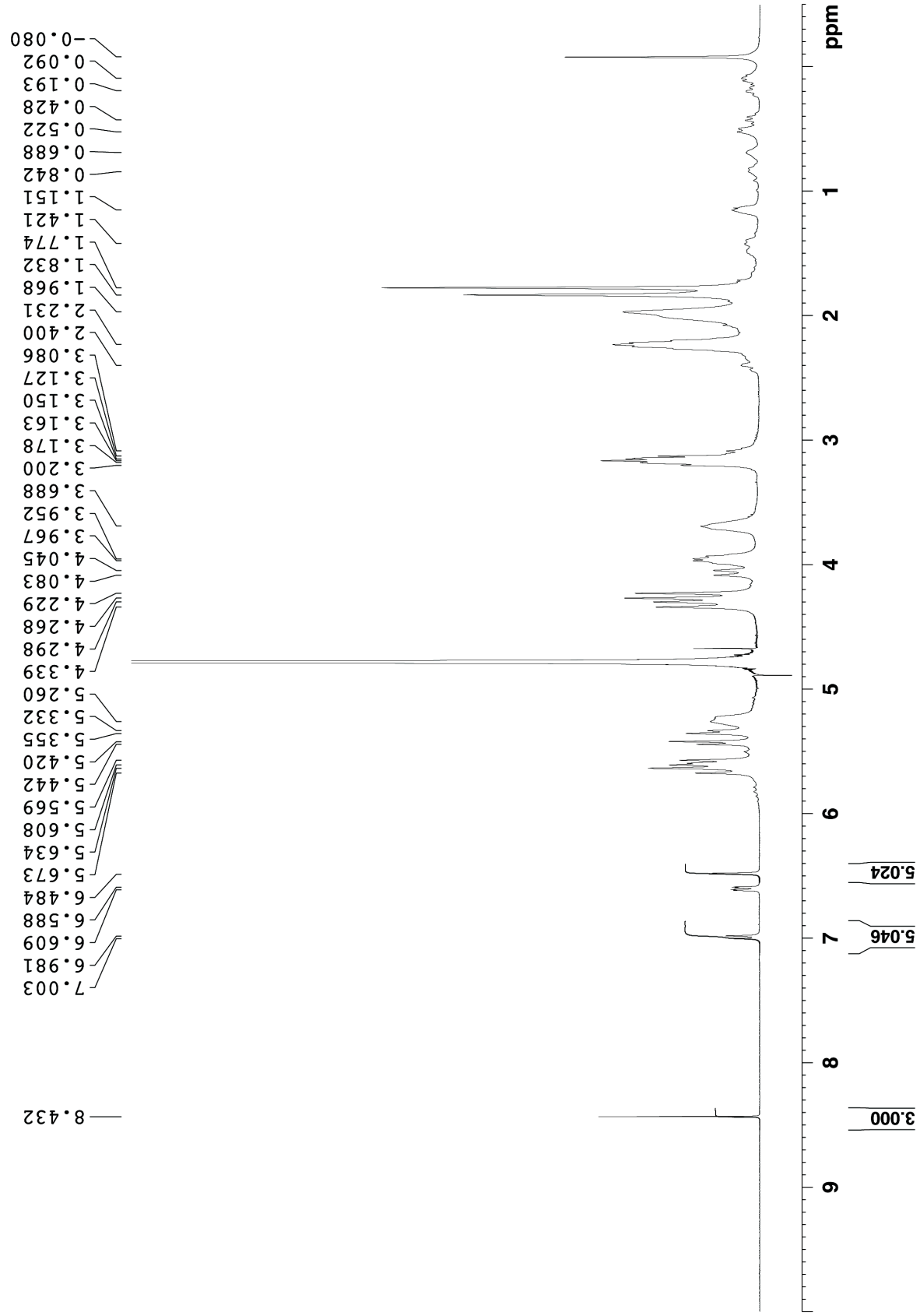

Figure S III-66. ^{1}H NMR recorded for pharmaceutical agent β-estradiol with **III-1d** (10 mM) (400 MHz, 20 mM NaD_2PO_4, pD = 7.4, RT, 1,3,5-benzenetricarboxylic acid as reference).

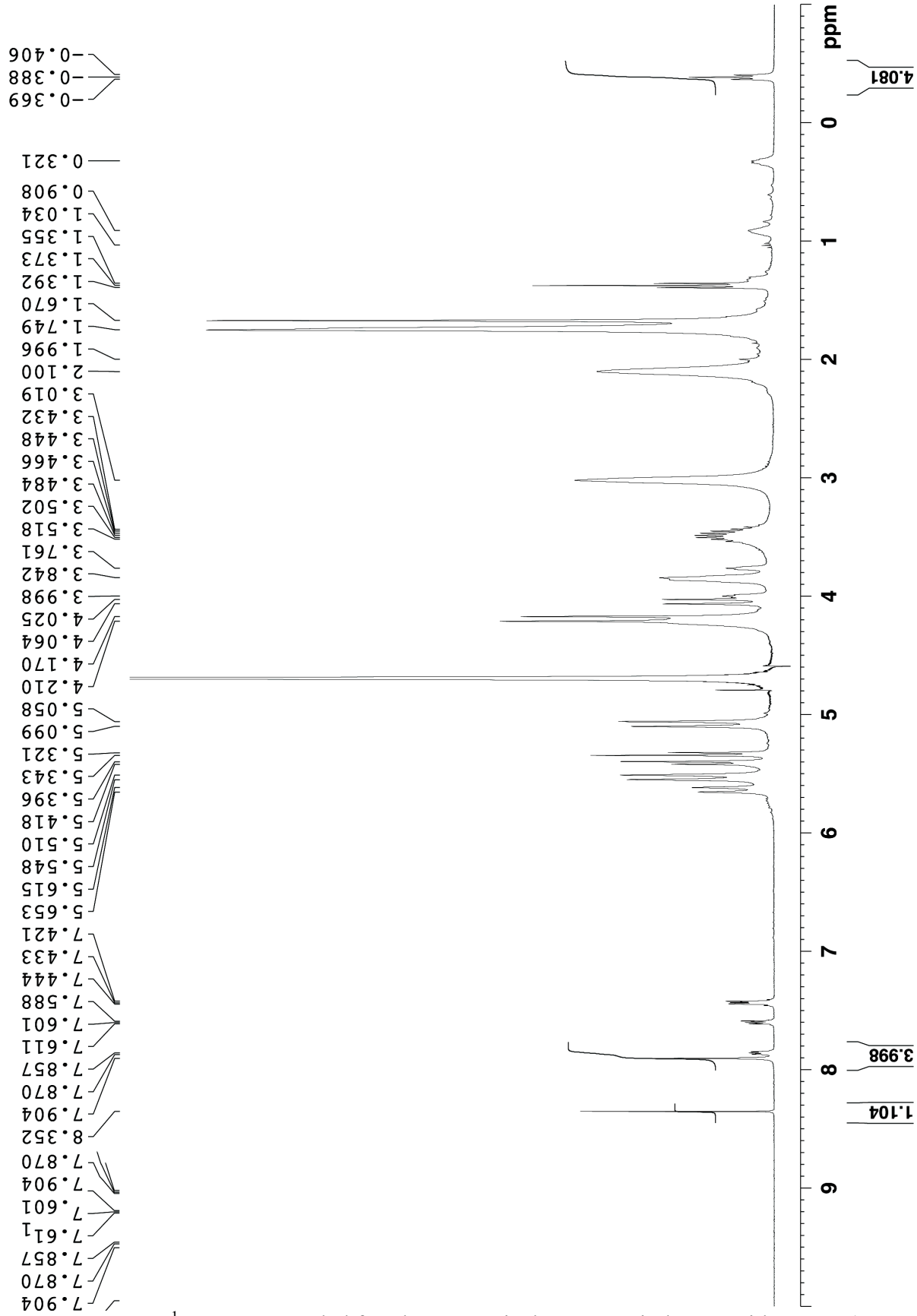

Figure S III-67. ^{1}H NMR recorded for pharmaceutical agent Amiodarone with **III-1d** (10 mM) (400 MHz, 20 mM NaD_2PO_4, pD = 7.4, RT, 1,3,5-benzenetricarboxylic acid as

reference).

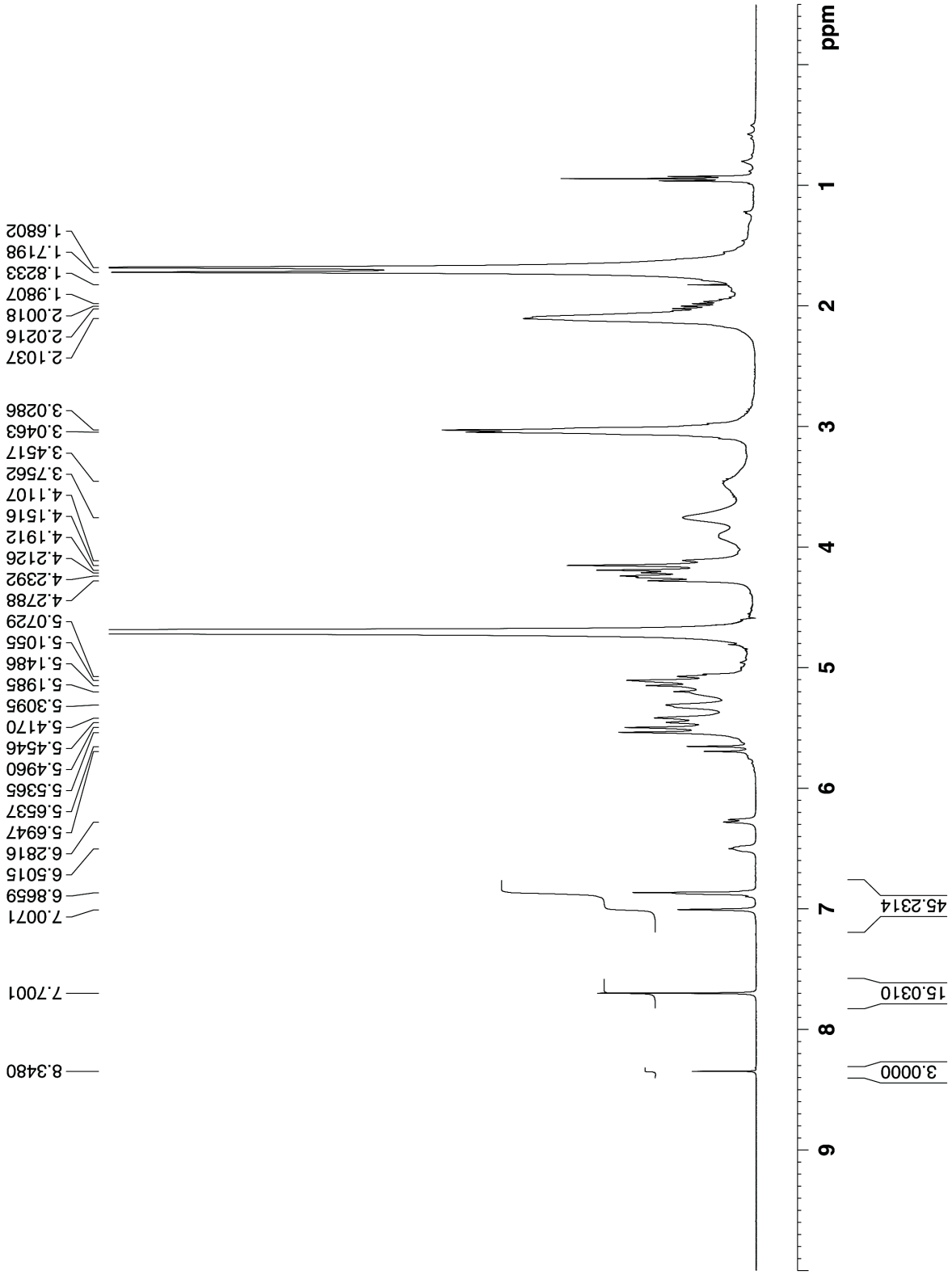

Figure S III-68. ^{1}H NMR recorded for pharmaceutical agent Camptothecin with **III-1d** (30 mM) (400 MHz, 20 mM NaD_2PO_4, pD = 7.4, RT, 1,3,5-benzenetricarboxylic acid as reference).

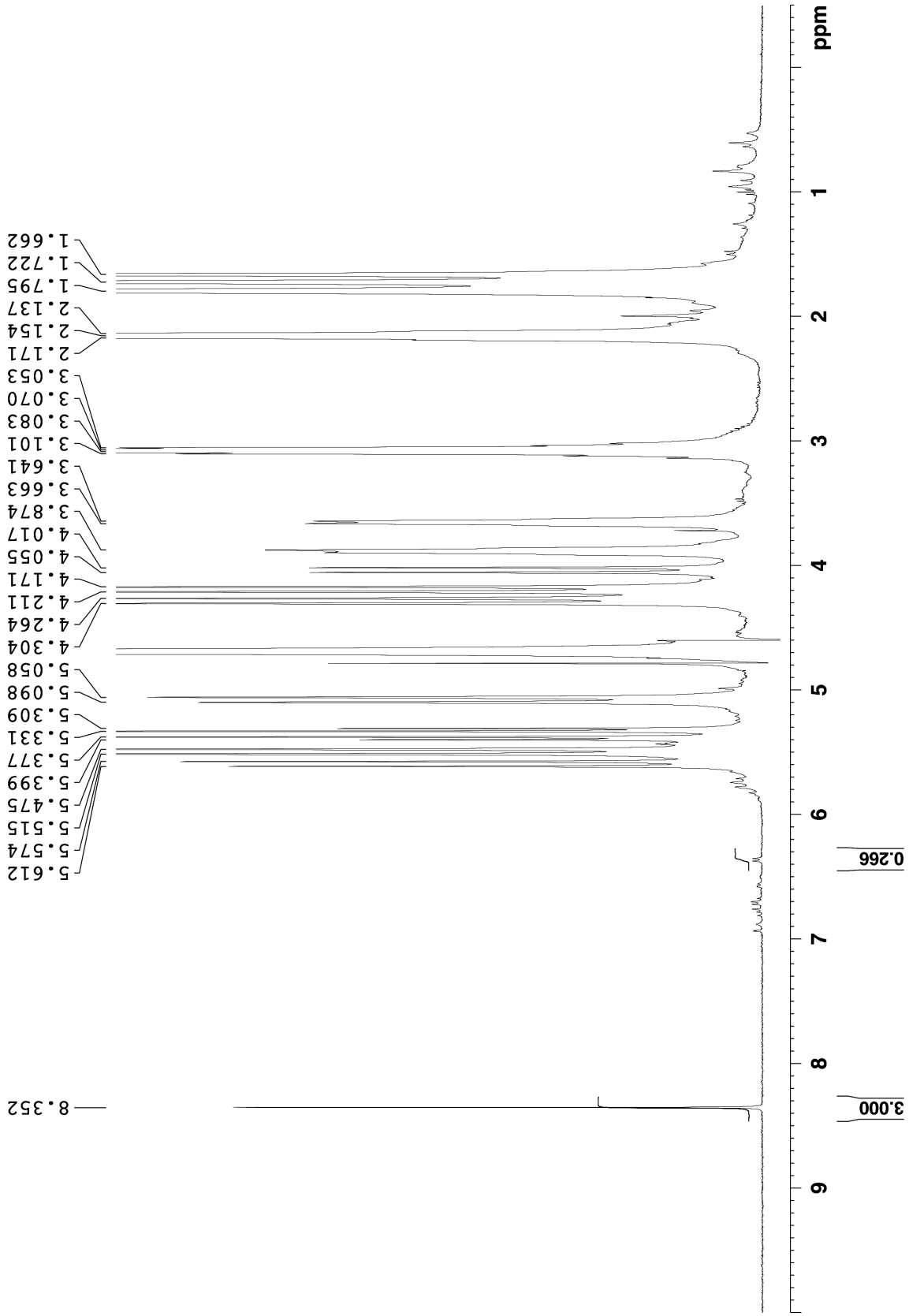

Figure S III-69. ^{1}H NMR recorded for pharmaceutical agent Indomethacin with **III-1d** (10 mM) (400 MHz, 20 mM NaD_2PO_4, pD = 7.4, RT, 1,3,5-benzenetricarboxylic acid as reference).

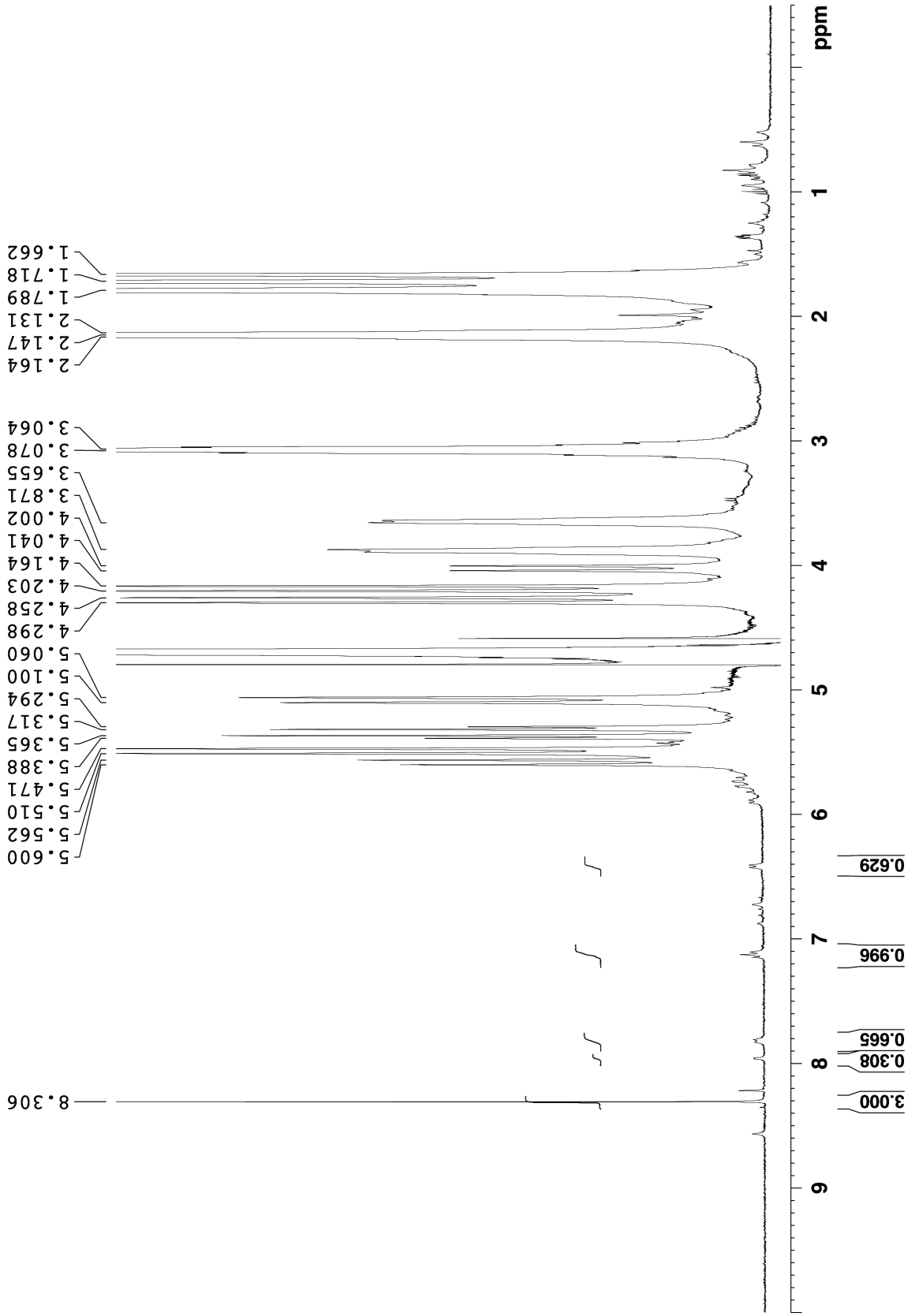

Figure S III-70. ^{1}H NMR recorded for pharmaceutical agent Itraconazole with **III-1d** (10 mM) (400 MHz, 20 mM NaD_2PO_4, pD = 7.4, RT, 1,3,5-benzenetricarboxylic acid as reference).

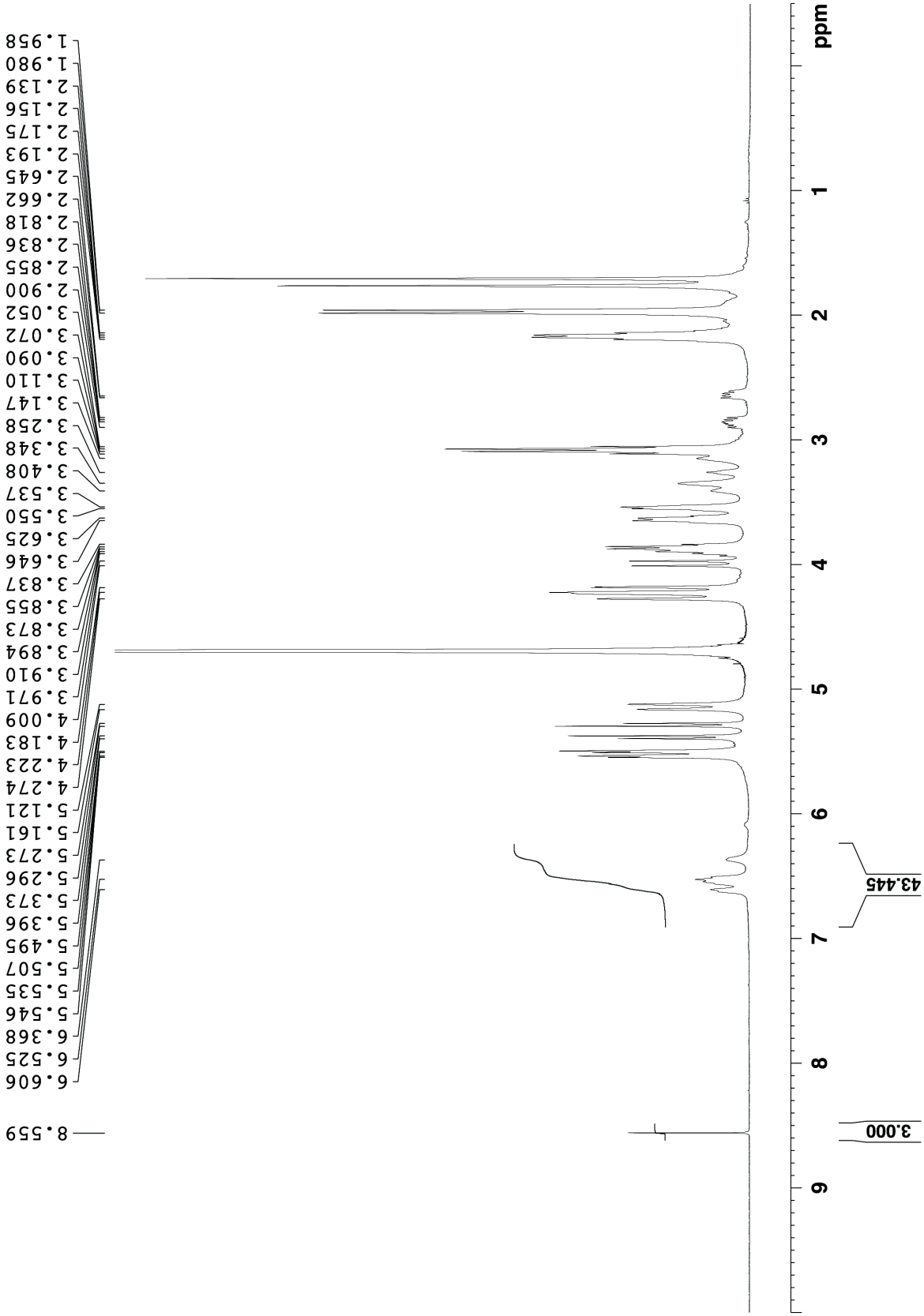

Figure S III-71. ^{1}H NMR recorded for pharmaceutical agent Melphalan with **III-1d** (10 mM) (400 MHz, 20 mM NaD_2PO_4, pD = 7.4, RT, 1,3,5-benzenetricarboxylic acid as reference).

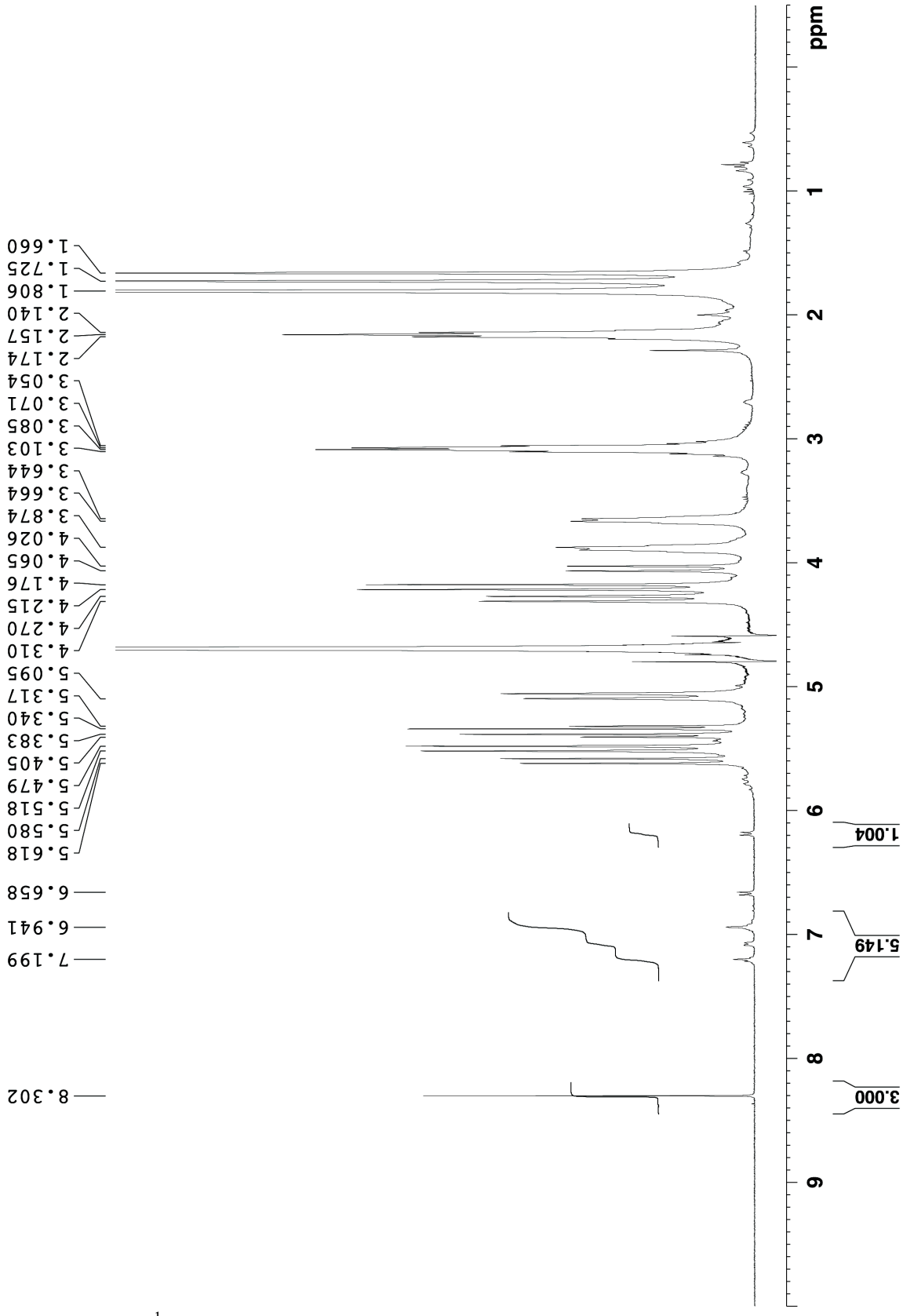

Figure S III-72. ^{1}H NMR recorded for pharmaceutical agent Tamoxifen with **III-1d** (10 mM) (400 MHz, 20 mM NaD_2PO_4, pD = 7.4, RT, 1,3,5-benzenetricarboxylic acid as reference).

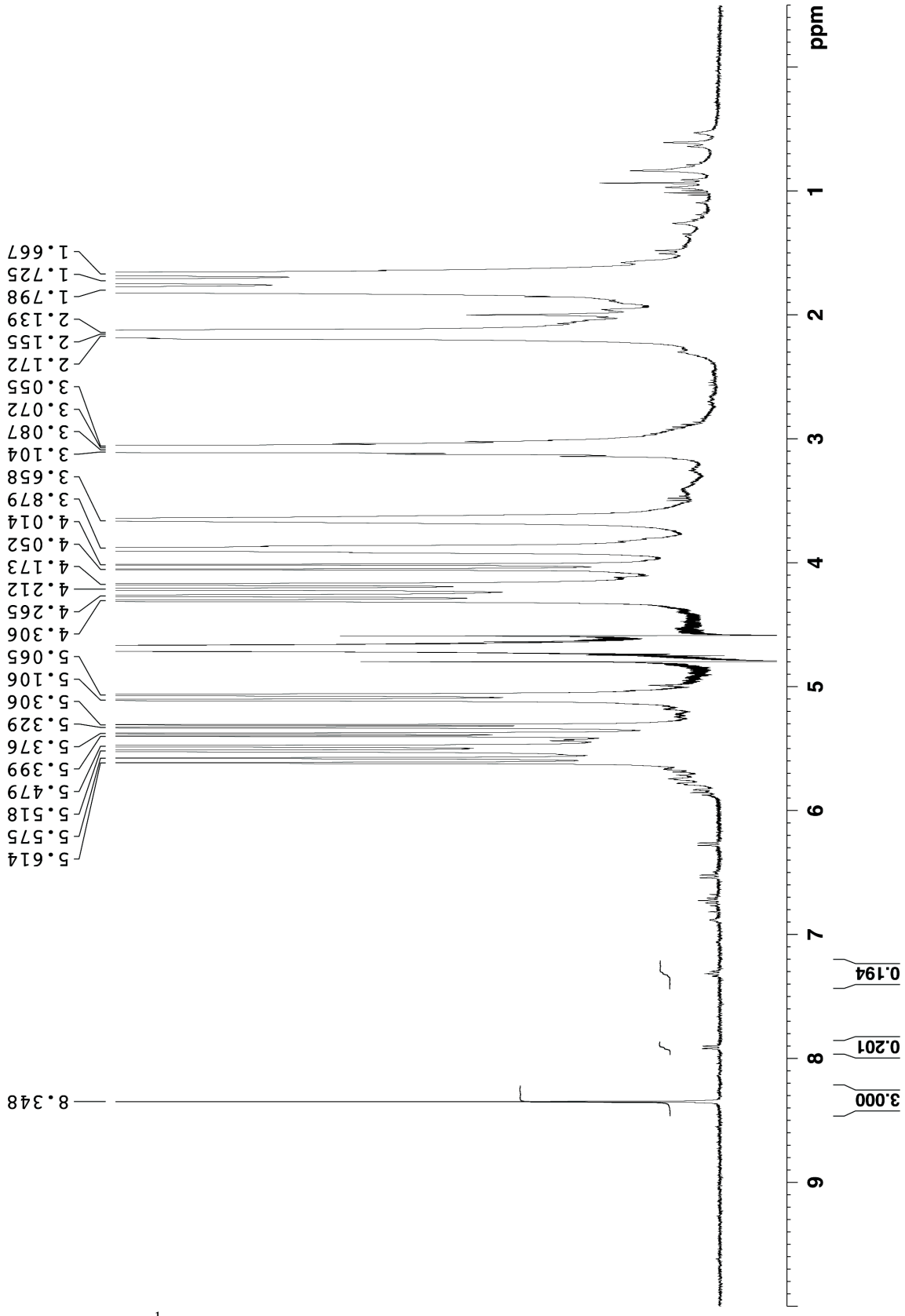

Figure S III-73. ^{1}H NMR recorded for pharmaceutical agent tolfenamic acid with **III-1d** (10 mM) (400 MHz, 20 mM NaD_2PO_4, pD = 7.4, RT, 1,3,5-benzenetricarboxylic acid as reference).

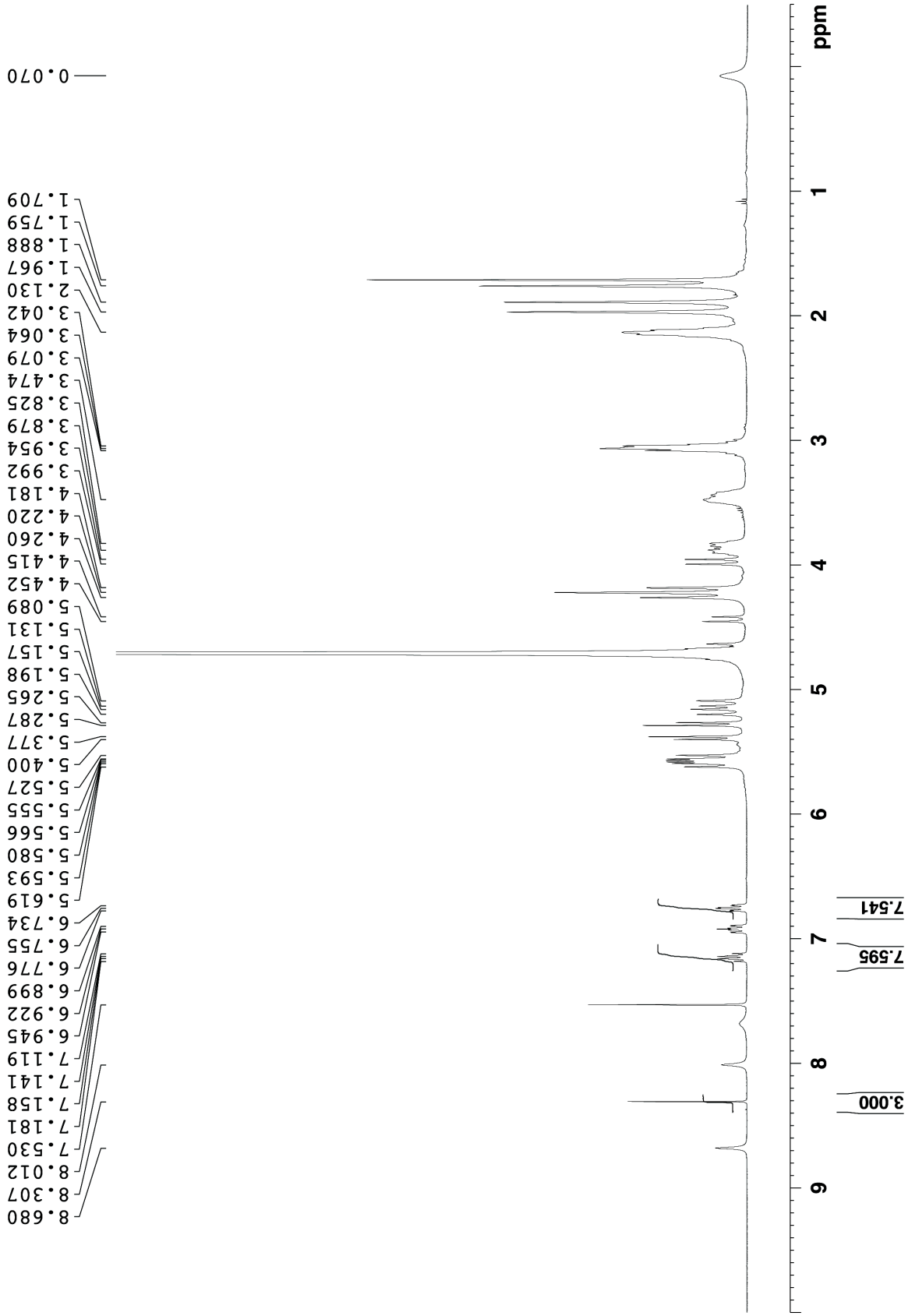

Figure S III-74. ^{1}H NMR recorded for pharmaceutical agent Voriconazole with **III-1d** (10 mM) (400 MHz, 20 mM NaD_2PO_4, pD = 7.4, RT, 1,3,5-benzenetricarboxylic acid as reference).

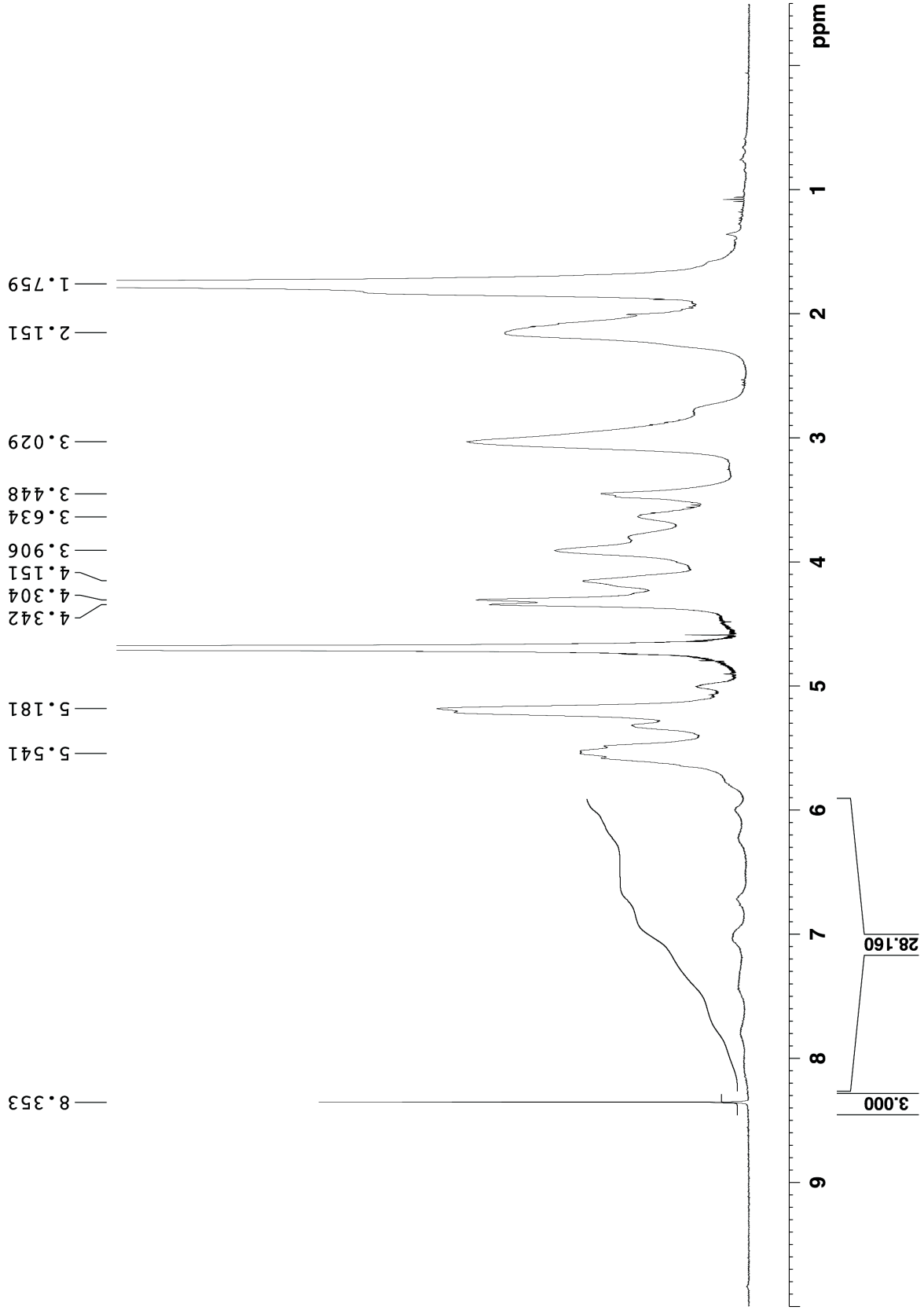

Figure S III-75. ^{1}H NMR recorded for pharmaceutical agent ziprasidone with **III-1d** (10 mM) (400 MHz, 20 mM NaD_2PO_4, pD = 7.4, RT, 1,3,5-benzenetricarboxylic acid as reference).

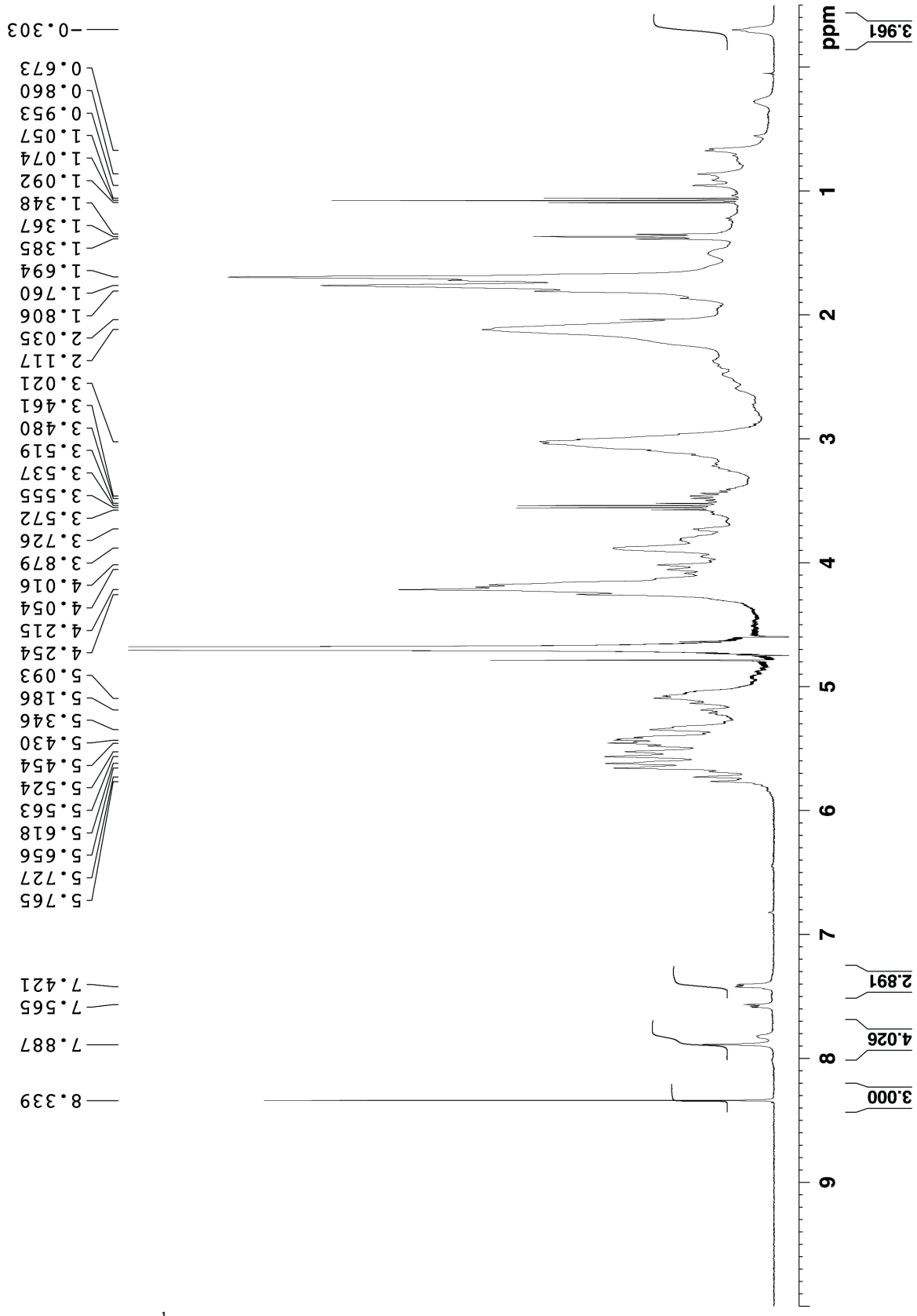

Figure S III-76. ^{1}H NMR recorded for pharmaceutical agent Amiodarone with **III-1e** (10 mM) (400 MHz, 20 mM NaD_2PO_4, pD = 7.4, RT, 1,3,5-benzenetricarboxylic acid as reference).

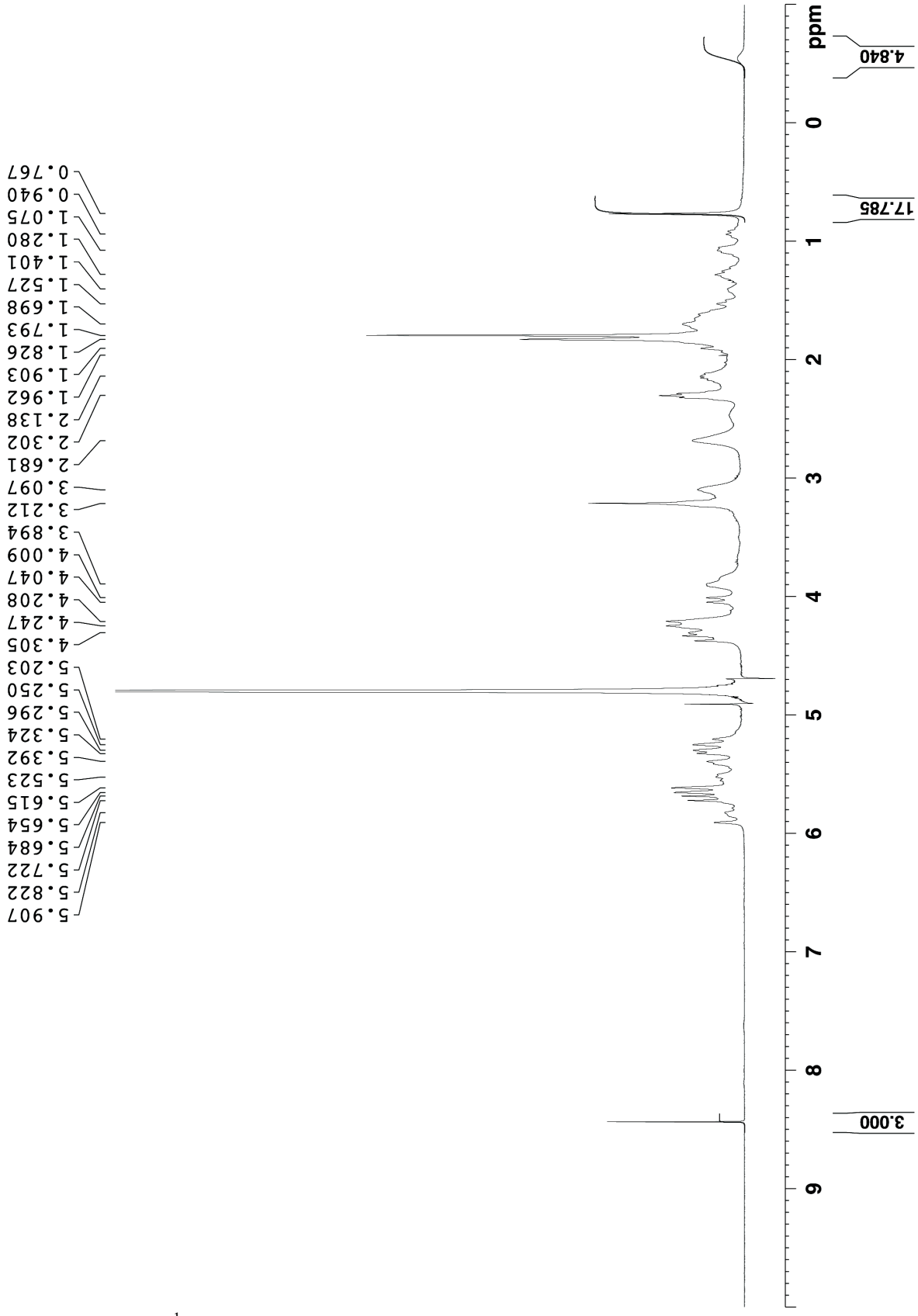

Figure S III-77. ^{1}H NMR recorded for pharmaceutical agent 17α-ethynylestradiol with **III-1e** (10 mM) (400 MHz, 20 mM NaD_2PO_4, pD = 7.4, RT, 1,3,5-benzenetricarboxylic acid as reference).

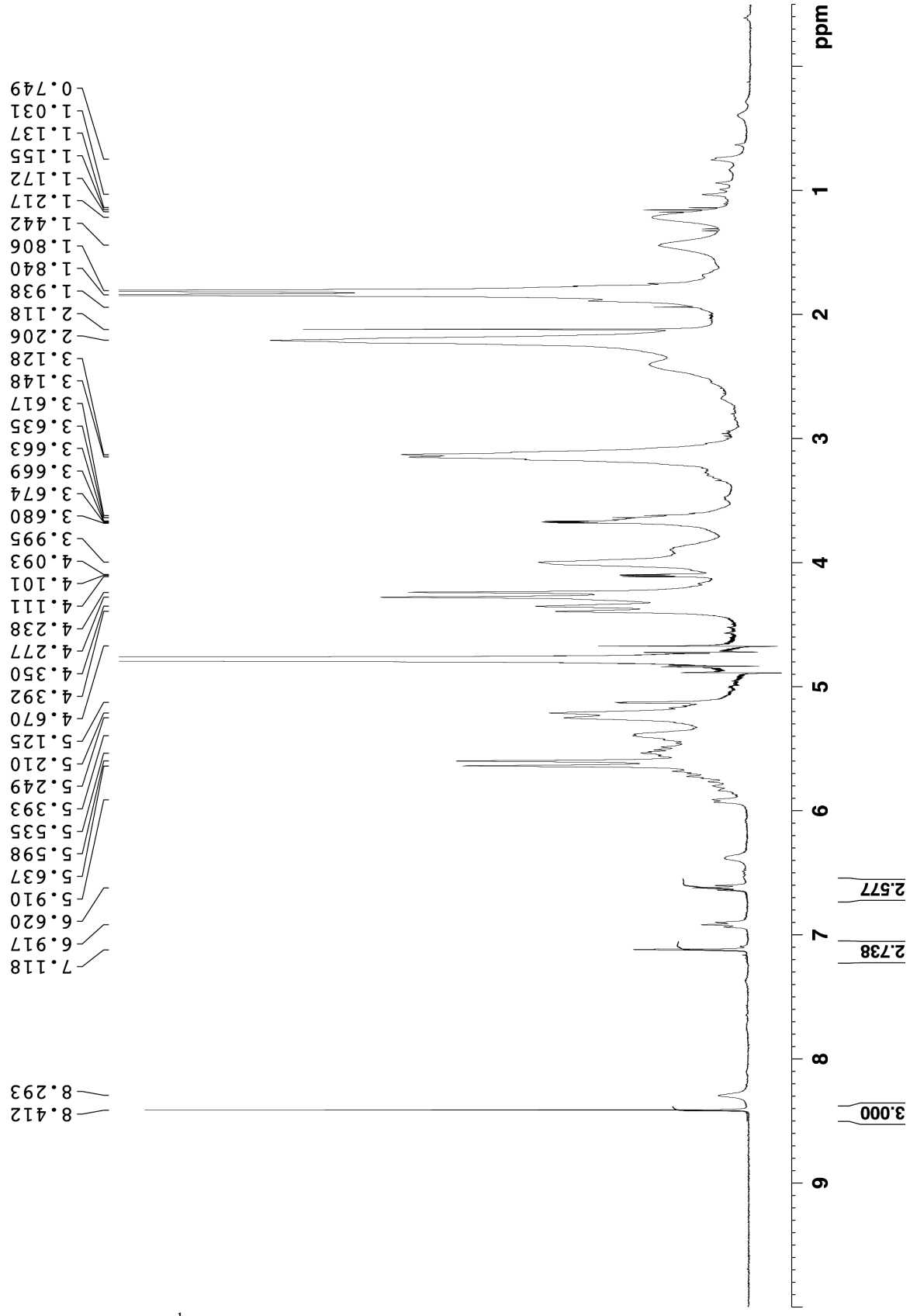

Figure S III-78. ^{1}H NMR recorded for pharmaceutical agent PBS-1086 with **III-1e** (10 mM) (400 MHz, 20 mM NaD_2PO_4, pD = 7.4, RT, 1,3,5-benzenetricarboxylic acid as reference).

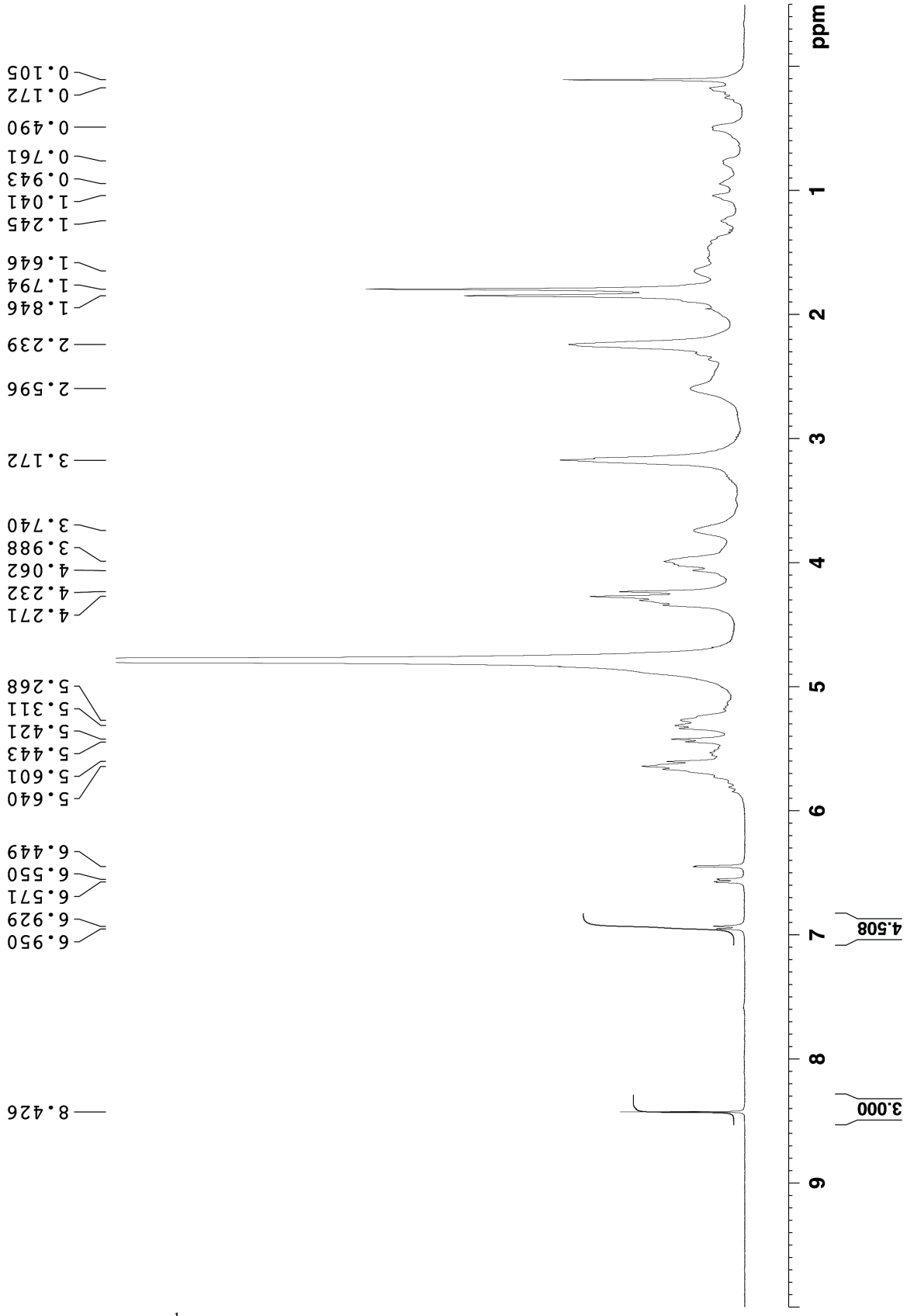

Figure S III-79. ^{1}H NMR recorded for pharmaceutical agent β-estradiol with **III-1e** (10 mM) (400 MHz, 20 mM NaD_2PO_4, pD = 7.4, RT, 1,3,5-benzenetricarboxylic acid as reference).

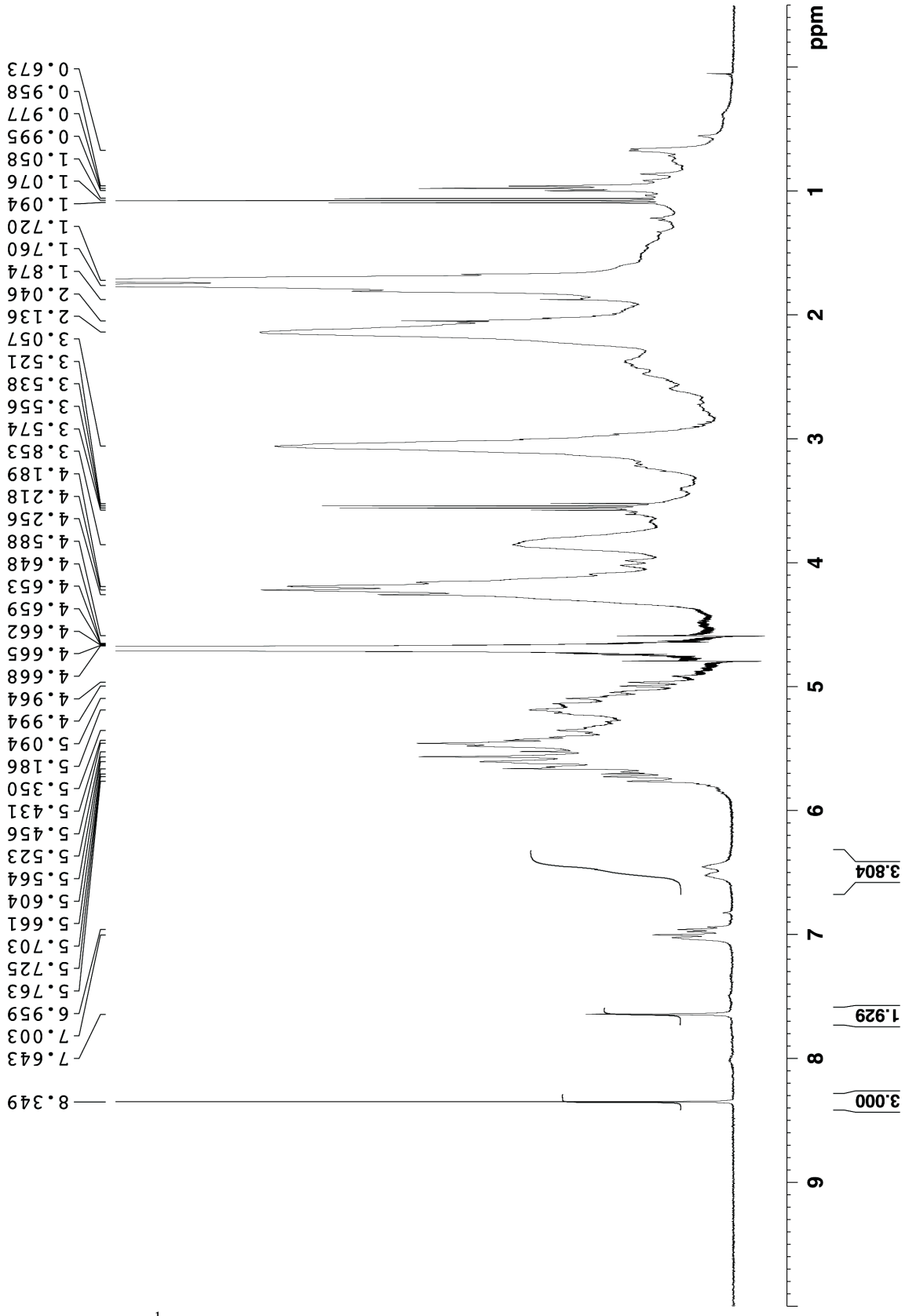

Figure S III-80. ^{1}H NMR recorded for pharmaceutical agent camptothecin with **III-1e** (10 mM) (400 MHz, 20 mM NaD_2PO_4, pD = 7.4, RT, 1,3,5-benzenetricarboxylic acid as reference).

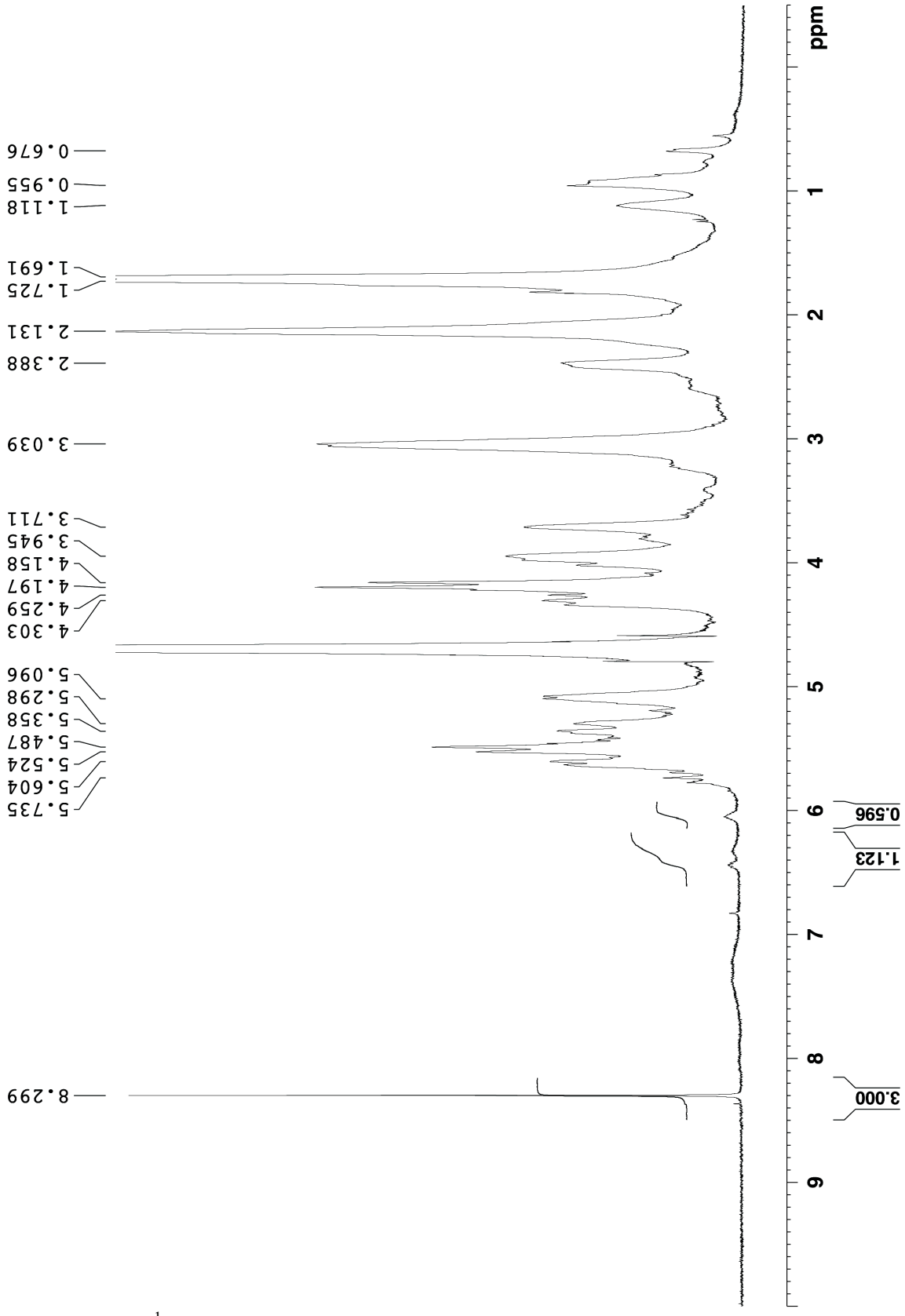

Figure S III-81. ^{1}H NMR recorded for pharmaceutical agent cinnarizine with **III-1e** (10 mM) (400 MHz, 20 mM NaD_2PO_4, pD = 7.4, RT, 1,3,5-benzenetricarboxylic acid as reference).

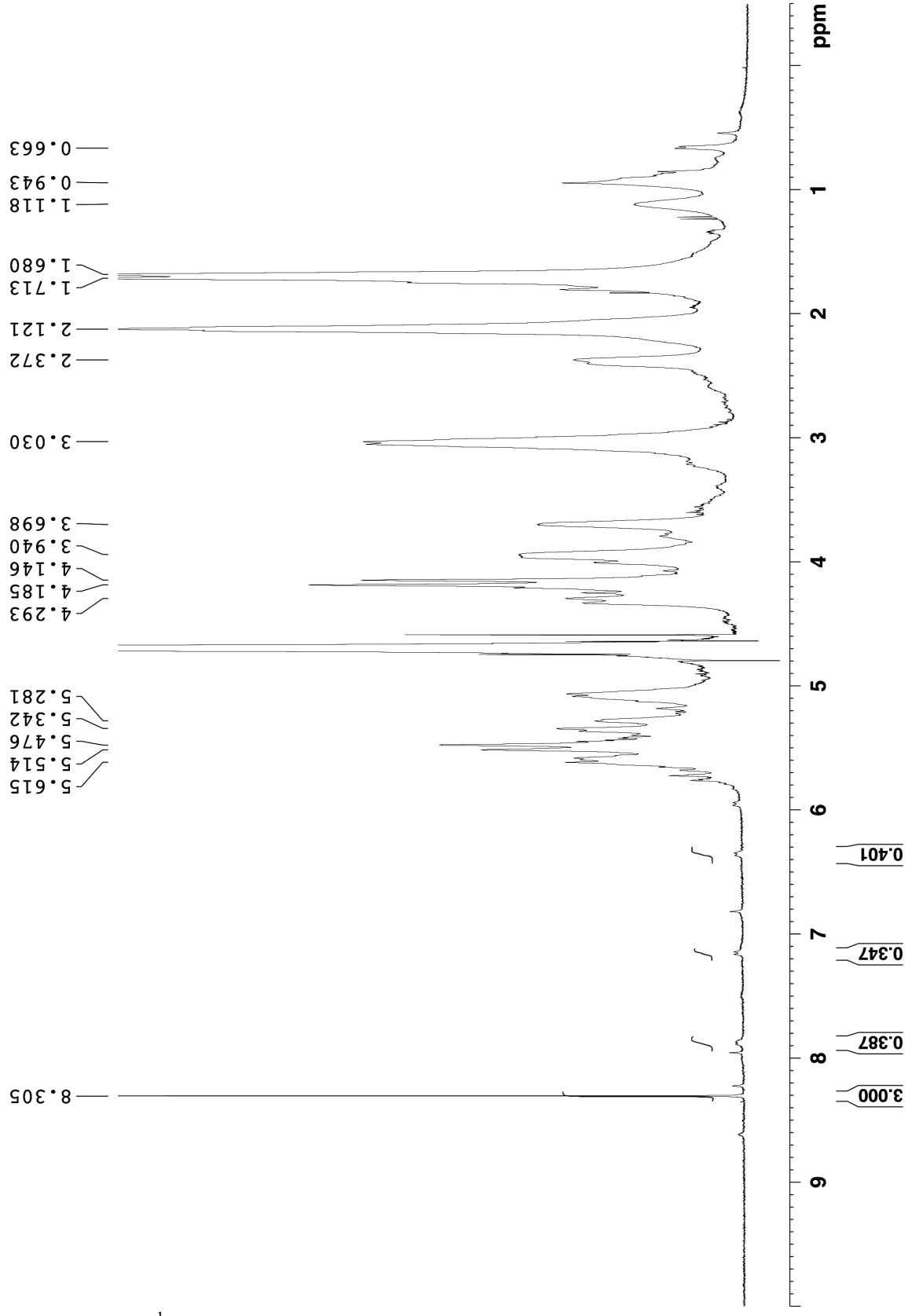

Figure S III-82. ^{1}H NMR recorded for pharmaceutical agent itraconazole with **III-1e** (10 mM) (400 MHz, 20 mM NaD_2PO_4, pD = 7.4, RT, 1,3,5-benzenetricarboxylic acid as reference).

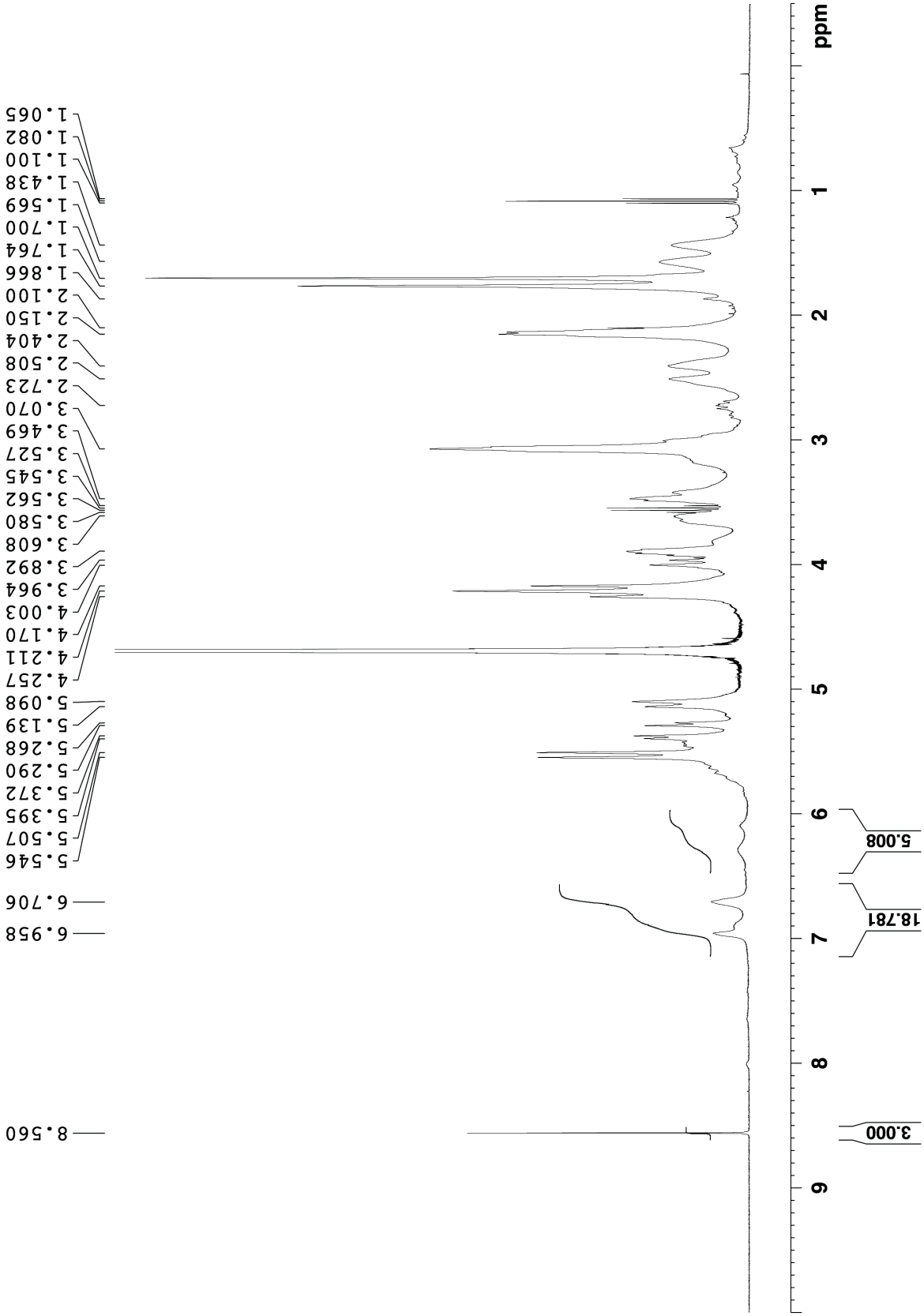

Figure S III-83. ^{1}H NMR recorded for pharmaceutical agent Melphalan with **III-1e** (10 mM) (400 MHz, 20 mM NaD_2PO_4, pD = 7.4, RT, 1,3,5-benzenetricarboxylic acid as reference).

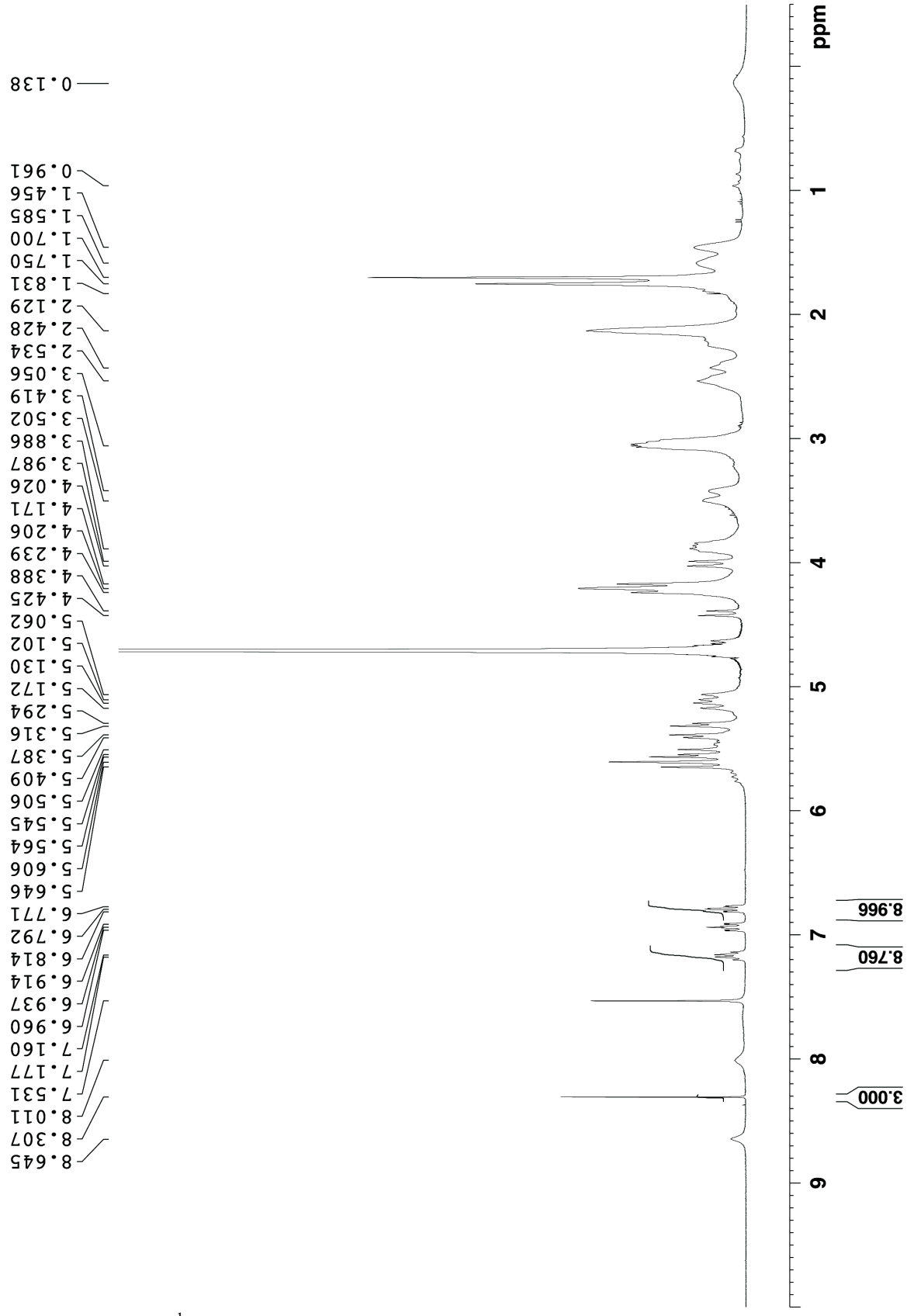

Figure S III-84. ^{1}H NMR recorded for pharmaceutical agent Voriconazole with **III-1e** (10 mM) (400 MHz, 20 mM NaD_2PO_4, pD = 7.4, RT, 1,3,5-benzenetricarboxylic acid as reference).

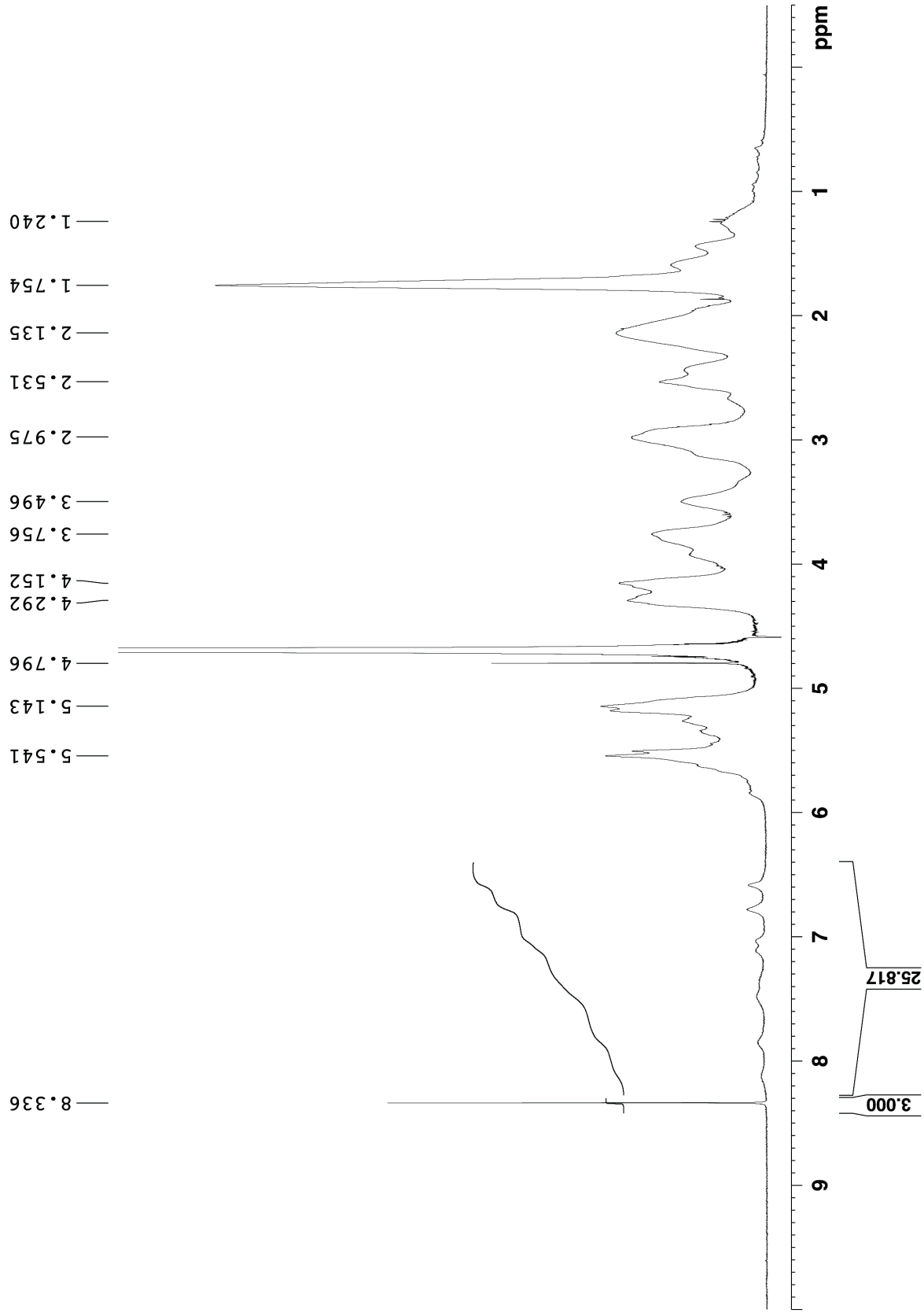

Figure S III-85. ^{1}H NMR recorded for pharmaceutical agent ziprasidone with **III-1e** (10 mM) (400 MHz, 20 mM NaD_2PO_4, pD = 7.4, RT, 1,3,5-benzenetricarboxylic acid as reference).

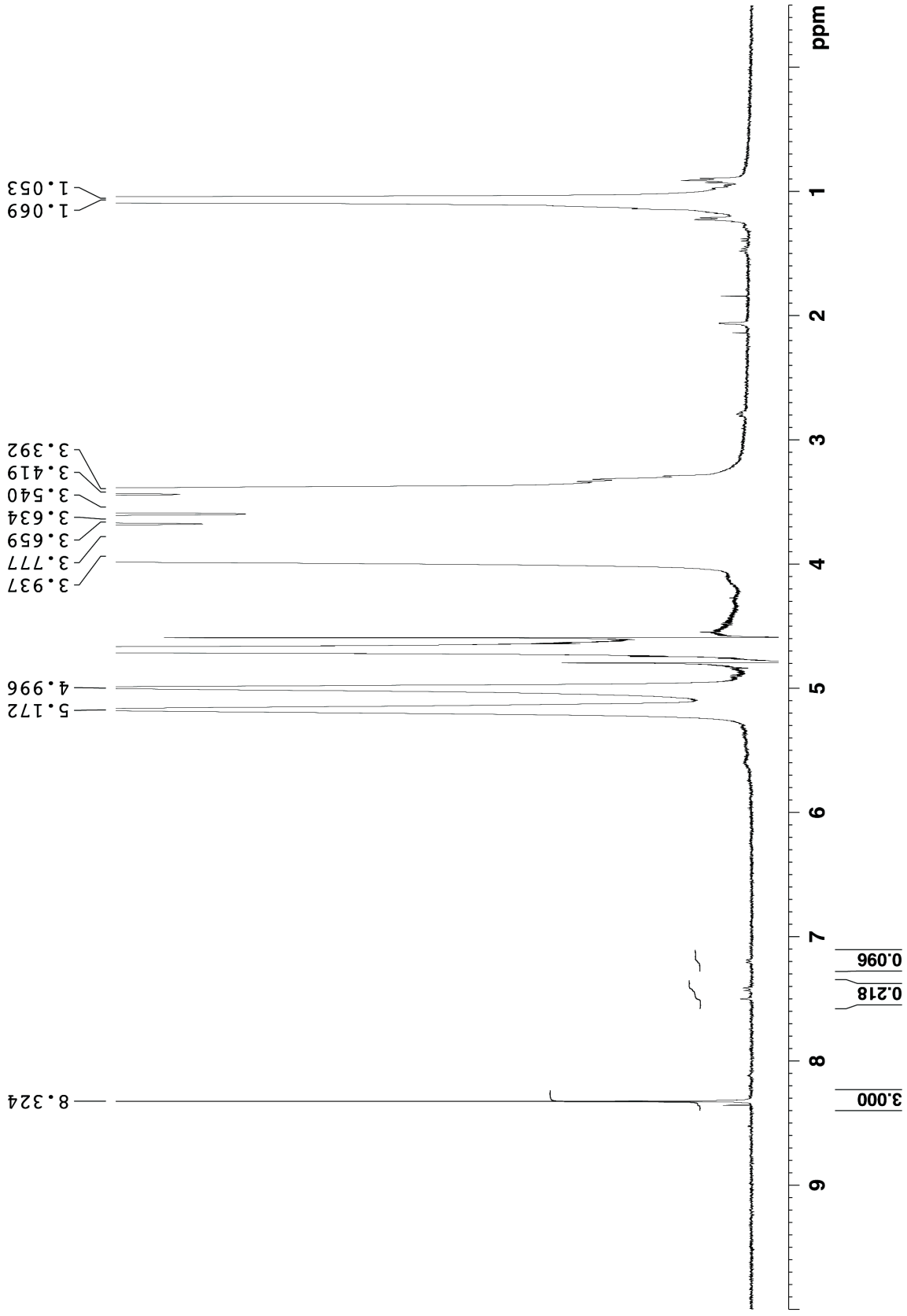

Figure S III-86. ^{1}H NMR recorded for pharmaceutical agent Albendazole with HP-β-CD (5 mM) (400 MHz, 20 mM NaD_2PO_4, pD = 7.4, RT, 1,3,5-benzenetricarboxylic acid as reference).

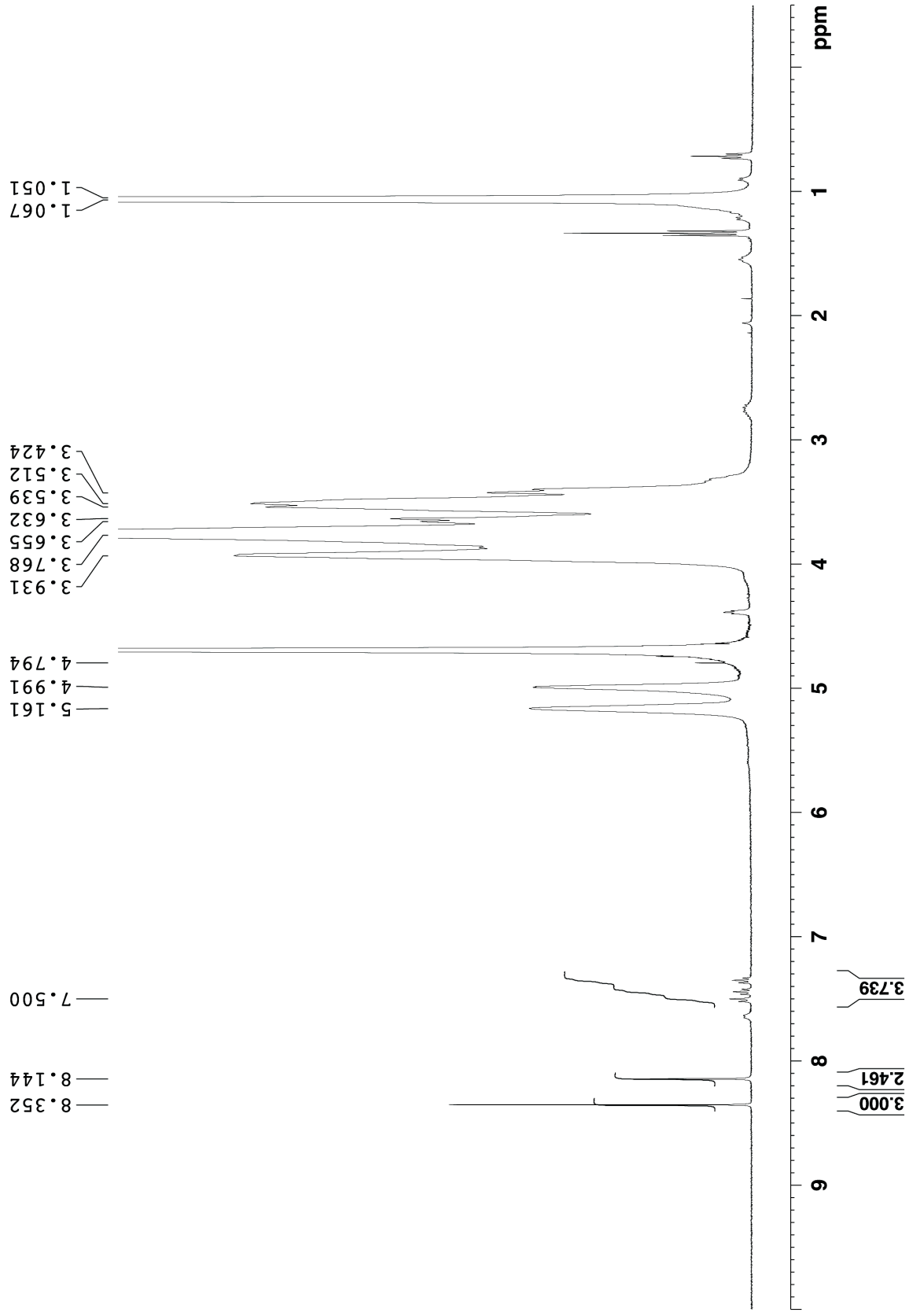

Figure S III-87. ^{1}H NMR recorded for pharmaceutical agent Amiodarone with HP-β-CD (10 mM) (400 MHz, 20 mM NaD_2PO_4, pD = 7.4, RT, 1,3,5-benzenetricarboxylic acid as reference).

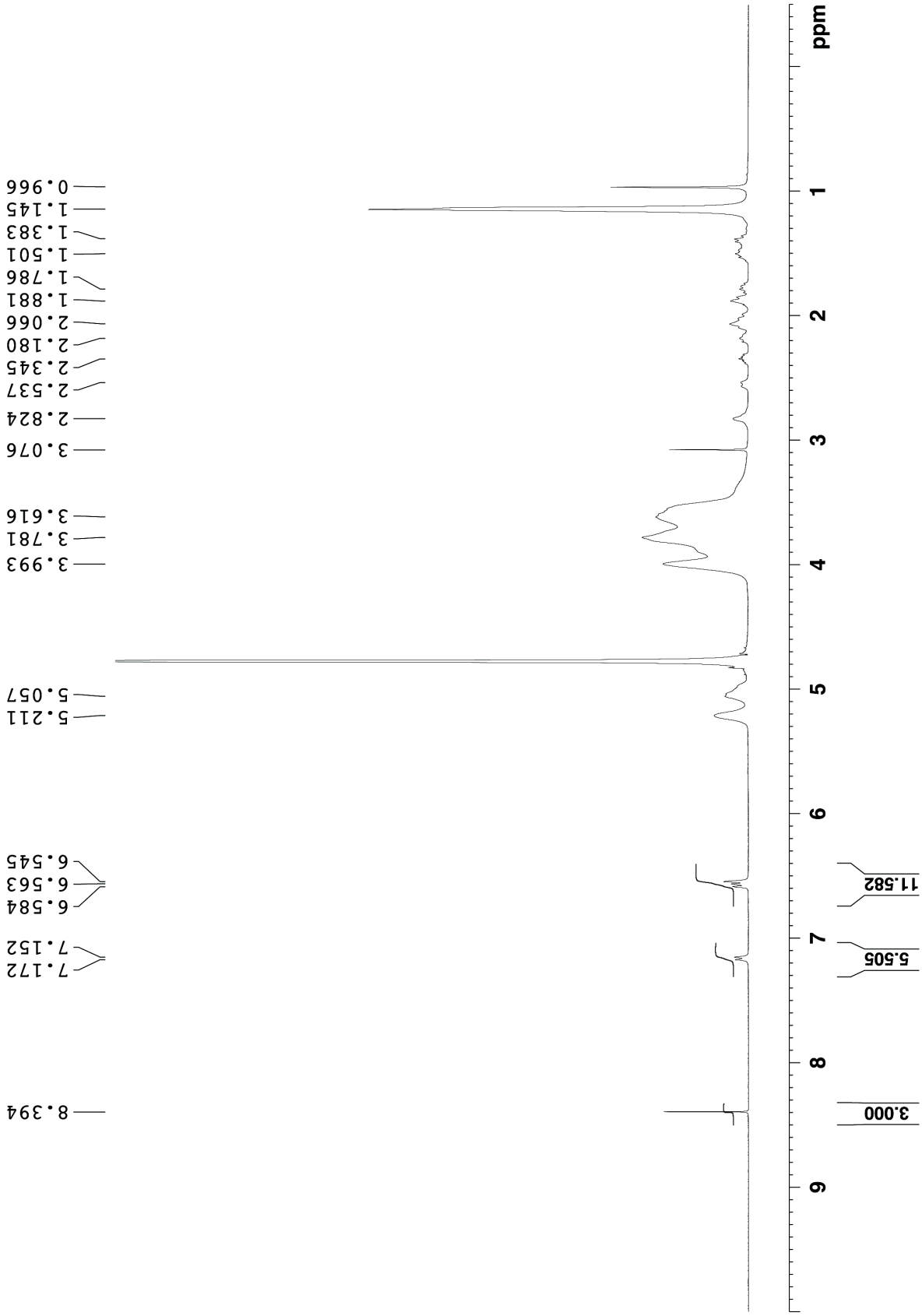

Figure S III-88. ^{1}H NMR recorded for pharmaceutical agent 17α-ethynylestradiol with HP-β-CD (10 mM) (400 MHz, 20 mM NaD_2PO_4, pD = 7.4, RT, 1,3,5-benzenetricarboxylic acid as reference).

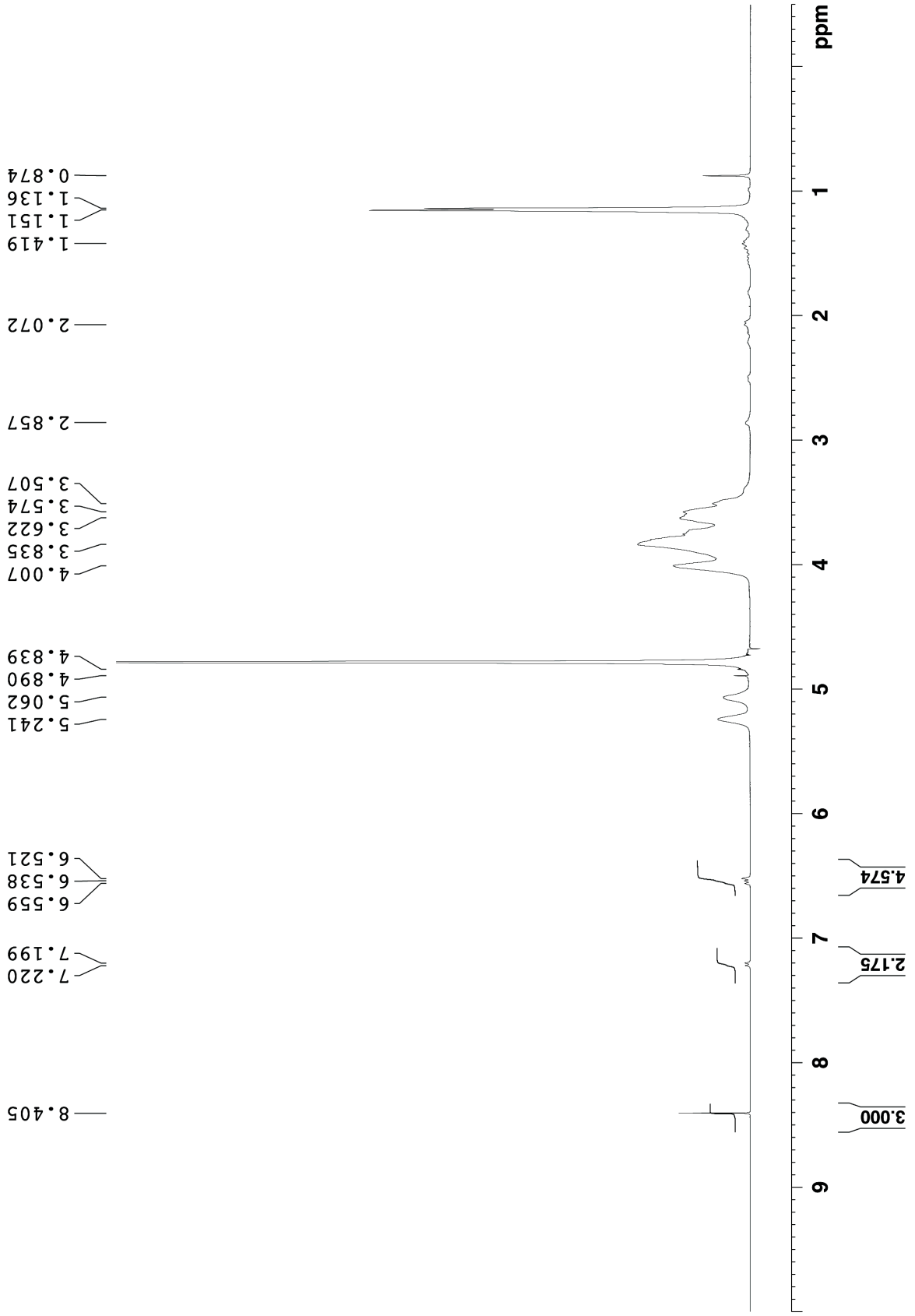

Figure S III-89. ^{1}H NMR recorded for pharmaceutical agent β-estradiol with HP-β-CD (10 mM) (400 MHz, 20 mM NaD_2PO_4, pD = 7.4, RT, 1,3,5-benzenetricarboxylic acid as reference).

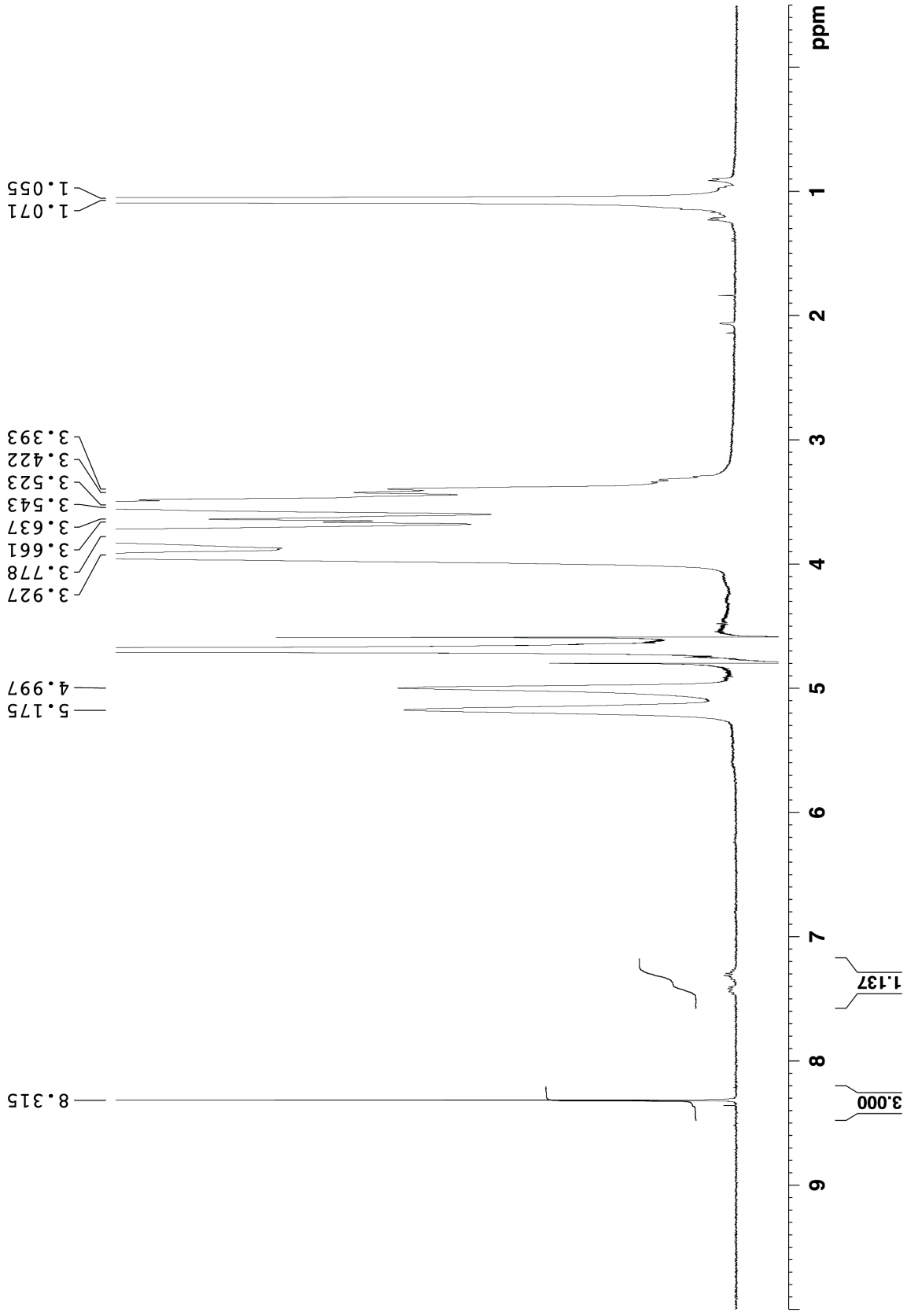

Figure S III-90. ^{1}H NMR recorded for pharmaceutical agent Cinnarizine with HP-β-CD (10 mM) (400 MHz, 20 mM NaD_2PO_4, pD = 7.4, RT, 1,3,5-benzenetricarboxylic acid as reference).

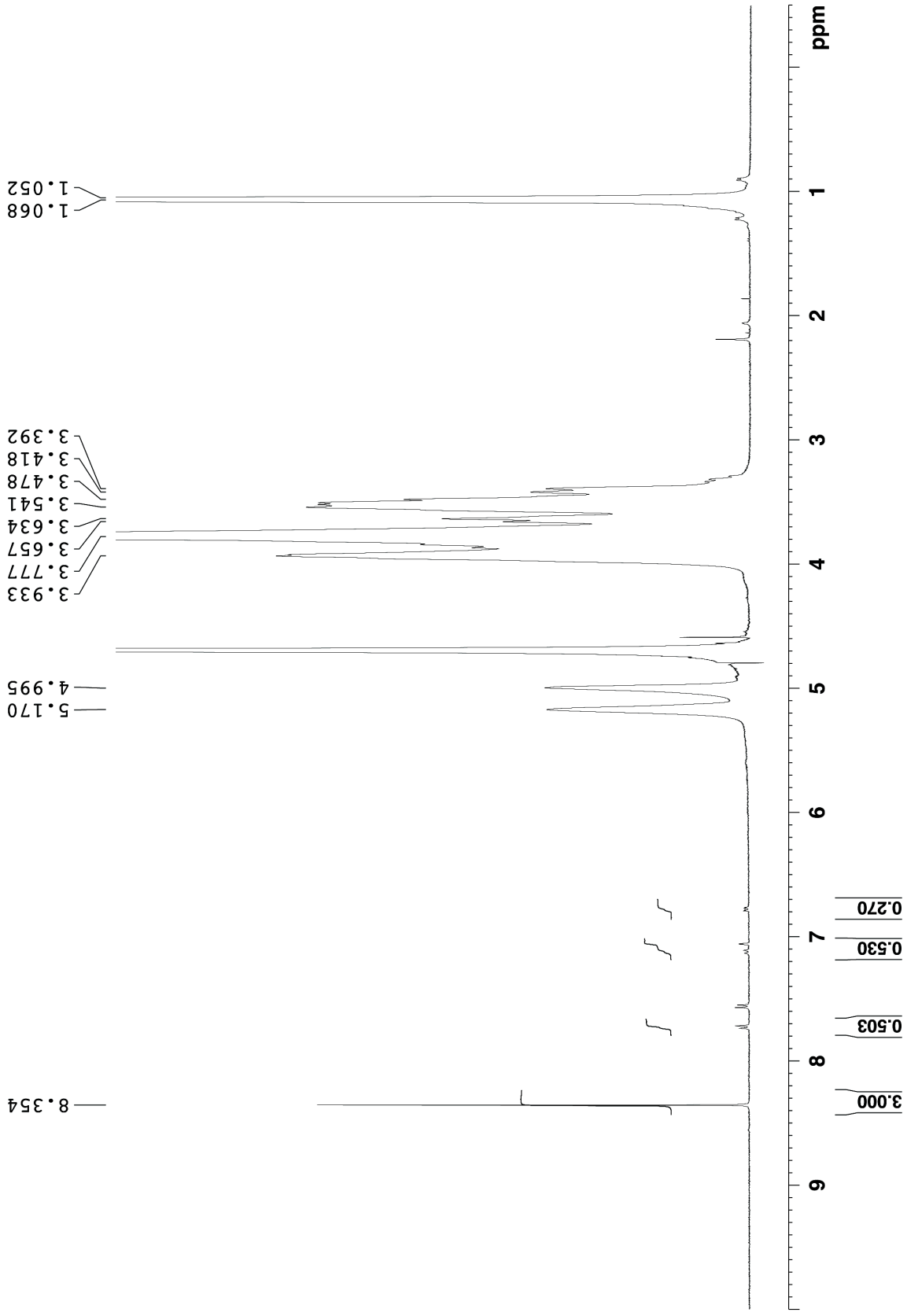

Figure S III-91. ^{1}H NMR recorded for pharmaceutical agent Indomethacin with HP-β-CD (10 mM) (400 MHz, 20 mM NaD_2PO_4, pD = 7.4, RT, 1,3,5-benzenetricarboxylic acid as reference).

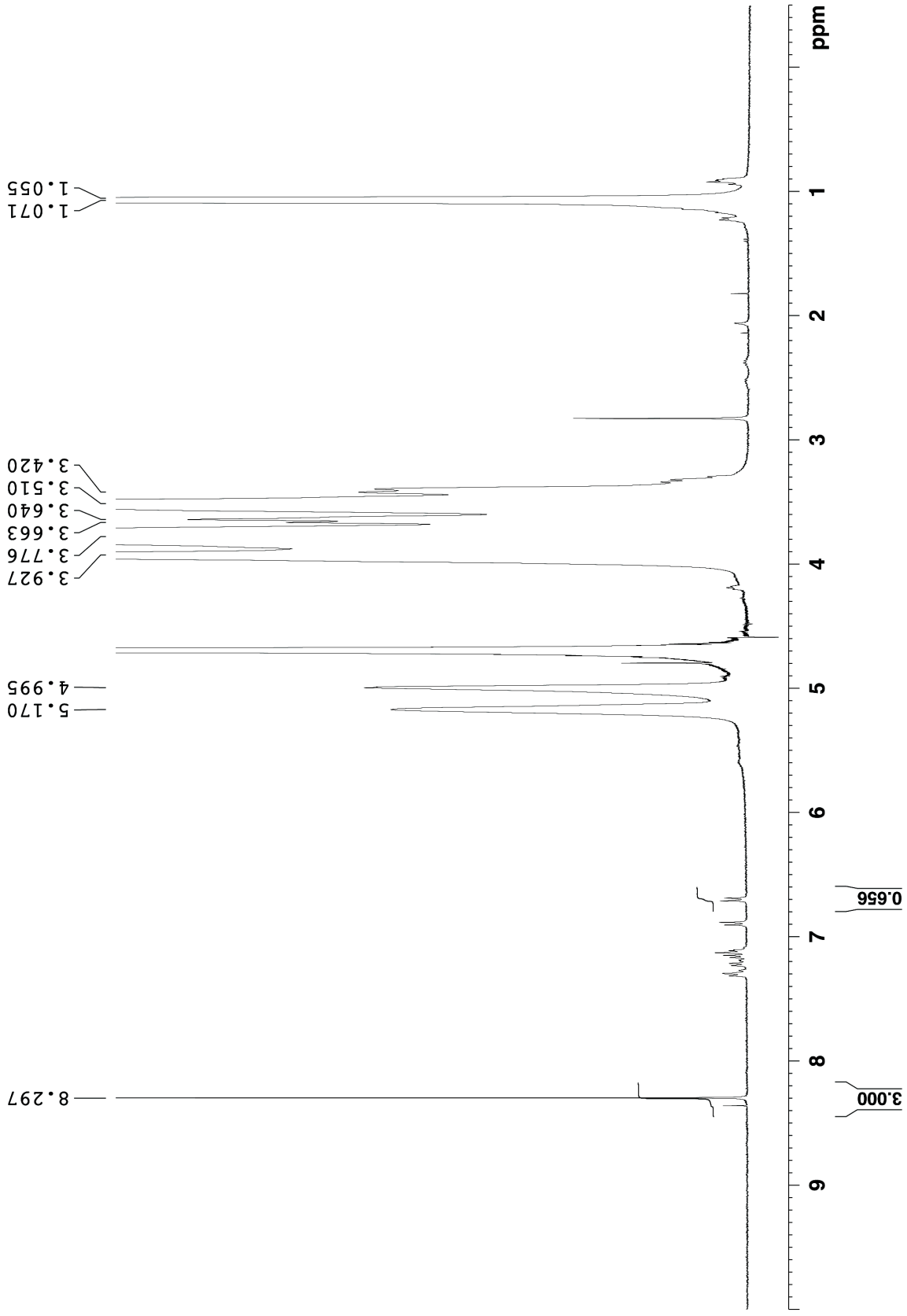

Figure S III-92. ^{1}H NMR recorded for pharmaceutical agent Tamoxifen with HP-β-CD (10 mM) (400 MHz, 20 mM NaD_2PO_4, pD = 7.4, RT, 1,3,5-benzenetricarboxylic acid as reference).

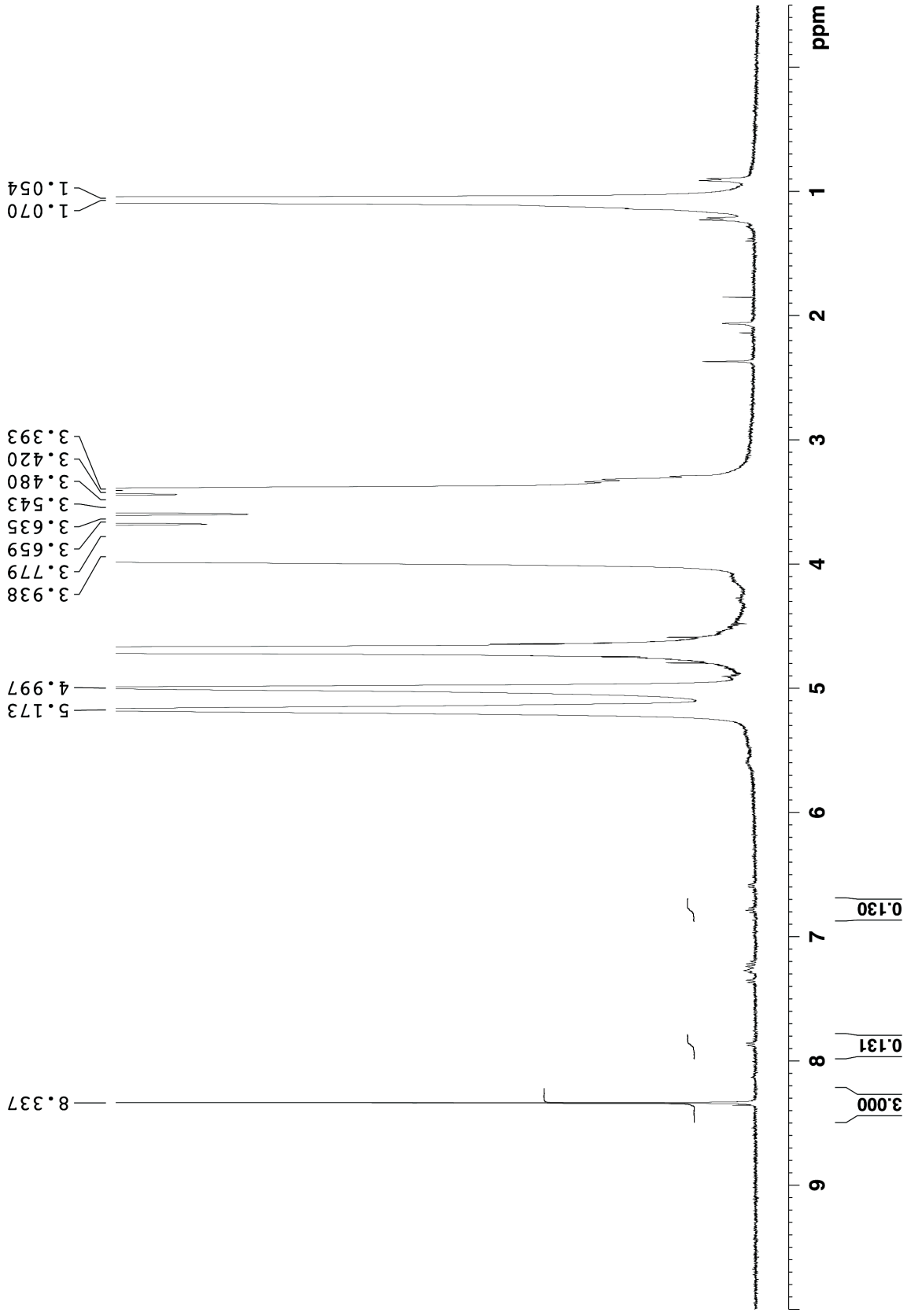

Figure S III-93. ^{1}H NMR recorded for pharmaceutical agent Tolfenamic acid with HP-β-CD (10 mM) (400 MHz, 20 mM NaD_2PO_4, pD = 7.4, RT, 1,3,5-benzenetricarboxylic acid as reference).

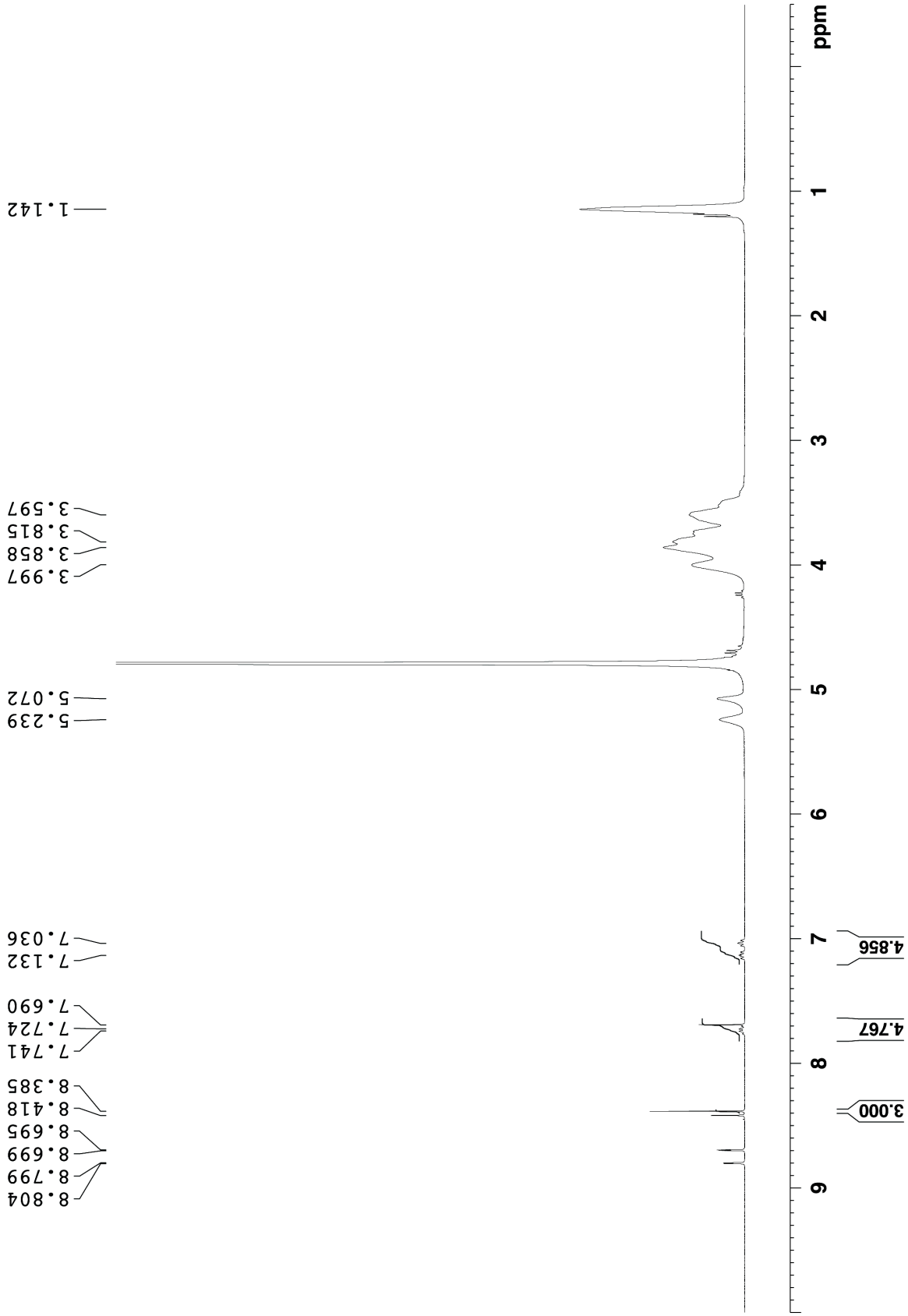

Figure S III-94. ^{1}H NMR recorded for pharmaceutical agent Voriconazole with HP-β-CD (10 mM) (400 MHz, 20 mM NaD_2PO_4, pD = 7.4, RT, 1,3,5-benzenetricarboxylic acid as reference).

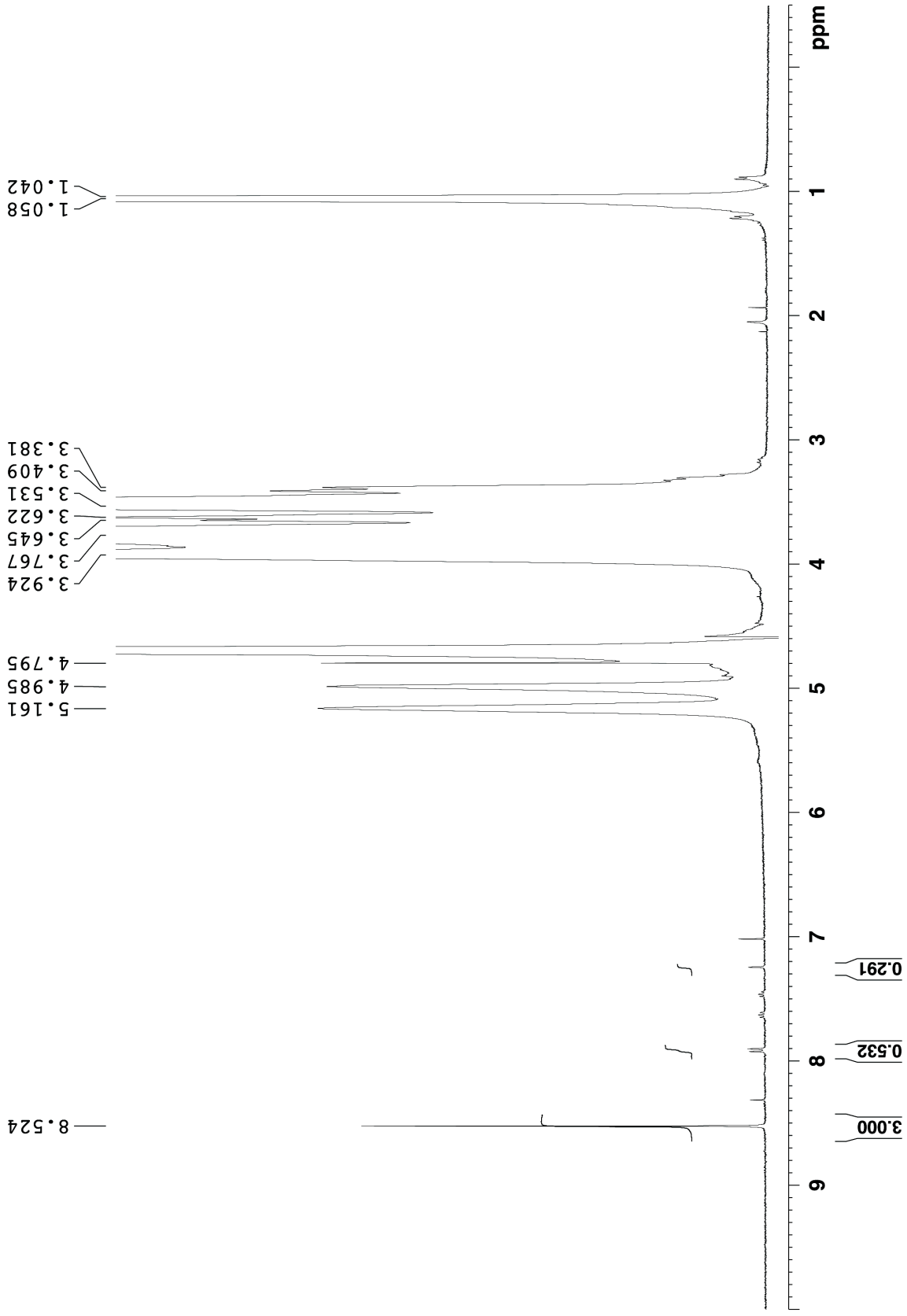

Figure S III-95. ^{1}H NMR recorded for pharmaceutical agent Ziprasidone with HP-β-CD (10 mM) (400 MHz, 20 mM NaD_2PO_4, pD = 7.4, RT, 1,3,5-benzenetricarboxylic acid as reference).

Bibliography

(1) Pedersen, C. J. *J. Am. Chem. Soc.* **1967**, *89*, 7017-7036.

(2) Behrend, R.; Meyer, E.; Rusche, F. *Justus Liebigs Ann. Chem.* **1905**, *339*, 1-37.

(3) Freeman, W. A.; Mock, W. L.; Shih, N.-Y. *J. Am. Chem. Soc.* **1981**, *103*, 7367 – 7368.

(4) Kim, J.; Jung, I.-S.; Kim, S.-Y.; Lee, E.; Kang, J.-K.; Sakamoto, S.; Yamaguchi, K.; Kim, K. *J. Am. Chem. Soc.* **2000**, *122*, 540-541.

(5) Day, A.; Arnold, I. A. P.; Blanch, R. J.; Snushall, B. *J. Org. Chem.* **2001**, *66*, 8094 – 8100.

(6) Liu, S.; Zavalij, P. Y.; Isaacs, L. *J. Am. Chem. Soc.* **2005**, *127*, 16798-16799.

(7) Day, A. I.; Blanch, R. J.; Arnold, A. P.; Lorenzo, S.; Lewis, G.; Dance, R. I. *Angew. Chem. Int. Ed.* **2002**, *41*, 275-277.

(8) Isaacs, L.; Park, S.-K.; Liu, S.; Ko, Y. H.; Selvapalam, N.; Kim, Y.; Kim, H.; Zavalij, P. Y.; Kim, G.-H.; Lee, H.-S.; Kim, K. *J. Am. Chem. Soc.* **2005**, *127*, 18000-18001.

(9) Huang, W.-H.; Zavalij, P. Y.; Isaacs, L. *Org. Lett.* **2008**, *10*, 2577-2580.

(10) Huang, W.-H.; Liu, S.; Zavalij, P. Y.; Isaacs, L. *J. Am. Chem. Soc.* **2006**, *128*, 14744-14745.

(11) Wittenberg, J. B.; Costales, M. G.; Zavalij, P. Y.; Isaacs, L. *Chem. Comm.* **2011**, *47*, 9420 – 9422

(12) Lagona, J.; Mukhopadhyay, P.; Chakrabarti, S.; Isaacs, L., *Angew. Chem. Int. Ed.* **2005**, *44* , 4844-70.

(13) Mock, W. L.; Pierpont, J. *J. Chem. Soc. Chem. Comm.* **1990**, *35*, 1509-1511.

(14) Kim, H.-J.; Jeon, W. S.; Ko, Y. H.; Kim, K. *Proc. Natl. Acad. Sci. USA* **2002**, *99*, 5007-5011.

(15) Jeon, W. S.; Ziganshina, A. Y.; Lee, J. W.; Ko, Y. H.; Kang, J. K.; Lee, C.; Kim, K. *Angew. Chem. Int. Ed.* **2003**, *42*, 4097-4100.

(16) Kim, J.; Jung, I. S.; Kim, S. Y.; Lee, E.; Kang, J. K.; Sakamoto, S.;Yamaguchi, K.; Kim, K. *J. Am. Chem. Soc.* **2000**, *122*, 540-541.

(17) Kim, H. J.; Heo, J.; Jeon, W. S.; Lee, E.; Kim, J.; Sakamoto, S.;Yamaguchi, K.; Kim, K. *Angew. Chem. Int. Ed.* **2001**, *40*, 1526–1529.

(18) Jeon, W. S.; Kim, E.; Ko, Y. H.; Hwang, I.; Lee, J. W.; Kim, S.-Y.; Kim, H.-J.; Kim, K. *Angew. Chem. Int. Ed*. **2005**, *44*, 87–91.

(19) Appel, E. A.; Biedermann, Frank, U.; Jones, S.; Zayed, J.; Scherman, O. *J. Am. Chem. Soc.* **2010**, *132*, 14251-14260

(20) Ghosh, S.; Isaacs, L., *J. Am. Chem. Soc.* **2010**, *132*, 4445-4454.

(21) Flinn, A.; Hough, G. C.; Stoddart, J. F.; Williams, D. J. *Angew. Chem. Int. Ed.* **1992**, *31*, 1475-1477.

(22) Jon, S. Y.; Selvapalam, N.; Oh, D. H.; Kang, J.-K.; Kim, S.-Y.; Jeon, Y. J.; Lee, J. W.; Kim, K. *J. Am. Chem. Soc.* **2003**, *125*, 10186-10187.

(23) Lee H.-K.; Park, K. M. J., Y. J.; Kim, D.; Oh, D. H.; Kim, H. S.; Park, C. K.; Kim, K. *J. Am. Chem. Soc.* **2005**, *127*, 5006-5007.

(24) Hwang, I.; Baek, K.; Jung, M.; Kim, Y.; Park, K. M.; Lee, D.-W.; Selvapalam, N.; Kim, K. *J. Am. Chem. Soc.* **2007**, *129*, 4170-4171.

(25) Ahn, Y.; Jang, Y.; Selvapalam, N.; Yun, G.; Kim, K. *Angew. Chem., Int. Ed.* **2013**, *52*, 3140-3144.

(26) Huang, W.-H.; Zavalij, P. Y.; Isaacs, L. *J. Am. Chem. Soc*. **2008**, *130*,8446–8454

(27) Lucas, D.; Minami, T.; Iannuzzi, G.; Cao, L.; Wittenberg, J. B.; Anzenbacher, P., Jr.; Isaacs, L. *J. Am. Chem. Soc.* **2011**, *133*, 17966–17976.

(28) Lucas, D.; Isaacs, L. *Org. Lett.* **2011**, *13*, 4112–4115.

(29) Cao, L.; Isaacs, L. *Org. Lett.* **2012**, *14*, 3072–3075.

(30) Minami, T.; Esipenko, N. A.; Zhang, B.; Isaacs, L.; Nishiyabu, R.; Kubo, Y.; Anzenbacher, P. *J. Am. Chem. Soc.* **2012**, *134*, 20021-20024.

(31) Vinciguerra, B.; Cao, L.; Cannon, J. R.; Zavalij, P. Y.; Fenselau, C.; Isaacs, L. *J. Am. Chem. Soc.* **2012**, *134*, 13133-13140.

(32) Lagona, J.; Fettinger, J. C.; Isaacs, L. *Org. Lett.* **2003**, *5*, 3745-3747.

(33) Burnett, C. A.; Witt, D.; Fettinger, J. C.; Isaacs, L. *J. Org. Chem.* **2003**, *68*, 6184-6191.

(34) Stancl, M.; Hodan, M.; Sindelar, V. *Org. Lett.* **2009**, *11*, 4184-4187.

(35) Ma, D.; Hettiarachchi, G.; Nguyen, D.; Zhang, B.; Wittenberg, J. B.; Zavalij, P. Y.; Briken, V.; Isaacs, L. *Nat. Chem.* **2012**, *4*, 503-510.

(36) Lipinski, C. A. *J. Pharmacol. Toxicol. Methods* **2000**, *44*, 235-249

(37) Hauss, D. J. *Adv. Drug Delivery Rev.* **2007**, *59*, 667-676.

(38) Porter, C. J. H., Trevaskis, N. L.; Charman, W. N. *Nature Rev. Drug Discov.* **2007**, *6,* 231–248.

(39) Leuner, C.; Dressman, J. *Eur. J. Pharm. Biopharm.* **2000**, *50,* 47–60.

(40) Muller, R. H.; Keck, C. M. *J. Biotechnol. 113,* **2004**, *113*, 151–170.

(41) Blagden, N., de Matas, M., Gavan, P. T.; York, P. *Adv. Drug Deliv. Rev.* **2007**, *59*, 617–630.

(42) Patri, A. K., Kukowska-Latallo, J. F.; Baker, J. *R. Adv. Drug Deliv. Rev.* **2005**, *57,* 2203–2214.

(43) Serajuddin, A. T. M. *Adv. Drug Deliv. Rev.* **2007**, *59*, 603–616.

(44) Stella, V. J.; Nti-Addae, K. W. *Adv. Drug Deliv. Rev.* **2007**, *59,* 677–694.

(45) Szente, L.; Szejtli, J. *Adv. Drug Deliv. Rev.* **1999**, *36*, 17–28.

(46) Villiers, A. *Compt. Rend.* **1891**, *112*, 536-538.

(47) Freudenberg, K.; Cramer, F. *Z. Naturforsch. B* **1948**, *3*, 464-467.

(48) French, D. *Adv. Carbohydr. Chem* **1957**, *12*, 189-260.

(49) Cramer, F. *Einschlussverbindungen (Inclusion Compounds)* Springer-Verlag: Berlin, **1954**.

(50) Rajewski, R. A.; Stella, V. J. *J. Pharm. Sci.* **1996**, *85,* 1142–1169.

(51) Stella, V. J.; Rajewski, R. A. *Pharm. Res.* **1997**, *14,* 556–567.

(52) Higuchi, T.; Connors, K. *Adv. Anal. Chem. Instrum.* **1965**, *4*, 117-212.

(53) Connors, K. A. *Binding Constants*; John Wiley & Sons: New York, **1987**.

(54) Okimoto, K., Rajewski, R. A., Uekama, K., Jona, J. A.; Stella, V. J. **1996**, *Pharm. Res. 13,* 256–264.

(55) Müller, B. W.; Brauns, U. *Int. J. Pharm.* **1985**, *26*, 77-88.

(56) Shiotani, K.; Uehata, K.; Hirayama, F.; Uekama, K. *Chem. Pharm. Bull.* **1994**, *42*, 2332-2337.

(57) Zia, V.; Rajewski, R. A.; Bornancini, E. R.; Luna, E. A.; Stella, V. J. *J. Pharm. Sci.* **1997**, *86*, 220-222.

(58) Thompson, D. O. *CRC Crit. Rev. Ther. Drug Carrier Syst.* **1997**, 1-67.

(59) Uekama, K.; Fujinaga, T.; Hirayama, F.; Otagiri, M.; Kurono, Y.; Ikeda, K. *J. Pharm. Pharmacol.* **1982**, *34*, 627-630.

(60) Husain, N.; Ndou, T. T.; de la Pen'a, A. M.; Warner, I. M. *Appl. Spectrosc.* **1992**, *46,* 652-658

(61) Brewster, M. E.; Loftsson, T.; Estes, K. S.; Lin, J. L.; Fridriks-dottir, H.; Bodor, N. *Int. J. Pharm.* **1992**, *79,* 289-299.

(62) Menard, F. A.; Dedhiya, M. G.; Rhodes, C. T. *Pharm. Acta Helv.* **1988**, *63,* 303-308..

(63) Liu, S.; Ruspic, C.; Mukhopadhyay, P.; Chakrabarti, S.; Zavalij, P. Y.; Isaacs, L. *J. Am. Chem. Soc.* **2005**, *127*, 15959-15967.

(64) Rekharsky, M. V.; Mori, T.; Yang, C.; Ko, Y. H.; Selvapalam, N.; Kim, H.; Sobransingh, D.; Kaifer, A. E.; Liu, S.; Isaacs, L.; Chen, W.; Moghaddam, S.; Gilson, M. K.; Kim, K.; Inoue, Y. *Proc. Natl. Acad. Sci. U. S. A.* **2007**, *104*, 20737-20742.

(65) Cao, L.; Sekutor, M.; Zavalij, P. Y.; Mlinaric-Majerski, K.; Glaser, R.; Isaacs, L. *Angew. Chem. Int. Ed.* **2014**, *53*, 988-993.

(66) Isaacs, L. *Acc. Chem. Res.* **2014**, *47*, 2052-2062.

(67) Ko, Y. H.; Kim, E.; Hwang, I.; Kim, K. *Chem. Comm.* **2007**, 1305-1315.

(68) Yang, H.; Yuan, B.; Zhang, X.; Scherman, O. A. *Acc. Chem. Res.* **2014**, 2106-2115.

(69) Kim, E.; Kim, D.; Jung, H.; Lee, J.; Paul, S.; Selvapalam, N.; Yang, Y.; Lim, N.; Park, C. G.; Kim, K. *Angew. Chem., Int. Ed.* **2010**, *49*, 4405-4408.

(70) Hettiarachchi, G.; Nguyen, D.; Wu, J.; Lucas, D.; Ma, D.; Isaacs, L.; Briken, V. *PLoS One* **2010**, *5*, e10514.

(71) Uzunova, V. D.; Cullinane, C.; Brix, K.; Nau, W. M.; Day, A. I. *Org. Biomol. Chem.* **2010**, *8*, 2037-2042.

(72) Jeon, Y. J. et al. *Org. Biomol.Chem.* **2005**, *3,* 2122–2125.

(73) Macartney, D. H. *Isr. J. Chem.* **2011**, *51,* 600–615.

(74) Walker, S., Oun, R., McInnes, F. J.; Wheate, N. J. *Isr. J. Chem.* **2011**, *51,* 616–624.

(75) Dong, N. et al. *Supramol. Chem.* **2008**, *20*,659–665.

(76) Koner, A. L., Ghosh, I., Saleh, N.; Nau, W. M. *Can. J. Chem.* **2011**, *89,*139–147.

(77) Dong, N., Wang, X., Pan, J.; Tao, Z. *Acta Chim. Sinica* **2011**, *69*,1431–1437.

(78) Miskolczy, Z., Megyesi, M., Tarkanyi, G., Mizsei, R.; Biczok, L. *Org. Biomol. Chem.*

2011, *9,*061–1070.

(79) Cao, L.; Hettiarachchi, G.; Briken, V; Isaacs, L. *Angew. Chem., Int. Ed.*, **2013**, *52*, 12033-12037.

(80) Zhang, B.; Zavalij, P. Y.; Isaacs, L. *Org. Biomol. Chem.* **2014**, *12*, 2413-2422.

(81) Pedersen, C. J. *Angew. Chem., Int. Ed.* **1988***, 27*, 1021–1027.

(82) Cram, D. J. *Angew. Chem., Int. Ed.* **1988***, 27,* 1009–1020.

(83) Lehn, J.-M. *Angew. Chem., Int. Ed.* **1988***, 27*, 89–112.

(84) Ogoshi, T.; Kanai, S.; Fujinami, S.; Yamagishi, T.-A.; Nakamoto, Y. *J. Am. Chem. Soc.* **2008***, 130*, 5022–5023.

(85) Xue, M.; Yang, Y.; Chi, X.; Zhang, Z.; Huang, F. *Acc. Chem. Res.* **2012**, *45*, 1294–1308

(86) Northrop, B. H.; Zheng, Y.-R.; Chi, K.-W.; Stang, P. J. *Acc. Chem. Res.* **2009***, 42,* 1554–1563.

(87) Rebek, J. *Acc. Chem. Res.* **2009***, 42,* 1660–1668

(88) Yoshizawa, M.; Klosterman, J.; Fujita, M. *Angew. Chem.,Int. Ed.* **2009***, 48,* 3418–3438

(89) Fiedler, D.; Leung, D. H.; Bergman, R. G.; Raymond, K. N. *Acc. Chem. Res.,* **2005***,38,* 349–358.

(90) Cram, D. J.; Tanner; M. E.; Thomas, R. *Angew. Chem., Int. Ed.* **1991***, 30,* 1024–1027.

(91) Klotz, E. J. F.; Claridge, T. D. W.; Anderson, H. L. J. *Am. Chem. Soc.* **2006***, 128,* 15374–15375;

(92) Tashiro, S.; Tominaga, M.; Kawano, M.; Therrien, B.; Ozeki, T.; Fujita, M. *J. Am. Chem. Soc.* **2005***, 127,* 4546–4547.

(93) Pluth, M. D.; Bergman, R. G.; Raymond, K. N. *Science* **2007***, 316*, 85–88.

(94) Mock, W. L.; Shih, N.-Y. *J. Org. Chem.* **1986**, *51,* 4440–4446.

(95) Dsouza, R.; Hennig, A.; Nau, W. *Chem.–Eur. J.* **2012***, 18*,3444–3459.

(96) Pemberton, B. C.; Raghunathan, R.; Volla, S.; Sivaguru, J. *Chem.–Eur. J.* **2012**, *18,* 12178–12190.

(97) Appel, E.; Barrio, J.; Loh, X. Scherman, O. *Chem. Soc. Rev.* **2012***, 41,* 6195–6214;

(98) Lee, D.-W.; Park, K.; Banerjee, M.; Ha, S.; Lee, T.; Suh, K.; Paul, S.; Jung, H.; Kim, J.; Selvapalam, N.; Ryu, S.; Kim, K. *Nat. Chem.* **2011***, 3,* 154–159.

(99) Dang,D.; Nguyen, H.; Merkx M.; Brunsveld, L. *Angew. Chem., Int. Ed.* **2013***, 52,* 2915–2919;

(100) Wittenberg, J. B.; Zavalij, P. Y.; Isaacs, L. *Angew. Chem., Int. Ed.* **2013**, *52*, 3690-3694.

(101) Muller, R. H.; Keck, C. M. *J. Biotechnol.* **2004**, *113*, 151-170.

(102) Baird, J. A.; Taylor, L. S. *Adv. Drug Deliv. Rev.* **2012**, *64* , 396-421.

(103) Okimoto, K.; Rajewski, R. A.; Uekama, K.; Jona, J. A.; Stella, V. J. *Pharm. Res.* **1996**, *13*, 256-264.

(104) Zhao, Y.; Buck, D. P.; Morris, D. L.; Pourgholami, M. H.; Day, A. I.; Collins, J. G. *Org. Biomol. Chem.* **2008**, *6*, 4509-4515.

(105) Zhao, Y.; Pourgholami, M. H.; Morris, D. L.; Collins, J. G.; Day, A. I. *Org. Biomol. Chem.* **2010**, *8*, 3328-3337.

(106) Saleh, N.; Koner, A. L.; Nau, W. M. *Angew. Chem. Int. Ed.* **2008**, *47*, 5398-5401.

(107) Chakraborty, A.; Wu, A.; Witt, D.; Lagona, J.; Fettinger, J. C.; Isaacs, L. *J. Am. Chem. Soc.* **2002**, *124*, 8297-8306. Freeman, W. A.; Mock, W. L.; Shih, N.-Y. *J. Am. Chem. Soc.* **1981**, *103*, 7367 – 7368.

(108) Lagona, J.; Wagner, B. D.; Isaacs, L. *J. Org. Chem.* **2006**, *71*, 1181-1190.

(109) Huang, W.-H.; Zavalij, P. Y.; Isaacs, L. *Angew. Chem., Int. Ed.* **2007**, *46*, 7425-7427.

(110) Huang, W.-H.; Zavalij, P. Y.; Isaacs, L. *Org. Lett.* **2009**, *11*, 3918-3921.

(111) Minami, T.; Esipenko, N.; Akdeniz, A.; Zhang, B.; Isaacs, L.; Anzenbacher, P. *J. Am. Chem. Soc.* **2013**, *135*, 15238-15243.

(112) Ma, D.; Zhang, B.; Hoffmann, U.; Sundrup, M. G.; Eikermann, M.; Isaacs, L. *Angew. Chem., Int. Ed.* **2012**, *51*, 11358-11362.

(113) George, W. N.; Giles, M.; McCulloch, I.; de Mello, J. C.; Steinke, J. H. *Soft Matter* **2007**, *3*, 1381-1387.

(114) Sijbesma, R. P.; Kentgens, A. P. M.; Lutz, E. T. G.; van der Maas, J. H.; Nolte, R. J. M. *J. Am. Chem. Soc.* **1993**, *115*, 8999-9005.

(115) Shen, C.; Ma, D.; Meany, B.; Isaacs, L.; Wang, Y. *J. Am. Chem. Soc.* **2012**, *134*, 7254-7257.

(116) Stancl, M.; Gilberg, L.; Ustrnul, L.; Necas, M.; Sindelar, V. *Supramol. Chem.* **2013**, *25*, 168 - 172.

(117) Connors, K. A. *Binding Constants*; John Wiley & Sons: New York, **1987**.

(118) Ma, D.; Zavalij, P. Y.; Isaacs, L. *J. Org. Chem.* **2010**, *75*, 4786-4795.

(119) Ma, D.; Glassenberg, R.; Ghosh, S.; Zavalij, P. Y.; Isaacs, L. *Supramol. Chem.* **2012**, *24*, 325-332.

(120) Anslyn, E. V. *J. Org. Chem.* **2007**, *72*, 687-699.

(121) Ghosh, I.; Nau, W. M. *Adv. Drug Deliv. Rev.* **2012**, *64*, 764-783.

(122) Shaikh, M.; Mohanty, J.; Singh, P.; Nau, W.; Pal, H. *Photochem. Photobiol. Sci.* **2008**, *7*, 408-414.

(123) Wu, J.; Isaacs, L. *Chem. Eur. J.* **2009**, *15*, 11675-11680.

(124) Tririya, G.; Zanger, M. *Synth. Commun.* **2004**, *34*, 3047-3059.

(125) Murahashi, S.-I.; Miyaguchi, N.; Noda, S.; Naota, T.; Fujii, A.; Inubushi, Y.; Komiya, N. *Eur. J. Org. Chem.* **2011**, 5355-5365.

(126) Fabre, C.; Mimura, N.; Bobb, K.; Kong, S.-Y.; Gorgun, G.; Cirstea, D.; Hu, Y.; Minami, J.; Ohguchi, H.; Zhang, J.; Meshulam, J.; Carrasco, R. D.; Tai, Y.-T.; Richardson, P. G.; Hideshima, T.; Anderson, K. C. *Clin. Cancer Res.* **2012**, *18*, 4669-4681.

(127) Rekharsky, M. V.; Inoue, Y. *Chem. Rev.* **1998**, *98*, 1875-1917

(128) Houk, K. N.; Leach, A. G.; Kim, S. P.; Zhang, X. *Angew. Chem., Int. Ed.* **2003**, *42*, 4872-4897.